UNIVERSITY OF SOUTHAMPTON

FACULTY OF SOCIAL, HUMAN AND MATHEMATICAL SCIENCE

School of Geography and Environment

The Dynamics of Cobble Dunes, Severn Estuary, United Kingdom

by

Akirat Abdulkade

Thesis for the degree of Doctor of Philosophy

November 2017

UNIVERSITY OF SOUTHAMPTON

ABSTRACT

FACULTY OF SOCIAL, HUMAN AND MATHEMATICAL SCIENCE

Geography and environment

Thesis for the degree of Doctor of Philosophy

THE DYNAMICS OF COBBLE DUNES, SEVERN ESTUARY, UNITED KINGDOM

Akirat Abdulkade

Dunes are one bedform type which can be found underwater and which have an impact on flow resistance and play an important role in engineering structure design, navigation as well as dredging strategies. Existing literature focuses on the formation and processes associated with dunes developed by sandy sediment and has paid little attention to those developed in coarse sediment, i.e. cobble dunes.

This research will focus on the dynamics of a set of coarse cobble dunes located on Hills Flats, in the Severn Estuary, UK. The features are composed of a range of sediment sizes; from small boulders, coarse cobbles, pebbles, to finer components. The dunes are exposed during low water period, especially during Spring tides, when direct measurements of the dunes could occur. Specifically, data related to dunes dynamics were collected by a number of techniques including measuring the dune shape by using dGPS, recording near-bed flow velocity data with current meter, sampling bedload transportation to imply the movements of pebbles or cobbles, and measuring the basic morphology of dunes located on the site and to obtain first interpretations of dune dynamics. Data from these techniques were processed to demonstrate the roughness effects on tidal flows and the subsequent influence on the bulk flow field. The results of this study show that the dunes, D_{50} ~ 16.7 mm, move only on the highest Spring tides and reverse direction of migration with each flood and ebb tide while little movement on Neap tides is recorded. The migration is low with the maximum rate only 1.1 cm per tide. The dune scale varies but usually less than 1 m high and 4 – 10m long. Water depth, flow velocity and bed shear stress over the dunes could exceed 10 m, 2 m/s and 80 N/m^2 respectively. The initial motion of pebbles could start in a range of 0.3 – 50 N/m^2. The dynamics of the bedforms are explained by the tidal asymmetry which mediates the temporal distribution of bed shear stress, understanding of which provide benefits to several aspects such as engineering of structures and environmental management planning in this area and other similar locations.

Keywords: cobble dunes; intertidal zone; bedform process; Severn Estuary

Table of Contents

List of tables

List of figures

DECLARATION OF AUTHORSHIP

I, Akirat Abdulkade, declare that this thesis and the work presented in it are my own and has been generated by me as the result of my own original research.

THE DYNAMICS OF COBBLE DUNES, SEVERN ESTUARY, UNITED KINGDOM

I confirm that:

1. This work was done wholly or mainly while in candidature for a research degree at this University;
2. Where any part of this thesis has previously been submitted for a degree or any other qualification at this University or any other institution, this has been clearly stated;
3. Where I have consulted the published work of others, this is always clearly attributed;
4. Where I have quoted from the work of others, the source is always given. With the exception of such quotations, this thesis is entirely my own work;
5. I have acknowledged all main sources of help;
6. Where the thesis is based on work done by myself jointly with others, I have made clear exactly what was done by others and what I have contributed myself;
7. [Delete as appropriate] None of this work has been published before submission [or] Parts of this work have been published as: [please list references below]:

Signed: .....

Date:.....

Acknowledgements

After an intensive period of four years, today is the day: writing this note of thanks is the finishing touch on my thesis. It has been a period of intense learning for me, not only in the scientific arena, but also on a personal level. PhD life has had a big impact on me. I would like to take this opportunity to thank people who have supported and helped me so much throughout this period as a researcher at School of Geography and Environment, University of Southampton. Without the following names, this research could not have been this success.

Firstly, I would like to thank my supervisory team, Prof Paul A Carling, Dr Julian Leyland and Dr Charlie Thompson for the continuous support of my PhD study and related research, for their patience, motivation, encouragement and immense knowledge. Their guidance through all the period of research, fieldwork supports and writing of this thesis are invaluable. I could not have imagined having a better advisors and mentors for my PhD study.

Besides my supervisory team, my study should not have been so smooth without assistance given by Geography technician; Peter Morgan, Liam Riddy, Tom Bishop, Darius Beben; postdoctoral and postgraduate colleagues; Arjan Reesink, Hai Q. Trieu, Chris Hackney, Hal Voepel, David Sutherland, Hachem Kassem, Quan Li Zong, Chloé Chatellino, Eliisa Lotsari; for the fieldwork data collections, equipment supports and lab works analysis. Moreover, I would like to thank these people for providing assistance in equipment and secondary data David Jones and Michael Smithson of the National Oceanographic Centre, Proudman Laboratory, Liverpool for the plankton tower sampler; Dr Jeff Warburton from Department of Geography, Durham University for Robotic Leica TCRP1205; Ross Jennings from Department of Geography, Environment and Earth Studies, University of Hull; and Mike Johnson from Gloucester Harbour Trustees for the bathymetry data of the Severn Estuary; The National Oceanography Centre, Southampton for the velocity current meters and suspended sediment sampler (KC Denmark).

I am particularly grateful for the financial support provided by the Office of the Higher Education Commission, Silpakorn University, and Royal Thai government, Thailand; otherwise, this research project would not have been possible.

Last but not the least, I would like to thank my family for their wise counsel and sympathetic ear through the duration of my study. You are always there for me. Finally, there are my friends including Geography fellows and Thai Soton family, who were not only able to support each other by deliberating over our problems and findings.

Definitions and Abbreviations

D	grain size
D_i	grain size percentile
D_{50}	median grain size
D_{mobile}	grain size likely to be moved
ff	The resistance coefficients/friction factor
F_D	drag force on each grain
Fr	Froude number
g	acceleration due to gravity
h	water depth
h/D_{50}	relative depth
H	height
H_s	significant wave height
H_{max}	maximum wave height
L	length
L_1	flat dune crest length
L_2	dune wavelength
L_U	dune length on the upstream/ up-estuary side
L_D	dune length on the downstream/ down-estuary side
L_1/L_2	flatness index
L_U/L_D	dune asymmetry
L_2/H	steepness
Q	discharge
Q_s	sediment load/ discharge of bed material load
R	hydraulic radius/ mean depth (could be replaced by “mean depth” for wide, shallow channels)
Re	Reynolds number
Re_p^*	particle shear velocity Reynolds number
S	slope
SSC	suspended sediment concentration (mg/L)
TSS	total suspended solids or dry weight of suspended sample (g)
T_1	wave period
u_*	Shear velocity
U	velocity (m/s)
U_W	wave orbital velocity amplitude at sea bed
W	channel width
y	height above the bed
Z	heights recorded above the bed
Z_0	bed roughness length
τ	shear stress
τ_*	dimensionless shear stress
τ_0	bed shear stress
τ_{0c}	critical shear stress
τ_{0s}	skin-friction bed shear stress

ρ	Density
ρ_w	water density
ρ_s	grain density
θ	Shields number
μ	dynamic viscosity
ϵ	eddy viscosity
γ	specific weight of water
δ_{sub}	thickness of laminar sublayer
η	packing coefficient related with grains per unit bed area
ϕ	internal friction between grains
α	lee slope
β	stoss slope
a	cross-section area
f	Darcy-Weisbach friction factor
ff	resistance coefficients/friction factor
κ	Karman's universal constant (κ = 0.4)
l	eddy penetration or mixing length
ν	kinematic viscosity

Chapter 1: Introduction

In natural rivers, bed characteristics and hydrodynamics are important factors related to bedform development and they are also interrelated to each other. The bed sediments are entrained and transported along stream by the power of the stream and are later deposited to develop into bedforms. The bedforms, in turn, affect the properties of flows, including turbulence. Several bedform types developing under water have been defined (Chapter 2). They are responsible for inducing flow resistance which is denoted as hydraulic roughness. Bed roughness found in natural systems ranges from small sediment particles, bed forms, vegetation, to any artificial obstacles (i.e. groynes). These elements act by protruding into water flow and enhancing shear stress and turbulence.

Dunes are one of the bedforms commonly found in many rivers as well as tidal and marine environment (Allen, 1984). They are usually developed in loose, non-cohesive sediments. Dune crests grow and reduce when bedload sediment increases and decreases respectively. The direction of migration of dunes is prone to be downstream as sediment are entrained from the upstream (stoss side) and moved towards the downstream (lee side). Dunes are classified by the height, length and amplitude and there are a wide range of sizes which have been reported (Wilbers, 2004).

The existence of dunes has an impact on flow resistance due to the additional form drag induced. The height of dunes is the important factor in creating roughness; the higher dunes are (occur when discharge increase), the more roughness the river bed has. The form resistance produced by dunes initiates turbulence downstream which in turn is related to dune development, especially the size and shape. Understanding of the geometry of dunes as well as the process in their development is useful for the analysis of bed roughness (Wilbers, 2004). Apart from effects on flow resistance, dunes can introduce channel depth limitations effecting flow conveyance and naivgation. All of these effects are significant in several aspects, such as the design of engineering structures, dredging strategies and storm tide prediction. Moreover, the changes in bedform morphology and the internal structures are useful in the process of interpreting ancient sedimentary assemblages which are believed to be of tidal origin (Carling *et al.*, 2006).

Several studies have described and observed the physical characteristics and development of dunes. For example, the classic contributions of Middleton (1991), Nio and Yang (1991) and Allen *et al.* (1994). Furthermore, several subaqueous dunes, both in fluvial and marine

environments, have been studied for many years, such as Kohsiek and Terwindt (1981), Van den Berg (1982), Berne *et al.* (1993), Gabel (1993), Allen *et al.* (1994), Larcombe and Jago (1996), Neumeier (1998), Kostaschuk and Best (2005), Choi and Jo (2015). Although, there are many studies describing the processes of subaqueous sand dunes, those formed in gravel-bed streams, coarse-gravel dunes as well as cobble dunes, are not well researched. A few studies have explained the processes of gravel dunes, such as Dyer (1970, 1971), Langhorne *et al.* (1986), Dinehart (1992a, 1992b), Carling (1996), Carling *et al.* (2006), Williams *et al.* (2006). However, there are no studies focused on intertidal dunes developed in coarse gravels. Therefore, this study will seek to develop a detailed understanding of the hydrodynamics, dunes dynamics, and sedimentary structure of coarse pebble and cobble dunes.

1.1 Aim and objectives

The main goal of this research is to understand the behaviour of subaqueous dunes developed in coarse gravel materials which have been found in the intertidal zone of the River Severn, United Kingdom (Figure 1.1) (see more detail of the study site in Chapter 2). The specific objectives of the study are:

1. To observe cobble dune movements by comparing the data of dune positions and shape measured in the field site.
2. To collect quantitative flow data and investigate flow hydrodynamics which will provide bulk flow parameters.
3. To examine the interaction between flow hydrodynamics, sediment transport and morphology of cobble dunes to gain an understanding of how flow interacts with the bedforms.
4. To study both the external and internal structure of the dunes developed in coarse sediments.

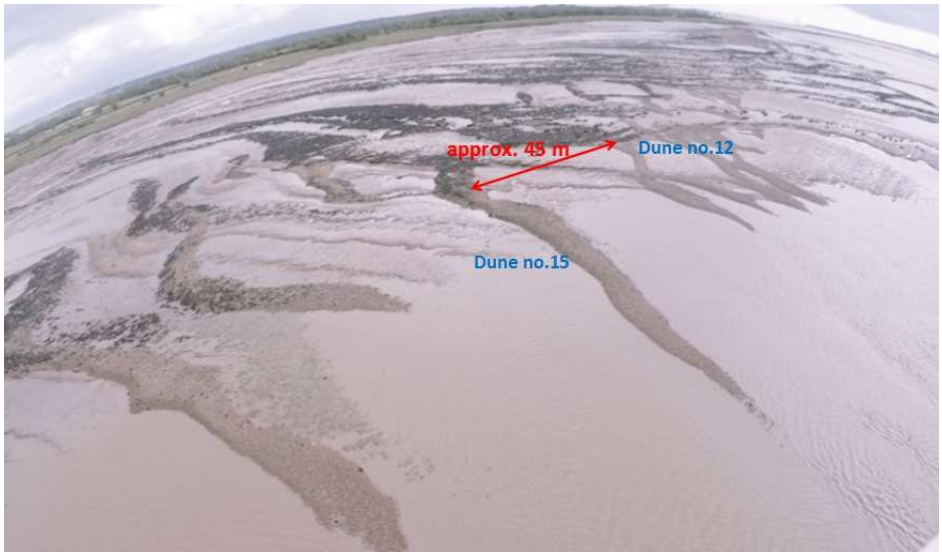

Figure 1.1 An oblique aerial image, taken on 19th May 2015, shows an area of the cobble dunefield found in the River Severn Estuary. Due to the strong wind on the day of survey, the images could not be made systematically and unable to specify the exact scale. However, the distance between the landward ends of dune no. 12 and 15 is about 45 m (red arrow).

Chapter 2: Literature review

This section aims to provide a detailed overview of the literature regarding bedform processes to describe the background and existing knowledge which will help to outline the framework of this study. The review is structured into six main parts. The first section describes theory and, secondly, principle related to general information of bedform development, followed by the details of flow mechanics that have impacts on sediment transportation and bedform process. The later section, details the existing literature concerning fluvial gravel bedforms, especially dunes and, finally, the dunes in bi-directional flows as a focus for the required area of study which helps in defining the aims of this research.

2.1 Bedform formation

A bedform, defined as "a single geometrical element such as a ripple or a dune" (Bridge, 2003), is developed by fluid processes acting on the surface in natural streams such that the sediment rarely exists as flat beds. Fluid controlled bedforms are developed within the interactions of the process elements; form, flow, and sediment transport (Leeder, 1982). Each element has impacts on the others. Stream flow strength and patterns are important factors impacting on sediment transportation as well as bedforms, which form resistance and also influence the flow pattern on a variety of scales. Bedforms lead to adjustment of flow across themselves. Thus flow conditions are different in each location and result in various types of bedforms. The relationship between the flow and the bed affects sediment transportation. The reflexive variations of these factors, at both temporal and spatial scales, result in different local characteristics of the bed forms. The changes in bedforms are the result of the adjustment of the stream (Knighton, 1998).

There are five main bed states occurring in unidirectional flows by relating their geometry with flows and sediment transport. They consist of ripples, Lower Stage Plane Bed (LSPB; including bedload sheets), dunes, Upper Stage Plane Bed (USPB; including low-relief bed waves), and antidunes including shoot and pool (Bridge, 2003). These bed states exist under different conditions and the changing conditions result in transition of bed configurations (Allen, 1984). Breakspear (2008) summarised the sequences of bedform transition with regard to the increasing Froude number (Fr), a ratio of inertial to gravitational forces, as having an impact on flows and sediment transport which will be described later in section 2.3, and sediment size (Table 2.1). Moreover, an illustration of bedform sequences with different grain size and flow

intensity is shown in Figure 2.1. For sand, starting from LSPBs, the increasing Fr would modify the bed to be ripples, dunes, USPBs, Upstream Migrating Antidunes (UMAs), and chute and pool as the final stage. Whilst fine to medium gravels would start from no movement state and transformed into LSPBs, dunes, Downstream Migrating Antidunes (DMAs), Upstream Migrating Antidunes (UMAs), USPBs and chute and pool as flow strength and Fr increase. Lastly, coarser gravels which are too coarse to form ripples have a smaller range of bedform sequence than finer grains. The bed state could change from no movement to LSPBs, UMAs, and USPBs and chute and pool. However, this is a general classification of bed configuration. In fact, the sequence of bedforms is complicated and generalised but primarily results from the relationship between flow velocity, water depth, and sediment size. In some cases, one type of bedforms might be skipped and replaced by another sequence, such as USPBs existing without any prior presence antidunes (Southard, 1971; Ashley, 1990; Carling, 1999; Breakspear, 2008).

Table 2.1 Summary of bed configuration sequences of different-size sediment

Sediment size	**No Move-ment**	**LSPBs**	**Ripples**	**Dunes**	**DMAs**	**UMAs**	**USPBs**	**Chute and Pool**
Sands		✓	✓	✓		✓	✓	✓
Fine to Medium gravels	✓	✓		✓	✓	✓	✓	✓
Coarse gravels (too coarse to form dunes	✓	✓				✓	✓	✓

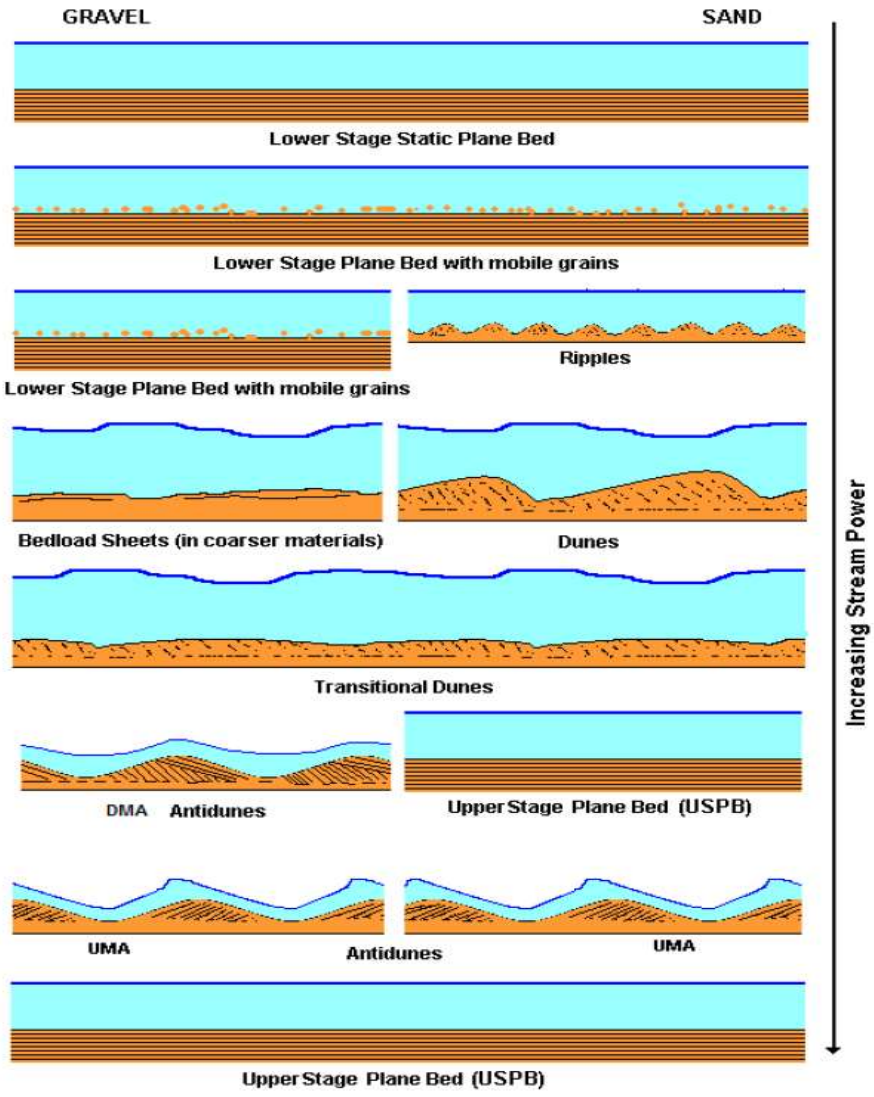

Figure 2.1 Sequence of bedform configuration. Flow from left to right (Breakspear, 2008).

2.2 Bedform classification

Many bed form classifications have been proposed using different criteria. Jackson (1975), for example, divided bedforms into three groups; microforms (i.e. ripples), mesoforms (i.e. bedload sheets, dunes, antidunes), and macroforms (i.e. bars). While Knighton (1998) has summarised into large-scale and small-scale forms of which bars are the bedform included in the large-scale type. For the small-scale bedform, the forms found include ripples, dunes, plane bed and antidunes.

Although the definitions of bedform types were mostly developed for sandy environments, Carling (1999) applied them to gravel bedforms. Many small-scale types can be found commonly in sand-bed streams. The small-scale bedforms in gravel bed streams have just been studied (i.e. Langhorne *et al*., 1986; Dinehart, 1992a, 1992b; Carling, 1999; Carling *et al*., 2006; Radecki-Pawlik *et al*., 2006; Williams *et al.*, 2006). It is stated that these coarse-grained bedforms exist in two main patterns; long axes parallel to the flow and the long axes transverse to the flow (Robert, 1990).

In addition, considering factors about bed form shape, flow, resistance to flow as well as sediment transportation processes, the forms can be classified into two types; lower-flow regime and upper-flow regime. In the lower stage, formations of plane bed, ripples and dunes occur, whilst plane bed, antidunes and a transitional zone between these two exist in the upper-flow stage (Knighton, 1998). Different types of bedforms are developed under different relationship of flow conditions and grain size. The bedform phase diagram (Figure 2.2) shows distinct fields of bedform types, for grain size upto 1.4 mm, which are commonly used.

In this section, the main purpose is to provide information on different types of subaqeous bedform, especially dunes which are the subject of this study. Apart from bedform types, the Lower and Upper Stage Plane Bed (LSPB and USPB) are also described as they are the important transition stages for dune formation. However, since this study aims to monitor the dynamics of coarse-gravel dunes, the review will focus in detail on dunes rather than other types of bedforms.

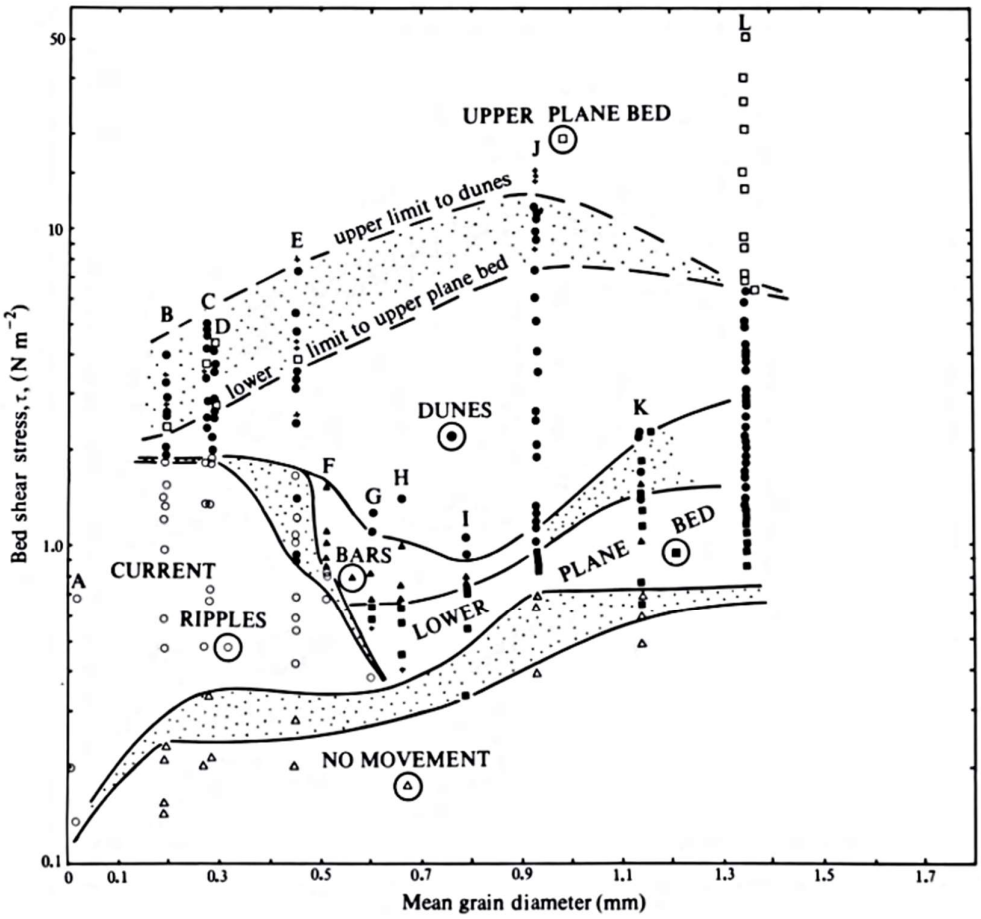

Figure 2.2 Bedform phase diagram (Leeder, 1982)which relates bedforms to mean grain size and the shear stress at the bed.

2.2.1 Lower stage plane beds (LSPBs)

The lower stage plane bed or lower plane bed (LSPB) refers to the flat configuration the bed of a river that is produced by low rates of sediment transport (Neuendorf *et al.*, 2005). According to the bedform phase diagram of Leeder (1982) (Figure 2.2), LSPBs exist in the coarse grains with diameter more than 0.7 mm approximately. This bedform replaces the existence of ripples which develop in very fine sand up to 0.7 mm. Shallow scours and narrow irregular grooves 2-3 grain diameters deep are exhibited over surfaces of this type. Moreover, it is also stated that "Net deposition on a lower-stage plane bed should give rise to crude planar laminations made up from shallow scours, but convincing examples have yet to be described from the sedimentary record" (Leeder, 1982).

2.2.2 Ripples

Ripples are small scale bedforms which can be found in both air and water environments. This undulating bedform is classified as a low flow regime bedform together with LSPB and dunes (Knighton, 1998). They exist transverse to the main flow with asymmetrical profiles, gentle sloping in the upstream with relatively steeper slopes in the downstream direction.

Normally, ripples form in subcritical and hydraulically smooth flow ($\frac{u_* D}{v} < 10$) and grain size must be less than 0.7mm (Yalin, 1972; Allen, 1984; Bridge, 2003). As a result ripples will develop in fine sediment environments of very fine to medium sand. There might be the case that they form occasionally in coarse sands. For mud, it is stated that ripples do not form as it is suspended once entrained from the bed. Only in some cases has it been reported that mud ripples occur if mud becomes sand-sized pellets (Bridge, 2003).

According to several studies, the formation of ripples is due to variation in velocity of near-bed turbulent flows and sediment transport rate (Raudkivi, 1963, 1966, 1997; Southard and Dingler, 1971; Williams and Kemp, 1971; Gyr and Schmid, 1989; Best, 1992, 1993, 1996; Coleman and Melville, 1996; reviews by Allen, 1984 and Bridge, 2003). Ripples start forming when intense turbulent flow exists, resulting in initial motion of grain. These bed-grains move in patches and become ridges with small spacing size from a few millimetres to centimetres and a few grain diameters high. This action creates depressions parallel to the flow and, here, would be called primary current lineations. Figure 2.3 shows the process of ripples formation in the early stages within the viscous sublayer. Turbulent fluid motion leads to erosion and deposition of sediment, piling it up to be a bed defect, or embryonic ripple, which is several grains high. Once the bed defect growth reaches enough height, flow separates in the lee side (downstream), turbulence increases towards the downstream, increasing further erosion downstream and other reattaching ridges could be formed. The process continues further downstream and the bed ridges continue growing until the whole bed has ripples with suitable mean size and shape. The degree of defect disruption in the viscous sublayer could imply the existence and geometry of ripples. For example, a small disruption is related to low intensities in reattaching separated flow, as well as variations of bed shear stress and sediment transport rate (Bridge, 2003).

Similar to most bed waves, ripples grow by amalgamation with smaller forms. Size can be identified by the geometry of ripples; height and length (wavelength). It has been reported that they are less than 0.02 – 0.04 m high and less than 0.6 m long (Allen, 1984; Knighton, 1998). One important factor having impacts on mean height and length of ripples is the grain size or grain Reynold number (U_*D/ν) (Yalin, 1972; Allen, 1984; Baas, 1994). Their size is related to and increases by size of grains, while the ratio of height and length depends on bed shear stress or bedload transport rate (Bridge, 2003). Unlike dunes, ripple size does not depend on the flow (water) depth. They form in flow with lower shear stress and shallower depth than dunes (Yalin, 1992; Knighton, 1998).

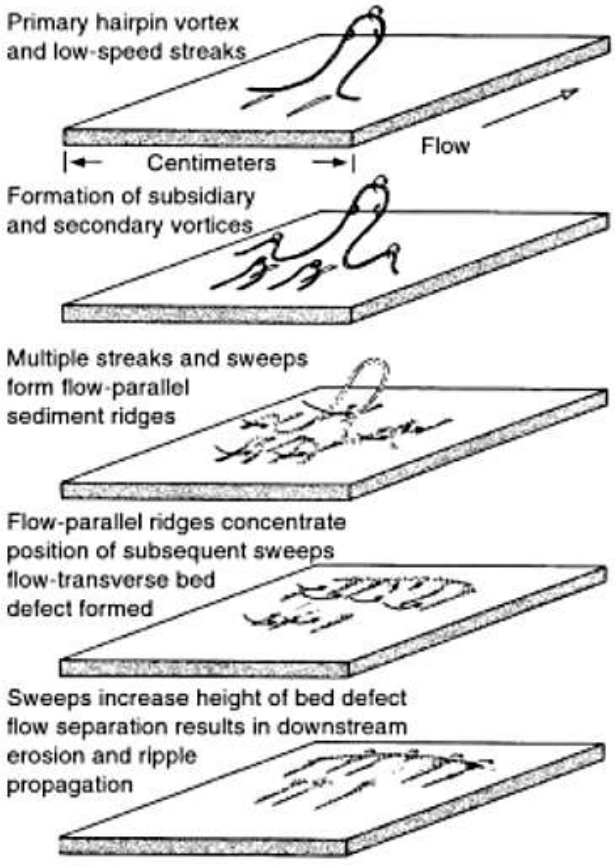

Figure 2.3 Formation of embryonic ripples or bed defect from primary current ridges (Bridge, 2003).

There are three main types of ripple shape presented in studies; straight crest, sinuous to linguoid crest-line, and lunate crest-line. The first type would be found in the low bed shear stress flows whilst the higher bed shear stress flow could develop the sinuous crests or even

modify straight crests to be curved-crest ripples given sufficient time. Finally the lunate type would be found in areas that have limited sediment supply (Bridge, 2003).

2.2.3 Bedload sheets

This bedform type exists in low-relief formed above the threshold of fluid motions. It can be found under transitional or rough flow with low bed shear stress and bed grain size greater than 0.7 mm. Flows across these sheets are stated to be distinct but the possibility of large-scale macroturbulent flow related to dunes over the sandy-gravel sheets is low (Best, 1996; Seminara *et al*., 1996; Carling, 1999).

The formation starts when the flow becomes transitional or rough flow together with the coarse grains affecting the viscous sublayer above the bed. The increasing flow energy leads to erosion and deposition as well as the growth of defects several grains high. Flow separation exists on the lee sides causing turbulence and having an impact on further erosion and deposition to upstream and downstream of the reattachment zone respectively. This process progresses downstream and forms the low-relief bedform which has been called bedload sheets or diffuse gravel sheets in previous studies (Bridge, 2003).

The scale of bedload sheets, both length and height, may be larger than ripples. Their length is proportional to flow depth and will decrease when bed shear stress increases. The ratio between wavelength and depth (L/h) ranges from 4 to 12. For the height, bedload sheets could grow up to 1-2 coarse grain size in height. A number of studies claimed that they could be formed up to 0.10 m high which could further develop into incipient dunes (Whiting, *et al.*, 1988; Kuhnle and Southard, 1990; Carling, 1999). Geometry of these sheets shares some dune- like characteristics which is the reason why they are sometimes regarded as incipient dunes.

Though bedload sheets are similar to dunes, bedload sheets are not as dependent on grain size sorting (Bennett and Bridge, 1995; Bridge, 2003) and Whiting *et al.* (1988) pointed out that well sorted gravels were poorly documented. Sheets are developed by a range of coarse sand and granules ($D_{50} \sim 2 - 5$ mm)(Carling, 1999). However, grain sorting by selective entrainment is important factor for this formation, especially in sandy gravels and there is a report that there are no sheets being developed with 100 per cent of gravels. This distinguishes bedload sheets from dunes (Iseya and Ikeda, 1987; Bennett and Bridge, 1995).

2.2.4 Dunes

This undulated flow-transverse bedform was recognised as the most common of bedforms which is formed by flowing water over a sand or gravel bed (Allen, 1984; Bridge, 2003). In previous decades, the term 'subaqeous dune' was not well-defined and various names were applied somewhat arbitrarily, especially in the 1960s. This resulted in confusing duplicated, and overlapping names existing for the large-scale, flow-transverse bedforms, for example, megaripples, large ripples, sand waves, and dunes. Consequently, criteria were developed to define dunes by Ashley (1990) and this study will follow these criteria. These criteria were separated by three descriptors ordered regarding to the importance of properties. These include size (height and spacing), shape, superposition, sediment characteristics, flow structure, etc.

Heights of dunes (H) usually exceed 0.1 m while wavelength (L) could be about 0.6 m and grow up to 100 m (Jackson, 1976; Ashley, 1990; Carling, 1999). The size of dunes was grouped by the bedform wavelengths and the mean heights as per Table 2.2 (Ashley, 1990);

Table 2.2 Dune scale criteria suggested by Ashley (1990)

Size	Wavelength (L)	Height (H)
Small	0.6 – 5 m	0.075 – 0.4 m
Medium	5 - 10 m	0.4 – 0.75 m
Large	10 – 100 m	0.75 – 5 m
Very large	> 100 m	>5 m

The scale of dunes, height and length, is often proportional to water depth in shallower flows (Figure 2.4) or to the boundary layer thickness in deeper flows. Smaller dunes, called incipient dunes, could also be found, for which the dimensions overlap with ripples as the bedforms are developing into small dunes that can be the equilibrium form (Carling, 1999). Moreover, there are a number of empirical relationships between water depth and mean height of equilibrium dunes that is in a range of $3 < h/H < 20$ (Bridge, 2003). Yalin (1964) proposed that $h/H = 6$ while (Allen, 1970) proposed that $h = 11.6H^{0.84}$ (where 0.1 m < h < 100 m). However, there is an argument that these relationship equations have low correlation coefficients as they do not represent the low-height dunes, nor non-equilibrium bedforms. Bridge (2003) also provided a major reason for the scatter that exists in the relationship between mean dune

height and depth in equilibrium flows. Dune height, including the mean, can vary from very small at the lower end of the dune existence field (transition from ripples or LSPB (as noted by Carling *et al.*, 2005) and again dune height diminishes at the transition to USPB and only reaches the maximum in the mid dune field. Another reason is the uncertainty in identifying when dunes are in equilibrium and indeed when equilibrium flow conditions pertain in natural time-varying flows. Lastly flow curvature can have a significant impact on dune scale. Apart from Yalin's (1964) dune scaling related to flow depth, there were a number of more complex dune scaling relations to other variables being proposed, such as grain size, transport stage, Froude number, current velocity and the dimensionless shear stress(Allen, 1968, 1978; Flemming, 1978; Rubin and McCulloch, 1980; van Rijn, 1984; Ashley, 1990; Karim, 1995; Carling, 1999; Bridge, 2003). Recently, Bradley and Venditti (2016) compiled the data of dune dimensions and flow characteristics from previous studies and assess the dune scaling relations. New depth scaling relations were proposed that differ between shallow and deep flows; a scaling break at 2.5 m deep, separates the two scale ranges. It is stated that strongly asymmetric dunes with high lee angles are commonly found in shallow flows (<2.5 m) of which heights are generally larger than $1/6h$, while in the deeper flows (>2.5 m) the dunes are more symmetrical with lower lee angles and their heights are less than $1/6h$. It is also added that dunes in deeper channel have the wider range of observed heights for a given depth (Bradley and Venditti, 2016).

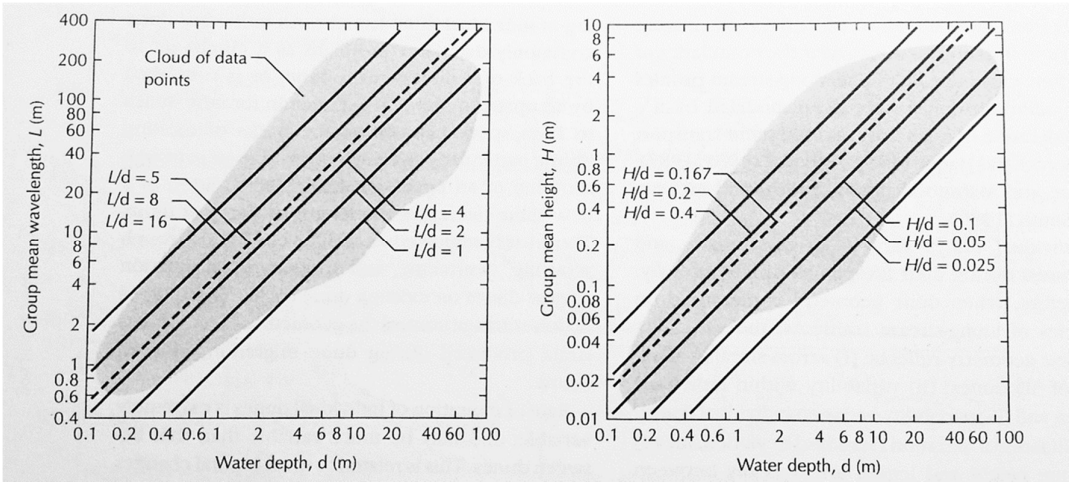

Figure 2.4 Relationship between water depth and wavelength or height of dunes (Bridge, 2003).

Steepness of dunes could be determined by ratio of the height and length (H/L). Figure 2.5 presents the variation of height and length against a range of bed shear stresses. Dune steepness is low at the lower boundary of the dune existence field and steepness typically ranges between 0.05 – 0.06 across a large region of developing dunes (Bridge, 2003). For sand dunes, it was stated that subaqueous dunes are close to equilibrium state at steepness ratio (H/L) equal to 0.08 (Ashley, 1990). Flemming (1988) and Ashley (1990) gave the relationship between maximum height (H) for minimum dune spacing (L) of equilibrium dunes as;

$$H = 0.0677L^{0.8098} \tag{2.1}$$

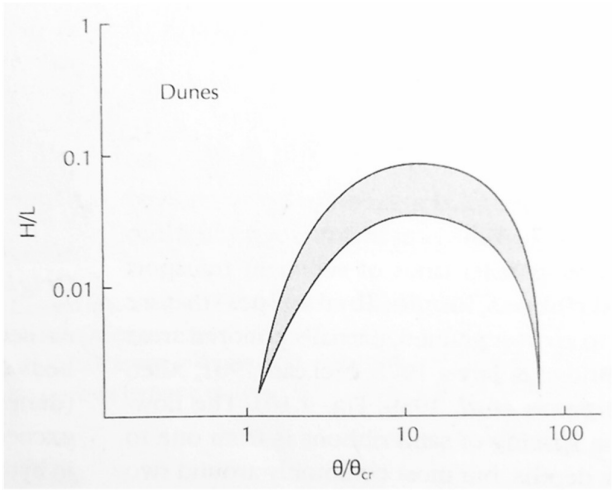

Figure 2.5 Variation in height and length of equilibrium dunes with dimensionless shear stress (Bridge, 2003).

Dunes exists in a range of shapes which is divided into two major types; two- and three-dimensional dunes. Two-dimensional (2D) dunes occur as gently sinuous or straight long crest lines transverse to the main flow while three-dimensional (3D) dune shape is short and sinuous or recurved lines or could have lunate or catenary crests (Figure 2.6) (Allen, 1984; Best, 1996; Breakspear, 2008). Geometry of both types is different. The 2D dunes could be described by one transect whilst 3D dunes, formed by scour pits and curved lee faces, are complex and need to be defined by three dimensions (Ashley, 1990). Venditti *et al.* (2005) suggests that 2D dunes could form and progress to be 3D dunes by the amplification of defects on the crest lines.

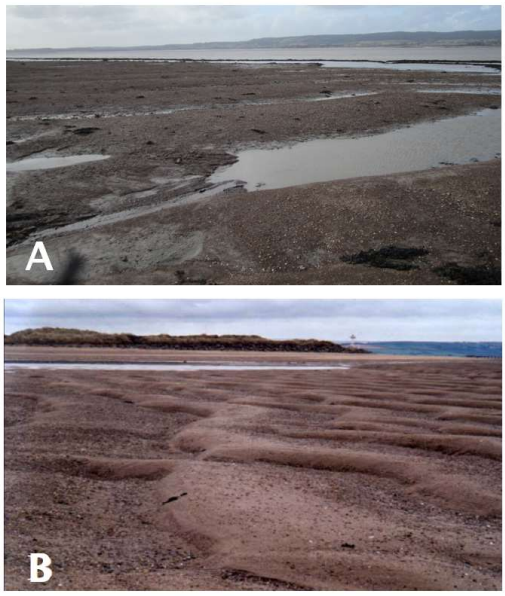

Figure 2.6 Types of dunes; (A) straight/sinuous crested gravel dunes at Hills Flats, Gloucestershire. Ebb flow was from bottom right to top left. (B) lunate dunes developed in sand-fine granules at Airy Point, Bideford, Devon. Flow is from the right (Breakspear, 2008).

Dunes could be developed in a range of sediment sizes, from 0.15 mm up to 60 mm both in field and flume conditions (Carling, 1999). Previously, there was a perception that dunes do not develop in gravels (Allen, 1993). But following Ashley's (1990) criteria of dune, height (H > 0.1 m) and length (L > 0.6 m), many studies have identified an existence of gravel dunes (Galay, 1967; Dinehart, 1989, 1992; Fahnestock and Bradley, 1973). However, there is no evidence that dune scale is related with grain size (Ashley, 1990; Best, 1996).

Normally, dunes, in cross section view, have asymmetric form with downstream migration which is the most common sedimentary structure of river deposit (Bridge, 2003; Breakspear, 2008). The upstream, or stoss side, is long and has a shallow slope while the lee side on the downstream side has a steeper slope, often being set by the angle of repose.

Generally, dunes are found in hydraulically transitional and rough flows, subcritical flows or low-flow regime with Shields number (θ) higher than 0.1, which could be lower for 2D dunes and higher for 3D dunes (Bridge, 2003; Breakspear, 2008). This should be related with flow velocity which flows forming 2D dunes have lower speed than 3D at a given grain size (Ashley, 1990).

Different states of flows have impact on shape of dunes. Bridge (2003) described the formation of straight and sinuous dune crests with straight crested dunes formed near the transitional stage from ripples to dunes. Once sediment transport rate and bed shear stress exceed this transitional stage, the wavelength of dunes decreases proportional to their height and flow depth ($L \sim 6h$) and the shapes start changing from straight to sinuous or linguoid. However, similar to ripples, Allen (1984) stated that lunate crested dune formation is related to the limitation of sediment supply. Apart from these, there are other flow conditions which are important for dune development and will be reviewed for more details in later section.

Ripples and dunes are both found in the lower-flow regime. They have some similar and some different properties. For similarities, it is stated that their migration direction moves downstream through erosion in the upstream slope and deposition on downstream face. Their profiles show a triangular shape which has a gentle slope in the upstream and a steeper one in the downstream direction. Their cross-bedding formations help in preserving and interpreting palaeohydraulic processes. Once the flow intensity and bed-load transport rates increase to the upper-flow regime, the last two bed forms are washed out, the upper stage plane bed exists and then antidunes can develop (Knighton, 1998).

2.2.5 Upper stage plane beds (USPBs)

USPBs are developed by higher bed shear stress and sediment transportation rate than ripples and dunes (Bridge, 2003). The flows are supercritical with Fr number 1.3 > Fr > 0.8 (Bridge and Best, 1997; Breakspear, 2008).

The geometry of USPBs is slightly similar to the LSPBs as they have low-relief formation and have larger areas of flat bed than ripples or dunes. This results from the increasing flow energy that decreases the length and height of bed waves, becoming flatter but not completely flat. The cross section shows that any transitional bedforms have asymmetric stream-wise shape and ratio between length and flow depth (L/h) is in the same range with the curved crested or incipient dunes of which height are not able to become higher (Bridge, 2003).

The process of formation of USPB can involve an increase in the suspended sediment transportation rate of which the concentration is high above the bed. There are two main arguments presented about the process of near bed suspended sediment and USPB. The first one states that high concentration of near bed suspended sediment dampens turbulence intensity over troughs resulting in less erosion at the trough (reattachment zone) and effecting less deposition on crests (Allen and Leeder, 1980; Bridge and Best, 1988). On the contrary,

several studies suggested that the high concentration will increase turbulence intensity (Bennett *et al.*, 1998). Moreover, it was proposed that "along-stream change in suspended-sediment transport rate lags behind along-stream change in bed shear stress and turbulence intensity" (Bridge, 2003). This results in erosion on the crests and deposition on troughs leading to decreasing height of bed waves. Due to the fact that this bedform type is dealing with high concentrations of suspended sediment, it could be explained that the USPBs is common in finer sand. Moreover, predicting the stability of USPBs could be made by using dimensionless bed shear stress as it determines the concentration of suspended sediment in flows (Bagnold, 1966; Allen and Leeder, 1980; Bridge, 2003).

2.2.6 Antidunes

Antidunes are another formation existing under stream flow which is less common than the previously mentioned bed forms. They could be found in broad, shallow channels with steep slopes. Several studies of this form have observed its behaviour, for example Cornish (1899), Owens (1908), Gilbert (1914), Kennedy (1960), Breakspear (2008). Antidunes have different phases of bedforms related with the increasing Froude number. These phases include Downstream Migrating Antidunes (DMAs), stationary antidunes, and Upstream Migrating Antidunes (UMAs) (Breakspear, 2008).

The wavelength and height of antidunes is varied even under the controlled condition of a flume study (Knighton, 1998). The amplitude of antidunes tends to be lower than equilibrium dunes because of the higher flow velocity. The length (L) of antidunes is related to water depth (h) as $L \approx 2\pi h$ (Kennedy, 1963) and can be also related with Fr of which relationship will be $L = 2\pi hFr$ (Allen, 1969). According to previous studies, lengths of antidunes are in the range of 0.1 to 30.5m and height varies between 0.01 – 1.5 m (Kennedy, 1960; Simons and Richardson, 1971).

Flow conditions across this bedform are in the supercritical stage or upper-stage regime and sediment transport rate over this kind of bed form is high. However, the Froude number of flows required to allow antidunes to replace dunes is varied but there is some data from sand-size sediment study which indicates that this value should exceed 0.84 for the transition to occur (Kennedy, 1960; Southard and Boguchwal, 1990). In turn antidunes may be replaced by upper stage plane bed if the flow has a higher Froude number (Carling, 1999) which is not over 1.7 (Gradowczyk, 1968). Due to the conditions of high energy (rapid) flow, the structure of antidunes are not constructed and preserved as well as ripples and dunes (Knighton, 1998).

Apart from the conditions mentioned above, the important properties of upstream migrating antidunes which make it more different from ripples and dunes are that it migrates short distance upstream (or remain stationary) through erosion on the downstream face (lee side) and deposition on the upstream face (stoss side) (Knighton, 1998; Carling, 1999). Gravel antidunes have been noticed that tend to be symmetrical, sinusoidal in profile, and of low amplitude (Carling, 1999). Additionally, antidunes are reported that are not well preserved in either sand or gravel beds and could be destroyed when water stages are falling (Bucher, 1919; Middleton, 1965; Foley, 1977; Carling, 1999).

2.2.7 Bars

Bars are classified as a macroscale flow transverse form (A.S.C.E. Task Force, 1966; Bridge, 1985; Bridge, 1993). The lengths are related to the channel width of the stream while the shape and position are varied and are generally used to classify them. Five types of bars are stated; point bars, alternate bars, channel junction bars, transverse bars, and mid-channel bars. They compose a variety of grain sizes. Many of them could be exposed at certain stages of flow and have important links with channel planform (Knighton, 1998). Seminara and Tubino (1989) classified bars into two distinct types; non-mobile “fixed bars” (e.g. alternate bars and point bars) and mobile “free bars” (e.g. braid bars and transverse bars). Identification of free bars could be confused with dunes as the scale of both forms may be limited by depth and width (A.S.C.E. Task Force, 1966; Bridge, 1985; Bridge, 1993).

These are the general concepts of the common bedforms being found and investigated by researchers, both in flume and field studies. This information provides a basic knowledge of a common range of bedforms that can be found in gravel beds. In practice the development processes and characteristics of each form might show some differences from theory and some types might share similar conditions leading to complexity in identifying the actual type of bedform and causing contention among researchers; for example the state of dune: antidune transition as well as the similar conditions of bedload sheet and incipient dunes.

2.3 Flow and sediment interactions with bedform development

Leeder (1982) states that the three process elements which interact in bedform development are form, flow, and sediment transport. Stream flows are the main control on sediment transportation and have an impact on changing of river morphology.

Flows have the ability to carve channel and river beds into different shapes and scales by eroding, transporting (entraining), and depositing sediment leading to a variety of bedforms. Stream flow strength and patterns are important factors having massive impacts on sediment transportation as well as bedforms whose morphology also influence the flow pattern at a variety of scales. Bedforms adjust to flow across their forms. Flow conditions are different in each location and results in various types of bedforms. Several parameters are related with flow hydraulics and mechanics, including velocity (U), water depth (h), channel width (W), slope (S), discharge (Q), viscosity (μ), density of water (ρ), and gravity (g) (Allen, 1984).

Bedforms under stream flow could not exist without the transportation of sediment. Strong flows have enough power to take grains out of the bed, to carry them along the stream, and drop them when current velocity decreases. However, these activities vary according to local conditions as well as responding to the grain size of sediment in each location. The form of sediments affects roughness over the bed. Bed roughness in turn has an impact on the energy of the flow. Richards (1982) explained that form roughness developed by high-energy flows and sediment transport would result in increasing flow resistance and a decrease in energy. The changing roughness, conversely, would control flow velocity.

The proceeding section will present the importance of flow parameters and conditions that relate to dune development as well as the interactions between these parameters that result in different flow properties in terms of flow conditions (steady or unsteady, laminar or turbulent flows, subcritical or supercritical flows). Moreover, the content will also explain sediment transport process which is related with flows, including initial motion of sediment.

2.3.1 Hydraulics and mechanics in water flows

The nature of flowing water in an open channel may be considered in terms of the variations of the flow properties in both the spatial and temporal sense. For spatial variation, flows are classified mainly by looking at pressure distribution, which have impact on streamline pattern. Flow could be classified into different types depending on a number of criteria; velocity within the spatial and temporal scale, Reynolds number and Froude number (Table 2.3). Considering

velocity, flows are classified into; steady/unsteady for velocity which is constant/variable with time and uniform/non-uniform flows for velocity which is constant/variable with position (Knighton, 1998; Bridge, 2003) or could be classified into three groups; uniform, gradually varied, and rapidly varied flows (Richards, 1982). For Reynolds and Froude numbers, the flows are classified into laminar/turbulent and tranquil/rapid respectively, of which the details will be explained later.

Flow in different positions along the stream are varied, but it is stated that the discharge is constant in both spatial and temporal scale (Figure 2.7) (Bridge, 2003). Stream discharge can be determined by the relationship between cross-sectional area and mean velocity which is known as the "continuity equation" (Richards, 1982) as following;

$$Q = a_1 U_1 = a_2 U_2 = \cdots \quad (2.2)$$

Where Q is water discharge

a is cross-section area

U is mean flow velocity.

Table 2.3 States of flow

States of flows	**Criterion**	
Steady flow	Velocity with time	Constant
Unsteady flow		Variable
Uniform flow	Velocity with position	Constant
Non-uniform flow		Variable
Laminar flow	Reynolds number (Re)	Re < 500
Turbulent flow		Re > 2500
Subcritical (tranquil) flow	Froude number (Fr)	Fr < 1
Supercritical (rapid) flow		Fr >1

Stream flows considered in the temporal scale concern the relationship between velocity and time and can be classified into steady and unsteady flows. **Steady flows** are flows whereby their parameters, i.e. velocity, discharge, and depth, do not change in time, while these parameters are not constant in **unsteady flows** (Richards, 1982; Bridge, 2003).

Uniform flows are constant along stream in terms of velocity, cross-sectional area, or flow depth. The bed, water surface, energy, and streamline in this flow are parallel. In contrast,

streamlines of the **non-uniform flow**, usually found in natural rivers, are not parallel due to variation in water depth, velocity, and cross-section area along the river. Patterns of streamlines reflect velocity variations. Speed of flow increases in convergence and drops when streamlines diverge (Figure 2.7B and C) (Richards, 1982; Bridge, 2003). Non-uniform flow can be considered as gradually varied flow and rapidly varied flow (Richards, 1982). The rapidly varied flow experiences more extreme changes than the gradually varied flow. Open channels having this kind of flow have considerable changes such as sudden change in water depth and hydraulic jumps and drop. The free fall over of a weir could be an example of this flow type. Apart from the temporal and spatial classification above, flows could be classified in more detail by considering others variations, such as energy, momentum, inertia, and viscosity. In natural river flow, non-uniform unsteady gradually varied flows are normally found. However, it is also stated that "in large rivers flood passage is often sufficiently slow that steady conditions can be assumed for short periods" (Richards, 1982). In non-uniform flow, the spatial deceleration is considered to be related to deposition, while the spatial acceleration is related to erosion (Bridge, 2003).

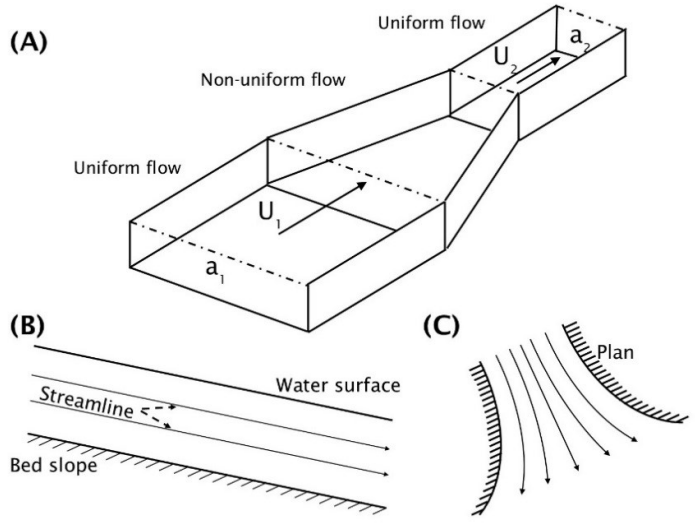

Figure 2.7 Definition of uniform and non-uniform flow (Redrawn from Richards, 1982 and Bridge, 2003).

The state of flow can be determined by two important dimensionless numbers which are the Reynolds number (Re) and the Froude number (Fr).

Laminar flow has smooth, linear streamlines and thin laminae with water sliding past each layer with constant velocity at a given point of flow. Bridge (2003) stated that "the magnitude and direction of vectors do not change within time at time scales of seconds or less". An experiment of Reynolds (1883) clearly showed that dyes injected into this state of flow will move in a straight line. Unlike laminar flow, streamlines of **turbulent flow** are curved due to swirling motions or eddies (Richards, 1982). This state can be found in natural streams. Turbulent flow has "the magnitude and direction of the flow velocity vectors at any point in the flow change with time over time intervals of fractions of a second to seconds" (Bridge, 2003). Inertial forces are predominant in this flow state. Secondary motion would occur in this flow and the injected dye within this flow show distorted movement (Richards, 1982).

To identify laminar and turbulent flow, the important indicator is Reynolds number (Re). It can be defined by the ratio between inertial and viscous forces as follows;

$$Re = \frac{\rho_w UL}{\mu} \qquad (2.3a) \qquad \text{or} \qquad Re = \frac{\rho_w UR}{\mu} = \frac{UR}{v} \qquad (2.3b)$$

where ρ_w is water density (1 g cm^{-3} = 1000 kg m^{-3})

L is characteristic length

μ is dynamic viscosity

R is hydraulic radius/ mean depth (could be replaced by "mean depth" for wide, shallow channels)

v is kinematic viscosity

In laminar flow, Re is normally less than 500 and viscous forces are significant in this kind of flow. In the turbulent flow Re could be higher than 2500 (Richards, 1982), while flows with Re between 500 and 2500 ($500 < Re < 2500$) is in the transitional state (Knighton, 1998).

Apart from the criteria and flow states above, the other important criteria is Froude number (Fr). Froude number is the dimensionless number based on the relationship between "the inertia of a unit mass of streamflow to the celerity of a shallow gravity wave" (Richards, 1982) as following;

$$Fr = \frac{U}{\sqrt{(gh)}} \qquad (2.4)$$

where g is gravitational force

h is flow depth

The value of the Froude number is used to distinguish critical flow state. Flow with Fr lower than one ($Fr < 1$) is subcritical (tranquil) while Fr higher than one ($Fr > 1$) is considered as supercritical flow (rapid) and flow with Fr equal to one (Fr = 1) is critical flow (Richards, 1982; Knighton, 1998; Bridge, 2003). Surface waves in supercritical flows are unstable and tend to break which has an impact on energy loss. This dimensionless number is one important indicator of the flows which lead to a transition between dunes and antidunes (Kennedy, 1963).

States of flow, classified by Reynolds and Froude numbers are varied regarding to water depth and flow velocity as shown in Figure 2.8 (Richards, 1982). Laminar flow exists in low values of velocity and water depth which are too small for most channel flows while turbulent flow exist in wider range of these two dimensionless numbers. Leopold *et al.* (1960) suggested that in natural, mobile-bed channels, the average Froude number is rarely greater than $Fr \approx 0.5$. However, these two numbers do not depend on the scale of rivers, so flow conditions in flume works are recommended to "aim to recreate the turbulence intensity and the Froude number of natural streams" (Richards, 1982).

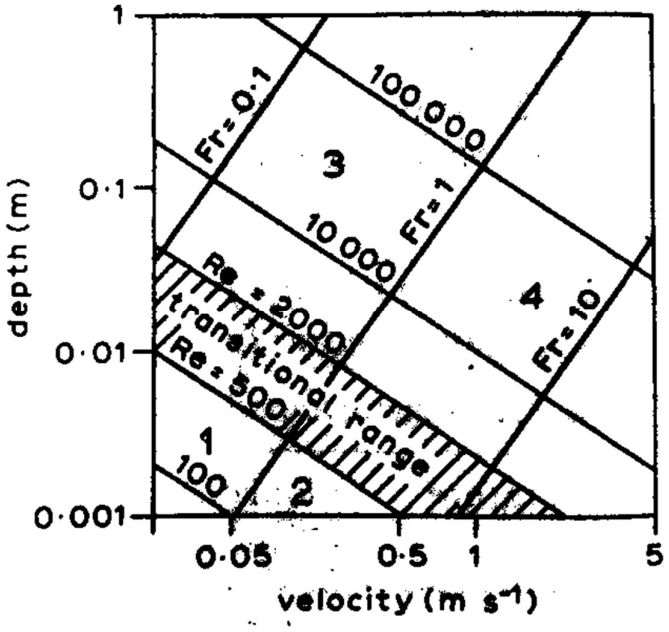

Figure 2.8 Flow states at different depth and velocity defined by Reynolds and Froude numbers (Richards, 1982).

Velocity and Flow resistance

Velocity is a vector quantity which is important in understanding flow regime. It has an important role in processes of sediment transportation and bedform development. It is sensitive and variable as it is related with many factors in both space and time, having an important role in morphological process and sediment transport. The velocity can be considered in four dimensions; A) distance from the bed, B) across the stream, C) downstream, which are illustrated in Figure 2.9, and D) time (Knighton, 1998).

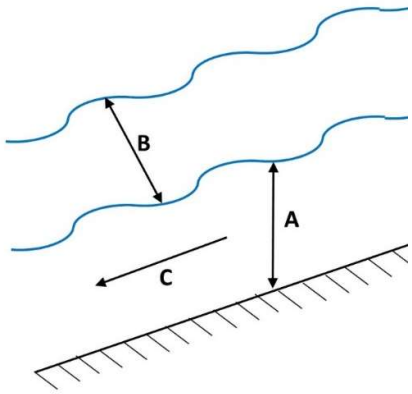

Figure 2.9 Dimensions of velocity in a stream.

(A) Distance from the bed to the stream surface: The velocity varies at different heights above the bed. The velocity close to the bed is slow and might equal zero, increasing with height above bed through the free stream at the edge of boundary layer. This will be later explained in the section of boundary layer theory and the velocity distribution.

(B) Across the stream: Velocity is also different with regards to the distance from the bank in a cross-section profile of a stream. At the same depth across the stream, velocity increases towards the centre of the channel so that flow is faster here than the velocity close to the river bank because the friction retards the flow close the banks. The important factors of velocity in this dimension are the ratio of channel width and depth, bed shape and alignment of the channel.

(C) Downstream: The rate of change in velocity may vary along the stream. This is related with the adjustment of velocity to accommodate the downstream increase in discharge. The rate of change (m) of velocity, calculated by $u = kQ^m$ and it is recommended that 0.1 of m value is an appropriate average.

(D) Time: Velocity measured at one point could vary significantly through time. In a small timescale of just a few seconds, the velocity may deviate by 60 – 70 per cent or more. However, Knighton (1998) stated that "the mean velocity at a section responds to fluctuations in discharge" at larger timescale; days, weeks, months. It is added that "the increase in depth with discharge tends to drown out roughness elements in the bed and thereby produce and increase in velocity, but the effect is not uniform and the velocity exponent *m* can vary considerably from section to section" (Knighton, 1998).

Variable quantities in the dimensions outlined above results in different velocities. The relationship of velocity distribution, cross-sectional shape, and erosive tendency would result in a velocity gradient for each position; for example the velocity gradient in wide-shallow channels is steepest at the bed resulting in greatest boundary shear stress against the bed, while a narrow-deep channel has a velocity gradient which is steepest against the banks.

Apart from considering these four dimensions, flow resistance is another factor related with velocity. It is among the important components on the interaction between flow and the boundary in channels. Many studies developed equations for this factor. However, the equation of Darcy-Weisbach is recommended due to the dimensional correctness and sounder theoretical basis (Knighton, 1998), which is written as:

$$ff = \frac{8gRs}{U^2} \qquad (2.5a) \qquad \text{or} \qquad ff = 8\left(\frac{u_*}{U}\right)^2 \qquad (2.5b)$$

where ff is the resistance coefficients/friction factor

s is slope of the energy gradient

(Knighton, 1998; Bridge, 2003). Normally, flow resistance consists of three components; (A) boundary resistance; the resistance resulting from frictional effect of the bed material itself and bedform development, (B) channel resistance; bank irregularities and changes in channel alignments have influence on this component, and (C) free surface resistance; this is caused by distortion of the water surface by waves and hydraulic jumps. Among these elements, boundary resistance is mainly concerned and is considered in subdivision as form and grain roughness (Knighton, 1998).

Bedforms developed in a sand-bed stream also provide form resistance which may be more important than grain roughness. Form could be varied in shape which is depended on flow conditions and sediment movements. Once the bed shape changes, the form roughness is altered providing different resistance. For example, flow resistance increases when the

discharge and sediment load increase until ripples develop into dunes. Moreover, the size of bedforms was considered to have a significant role in increasing total flow resisitance over coarse beds as the bedform sizes increase (Knighton, 1998).

Although form roughness provides a considerable contribution to boundary resistance, especially in sand bed stream, grain roughness is the other component in boundary resistance, which is also important in coarser grained beds. It can dominate, especially in coarse grain beds, i.e. gravels (2 - 64 mm) or cobbles (64 - 256 mm). Grain roughness is defined as "a function of relative roughness (h/D or R/D)" (Knighton, 1998) and can be written as

$$\frac{1}{\sqrt{ff}} = c \log\left(a \frac{R}{D_x}\right) \tag{2.6}$$

where c and a are constant

D_x is measure of the size of roughness element, which is equal to grain size in uniform material while D_{84} is commonly used in non-uniform material. However, it was stated that this equation is less applicable when $R/D_{84} < 4$ and $W/h < 15$ (Knighton, 1998).

According to this equation, Knighton (1998) summarised that "as depth increases with discharge at a cross-section, the effect of grain roughness is drowned out and flow resistance decreases, although possibly at a declining rate with higher discharge. Consequently, velocity may also tend to change more slowly at higher flows, producing non-linearities in hydraulic geometry."

There are other components having an impact on resistance. The bank irregularities and channel curvature would increase additional resistance and be a reason for energy loss. An increase in suspended sediment can lead to increasing viscosity and a damping down of turbulence which could reduce resistance by 5 - 28 per cent (Vanoni and Nomicos, 1959). However, the effect of suspended sediment is considered to exist at times of very high concentration rather than natural conditions. Lastly, height, density and flexibility of vegetation also have influence on resistance (Knighton, 1998).

Flow resistance is an important element in flow behaviour as it is related with bed material properties, sediment transport, and energy consumption of flows. Resistance can be calculated

using the equations have been proposed, including the Darcy-Weisbach equation mentioned above, by visual comparison with representative reaches, or by direct measurement.

Boundary layer theory and the velocity distribution

In river channels, the resistance of the bed as well as the banks has the impact of slowing water flow, especially the flow close to the solid boundary where current speed of a thin layer of water adjacent is slowed to a stop, while the shear resistance between each adjacent layer and retardation decrease as the flow is far from the boundary. In this layer, there is a velocity gradient, the rate of change of velocity with height above the bed ($\frac{dU}{dy}$) (Knighton, 1998), which results in different flow speed in different height above the bed. Velocity is highest at water surface and decreases where the flow is close to the bed, which is known as the velocity distribution (Figure 2.10). This velocity gradient exists in the boundary layer, which is affected by the boundary drag. This layer extends to the water surface in rivers. Momentum per unit volume of the upper layers is greater than the lower layers and it is transferred from higher to the lower momentum. It is also stated that the retardation in faster layers indicates the shear resistance which is considered to be related with the degree of interference and contrast in momentum between the two layers (Richards, 1982).

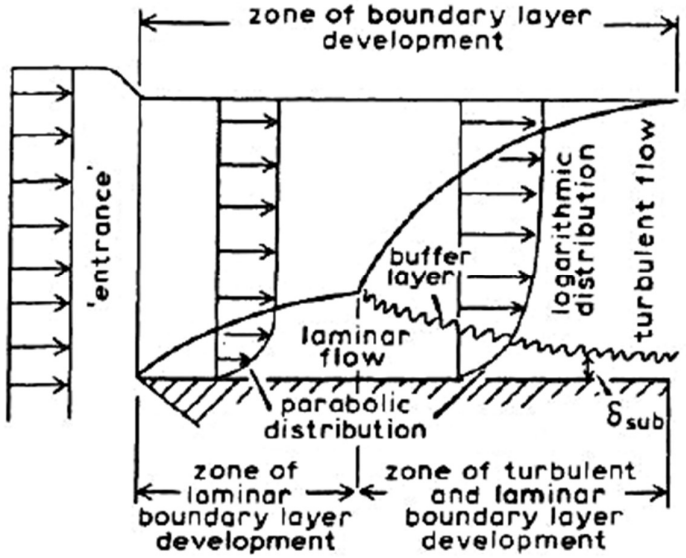

Figure 2.10 Boundary layer development in a stream over solid surface; δ_{sub} is the laminar sublayer (Richards, 1982).

Characteristics of laminar and turbulent flows are the key in considering velocity profiles, which present variation in velocity with height above the bed. The profiles are initially considered in two dimensions for wide flow with no side-wall effects (Richards, 1982). The analysis of velocity profiles in turbulent flow is more complicated than profiles in laminar flow.

In laminar flow, flow layers move by gliding over one another layer which has moving molecules exist between layers. This movement results in changing momentum by increasing in the slower layers at the bottom and decreasing in the upper layers where there is faster velocity. The rate of changing momentum is measured as 'kinematic viscosity' (ν). The shear stress at any point in the vertical within laminar flow can be written as;

$$\tau = \rho_w g(h - y)s \tag{2.7}$$

or;

$$\tau = \rho_w \nu \left(\frac{dU}{dy}\right) \tag{2.8}$$

where τ is shear stress

y is height above the bed

$\frac{dU}{dy}$ is the velocity gradient or rate of change of velocity with depth

(Richards, 1982; Bridge, 2003). As the equations 2.7 and 2.8 are equal, the both are combined and integrated which results in an equation of velocity profile with parabolic function of distance from the solid boundary (Figure 2.11) as

$$U = \left(\frac{gs}{2\nu}\right)(2yh - y^2) + C_1 \tag{2.9}$$

where C_1 is a constant of integration (Richards, 1982).

Unlike laminar flow, turbulent flow moves in irregular paths and mixing. This kind of flow does not have momentum transfer at the molecular scale, but it happens between layers. This is due to eddies which momentum can transfer at a greater distance than the molecular scale. The high momentum close to the water surface can transfer deep down close to the bed, so the near bed velocity can increase immediately. On the other hand, the low momentum going upward would delay increases in velocity near water surface. "Eddies of varying size are generated and superimposed on the main downstream flow in both the vertical and the horizontal planes, constituting elements of a coherent structure of turbulence which is

beginning to emerge. They give rise to unsteady flow events acting both towards ('sweeps') and away from ('ejections') the bed, which have important implications for the entrainment and suspension of non-cohesive sediment" (Knighton, 1998). This results in a steep velocity gradient near the bed. The shear stress of turbulent flow at any point can be defined as

$$\tau = \rho_w(\epsilon + \nu)\left(\frac{dU}{dy}\right) \quad (2.10a) \quad \text{or} \quad \tau = \epsilon\left(\frac{dU}{dy}\right) \quad (2.10b)$$

where ϵ is eddy viscosity which is related with eddy penetration or mixing length (l) and can be determined by Karman's universal constant ($\kappa = 0.4$) as followings;

$$\epsilon = l^2 \frac{dU}{dy} \quad (2.11)$$

$$l = \kappa y \quad (2.12)$$

This equation is similar to equation 2.8, except the kinematic viscosity (ν) which is neglected and replaced by eddy viscosity (ϵ) as it is a more significant factor in turbulent flow which results in larger shear stresses at the same velocity gradient and a steeper near bed velocity gradient (Richards, 1982; Knighton, 1998). However, an analysis of velocity profile of turbulent flow, which often occurs in nature, is complicated as the eddy viscosity varies with distance from the bed and is not constant. With the mathematical analysis considering factors related with eddy, laminar sublayers, Richards (1982) and Knighton (1998) provided the shear stress close to the boundary (τ_0) as;

$$\tau_0 = \kappa^2 y^2 \rho_w \left(\frac{dU}{dy}\right)^2 \quad (2.13a) \quad \text{or} \quad \tau_0 = \gamma R s \quad (2.13b)$$

where $\boldsymbol{\gamma}$ is the specific weight of water

For the velocity profile of turbulent flow is written as;

$$U = \frac{u_*}{\kappa} \ln \frac{y}{y_0} \quad (2.14)$$

where u_* is shear velocity which can be derived from

$$u_* = \sqrt{(\tau_0/\rho_w)} \quad (2.15)$$

However, Richards (1982) also provided universal velocity profiles which define the logarithmic "law of the wall". These profiles, converted to common logarithms, differ for the cases of turbulent flow for smooth and rough boundaries as demonstrated by Equations 2.16 and 2.17.

$$U = 5.75u_* \log\left(\frac{u_* y}{\nu}\right) + 5.5u_* \quad (2.16)$$

$$U = 5.75u_* \log\left(\frac{y}{D_{65}}\right) + 8.5u_* \quad (2.17)$$

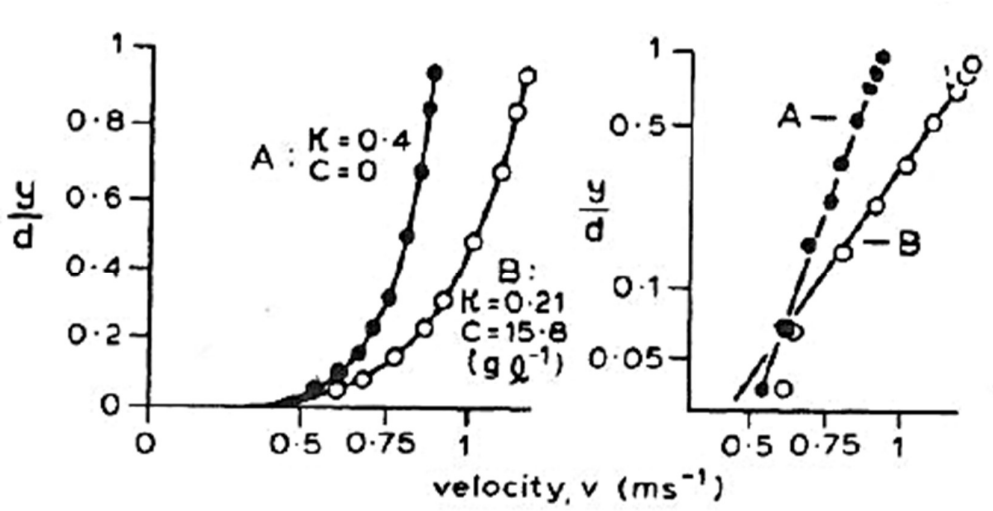

Figure 2.11 Velocity gradient in laminar flow (left) and turbulent flow (right) (Richards, 1982)

Initial motion of particles

Physical properties of sediments developed on the stream bed have impacts on the movement of bed materials. Not only does grain size have a direct influence on the process, shape, density, and structural arrangement of bed material, but it also has an influence on movements as well. Bed material is classified into two main types; cohesive and non-cohesive materials. Cohesive material consists of particles in the silt-clay range where resistance to erosion depends on bonds between particles. Unlike cohesive material, non-cohesive types, found in most stream beds, consist of loose grains in sand and gravel ranges. Resistance to erosion is related with their physical properties (Knighton, 1998).

The flows passing above the bed have an influence on bedload transport process. In natural streams, bedload movements start when flow intensity increases until it exceeds a threshold, where a force to move particles is equal to the resisting motion. At this point, the particles will be lifted from the bed and transported through the stream. The flow intensity to initiate movement can be determined by the critical shear stress (τ_{0c}), critical velocity or stream power. The lowest flow intensity that is able to create initial motion of particles on the river bed is known as the critical flow. Flow competence is defined as the maximum particle size which could be transported (Richards, 1982; Knighton, 1998).

Many studies have tried to explain this process and it is challenging to physically measure the critical stage of initial motion of transport. There are a couple of techniques to identify the initial movement of particles. Increasing flow intensity over a flat bed has an impact on small particles and starts to move them which eventually leads to the movement of larger grains. The visual identification in flumes is one of those techniques can be used to identify the movements. However, this technique might not be suitable in turbulent flow which has fluctuations in velocity causing movements of particles sporadic. The threshold gained by this method is considered to be highly subjective (Richards, 1982). Another method is to investigate the relationship between bedload transport and flow properties such as velocity and shear stress. The linearized curve obtained from the relationship between bedload transport and shear stress or flow velocity can be projected to zero bedload transport and the critical stress or velocity can be obtained at this point. However, deviation of the data from a linear function often occurs close to the threshold because of the statistical aspect of particle motions and the transport through the measuring section of imported particles already in motion"(Richards, 1982) (see example in Figure 2.12) rendering this method unreliable. Alternatively, a number of techniques have been used to measure particle movement in gravel-bed streams, i.e. tagging, painting, or aluminium wire wrapping (i.e. Butler, 1977; Keller, 1970; Richards, 1982). The distance particles are transported along stream can be related to the peak shear stresses of stream flows and using such a function the threshold stress for given grain sizes can be assessed, which increase with size of particles (Richards, 1982).

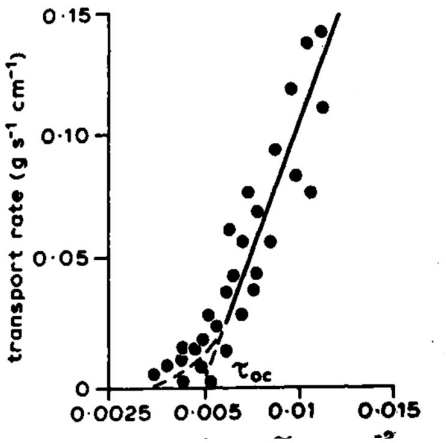

Figure 2.12 Definition of critical shear stress using a sediment transport relation (Richards, 1982).

According to the above techniques, the most common method widely used is relating time-averaged flow properties with bedload transport. A lot of studies explain the relationship between bedload transport and flow properties. HjulstrÖm (1935) presented a curve of sediment grain size against velocity (Figure 2.13). The lowest threshold velocity is found in well-sorted sands, 0.2 – 0.5 mm, while the larger and heavier grains, i.e. gravels and pebbles, and smaller size, less than 0.2 mm, like cohesive clays, which may be protected in laminar sublayer, need higher velocity to entrain them. However, flow depth, slope, sediment sorting, and consolidation have an influence on variations of critical velocity for a given sediment size and critical conditions for gravels exist for sliding and overturning (Sundborg, 1956, 1967; Novak, 1973; Richards, 1982). Francis (1973) reported that the flow velocity within which termination of bedload transport occurs is dependent on shear velocity ($u_* = \sqrt{(\tau_0/\rho_w)}$) and fall velocity. The transport of gravels as bedload tends to stop and deposition starts when the velocity drops to two-thirds of the critical velocity. In contrast the suspended sediments, including silt and clay, can be transported in the flow with a wider range of velocity between threshold and fall velocity (Richards, 1982).

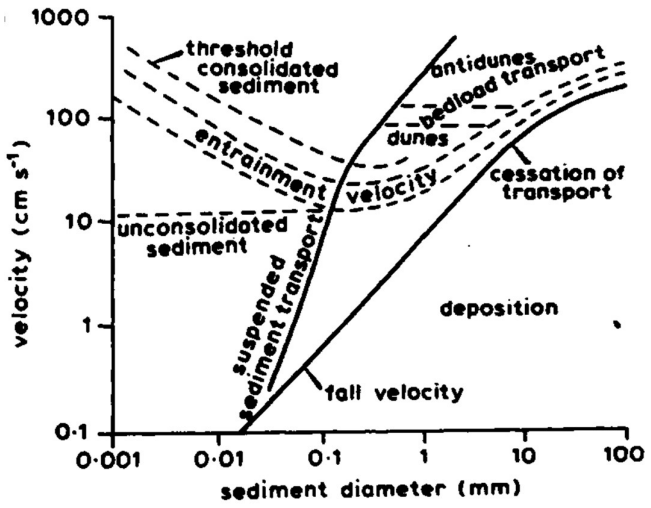

Figure 2.13 Threshold velocities, transport, deposition and bedform regimes (Richards, 1982).

Later, another important method was proposed by Shields (1936). In this study mean bed shear stress (τ_0) was used as a criterion and it was proposed that critical bed shear stress (τ_{0c}) increases with grain size and is also influenced by bed roughness condition. The dimensionless critical shear stress or Shields number, is defined as

$$\theta_c = \frac{\tau_{oc}}{(\rho_s - \rho_w)\, gD} \tag{2.18}$$

where ρ_s is density of sediment

D is particle size (mm)

(Richards, 1982; Knighton, 1998). This Shields number value results from the relationship between critical bed shear stress and the submerged weight of the sediment grain which is subject to the imposed bed shear stress (Richards, 1982). While bed roughness could be defined by a particle Reynolds number (Re_p^*):

$$Re_p^* = u_* D/v \; = 11.6 D/\delta_{sub} \tag{2.19}$$

where δ_{sub} is thickness of laminar sublayer

The dimensionless critical shear stress, or Shields number (θ_c), is commonly shown to vary as a function of the particle Reynolds number, (Re_p^*), and the effect of relative particle exposure which mediates a probalistic approach to entrainment is given as a function of $\theta_c \propto D/\delta_{sub}$ which is shown in Figure 2.14A (after Richards, 1982). The hydraulically smooth bed surface exists when Re_p^* is lower than 3.5 and grains are submerged within laminar sublayer (D/δ_{sub} < 0.3). The smoother bed surface is, the higher Shields number is required to move grains. However, θ_c in rough surface is not dependent on Re_p^* and "rapidly attains a constant value k", ranging from 0.03-0.06 with 0.045 as an accepted good approximation (Richards, 1982; Knighton, 1998). So the critical bed shear stress (τ_{0c}) on a hydraulically rough bed surface could be written as

$$\tau_{0c} = \kappa(\rho_s - \rho_w)\, gD \tag{2.20}$$

In a rough bed with grain size from 0.18 to 0.7 mm, which is commonly found in natural streams, the minimum value of θ_c is about 0.03 at low value of D/δ_{sub} where smooth turbulent stream exists. A decrease in shear stress over a rough bed resulting in a decrease in maximum grain size being transported (Inman, 1949; Simon, 1971; Richards, 1982). On the other hand, the finer grains, less than 0.2 mm, in a hydraulically smooth bed need higher θ_c to entrain sediments as the grains are finer than the laminar sublayer which is not subject to greater stress produced by turbulent flow. Furthermore, critical conditions can be also defined by the relationship between flow velocity and grain size which presents the same trends

(Figure 2.14B). It is also revealed that the most easily eroded grain size is about 0.25 – 0.5 mm (medium sand) (Knighton, 1998).

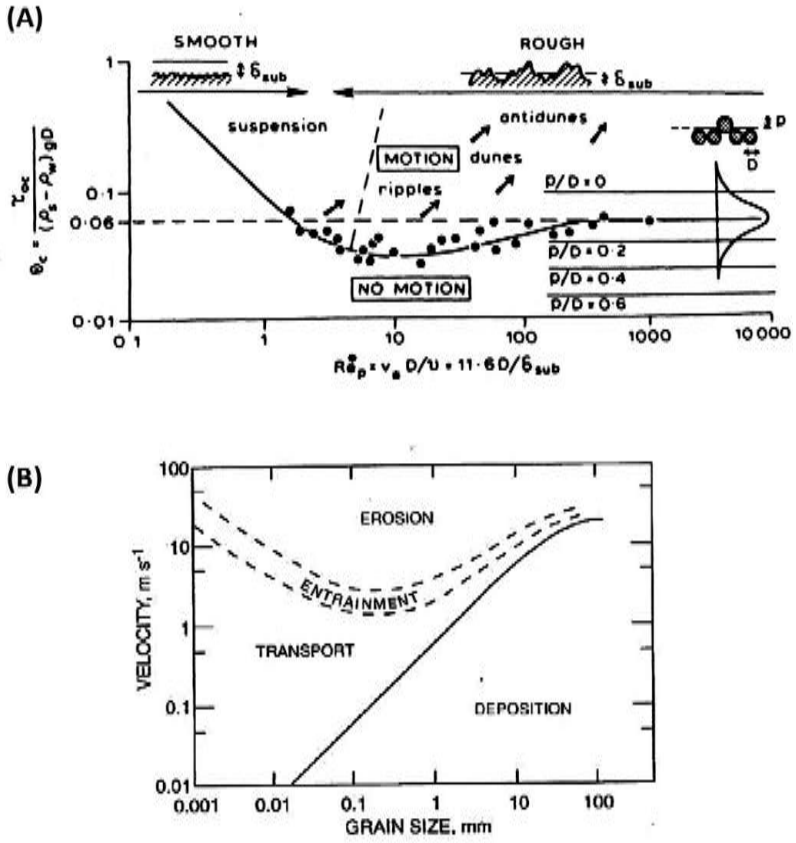

Figure 2.14 (A) The Shields entrainment function, showing threshold state and the effects of relative particle exposure and the concept of probabilistic entrainment (Richards, 1982). (B) Erosion and deposition criteria defined in terms of threshold velocities (Knighton, 1998).

Although mean velocity may be not considered the most relevant parameter (Knighton, 1998), bed velocity is an important factor of grain movement and depends on different shear velocity and bed roughness. Different sediment sizes have different values of critical bed velocity. Fitting a logarithmic velocity profile to current meter data, and projecting it to the bed level can be utilised to gain an estimate of bed velocity (Richards, 1982). The approaches mentioned above are beneficial in determining an average indication of the threshold state. However, there are some limitations in these approaches, especially data scatter in the Shields curve which would result from differential grain exposure (Richards, 1982). Many studies defined different Shields value under different conditions. For example, Fenton and Abbott (1977) recommend Shields value (θ_c) at 0.01 for natural stream with rough beds having grains

that are easily moved or "over-loose" bed. On the other hand, Carling (1983) suggested θ_c = 0.3 for compact gravelly sediment or "under-loose" bed. Williams (1983) suggested lower and upper limits for Shields parameter (θ) of the grains, which are greater than 10 mm, as 0.01 and 0.25 mm respectively.

Unsteady flow conditions and mixed sizes of bed materials are considered as the important factors contributing to the scatter of points around the Shields curve. These issues include the problem of definition of entrainment threshold, measurement and spatial variability of shear stress or velocity, intensity of turbulence, channel size, degree of exposure of grains, pivoting angles, degree of packing, grain shape, etc. (see more in Table 4.4 of Knighton, 1998). The differences in each factor may result in different processes of entrainment. For example, the short term fluctuation creates instantaneous stress greater than the average value. As a result, an entrainment of grains may occur at stresses lower than predicted. At a given grain size, critical shear stress in narrower channels tends to be higher than in wider channels. The degree of packing, in grains coarser than 8 mm, leads to different Shields value (Knighton, 1998). Within the Shilds diagram, a relationship between sediment size, shear stress and flow velocity is suggested; for fine sandy sediment, sediment movement seems to vary as a function of the critical shear stress as the particle Reynolds number varies. On the contrary, the entrainment of coarse sediment generally occurs at a constant mean shear stress although the particle Reynolds number continues to vary (Rubey, 1938; Richards, 1982).

Keller (1970) shows that the size and shape of grains as well as the bed velocity have an impact on pebble movement. The first two factors are dominant controls on the distance of pebble movement from deeper pools of water, while the latter one is dominant in the shallower, more turbulent, flow of riffles (Richards, 1982). However, it is suggested that not only the absolute size, but also the relative size of particles should be considered in order to define the critical shear stress (Knighton, 1998). It was proposed in the studies of Parker *et al.* (1982) and Andrews (1983) and Carling (1983) that in mixed beds, "the hiding and protrusion effects of larger grains are regarded as sufficient to compensate for their greater submerged weight, so that all grain sizes become mobile at approximately the same shear stress" (Knighton, 1998). On the other hand, later research pointed out that there is size-selective entrainment in coarse grain channels, "although not to the extent predicted by the Shields curve for unisize material (where $\tau_{cr} \propto D$)" (Knighton, 1998). "In grain mixtures the critical shear stress is reduced for coarser grains relative to the unisize Shields value (because of greater exposure and reduced resistance to motion) but increase for the finer ones (because of reduced exposure and increased resistance to motion)." (Knighton, 1998).

The stability of grains is one point being analysed by consideration of "turning moments acting about the downstream fulcrum" (White, 1940; Richards, 1982). Generally, each grain entrained by flow is dealing with a number factors; drag force (F_D), submerged weight, internal friction between grains (ϕ) existing at contact point (point A in Figure 2.15). The drag force on each grain is gained by relationship between shear stress and the exposed area per grain (D^2/η) as

$$F_D = \tau_0 D^2/\eta \tag{2.21}$$

where η is packing coefficient related with grains per unit bed area ($n = \eta/D^2$). This equation is assumed as the drag force is the only force on grains, not including form drag of bedforms. The equilibrium state exists when drag force equals the submerged grain weight which is written as

$$F_D\, x = m'\, g y \tag{2.22}$$

where x is $\frac{D}{2}\cos\phi$

y is $\frac{D}{2}\sin\phi$

$m'\,g$ is submerged grain weight, equal to $\pi\,\frac{D^3}{6}(\rho_s - \rho_w)g$

The relationship of these forces can be considered in terms of shear stress ($\tau_0 = \tau_{0c}$) by substuting the value F_D in equation 2.21 to equation 2.22 which can be written as

$$\tau_0 = \eta\frac{\pi}{6}(\rho_s - \rho_w)gD\tan\phi \tag{2.23}$$

Critical shear stress is defined for spherical grains of diameter D on a flat bed and theoretically justified for the Shields entrainment function (θ_c). However, this relationship is considered on the basis of zero slope. For steeper slopes, it could be modified by an adjustment for the additional downslope component of gravity force (Figure 2.15). According to this equation, it could be implied that the grain size has a major impact on initial movement, such as $u_c \propto D$ or $\tau_c \propto D$, together with grain shape and degree of packing (Richards, 1982; Knighton, 1998) (Richards, 1982; Knighton, 1998) and "maximum particle weight transported by a current varies as the sixth power of velocity ($D^3 \propto u^6$)" (Richards, 1982). It is stated that the Equation 2.23 may be applied both to the entrainment of bed material and to derivation of fall velocities (Richards, 1982).

However, "mean shear stresses at incipient motion calculated from $\tau_{0c} = \rho_w g d s$ were about one-half those expected" (White, 1940; Richards, 1982) and it is considered a limitation found in this equation (Knighton, 1998). This is due to lift forces and the instantaneous velocity variation in turbulent flow were ignored (Richards, 1982). The lift force is another type of force which is important in moving grains, at least in sand-bed streams. This force is created by the steep velocity gradient over a particle, which close to the bed is greater than the velocity under the grain resulting in the difference in pressure (pressure gradient). Moreover, it can be also created by turbulent eddies which have velocity components moving upward over the bed. This lift force tends to decrease relative to the distance from the bed because of the declination of velocity and pressure gradients. However, lift forces are negative and help to resist erosion within a laminar sublayer over smooth boundary (Richards, 1982; Knighton, 1998). One interesting experiment on initial movement of pebbles was presented by Helly (1969). The study used drag forces (Equation 2.23) together with the lift-force effect succeeded in predicting the initial movement of particles and provided explanation of saltation (movements in a series of hops) (Richards, 1982; Knighton, 1998).

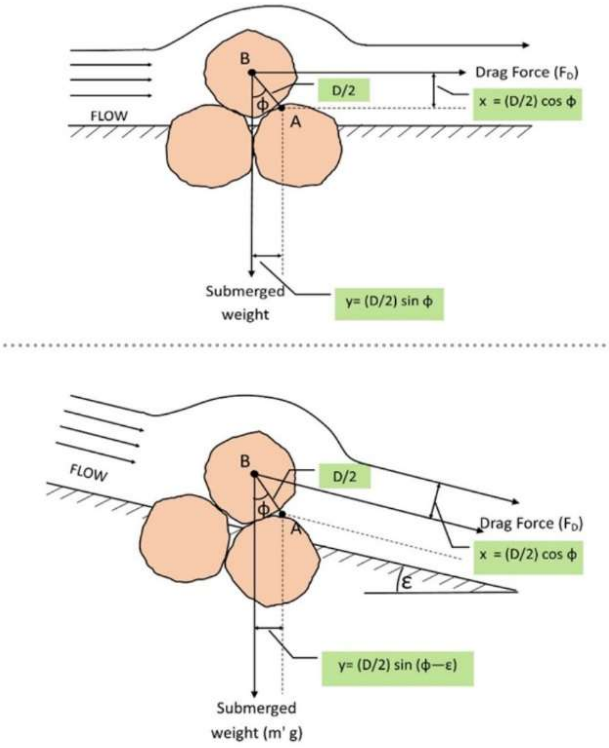

Figure 2.15 Forces acting on grains on a horizontal bed; A is the pivot point

2.3.2 Sediment transport

Sediment movement in rivers consists of a variety of elements (Figure 4.6 of Knighton, 1998). Considering the case of transportation, there are three components; dissolved load, wash load and bed-material load. The first two loads are the main components of catchment denudation, while the last one is important in geomorphological aspect as it has an impact on bedform adjustment. As a consequence, the bed-material load is more focused on in this section.

The bed-material load, mainly supplied by the channel bed, consists of grains with size generally coarser than 0.062 mm as finer fractions are regared as washload which can be deposited within the intertices of the bed but which does not contribute to the fabric of the bed in any substantial fashion. This bed-material load is transported in the form of bedload or as suspended load. Bed-material transport is difficult to measure accurately in the field due to errors in devices and temporal variations in transport rate. Methods in measurement are divided into direct and indirect measurement. Direct measurement includes pit traps, sampling device put on the bed and the indirect methods are tracers, impact plates, repeated surveys etc. There is no completely perfect method for measurement but the indirect field surveys provide enough details, more reliable results and have minimum disturbance to flow and time integrated sampling (Knighton, 1998).

Several variables are associated with flow, fluid, and sediment properties as well as gravity force and planform geometry. The basic issues in studying bedload transportation are understanding the dynamics of bed material movement and establishing a relationship between sediment transport rate and flow, fluid, and sediment properties (Knighton, 1998).

Dynamics of bed material movement: As stated in initial motion section, the grains start to be entrained when flow conditions at the bed exceed the threshold ($\tau_0 > \tau_{0c}$). The **bedload sediments** move by rolling, sliding, or saltation on the bed in shallow zone with a few grain diameters thick at the less velocity than surrounding flow. While **suspended load sediments** are the finer particles which may be carried within the flow resulting from turbulent mixing processes and transported in suspension, “possibly once a second threshold has been reached” (Knighton, 1998).

The differentiation between two modes of transport is arbitrary as their particles are interchangeable. Particles in sand bed streams tend to transport in groups as bedforms like ripples, dunes, or antidunes, whilst in gravel bed stream grains moves individually or move as discontinuous sheets. The transport rate of bed materials is related to the capacity of the flow,

which the armour layer might limit. Several experiments have been done to explain grain movements. Single grains, ranging from 5 to 10 mm, were traced photographically in the experiment of Abbott and Francis (1977) using transport stage (u_*/u_{*0}) as the driver for variable Q_s values. It is possible for all modes of transport to occur simultaneously over a wide range of flow conditions, but there might be one of them which dominates at a given stage. Moreover, phases of transportation in gravel-bed streams were defined by looking at dimensionless shear stress (τ_*) (Andrews and Smith, 1992). The first phase (Phase I) is called marginal transport which exists when the fluid force is strong enough to rotate grains from where they lie to roll over until they are settled in new places. Generally, the number of grains in motion changes depending on the level of dimensionless shear stress (τ_*) which is between 0.020 and 0.060 ($0.020 < \tau_* < 0.060$) for uniform grains. The second phase (Phase II) exists in higher shear stresses which exceed value of 0.060 ($\tau_* > 0.060$). At this phase the mobility of bed material is significant. Most of the bed is mobile and saltation is a significant transport mode. For many gravel bed rivers, a considerable portion of material is transported in marginal conditions (Phase I). Moreover, data gathered in gravel-bed rivers by Andrews (1984) show that there are an average of 12 days per year that the shear stress is greater than 0.030 but rarely higher than 0.070 (Knighton, 1998).

Armour layers play an important role in sediment transport. The development of this type of feature moderates supply in sediment transport processes and affects the characteristics in the two phases mentioned above. With the armour layer, a study by Carling (1987) shows that the passage of finer fractions is found over a stable coarser bed where the marginal transport condition (Phase I) exists. For Phase II, the substantial sediment transport could occur when the armour layer is breached when the channel morphology is modified by strong flows (Knighton, 1998).

Suspended load dynamics are related with sand fraction and turbulent properties over the bed, as well as the topography of the bed. In a field study of Lapointe (1992), the ejection events of eddies, moving fluid parcels away from the bed, tend to have an effect on suspended sediment concentration (SSC) which could be as much as 90 per cent of vertical mixing. The balance between the fall velocity and the vertical flow of an eddy results in vertical distribution of suspended sediment in which the SSC and grain size decreases away from the bed (Knighton, 1998).

Knighton (1998) stated that “The transport velocities of entrained particles are so low relative to flow velocities”, about 2-15 per cent. So the tranported distances are very short especially

during the marginal transport phase. Considering individual grains, they usually move in a series of steps and have rest periods, consequently bedload is transported intermittently (Knighton, 1998). The gravel-bed stream study of Carling (1987) has shown that particle velocity, including rest periods, range from 2 cm/h to 26 cm/h from intermediate flow to the bankfull discharge respectively. Although, the relationship between mean distance of grain travel and the excess stream power is weakly correlated (Knighton, 1998), grain size results in differences in this relationship. For large particles, a study of Hassan and Church (1992) shows that the distance of travel decreases with increasing grain size, while the distance of small particles is insensitive to grain size because they are inhibited by bed surface structure (Church and Hassan, 1992). However, these effects are less noticeable in Phase II (Knighton, 1998).

For **sediment transport rate**, many formulae have been proposed to "express the maximum amount of sediment (capacity) that can be carried for a given flow, fluid and sediment conditions" (Knighton, 1998). These equations are based on the relationship between the sediment transport rate per unit width and either excess shear stress ($\tau_0 - \tau_{cr}$), excess discharge per unit width ($Q - Q_{cr}$) or excess stream power per unit width ($W - W_{cr}$) (Knighton, 1998; Equation 4.11, 4.12, 4.13). However, there are no expressions which provide satisfactory prediction and which are accepted widely. The difficulties of developing bedload formulae are due to several factors, including fluctuation in sediment supply, heterogeneity of most channel beds, especially gravel beds, and inherent variability of bedload transport rates (Knighton, 1998).

Determining the maximum bedload transport is challenging, especially in the gravel-bed stream where an armour layer has developed. The armour layer is a feature developing over relatively finer materials and which protects them. Its thickness is usually no more than one grain diameter. This layer helps to limit material supply, especially during marginal transport conditions, resulting in lower sediment transport rate than that predicted by the formulae mentioned above. The stability of this feature is uncertain but it is expected that the layer does not grow under ephemeral flood regimes (Knighton, 1998).

Variations in bedload transport rate could be considered as ***spatial variations*** which occur at various scales. In bimodal sediment beds, the amount of sediments in finer strips is larger than those in coarser ones. The varied width of the channel bed also affects bedload transportation across the channel. Even though the river discharge is constant the bedload rate is rarely uniform as the width of channel bed varies with river stage, especially in meandering channels. For ***temporal variations***, 'bed-load pulses' are a common feature in bed material transport**.**

The pulses have been related with several mechanisms at different time scales (Knighton, 1998; Table 4.8). Among these mechanisms, "the migration of coherent bedforms or groups of particles is probably the most prevalent cause of variability" (Knighton, 1998). In the case of dunes, the maximum rate of transported sediments are related with the passage of dune peaks, whilst the smaller amount is related with troughs (Leopold and Emmett, 1976). Some types of bedform, such as large bars in gravel-bed streams, may take a longer time scale, a season or more, to migrate (Knighton, 1998).

2.4 Important factors on dune development

2.4.1 Flow parameters having impact on dune development

A number of parameters have been considered as factors affecting dune scale, which depends on the relationship between height (H) and wavelength (L) of dunes. These flow parameters include water depth (h), current velocity (or boundary layer thickness), bed shear stress, Froude number, grain size (Flemming, 1978; Rubin and McCulloch, 1980; Allen, 1984; Ashley, 1990; Carling, 1999; Francken *et al.*, 2004).

Current velocity (U): The distribution of velocity in the vertical and across the channel is considered an important factor controlling dune dynamics (Richards, 1982). According to McCave (1971), who studied the relationship between dune dimension, height, length, water depth, velocity and sediment transportation, current velocity is related with a growth in dune height. It was stated that "an increase in velocity produces an increase in dune height, until suspended sediment transport becomes large relative to the bedload transport rate, causing a decrease in dune height." On the other hand, the higher velocity could diminish dunes and result in flat bed when $\tau_{0s} > 0.8g\rho_w(s-1)D$ is fulfilled; τ_{0s} is the skin-friction bed shear-stress, g is the acceleration due to gravity, ρ_w is the water density, s is the relative density of the sediment and D the grain diameter.) However, a number of studies did not present a clear relationship between the flow velocity and dune dimension (Terwindt and Brouwer, 1986; Harbor, 1998; Francken *et al.*, 2004).

Bed shear stress (τ_0): Apart from the current velocity, the distribution and magnitude of bed shear stress created by flows is one of flow conditions that should be determined in order to understand bedform development (Richards, 1982). Bed shear stress is related with a number of factors including flow velocity (Equation 2.13a and 2.13b). Increasing in flow velocity over a dune will increase the shear velocity and shear stress in the boundary layer above the dune

(Francken *et al.*, 2004). The values of bed shear stress on the crest and trough are different. Moreover, there are some parameters having impact on the bed shear stress, such as water temperature and suspended sediment concentration. With the different conditions of these parameters, flows for the same depths and the same velocities would have different bed shear stress (Rubin and McCulloch, 1980). Initial motion of grains, as explained above in relation to the Shields diagram, will happen when flow reaches the critical bed shear stress (τ_{0c}) which is variable due to different related factors dependent on the flow conditions and grains properties in particular.

Froude Number (Fr): As was noted above, Froude number is one factor having an impact on river bedform especially in dune development as well as the transitional state of dunes, including transition between dunes and antidunes (Kennedy, 1963; Carling, 1999). Specifically, a number of studies were conducted to observe the process and development of dunes in terms of effects of Froude number to the dunes, for example Gilbert (1914), Williams (1967), Cooper *et al.* (1972), Vanoni (1974, 1977), Shaw and Kellerhals (1977), Whittaker and Jaeggi (1982), Ikeda (1983), Smart and Jaeggi (1983), Bathurst *et al.* (1987), Pitlick (1992) and Marion and Fraccarollo (1997). Many of these studies provide Froude numbers across the dune: antidune transition. They noted that, for gravel beds, a LSPB stage or dune bed could transform to gravel antidunes when Froude number exceeds 0.84.

Relative depth (h/D_{50}): It is the other factor being observed. Some studies investigated the relationship between Froude number and relative depth which could result in bedform changes. Williams (1967) and Vanoni (1974, 1977) studied coarse sand dunes, $D_{50} \approx$ 0.93 -1.35 mm. They used Froude number to distinguish dunes and antidunes and also considered the relative depth (h/D_{50}). The results show that once the relative depth is less than 100, the transition zone from dunes to antidune would occur at Fr value of 0.84. However, Fr would decrease if the relative depth exceeded 100. Apart from the critical Froude number for the dune transition from both field and flume works dunes are in the equilibrium stage at Fr ~0.70-0.75. The higher Fr will diminish dunes (Gilbert, 1914; Ikeda, 1983). In the transition to upper stage flows, diminishing dunes were lengthened and lowered in height before being replaced by a plane bed (Dinehart, 1992a)

Water depth (h): The depth of flow, or boundary layer thickness, is one important factor influencing dune scale (Allen, 1968; Yalin, 1972; Francken *et al.*, 2004). A large number of studies have tried to determine and explain the relationship between dune geometry and water depth. Dune wavelength and dune height is in proportion with water depth (h) or the

boundary layer thickness (Best, 1996; Carling, 1999). For example, Allen (1968) proposed the relationship between length and depth as $L = 1.66h^{1.55}$. Data from other studies shows that this relationship should not be generalised (Lane and Eden, 1940; Jordan, 1962; Flemming, 1978; Terwindt and Brouwer, 1986; Francken *et al.,* 2004). Apart from the wavelength, the height of the dune relative to water depth has also been investigated. Rubin and McCulloch (1980) proposed that $H \leq 1/6$ of mean flow depth. However, the correlation between height and water depth varies between systems and the height increases with the scale of the flow system (Allen, 1984). It is stated that the maximum ratio between height and depth could not be reached if the current velocity and grain size were less than optimal, showing that depth might not be the only controlling factor.

2.4.2 Grain size and dune geometry

Previously, bedform formations developed by a wide range of sediment sizes have been studied, including dunes. Although flow depth is considered to be an important factor on dune growth, grain size is the other factor that possibly affects dune development. This is supported by the statement that "water depth will limit further dune growth once the velocity above the dune crest exceeds a grain size dependent critical shear velocity" (Francken *et al.*, 2004). Several studies agreed that an increase in grain size leads to an increase in the size of dunes (Simons *et al.*, 1965; McCave, 1971; Rubin and McCulloch, 1980). In contrast, a number of comments in other studies contradicted this, such as Carling (1999) who stated that coarse grains (sand-gravel) does not obviously affect the size of dunes. Dunes developed by fine grains have a smaller equilibrium size than those developed by coarse grains (Francken *et al.*, 2004). However, it was suggested that if the two sediments sharing the same median grain size but have difference in other properties like sorting, density, or shape, the bedform probably develop differently even that they are under the same conditions of mean depth and velocity (Rubin and McCulloch, 1980). This is supported by a report of Wilcock (1992) that "sorting has a measurable effect on the size and shape of sandy bedforms" (Francken *et al.*, 2004). Thus it may be concluded that although grain size does not seem to be a major factor in limiting the occurrence of dunes, the size of the sediment together with the sorting and other properties might effect the dune form although this is poorly understood.

2.5 Gravel dune bedforms

Although there are many studies focusing on subaqueous sand bedforms, the dunes developed in gravels have not been well studied. In the past, gravel bedforms were understood only to exist as LSPBs in fast, competent flow or as USPBs and antidunes (Menard, 1950; Harms and Fahnstock, 1965; Carling, 1999). Consequently, the assumption was incorrectly made that mesoscale undulations in gravel beds are antidunes (Carling, 1999). Moreover, bedform phase diagrams from several studies (i.e. Leeder, 1983; Allen, 1984; Southard and Boguchwal, 1990; Ashley, 1990) do not include dunes with coarse grain sizes and higher flow strength. These diagrams are based on experimental data on shallow flows with sand-size sediments. Data of dunes and transitions to antidunes or plane beds with coarser sediment (> 5mm) are not sufficient, so "identification of the boundaries between gravel bedform existence fields with any certainty" was impeded. However, Carling (1999) has gathered data and plotted phase diagram with wider range of grain size and include the coarse grains up to 10 mm (Figure 2.16).

The other common misconception is about the state of flow in gravel bedform. It used to be conceived that the LSPB and USPB simply are related to subcritical and supercritical flows respectively (Carling, 1999). A number of studies show the concept is not necessarily so clear-cut as previously mentioned. For example, an experiment of Cooper *et al.* (1972) found that a LSPB in gravel within shallow sub-critical flows persisted, without any change in bed state, when a high value of Froude number ($Fr > 1.0$) developed. Thus this situation might be viewed as a LSPB persisting into upper-stage flow or a transition from LSPB to USPB without any evident change in bed state. On the other hand, bulk flows with low Froude number ($Fr < 1.0$) are able to develop USPB or antidunes locally when the relative depth decreases (Cooper *et al.*, 1972; Allen, 1984) for example on the crest of dunes. Although some authors stated that coarser grain size has a limiting influence on development of gravel dunes (e.g. Costello and Southard, 1981; Flemming, 1988), the examples above together with results from a number of studies, present the argument that there should be no limitation in grain size to form the steep dunes if the flow power and water depth are enough to adjust growth (Carling, 1999).

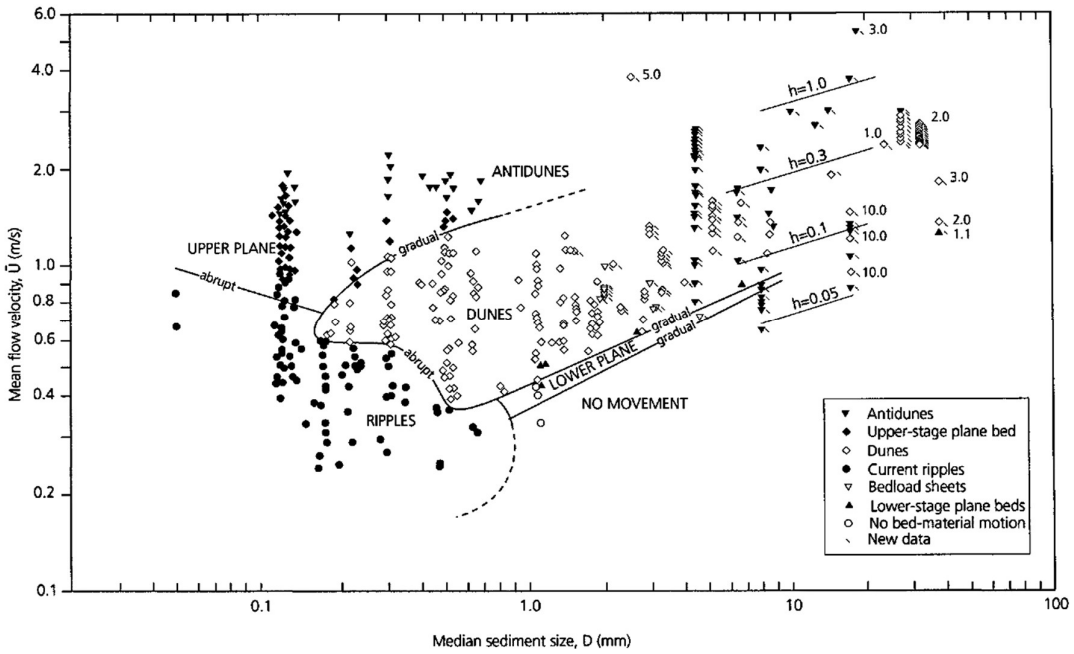

Figure 2.16 Bedform phase diagram (Carling, 1999).

Difficulty in classifying dunes and bars as well as inadequate experimental data for the development of gravel beds are reasons that the identification of gravel dunes is uncommon (Carling, 1999). Even though in the older literature several non-generic terms to designate flow-transverse gravel bedforms have been reported; such as gravel ripples, gravel waves, gravel bedforms, gravel dune-like bedforms, gravel bars (for example Gomez and Church, 1989; see Carling, 1999), these terms are not appropriate where the flow conditions are clearly associated with dune development. Notably the designation of gravel ripples is not appropriate given the scale of fluvial gravel bedforms (Carling, 1999). It has long been known that ripples do not form in in bed materials coarser than about 0.7 mm (Costello and Southard, 1981; Allen, 1984; Carling, 1999) because hydraulically smooth flow, $u_* D/v < 10$, is required for ripples to develop (Yalin, 1972; Allen, 1984; Carling, 1999). In the case of coarser bed material such as granules and coarser gravel the flow is invariably rough turbulent when coarser bed material is mobile (Carling, 1999). Consequently, most of this section will focus on the the processes and properties of gravel dunes and gravel antidunes.

Considering the bedform profile in vertical section, Carling (1999) noted that gravel and sand bedforms have similarities in ratios between height and wavelength ($H{:}\,L$), both of which could approach zero. Thus, he suggested that height of "gravel dunes should reach an

equilibrium value equivalent to that for sand". The maximum $H:L$ ratio of sand dunes in equilibrium is stated to be about 0.08 (Ashley, 1990). However, conditions in experiment and field works are constricted, so the evidence to support understanding in gravel dunes is limited and data are related to non-equilibrium and depth-limited conditions (Carling, 1999). Most studies results showed low $H:L$ ratios of gravel dunes, only few are similar to equilibrium values of deep-water sand dunes (i.e. Galay, 1967; Dinehart, 1992a, 1992b).

For planform of dunes, there are fewer studies of gravel dunes than sand dunes. Different types of gravel dunes have been studied in the field. 2D Quaternary gravel dunes with straight or sinuous crests were described by Baker (1978), Shaw and Gorrell (1991) and Carling (1996). Quaternary 3D gravel dunes with short crests were also described by Carling (1996). Examples of studies of short crested 3D gravel dunes in modern rivers are those of Gustavson (1978), Galay (1967), Galay and Neill (1967), Clague and Rampton (1982), and Scott (1982). Besides, Germanoski (1989, 1993) studied gravel bedforms both in field and flumes. Examples of flume studies on gravel bed dunes have been also presented by Ikeda (1982, 1983). These studies used morphological criteria for dune identification.

Although it was mentioned in the previous section on bedform classification that water depth controls scale of dunes, while scale of bars are dependent on water depth and channel width are considered to have impact on both of their scales and an identification of these two bedform types could be confused (A.S.C.E. Task Force, 1966; Bridge, 1985, 1993). Moreover, $H:L$ ratio of them may be low so that some periodic free bars may be related to the morphological process of equilibrium gravel dune development (Smith, 1978; Carling, 1999). The important study of Ikeda (1983) supports this statement and the result shows formation of mesoscale, low-relief dunes, developed from mobile macroforms, alternate or transverse bars, by increasing flow strength and bedload transport rate. The parameters influencing the distinction between macroscale and mesoscale gravel bedforms are also stated in his study.

2.5.1 Gravel dunes Vs gravel antidunes

Flow Criteria

In bedform development processes, especially transitional states from dune to antidune, Froude number is one potential factor having an impact on this bed transformation and could be used as criteria to separate dunes and antidunes (Kennedy, 1963; Carling, 1999). Though only a few gravel dune studies, both from field and laboratory works, have been completed, they show that, in gravel beds, the LSPBs would transform to antidunes under flows with

Froude number greater than 0.84 (i.e. Shaw and Kellerhals, 1977; Whittaker and Jaeggi, 1982; Smart and Jaeggi, 1983; Bathurst *et al*., 1987; Pitlick, 1992; Marion and Fraccarollo, 1997). Besides, some studies also considered relative depth. Dunes and antidunes developed by coarse sands (D_{50} = 0.93-1.35mm) were investigated by Williams (1967) and Vanoni (1974, 1977) and results, similar to other studies, show Froude number at transition is about 0.84 and there was no prevailing USPBs between transition between these two bedform types. However, it was added that this value of Froude number exists in flow with relative depth (h/D_{50}) less than 100. In contrast, Vanoni stated that Froude number at transitional phase "declined monotonically" for a relative depth higher than 100. However, hydraulics data from the early studies are not sufficient to define Froude number or relative depth. As a result, theoretical calculations for assessing subcritical Froude numbers were created to support an interpretation of Quaternary gravel dunes (Baker, 1973; Carling, 1996). Steep equilibrium dunes were found when Froude number is 0.70 - 0.75 approximately (Harrison, 1950; Gomez *et al.,* 1989; Dinehart, 1992a) and higher Froude numbers will diminish dunes (Gilbert, 1914; Ikeda, 1983) and they will be replaced by other bedform types, such as USPB or antidunes.

During transition to other types, the geometry of bedforms is changed. For dunes changing to USPB or antidunes, their lengths increase and heights decrease and become a plane bed during transition to USPB (Dinehart, 1992). Studies of Gilbert (1914) and Ikeda (1983) present information of gravel dunes and their transitional state to antidunes. Gilbert reported low-relief gravel dunes with grain size of 3.17 mm. The scale of these dunes were a maximum of 0.05m high and 0.61m long. Dunes changed to plane bed and transition to USPB starts when flows have increasing bed shear stress and lower water depth and in a Froude number range from 0.83 to 1.07. Ikeda studied low-relief dunes in 8 mm gravel bed. Results show that dunes in this gravel bed developed at Froude number of 0.78 – 0.80 and the antidunes were found for Froude numbers of 0.78 – 1.33. Though the range of Froude numbers of these two bedforms overlap, Ikeda explained differences that, at Fr = 0.78, antidunes develop on steep slope, shallow water, and high bedload transport rate, while dunes develop on gentler slope, in deeper water, and lower bedload transport rate than antidunes.

Information of transition from dunes to LSPB is presented by Galay (1967) and Fahnestock *et al.* (1969). Geometry of dunes during changing to LSPBs is similar to those transition of dunes to USPBs or antidunes which dunes length increases while height decreases leaving very small mounds at low flow. Moreover, steepness is also expected to decrease when water depth decreases (Carling, 1999).

A diagram of the relationship between Froude number and relative depth in gravel bedforms, dunes, transition, and antidunes, was created by Carling (1999) (Figure 2.17). Many bedforms exist with Fr around 0.84, especially the transitional bedforms but data with a relative depth higher than 100 are few. Antidunes seem to occur when the Fr is higher than 0.84 and in relative depths lower than 100, whilst gravel dunes exist with Fr under 0.84 and most of them were found in deeper water with relative depths over 100.

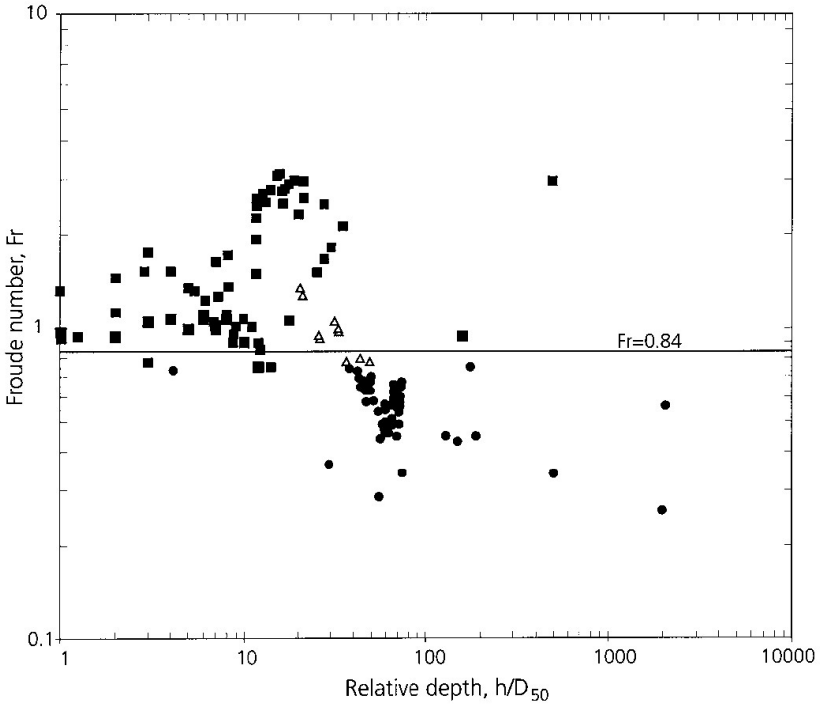

Figure 2.17 Froude number and relative depth for gravel bedforms (Carling, 1999) including gravel dunes (●), transitional bedforms (Δ) and antidunes (■).

Morphological and sedimentological criteria

Apart from using Froude number criteria above, morphology and sedimentology could be used as the criteria classifying gravel dunes and antidunes. Information of stratigraphic studies on gravel dunes and antidunes are summarised as follows;

For dunes, planar-tabular cross-strata are found in well-preserved 2D gravel dunes, while trough cross-strata are common in 3D dunes. Alternating cobble and pebble beds usually exist in bedding and the inclination of beds are varied in individual dunes, shallow or steep inclination as well as angle of repose beds may occur (Carling, 1999). Grain size in some dunes show the coarser grains occur down the lee slope or at the toe of cross-beds (Baker, 1973;

Carling, 1996). For antidunes, a number of studies of antidunes have been reported and described in terms of morphology and sedimentary structure, i.e. Bucher (1919), Middleton (1965), Foley (1977), Whittaker and Jaeggi (1982), Shaw and Kellerhals (1977), Carling (1999), Breakspear (2008).

2.5.2 Gravel dune morphology

Cross section

Previous important studies on the longitudinal geometry of Quaternary gravel dunes were done by Baker (1973) and Carling (1996) who showed that they have humpback forms. The evidence showed that the crests were flattened by falling water levels. However, there is only a little impact on the steepness (H/L) (Carling, 1999). Slopes of stoss and lee sides in both studies tended to steepen as dune height increased and it was stated that "there is no definitive relationship between steepness and asymmetry (L_{stoss}/L_{lee}). Most of the dunes observed in Siberia are asymmetric with high L_{stoss}/L_{lee} ratio of greater than 1 (Carling, 1999). Ashley (1990) suggested H/L ratio (steepness) of near equilibrium dunes in fine to coarse sand as 0.08. On the other hand for dunes with coarser grains, including sand and gravel, steepness is related to the non-dimensional bed shear stress.

Sediment grain sorting

Differences in sizes of grains might result in different grain sorting in bedforms. It is also suggested to closely consider the relationship between bed sediment size and dune morphology as the specific influence of grain size on gravel dune morphology has not been isolated (Carling, 1999).

As gravel dunes and sand dunes tend to develop similar steepness which implies "dynamic similarity in dune form for a wide range of grain sizes", it was claimed that morphology of coarse-sediment dunes is not mainly influenced by the median grain size (Carling, 1996a; Carling, 1996b). Carling (1999) supported this statement by combining data from many sources and creating two plots of median sediment size against dune height and length (Figure 2.18).

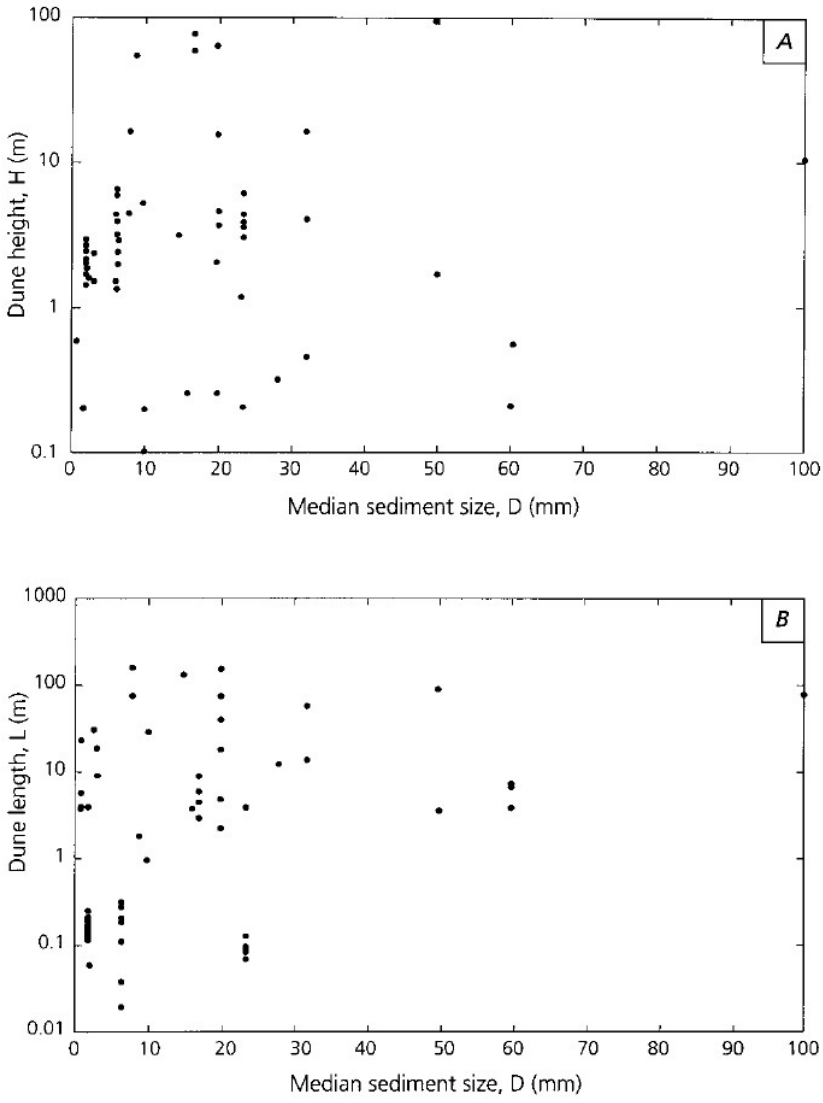

Figure 2.18 Relationship of A) dune height (H) and B) dune length (L) to median sediment size (Carling, 1999).

When looking at sediment sorting, Wilcock (1992) stated that mixture sorting has an impact on size and shape of sandy bedforms in which sediment is unimodal. On the other hand Wilcock also claimed that in there is a tendency for grain separation in bimodal sediment, including fine gravels, whereby the coarser grains settle under the sand dunes. This behaviour is supported by the flume study of Harrison (1950). The grain segregation was observed during bedload transport and fine gravel dunes were found developing and migrating over coarse gravel bed. Moreover, Snishchenko *et al.* (1989) studied effects of bed sorting in gravel dunes, with D_{50} ranging from 1.55 mm to 8.5 mm. They showed that dunes with uniform bedstocks are higher and longer than those in mixtures. Apart from the effect on height and length of dunes,

sediment sorting also has impact on celerity. “Flow resistance and bedform celerity were greater in both coarser and nonuniform bedstocks, whereas height and length were inversely related to D_{50}” (Carling, 1999). Though these studies showed similar findings, the study of Wilcock (1992) showed difference in dune length which tended to be shorter in unisize sediment than in the mixture.

Understanding the effect of sediment sorting of gravel dunes is complicated due to “variability of dynamic sorting in multimodal or broadly size sediments” (Carling, 1999). Moreover, it was stated that effects of mixed grain density and mixed grain shape have not been well studied and added that they “should be manifest by differences in particle mobility and sorting over gravel dunes” (Meyer-Peter and Müller, 1948; Maizels, 1989, 1997; Nakayama *et al.*, 1997, Carling, 1999).

Equilibrium

Data of height and length in gravel dunes were gathered and both of them were plotted against each other by Carling (1999) (Figure 2.19). From these data, a few gravel dunes are less than 0.6m long and 0.1m high and most of the smallest bedforms in these data were considered as bedload sheets. Among several studies, secondary dunes were found in studies of Gomez *et al.* (1989) and Dinehart (1992a), however they were not included in this diagram.

Figure 2.19 shows the steepness of gravel dunes. Two possible limit lines were created to define maximum steepness (Carling, 1999). The first curve, $H = 0.0073L^{1.5}$, is derived from studies on Quaternary long-crested (2D) dunes of Baker (1973) and Carling (1996a, 1996b). It represents maximum steepness of dunes. From other studies, several 2D dunes scatter below the curve showing that their steepness is less than the maximum value. On the other hand, a number of gravel dunes appear above this maximum steepness trend, most of which are short-crested (3D) dunes, including those studied by Dyer (1971). The steepness 3D gravel dunes tend to have an upper limit which is similar the limit of subaqueous dunes suggested by Ashley (1990). This function is defined as $H = 0.18L^{0.84}$. Consequently, it is possible that these gravel dunes might be in equilibrium state under flow (Carling, 1999).

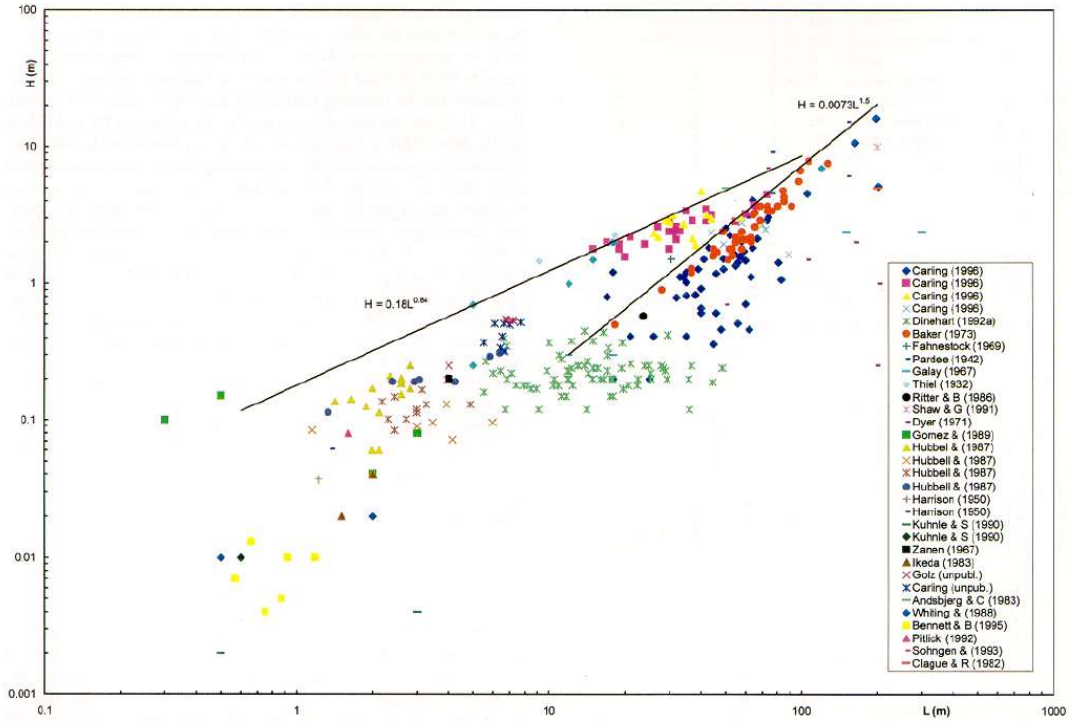

Figure 2.19 Compilation of data for gravel bedload sheets and gravel dunes depicting bedform height (H) as a function of bedform length (L) (Carling, 1999).

2.5.3 Bedform processes and flows

An increase or decrease in flow strength has an effect on the formation of the bed. Growth or decay of dunes also effects changes in flow conditions. In this section, the review is about gravel bedforms changing to and from gravel dunes, including LSPBs to dunes and dunes to USPBs.

Most early studies on bedform and hydraulic parameters concerned finer sediment with sizes less than 2 mm. Some studies considered coarser grains, with D_{50} up to 5 mm and show that an increase in the amount of gravel causes bedforms to disappear (i.e. Iseya and Ikeda, 1987; Dietrich *et al*., 1989; Kuhnle, 1993). However, Carling (1999) stated that this might be related to limitations of laboratory conditions.

Due to the constraints in laboratory works, theoretical calculation was used to find the threshold conditions of sediment movement as well as growth and decay of gravel dunes (i.e

Carling, 1996a). Moreover, observation of sediment movement on active modern gravel dunes is useful for determining essential parameters such as non-dimensional critical bed shear stress (θ) which helps indicate movement of particles, including the initial movement. The value of non-dimensional critical bed shear stress can be calculated using the following equation (Carling, 1999) which is the Shields number mentioned in the previous section (Equation 2.20) wherein reference was made to the critical shear stress, θ_c.

$$\theta = \frac{\tau_o}{(\rho_s - \rho_w)\, g D_i} \tag{2.24}$$

where θ is non-dimensional critical bed shear stress. This non-dimensional critical bed shear stress were more specifically identified as bed shear stress at initial motion (θ_c), the LSPB:dune transition ($\theta_{lspb:d}$), and the dune:USPB/antidune transition ($\theta_{d:USPB}$)

τ_o is mean bed shear stress

D_i is grain-size percentile

Transition from LSPB to dune

From previous studies, not many field data of the transition from LSPB to dune were observed. Estimation of critical bed shear stress in the transition from LSPB to dune ($\theta_{lspb:d}$), by using maximum flood stage indicators, were made by Baker (1973, 1978), while the transition value was directly measured by Dinehart (1992a) and he also found the conditions of near-equilibrium dunes. More studies were done by Dyer (1970a, 1970b, 1971, 1972) which investigated asymmetrical gravel dunes in a shallow tidal environment. The initial motion (θ_c) was measured both over dune crests and troughs. The results provide a ratio of maximum initial motion over crest and troughs equal to approximately 2. However, he added that dunes did not start migrating until the ratio of initial motion over crest and trough is higher than 4 and initial motion over crest exceeds 0.08. Initial motion over crest of dunes with grain size of 4 - 32 mm was reported as 0.043 by Langhorne *et al.* (1986). This value is close to general threshold of motion for gravels such as θ = 0.045 presented by Komar (1996).

There are not many studies describing the behaviour of bedform development for grain sizes larger than 5 mm. A number of these studies observed some LSPB or gravel sheet existence which would later forms asymmetric dune-like bedforms. For example, a study of Ikeda (1983) reported "low-relief dunes" on a gravel bed, with grain size > 8 mm, under low bed shear stress flow. However, conditions for development from gravel sheet to dunes are not identified (Whiting *et al.*, 1988; Whiting *et al.*, 1988; Kuhnle and Southard, 1990; Carling, 1999). The study of Meyer-Peter and Müller (1948) on coarser bedstock, with a range of 2.8 mm to 28.65 mm, show that development of low-relief bedforms result in an increase in flow resistance. With their data, Smart and Jaeggi (1983) as well as Griffiths (1989) suggested a relationship between flow resistance and mesoscale bedforms (Carling, 1999).

Comparing coarse and fine grains, bedforms developed with coarser grains (D_{50} = 6.5 mm) were reported to be poorly formed, while the fine grains (D_{50} = 2.1-3.97 mm) formed better (Hubbell *et al.*, 1987; Gomez *et al.*, 1989). Moreover, it was stated that the unstable bedload transport over 23.5 mm gravel bedstock in the LSPB flow regime created long-wavelength undulated forms with a few grains high (Carling, 1999).

Transition from dune to USPB

According to laboratory studies, height of dunes increases with an increase in flow strength. Once the bed shear stress exceeds 0.25-0.3, the height would stop growing and dunes are flattened (e.g. Bridge, 1982; Allen, 1984; Carling, 1990). So it was presented that the relationship between H/L or H/h and increasing bed shear stress follows a bell-shaped relationship. However, although several studies provided data on the bed with grains as coarse as 5.1 mm (i.e. Allen, 1978, 1984; Yalin, 1992), only a few studies show the results of the relationship for even coarser grain size data, for example, Dyer (1970a, 1971, 1972), Dinehart (1992a), and Pitlick (1992).

Dyer studied dunes with a median grain size of 16 mm. He stated that dunes started growing when θ_c was exceeded on the stoss side and the USPB transition also created on the crest for finer fractions (D = 4 mm and θ = 0.31). This was considered to induce "a degree of size sorting and crestal flattening" (Carling, 1999). Irregular steep bedforms were found by Pitlick (1992) which were considered as antidunes or transitional stage. A plane bed or dunes were stated to exist prior to development of these irregular bedforms beginning in critical flow with θ = 0.20-0.45. Dinehart (1992a) recorded dunes with maximum height when θ = 0.25 but height started decreasing to "featureless" USPB when θ = 0.30. Moreover, data from a study of Dinehart (1992b) showed falling stage bed shear stresses have impact on dune height changes. Height

increased when θ= 0.2-0.27 and decreased when θ fell further to 0.16. USPB was also reported to exist with θ between 0.25-0.3 for high stage flow. According to the empirical polynomial functions in the study showing trends of maximum values for H/L or H/h, the turning point exist with θ= 0.21 when H/h = 0.25 or θ= 0.25 when H/L = 0.06. So it was concluded that the transitional stage between maximum height and USPB of Dinehart's dunes exists with θ from 0.21 and 0.3 (Carling, 1999).

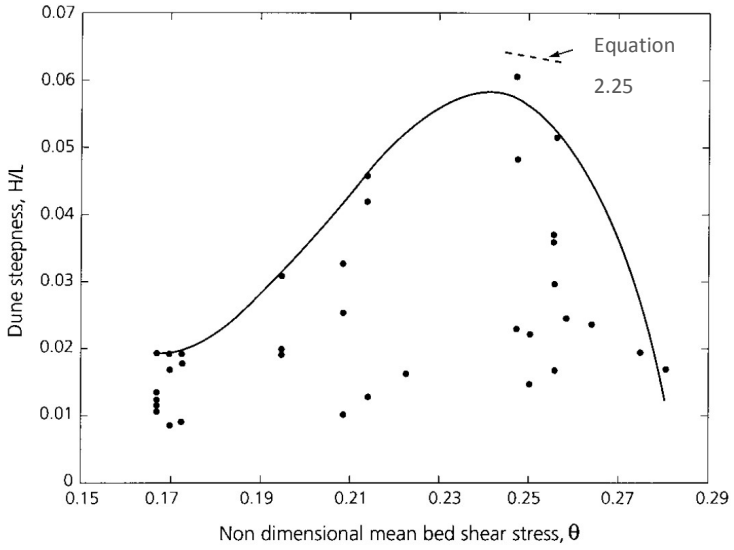

Figure 2.20 Variation in dune steepness (H/L) as a function of non-dimensional bed shear stress (θ) through time. The data represent a suite of dunes growing to maximum steepness before decaying in height (data from Dinehart 1992b, table 1, time = 61.21 hours to 85.72 hours) (Carling, 1999).

Apart from the studies previously mentioned, dune steepness of equilibrium dunes has been considered and could be applied with Dinehart's gravel dunes (Figure 2.20). A parabolic function for dune steepness, relating to the Shields parameter, was presented by Fredsøe (1975) as follows;

$$\frac{H}{L} = \frac{0.02}{\sqrt{f/8}}\left(1 - \frac{0.06}{\theta} - 0.4\theta\right)^2 \qquad (2.25)$$

where H is dune height

L is dune length

f is the Darcy-Weisbach friction factor

This equation was stated to apply to "equilibrium dunes in steady uniform flow, whereas many of Dinehart's dunes developed during unsteady flow, and only a few may have been equilibrium bedforms" (Carling, 1999). However, there is another means to write the equation relating to the relationship of height and water depth as;

$$\frac{H}{h} = \frac{\alpha 0.125}{\sqrt{f/8}}\left(1 - \frac{0.06}{\theta} - 0.4\theta\right)^2 \quad (2.26)$$

where α is the coefficient in van Rijn's (1982) relationship between equilibrium dune length and water depth ($L = \alpha 2\pi h$)

f is the Darcy-Weisbach friction factor

The latter equation is an application of van Rijn's to Dinehart's L: h data. The outcome shows that α was about 0.52-0.89 during dune growth which was stated to be consistent with data from sand dunes. Only few data from Dinehart (1992a, 1992b) where α >1.0 are considered as non-equilibrium forms.

Both equations have reasonable agreement with Dinehart's dune data. The observed and predicted (calculated with equations) values of H/L are in agreement when Dinehart's dunes were steepest. For the latter equation, θ, f and α from Dinehart's data were used. The calculated relative depth (H/h) were in agreement with the observed value for steepest dunes when measured f and α are about 0.15 and 1.52 respectively. However, the observed H/L and H/h were lower than predicted values when the dunes were not close to equilibrium. The f values of flow conditions recorded by Dinehart shows that dune height increased and length decreased when f was 0.1, and the height declined while the length amplified when f was lessened to 0.07 (Carling, 1999).

2.6 Marine dunes/ dunes in bidirectional flows

In tidally dominated environments, dunes are commonly found under tidal currents with speed typically over 0.5 m/s and fine to medium sands (Dalrymple *et al.*, 1978; Dalrymple and Rhodes, 1995; Masselink *et al.*, 2009; Choi and Jo, 2015). Previously, there are a number of studies measuring dune migration in tidal environments (i.e. Terwindt and Brouwer, 1986; Allen *et al.*, 1994; Larcombe and Jago, 1996; Hoekstra *et al.*, 2004; Choi and Jo, 2015).

However, these studies are done within fine sediment bedforms. Reports on cobble dunes in the tidal environment are rare.

According to previous studies of dune behaviours in tidal/estuarine environment, factors on these dunes are similar to those in rivers, which are developed in unidirectional flows. However, they are more complicated in development and structure which results from different flow hydrodynamics which are related to bidirectional of tidal currents, changing tidal levels and time-velocity asymmetry, and occasional presence of waves (Dalrymple and Rhodes, 1995; Choi and Jo, 2015). As a consequence the study of dunes in tidal environments needs to consider differences between two directional flows of flood and ebb tides.

Flood and ebb tides create two different flow directions which probably result in tidal asymmetry. This asymmetry usually refers to "the distortion of the tidal wave that makes the flood period unequal to the ebb period" (Wang *et al.,* 1999). If the longer period is the flood tide, it would be called flood-dominant, on the other hand it would be called ebb-dominant. Tidal asymmetry is related to morphological development and sediment transport (Wang *et al.,* 1999) which probably have impacts on dune behaviour. Asymmetry of flood and ebb can be considered in terms of water level variation and current velocity which is important to and proportionated with dune migration rates (Terwindt and Brouwer, 1986; Dalrymple and Rhodes, 1995; Wang *et al.*, 1999; Kostaschuk and Best, 2005; Villard and Church, 2005; Choi and Jo, 2015). Tidal asymmetry tends to happen during spring tides (e.g. Boersma and Terwindtt, 1981; Choi and Jo, 2015). Proportion of flood and ebb tides in terms of velocity and discharge has impacts on morphology, structure, and migration rates. The dunes developed under dominance of either flood or ebb tides tend to migrate toward the same direction of the dominant tide and exist in asymmetric form while dunes formed under symmetrical tidal currents tend to have near-zero migrations (Lee *et al.*, 2006).

Choi and Jo (2015) studied medium to coarse sand dunes on the west coast of Korea where simple and compound dunes were found. They have ebb-asymmetric shape where the simple dunes tend to be more asymmetric and migrate faster than compound dunes while the compound dunes have longer length as well as steeper lee side. Ebb flows dominant the hydrodynamics of dune formation, peak flood velocities in minor channels and major channels are 0.9 m/s and 1.2 m/s respectively, while the peak ebb velocities are 1.2 m/s and 1.4 m/s respectively. They added that dune migration mostly exists during spring tides, when the peak tidal current is greater than 0.8 m/s, but not during neap tides as tidal currents might be below

the threshold of dune migration. However, it was reported that during the study these dunes move both seaward and landward at different rates.

The tidal asymmetry is not the only indicator that dunes might migrate towards that direction. There are also other factors having an important role on migration, including wave intensity and discharge fluctuation. During tidal currents, it is possible for dunes to migrate toward another tide sometimes. There are some factors which should not be neglected including storm events; wind, waves, as well as period of spring/neap tides. The study of Choi and Jo (2015) shows that even the hydrodynamics in the study area is ebb-dominant and dunes tend to migrate seaward, but that sometimes during the study period, dunes migrate landward. One reason is that stormy conditions during spring tides which lead to wind-induced waves and large waves with wave orbital velocity higher than 0.3 m/s (Hoekstra *et al.*, 2004). The high intensity of waves together with spring tide period would lead to accentuation of dune migration toward direction of residual tidal currents. It was suggested that dune height could decrease due to the erosion on the top caused by these intense waves (Terwindt and Brouwer, 1986; Hoekstra *et al.*, 2004; Ferret *et al.*, 2010; Choi and Jo, 2015). It is reported that waves with a height greater than 0.4 m were measured in the same period as landward dune migration. Though the flood tidal current is very strong or there is a storm event but there is the low wave height or it happens during peak neap tides, when wind-induced waves are unlikely to occur, dunes do not migrate and tend to have aggradation of dune tops.

Apart from the hydrodynamics and storm events mentioned above, another factor affecting the migration of dunes is the morphological changes occurring within the area. Choi and Jo (2015) reported the effect of channel migration on compound dune morphology. Dunes might be eroded by channelized flow or they might have deposition of sediments transported by the tributaries of which position is changed. According to continuity equation, once channel width is changed, the flow conditions would alter. Narrower channel would result in faster flow or, in contrast, wider channel would have less flow velocity.

Chapter 3: Study site

This chapter describes the location of the study site and surrounding areas. The chapter includes the study location in the broader area, the estuary and the Bristol Channel, followed by information of a more specific location, Hills Flats, where the fieldwork took place. It summarises the general information of the area, including the geographical setting, geology, tidal cycles, and wave regime in order to provide background for this study.

3.1 Severn Estuary and Bristol Channel

3.1.1 Location

The Severn Estuary is located in the southwest of Britain. It is one of the largest coastal inlets of Britain with a high tidal range (Allen and Fulford, 1996) and is connected to the Bristol Channel which is on the shelf surrounded by the English Channel, Celtic Sea, and St. George's Channel and separates Wales and Southwest England (Figure 3.1). This channel comprises a large, partially enclosed body of tidal water with an approximate length of 250 km and is renowned as a major waterway (Hashemi *et al.*, 2008; Uncles, 2010).

Many researchers have paid considerable attention to this estuarine system. For example, the large tidal range and energy of this area have drawn the attention of oceanographers to look at energy propagation, dissipation as well as power generation (Uncles, 2010). Other important case studies in this tidal system are applied to a variety of aspects; such as ecology, meteorological forcing, and water quality (Uncles, 1982; Wolf, 1987). Apart from these research topics, over the last 20 years, there are many studies focused on physical properties and processes including bed-form behaviour, sedimentation process and transportation, within the channel as well as the Severn's intertidal area (Kirby and Parker, 1982; Dyer, 1984; Allen and Rae, 1988; Carling *et al.*, 2006; Williams *et al.*, 2006; Uncles, 2010).

The Severn Estuary and Bristol Channel cover a very large area with different properties. Uncles (2010) divided this area into five zones; outer channel, central channel, inner channel, lower Severn, and upper Severn where the study location is in (Figure 3.1). However, in this study, the definition of the Severn Estuary is based on the Admiralty Chart SC1179 which is shown in Figure 3.2. The estuary starts from the middle estuary at the villages of Aust and Beachley at the downstream and ends at the Maisemore weir at Gloucester in the upstream. The outer estuary, from Aust to the Bristol Channel, is significantly influenced by the marine

environment (Allen and Duffy, 1998; their Figure 1). This definition is in the same area as the upper Severn as defined in a study of Uncles (2010).

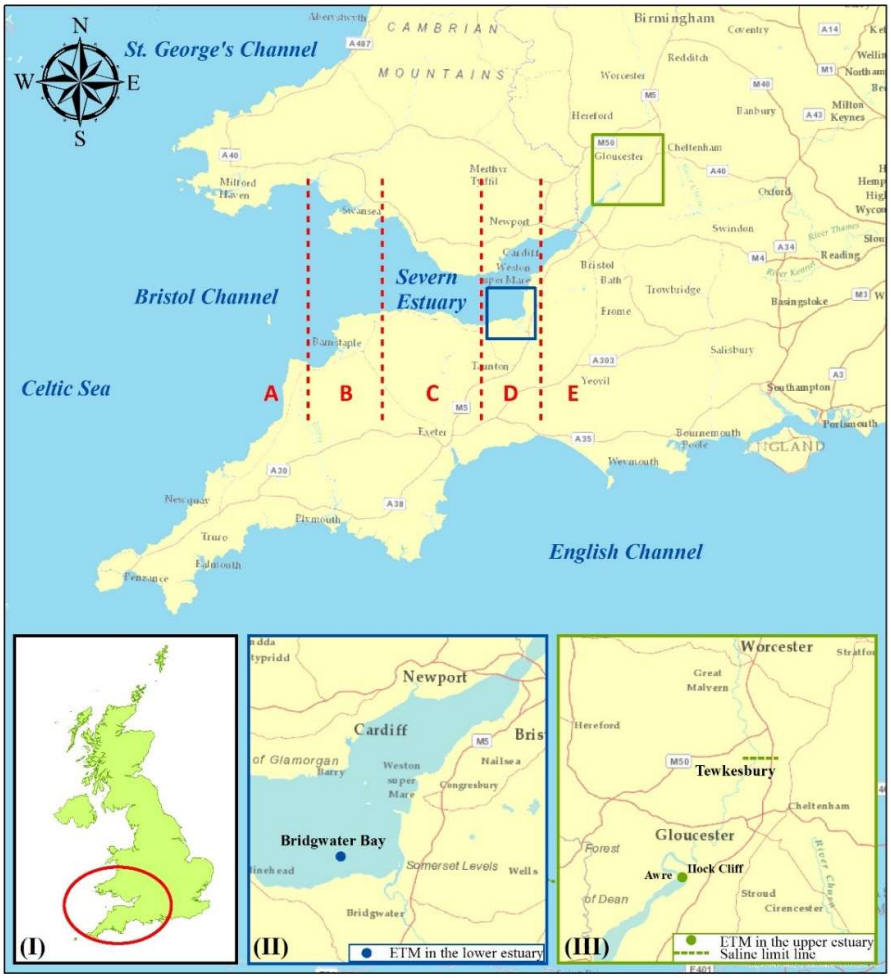

Figure 3.1 Location of the Severn Estuary and Bristol Channel in the UK (red circle in the inset map) and surroundings area. This area is categorized into five zones (Uncles, 2010). Red-dashed lines separated these zones approximately; (A) outer channel, (B) central channel, (C) inner channel, (D) lower Severn, and (E) upper Severn. The inset map (I) shows the location of the estuary and the channel within the United Kingdom. The other two inset maps, (II) and (III), show the areas of where the estuarine turbidity maximum (ETM) in the estuary were reported (the blue and green dots in these two insets) (Manning *et al*., 2010; Carling *et al*., 2015). Moreover, the saline limit is reported to be in the upper Severn (the green dash line at Tewkesbury in the inset (III) (Uncles, 2010; Carling *et al*., 2015).

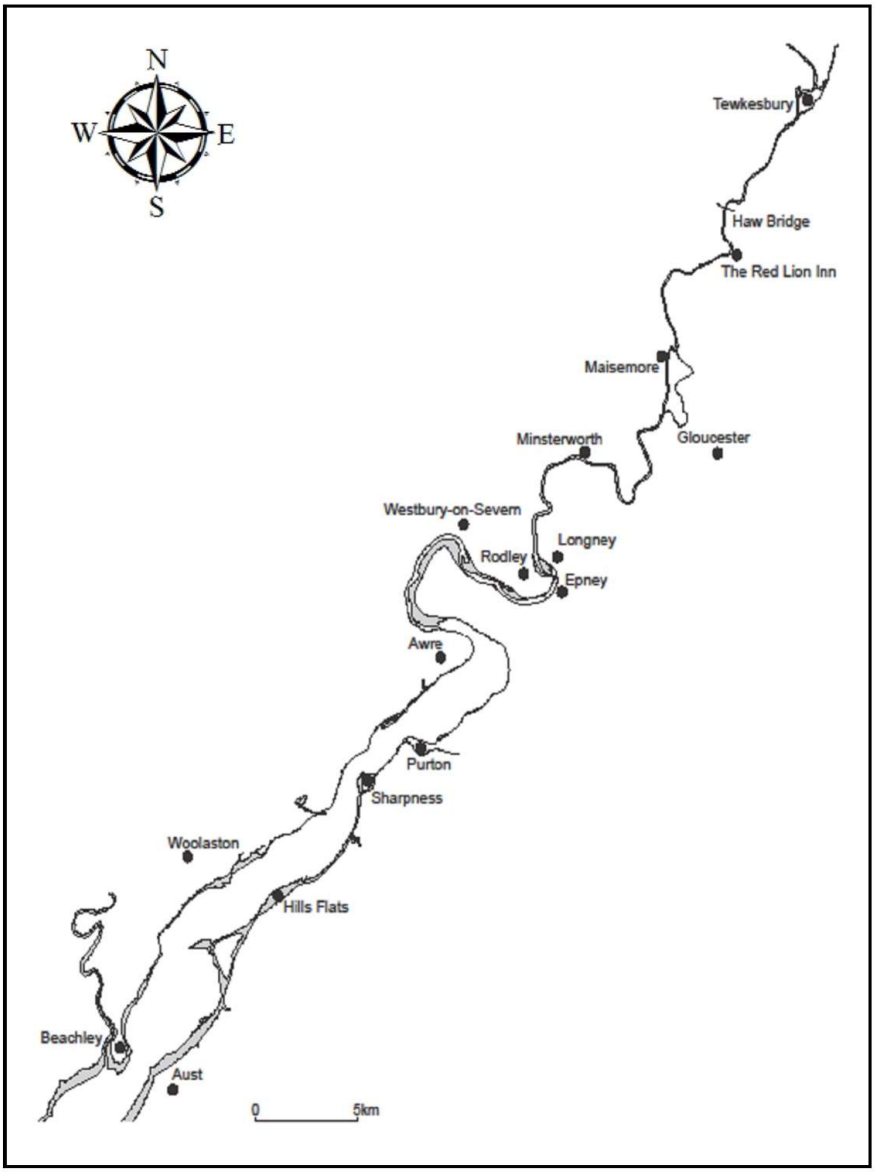

Figure 3.2 An area of the upper estuary of River Severn, starting from Aust which is a little upstream of Avonmouth toward Tewkesbury, the inner zone of the Severn Estuary.

3.1.2 Geology and sediment

The geology of the Severn Estuary was estimated to develop from about 400 million to 200 million years ago (Severn Estuary Partnership, 2011) and the geological and geomorphological development in this area are various and slightly different regarding to locations. The oldest one is rocks of ***Devonian Old Red Sandstones***, following by ***Carboniferous rocks*** (hard-grey limestones), ***Triassic rocks*** (known as Mercia Mudstone Group formed from silty clay which limestones and mudstones formed) and ***Jurassic rocks*** (limestones and mudstones). The

Devonian rocks are poorly exposed, while the other three rocks dominates in this area. It is also added that deposits of sediment over the past two million years consist of riverine alluvium, peats and marine clays as well as glacial deposits of sands, clays and gravels (English Nature, 1997; Severn Estuary Partnership, 2011). Jurassic and younger mudrock-dominated beds, with muds and muddy sands, are also found on the floor of Bristol Channel and the Celtic Sea (Allen, 1991). The generalised bedrock geology of the Severn estuary of Allen (1991; Figure 1) shows that most of the English side is formed of Mesozoic rocks while there are Palaeozoic and older rocks on the Welsh side. Moreover, throughout the estuary, including the study area at Hills Flats, there are four Holocene components: the Wentlooge formation (pale green estuarine silt clays); the Rumney formation (pink sandy to silt clays); the Awre formation (pink to grey sandy to silt clays) and; the Northwick formation (grey sandy to silt clay). These components started to accumulate 2500 to 3000 years ago and formed a stair-like succession on the salt marshes and high mud flats (Allen and Rae, 1987; Allen and Fulford, 1996). The sequence and relationship of linked geomorphological and lithostratigraphy of these formations lying often above the Triassic Mercia Mudstone bedrock in the Severn Estuary are presented in Figure 3.3.

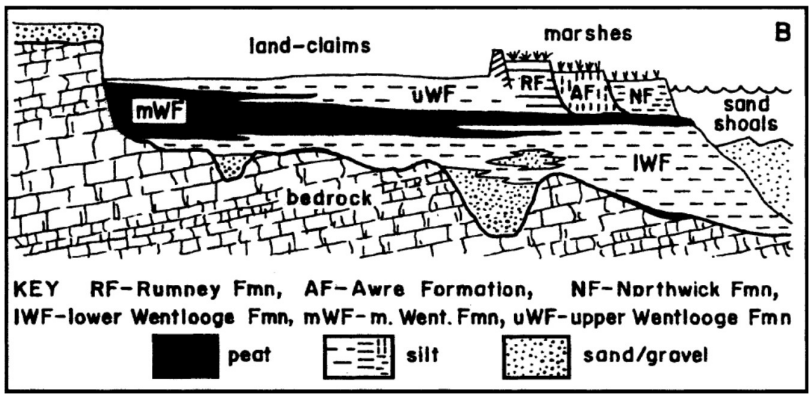

Figure 3.3 Schematic of the typical Holocene stratigraphy in the Severn Estuary (after Allen, 2004; Figure 1).

The Bristol Channel and the Severn Estuary have a wide range of bed sediment sizes. There are a number of reviews for sediment processes; i.e. Kirby and Parker (1982) and Dyer (1984). The coastline of this estuary consists mainly of mud, sand or gravel beaches found along the margins of the estuary. The sea floor in the inner Channel largely consists of rock with some sandy barforms and occasional gravel patches, especially in the north of the inner channel. In the inner estuary, the bed is also cut into bed rock but is mainly covered with a layer of muddy and sandy sediment on the Welsh and English sides respectively (Dyer, 1984; Figure 1).

Erosion of the Holocene estuarine alluvium is one of the main sources that supply fine sediment to the lower River Severn with deposits about 10 m in thickness, increasing in thickness into the Severn tributaries. However, despite the fine sediment supply from the river, there is still recession of the shore rather than progression because the rising of relative sea level (Allen and Fulford, 1996). Most of the gravel constituting the cobble dunes at Hills Flats is sourced from erosion of the underlying Triassic mudstones and muddy limestones which form the bedrock shelf along the English shoreline in this vicinity. A small quantity of finer gravel is sourced from the base of the Wentlooge Formation (Allen, 1987; Allen and Rae, 1987).

Suspended sediment is one important factor for turbidity. For the River Severn and estuary as well as the Bristol Channel, turbidity was concluded to be mainly a result of sediment resuspension by tidal currents and waves, and increases from its mouth to upper reach with 0.001 – 50 g/L of suspended particulate matter (SPM) (Collins, 1983; Uncles, 2010). It was stated that "the estuary is highly turbid with fine sediment concentrations peaking in the winter months (Allen and Duffy, 1998; Hamilton, 1979) such that large quantities of muddy fine sediment may be deposited and resuspended on the intertidal areas during individual tidal cycles" (Carling *et al.*, 2006). Dyer (1984) studied vertical profiles of turbidity and reported a variation of suspended sediment concentration throughout individual tidal cycles and the neap-spring cycle. The concentration tends to be uniform from the surface to bed at a maximum current during spring tides. Nevertheless, once the current strength decreases and the suspension and particles start settling, there are different steps in profiles of suspended sediment concentration, termed lutoclines by Kirby and Parker (1983), which shows lower concentration away from the bed but higher concentration near the bed. There are many tributaries that flow into the estuary and the River Severn is dominant as most of fine sediment in the estuary is derived from this river (Allen, 1990, 1991). It was reported that, each year, some 1.6×10^6 tonnes of suspended fine solids were supplied to the estuary by the Severn (Collins, 1987) which equals to two-thirds of the annual fine sediment supply to the estuary (Allen, 2004) and for the whole estuary, there are up to 30×10^6 tonnes of fine sediment suspended at MHWST (Allen and Duffy, 1998). Joint (1983) reported survey results of SPM concentrations that concentrations are very low, (ca. less than 10 mg/L) in the outer channel while those in the inner channel are high (ca. 50 mg/L) and increase upstream into the estuary, which could reach 500 mg/L or more. However, the specific data of suspended fine sediments in the head of the estuary is not well reported while high concentrations of them are found in the middle and outer estuary for all tidal states (Hydraulics Research Station,

1981b; Crickmore, 1982; Kirby, 1986). Two estuarine turbidity maxima (ETM) were reported in the Severn Estuary. The first one is in the upper estuary near Gloucester, between Awre and Minsterworth (Figure 3.1 (III)) (Manning, 2010; Carling *et al.*, 2015) whilst the other ETM is in the lower estuary in the vicinity of Bridgwater Bay (Figure 3.1 (II)) (Manning, 2010).

3.1.3 Flow and tidal regime

Among other tributaries discharging to the estuary, the River Severn is the largest resource of fresh water flow with the average daily flow rate of about 100 m^3/s (IH, 1998). The record of average monthly discharge from 1971 to 1994 shows flow variations in different seasons, from a low flow in summer (July), 2.6×10^6 m^3/d, to a peak flow in winter (January), 17.2×10^6 m^3/d. The fluvial discharge has an important influence on fine sediment regime in the inner most reach of the estuary (Kirby, 1986). The River Severn gauging station providing river discharge available nearest to the study site, Hills Flats, is at Haw Bridge (Figure 3.2), where peak daily fluvial discharge is typically 93 m^3/s (Carling *et al.*, 2015).

As the Severn Estuary has a high tidal range, this results in the strong tidal stream and the discharge of water with a high amount of silt. This estuary is a large well-mixed extreme macrotidal or hypertidal system in the semi-diurnal tidal cycle (Archer, 2013). The tidal range, which could reach approximately 7 to 14 m high, is acknowledged as the second largest range in the world which is increasingly tidal and turbid from its mouth to the upper Severn (Somerville, 2005; Carling *et al.*, 2006; Hashemi *et al.*, 2008; Uncles, 2010).

The general flow and tidal characteristics of this channel were summarised by Uncles (2010). At the mean spring tides (MST), the tidal currents could exceed 1 m/s and 2.5 m/s at the mouth of channel and in the upper channel respectively. Whereas the current speed at the mean neap tides (MNT) reduces by half but shares the same trend (Figure 3.4A, B). The Mean Spring Tides Range (MSTR), which is the difference in water-levels between mean high water and mean low water of spring tides, ranges from 3 m, at the shelf break, to 12 m, in the upper estuary. Inside the channel, Allen and Fulford (1990) have reported the mean high water Spring tides of the inner estuary as 8 – 8.5 m OD while Uncles (2010) reported the mean spring tidal range of the upper reaches increases from 7 to 12 m. The highest tidal range in the outer estuary is about 15 m and decreases in the upper part of estuary as an increase in frictional drag across the shallower bed (Uncles and Jordan, 1980). Besides, Mean High Water Interval (MHWI), water-level elevations during storm surge as well as the current speeds of storm surge were also explained. It can be summarised that the MSTR and MHWI share slightly

similar patterns in that the values of these characteristics of the inner channel are higher than the outer zone (Figure 3.5A, 3.2B). Water levels and current speeds influenced by storm surges were also illustrated in Figure 3.5C and D that water level would raise from 0.5 to 1.25 m in the outer channel while in the Bristol Channel the elevation could go up to more than 1.5 m. For the storm surge current speeds, the maximum increase of speed near the shelf break is about 0.2 m/s , growing to 0.4 m/s in the Celtic sea and drops again to 0.2 m/s in the Bristol Channel and in the upper estuary.

During Spring tides, the high and low water can vary by as much as 15 m. The maximal range of inland amplification of tides, exceeding 13 m, was recorded at Avonmouth on the coast near Bristol, which is in accordance with the record of tides 14.8 and 14.6 m high at Avonmouth stated by Allen and Fulford (1996) and Carling *et al.* (2006) consecutively. However, it was claimed that tidal range decreases further upstream to the River Severn (Archer, 2013). This high range leads to very strong currents, whirlpools and eddies, and large areas of sand, mud, as well as rocks exposed during the low water period (Somerville, 2005). Due to its high tidal range and the potential energy of tides within this region, the dynamics of sediments; erosion, transport, and deposition; could cause extreme and short-term variability (Archer, 2013).

Inside the estuary, the funnel-like channel is narrower than the outer estuary. Together with the high tidal range, the current speed within the upper estuary towards the estuarine head becomes stronger and leads to high turbidity. Moreover, the channel in the upper estuary becomes shallower and has fast currents. This results in the distorted temporal curves of water levels and currents, with a pronounced tidal asymmetry in which peak flood currents exceed peak ebb currents when river runoff is small (Uncles, 1981). Even if there is no exact evaluation for their relationship, fluvial discharge is likely to have an impact on tidal behaviour (Cai *et al.,* 2014). As the flood tides travel into the inner estuary, which comprise a narrowing and winding channel, tidal bores can be found in this region. This bore can be found from 16 km approximately downstream of Gloucester and it travels up estuary. The bore seems like a wave up to 2 m in height that travels upstream against the river current, breaking over bars and against the banks, through a reach that can be considered transitional fluvial-marine. The extent of the transitional reach has not been formally defined. Low salinities, turbidity maxima, high concentrations of floating woody-debris trapped at the head of the estuary, and the presence of both freshwater and marine fishes are considered to be evidence for this fluvial-marine transitional area (Allen, 1993; Potter *et al.*, 2001; Van den Berg *et al.*, 2007). However, distinct tidal bores form only during spring tides. In addition, the spring and autumn equinoxes together with spring tides can produce massive tidal bores every 130 days. An

anthropogenic influence reduces bore height and inland progressive of tidal bores, for example the channel-cross weir at Gloucester. The bore is used extensively for surfing and kayaking (Somerville, 2005; Archer, 2013).

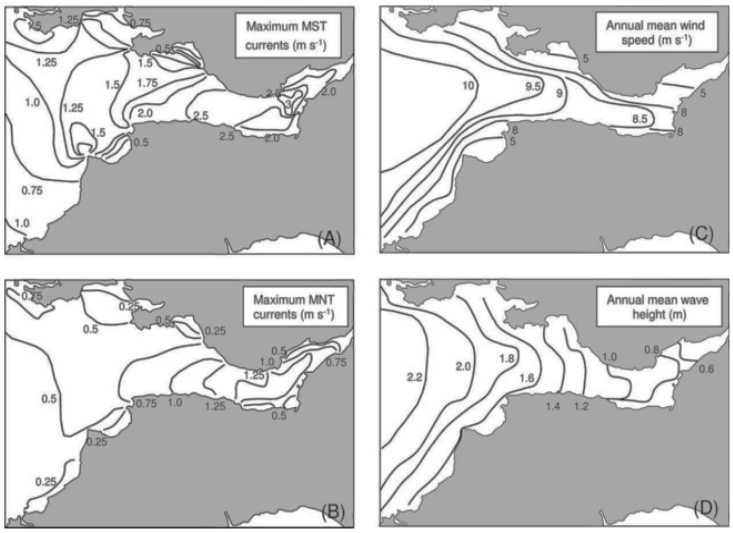

Figure 3.4 Simulated maximum tidal current speeds at mean spring tides (MST, (A)) and mean neap tides (MNT, (B)) together with simulated annual mean wind speeds at 80m above sea level (in m/s, (C)), and simulated annual mean significant wave heights (in m, (D)). Taken from Uncles (2010); his Figure 4.

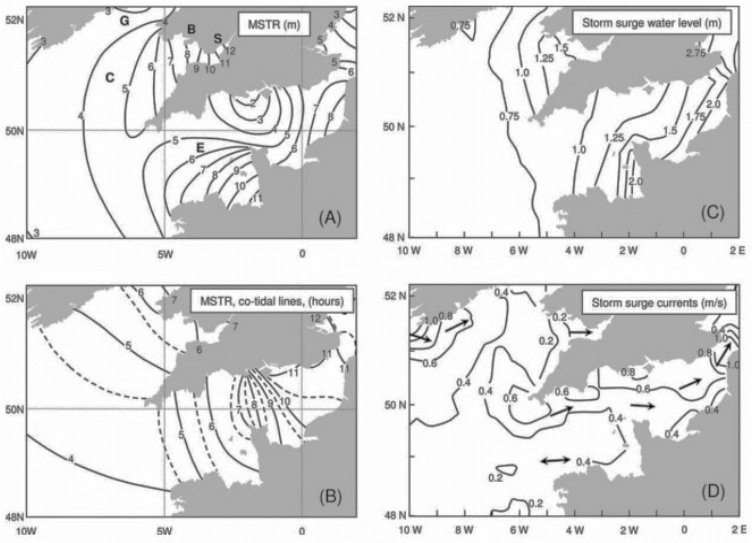

Figure 3.5 (A) Mean spring tidal range at a location ('C' = Celtic Sea; 'G' = St. George's Channel; 'E' = English Channel; 'B' = Bristol Channel; 'S' = Severn Estuary). (B) Co-tidal lines, drawn through locations of equal Mean High Water Interval. (C) Storm surge water-level elevations (in m). (D) The maximum expected storm surge current speeds (in m/s) for a 50-year return period. Taken from Uncles (2010); his Figure 1.

The time-series of predicted maximum and minimum tides over the study period represent the class 'A' tide gauge at Avonmouth (https://www.bodc.ac.uk/data/online_delivery/ntslf/#time_series), the closest station to the site. The available data used in this study, from 2010 to 2016, were from two sources. The first source (source A) is the software package, POLTIPS, produced by the National Oceanography Centre, UK (http://noc.ac.uk/tag/poltips). However, the data available from this software are for the period between 2014 and 2016, so the online data (source B) (http://www.tides4fishing.com/), was the other source to obtain tidal data from 2010 to 2013. However, initially comparing the overlapped data in 2014 from these two sources, revealed that some predicted values from both sources are slightly different. The statistical comparison (from data in January 2014) shows that the data from source A could be lower and higher than source B by 0.5 m and 0.3 m respectively (-0.5 m < source A-B <0.3 m). The average difference is about 0.1m lower (-0.1 m) and the standard deviation (SD), median and mode between both sources are 0.157, -0.1 and -0.09.

The predicted maximum and minimum Avonmouth tides from 2010 to 2016 do not show a significant increase or decrease during that period (Figure 3.6). Considering the whole series, the highest tide levels (Figure 3.7) have been stable, not highly fluctuated, such that the maximum tides could exceed 14 m OD, except those in the year of 2012 and 2013; most of which are below 14 m. Similarly, the lowest tides have not fluctuated much. In the years of 2012 and 2013, the lowest tides were not as low as the tides in 2010-2011 and 2014-2016 when the lowest were close to 0 m. Looking at the specific period of this study from March 2013 to March 2016, it can be seen that at the beginning of the study, 2013, there were lower maximum and higher minimum tidal levels and a slight change, ±0.5 m approximately, in the last two years of data collection, 2014-2015. These systematic changes are due to lunar and solar declination changes rather than the diurnal and semi-diurnal system. The maximum and minimum tides of the whole period from 2010 to 2016 and the values in each year are shown in Table 3.1. The highest tide reached 14.65 m on 21st February 2015 and the lowest tides was -0.19 m on 21st March 2015. The time-series of predicted tides within 7 years, 2010 to 2016, shows an extreme astronomical tidal range which the high tides could reach 14.6 m (Figure 3.7). There is a difference between the Spring and Neap tides in that the high tidal heights during Spring tides can be approximately 1.5 m greater than those in Neap tides (Figure 3.8). The mean high water during this study period is about 11.95 m. The majority of high waters is between 12-13 m, followed by 11-12 m and 13-14 m. While the predicted high tides that exceed 15 m have not existed in this period (Table 3.1). Compared with the previous studies (i.e. Carling *et al.*, 2006) at Hills Flats, the high tides are in the similar range of height. However,

the distribution of predicted high tides between 2010 and 2016 does not show any tide higher than 15 m. (Figure 3.9) unlike the tides in 2001 to 2004 when there was a number of tides exceed 15 m (Carling *et al.*, 2006).

The spring and neap tidal cycle close to the study site lasts for a month approximately. The duration of the Spring and Neap tidal cycles takes about two weeks (30 tides) each. During the transition period, the tide height is about 10 m and it increases to the peak of spring and neap tides during which the heights could reach 14-15 m (spring tides) and 12-13 m (neap tides). The increase in tide heights to the maximum Spring tides occurs over a week before decreasing to smaller tides, through a transition period, and then a similar cycle begins for the neap tides. Although the high spring tides are higher than high neap tides, on the other hand the low spring tides exhibit lower levels than low neap tides which can reach 0 m in contrast to slightly below 2 m for neap tides. A representation of predicted tide heights at Avonmouth changing between spring and neap tides is presented in Figure 3.10.

Investigating the annual predicted tide level in the study period, from 2013 to 2015 (Figure 3.11), the cycles of spring and neap tides can be clearly seen. However, around twice a year the maximum spring tide is as high as the maximum neap tide. This behaviour of spring tides exists twice a year (the tides in the black frame in Figure 3.11).

Table 3.1 Maximum and minimum predicted tides at Avonmouth from 2010 - 2016

Year	Maximum tide height (m)	Minimum tide height (m)
2010-2016	14.65	-0.19
2010	14.3	0.2
2011	14.2	0.3
2012	14	0.6
2013	14.1	0.4
2014	14.57	-0.15
2015	14.65	-0.19
2016	14.51	-0.01

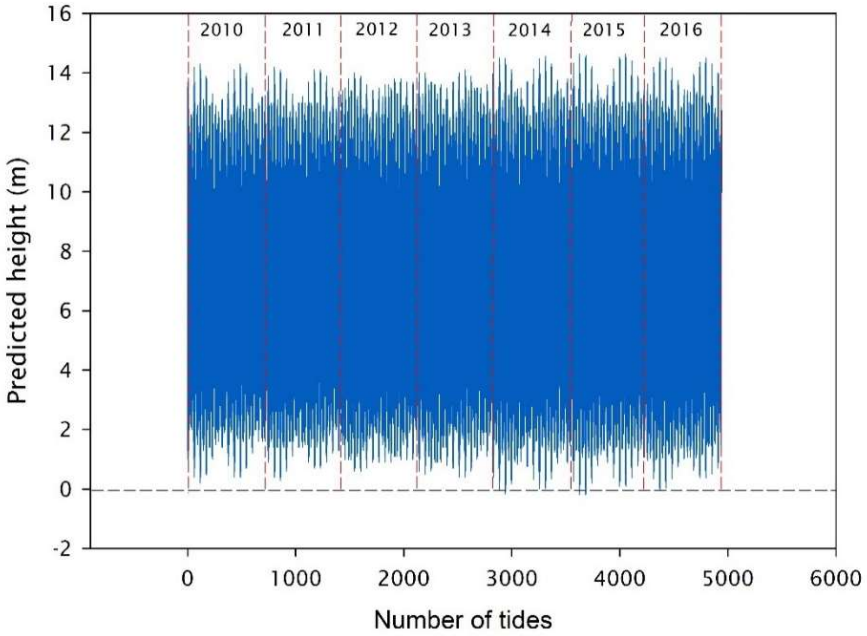

Figure 3.6 Predicted high and low tide height at Avonmouth 2010 to 2016

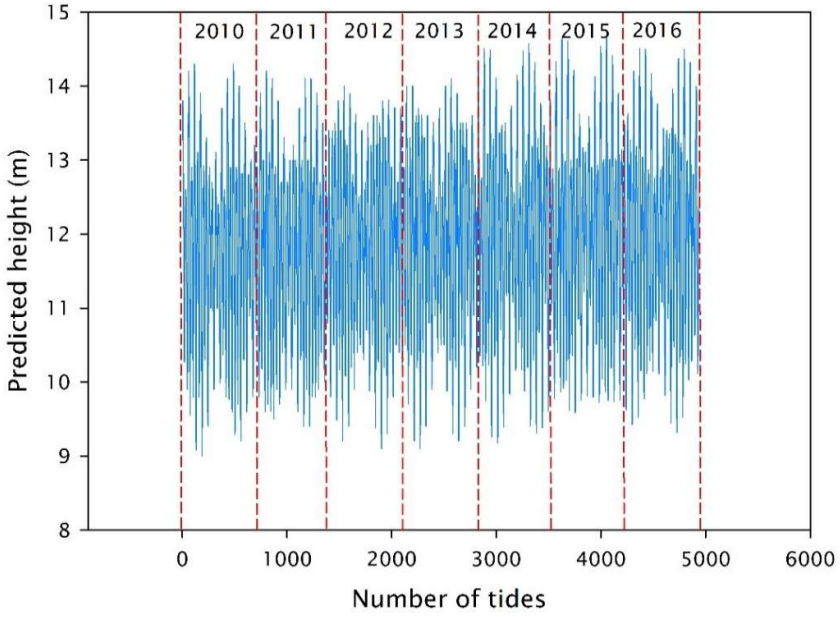

Figure 3.7 Predicted high tide height at Avonmouth 2010 to 2016

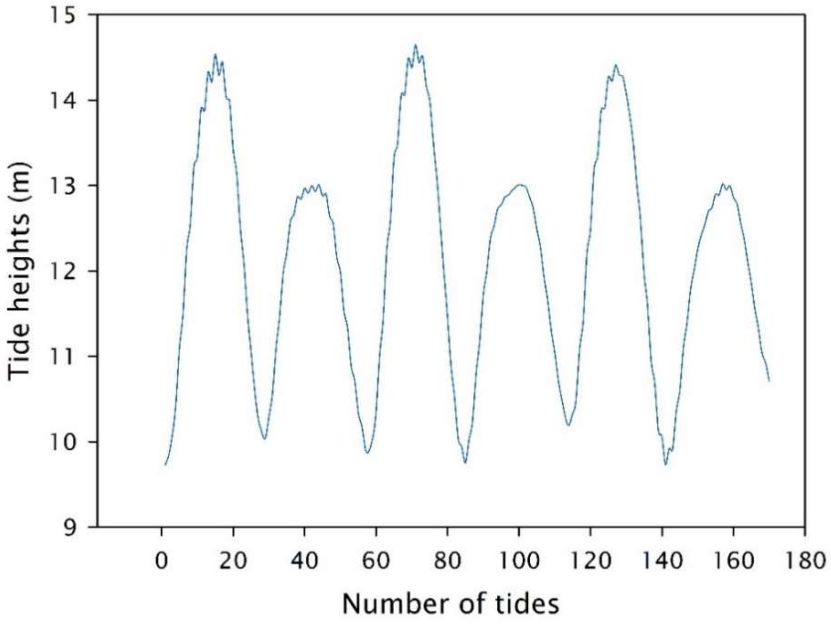

Figure 3.8 Representative series of predicted spring to neap tides (24th August 2015 to 20th November 2015)

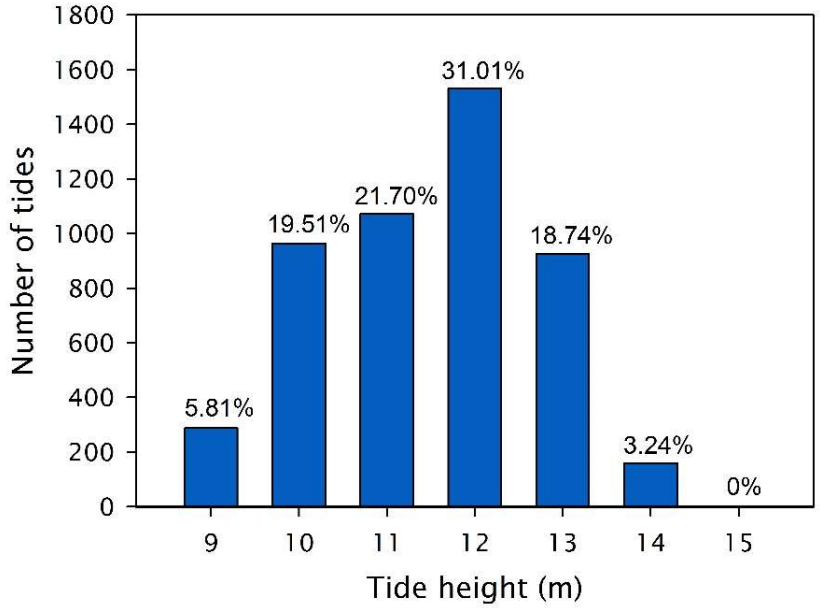

Figure 3.9 Distribution of predicted tidal heights at Avonmouth 1st January 2010 to 31st December 2016

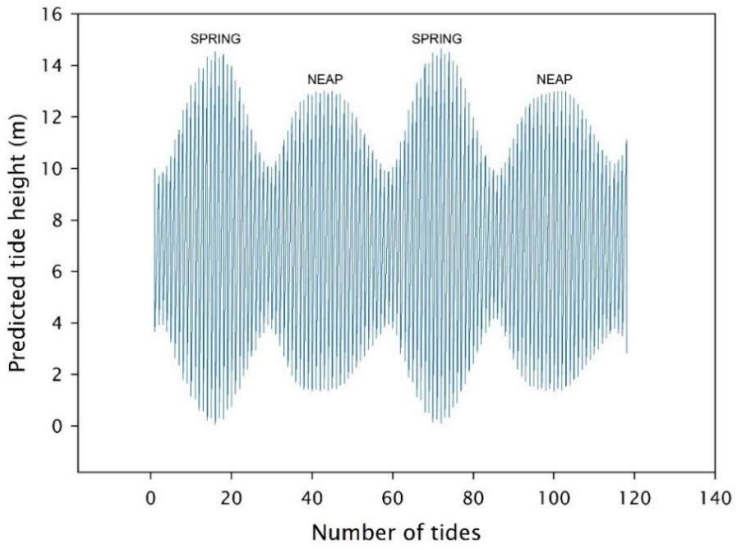

Figure 3.10 Representative of tides showing a trend of tidal cycle at Avonmouth from 24th August 2015 to 23rd October 2015

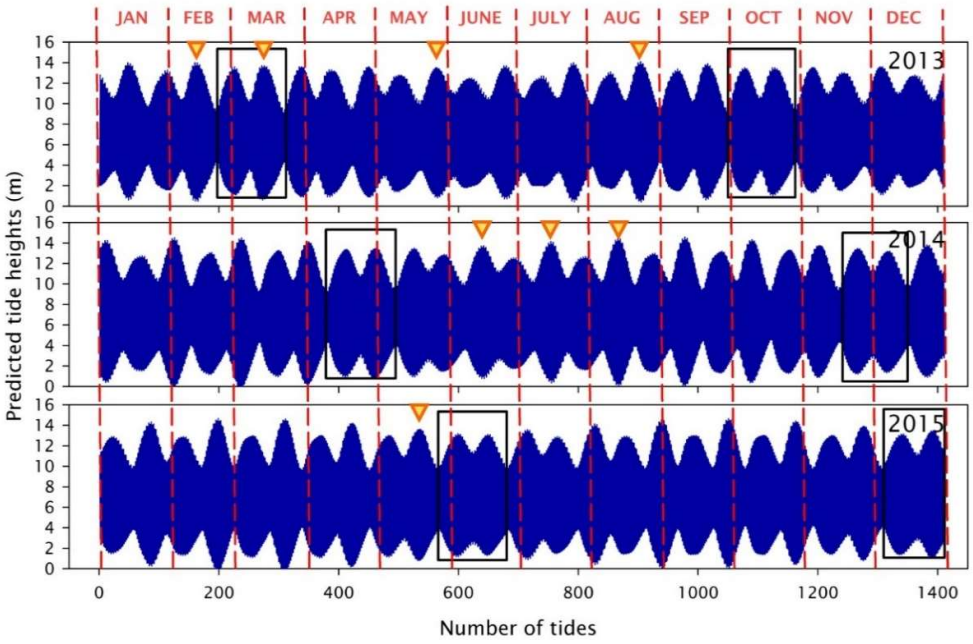

Figure 3.11 Annual predicted tides at Avonmouth from 2010 to 2016. The black frames show periods when maximum level of spring and neap tides almost equal and the period that spring tide exists following the previous tides without neap tides. The orange triangles show the time that data were collected.

3.1.4 Wind and wave regime

According to a numerical model of Pingree and Griffiths (1980), presenting currents on the sea shelf, there are two types of simulated steady winds; the southwest and southeast winds. Both winds are north-flowing across the Bristol Channel but have different impacts on the channel. The southwest wind, which approximates to winter conditions, produces the south-flowing return in the central St. George's Channel while the southeast wind produces no return flow. In addition, both winds have different impacts on water level in this region. During the southwest wind the inner channel has higher levels than the outer zone. In contrast, the water level of the outer channel is higher during the southeast wind (Uncles, 2010) (see Figure 3.5).

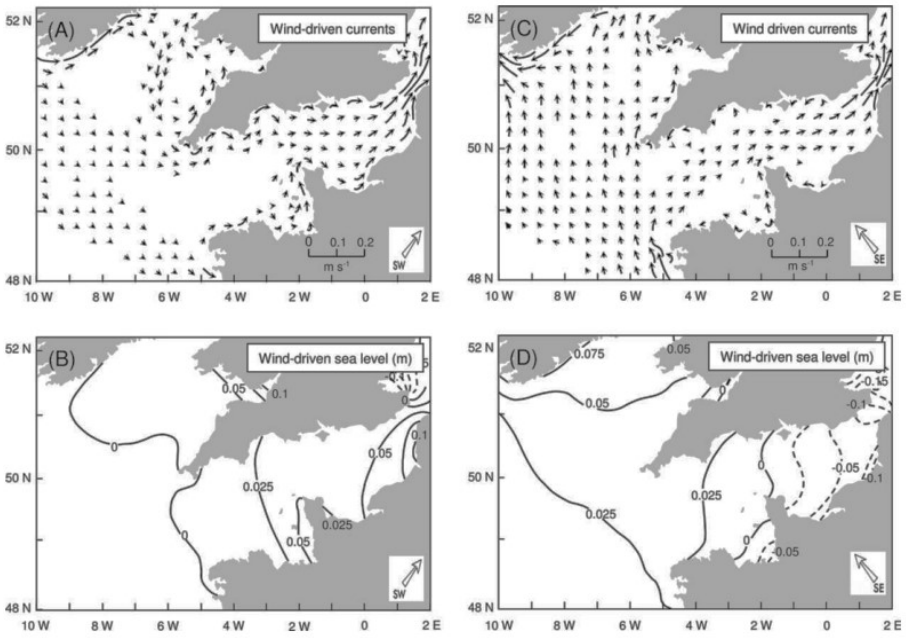

Figure 3.12 (A) Wind-driven residual currents resulting from a uniform southwest wind with a wind-stress of 0.16 Pa. The length of a current vector determines the strength of the current at its central point. The current arrows are slightly curved to conform to the direction of current flow. Only about one tenth of the current vectors have been drawn and values less than 0.0125 m/s have been omitted. (B) Sea level (in m) corresponding to the southwest wind residuals shown in (A); currents and water levels for a southeast wind with a wind-stress of 0.16 Pa are shown on (C) and (D), respectively. Taken from Uncles (2010); (his Figure 2).

For more details of the inner estuary, closer to the study site, Uncles (2010) also summarised and illustrates a set of maps using the modelled data of BERR (2004) (Figure 3.12). The mean sea level increases relative to land in the region and the sea level tends to rise about 5 mm per year in the upper Severn. The tidal current speed is dependent on the range of MSTR; the fast currents exist with the large MSTR. Moreover, the annual mean wind speed and annual mean wave height were also presented and it could be summarised that both wind speed and wave height are higher in the outer channel and tend to decrease in the inner channel and upper zone of the Severn estuary (Figure 3.12C and D). It is stated that the annual mean wind speeds from the mouth of the channel is around 10 m/s and decreases towards the middle reaches of the Severn. The annual maximum wind speed is in winter (12 m/s) whilst the minimum is in summer (7.5 m/s). This wind pattern conforms to the wave height pattern, both of which have the higher value in the outer channel and decline when they reach the inner and upper estuary. Draper (1991) showed that the waves in the outer channel are more than 3 m high for 10% of the year and fall to less than 1 m in the Severn estuary.

The studies of Allen and Duffy (1998a, 1998b) provides wind data at Avonmouth and a few data for Cake Pill which is situated between the study site, Hills Flats, and Avonmouth. According to these studies, two periods of wind data at Avonmouth were presented, from (A) 1970 to 1988 and from (B) June 1991 to June 1993. During these two periods the same trends occur; the wind speed is mainly in a range of 5.5-7.9 m/s (30%); followed by 3.4-5.4 m/s (27%), 1.6-3.3 m/s (17%), <1.5 m/s (11%) and 8.0-10.7 m/s (10%). Only a few occasions occur when the wind speed is greater than 10.8 m/s which is about 5% of the total data. There are some deviations between these two periods, when the average speed for period (A) and (B) was 5.64 and 5.06 m/s. For wind direction, there are various sectors represented in the whole data. Most winds blows towards 210˚-240˚ and 30˚-60˚. Moreover, it was also reported that detailed characterisation of waves in the inner Bristol Channel and outermost estuary, are restricted to a three years observation period (1979 – 1981). During this time the significant wave heights (H_s), which are greater than 1 m, were observed during 15% of the time and the extreme value could reach 3.5 m.

3.1.5 Salinity

Uncles (2010) observed the salinity in the Bristol Channel and Severn Estuary and reported that there are differences in the level of salinity. Salinity in the outer channel reaches 34.6 ppm (effectively seawater) in the west and decreases towards the inner channel where the salinity decreases to less than 2 ppm. This trend is related with the distance from the effect of

freshwater discharge from the rivers draining to the estuary, including the River Severn. However, it is stated that in the inner channel "there was a strong inverse relationship between tidally-averaged salinity and freshwater runoff into the estuary" (Uncles, 2010). In the estuary, salinity measured in the lower Severn has only a small difference between surface and bed and the salinity level decreases when the tidal range decreases. In the upper Severn, saline intrusion can occur as far upstream as Tewkesbury weir during high Spring tides (Figure 3.1) (Uncles, 2010; Carling *et al.*, 2015). Salinity at Tewkesbury weir usually equals zero and starts increasing from the weir downstream with a value greater than 25 ppm at 90 km from the weir near Avonmouth (Uncles, 2010). River discharge in the estuary and the River Severn have an impact on variations in salinity. During winter, the flow discharge is greater resulting in lower salinities in the estuary. This observation conforms to the study of Collins and Williams (1981) who stated that, in winter, salinity in the head of the estuary may be less than 20 ppm and decreases to zero in the tidal river Severn.

3.1.6 Sea level rise

There was also a report about sea level trends by Phillips and Crisp (2010). This study provided 15-year tidal gauge records (1993 to 2007) of mean sea level, maximum extreme sea level and minimum extreme sea level. The data, from four gauges (two in the outer channel and the others within the estuary), were analysed and compared together with others studies as well as the North Atlantic Oscillation (NAO) Index. Although, it is stated that the water level could vary due to different locations, results showed that trends of maximum sea level decreases, while the minimum sea level is increasing. This implies that the tidal range would decrease due to the convergence of maximum and minimum extremes. Mean sea level (MSL) has also been increased (2.4 mm/yr) and the projected of MSL for the year of 2050 is predicted as 0.370 m above OD With these changes, there might be impacts occurring to the environment and surroundings area as sea level has a causal relationship with several factors i.e. sediment supply, wave energy, probably leading to changes to flow conditions and bedform geomorphology.

3.2 Hills Flats

3.2.1 Location and geographical settings

Hills Flats, located at approximately 51° 40.45'N: 2° 33.24'W (Carling *et al.*, 2006), is in an intertidal zone on the Avon-Gloucestershire border in Severn Estuary, the inner zone of Bristol Channel and closed to the upper Severn zone (Allen and Fulford, 1996; Uncles, 2010). The site is on the left bank of the estuary in Southwest Britain and consists of a rock platform 3 km long and 650 m wide approximately and lies in north-east to south-west direction. The surface of this location is uneven with varied elevation, from the Ordnance Datum to a few metres above. The highest elevation is towards the landward area which is the location of an artificial sea bank along the shoreline of the Severn. Seaward of the sea bank there is rough pasture, followed by small near-vertical marsh cliffs, salt marshes as well as the bedrock platform. The lowest area of the Hills Flats platform extends toward the river in the north-west direction (Figure 3.13) (Allen and Fulford, 1996; Carling *et al.,* 2006).

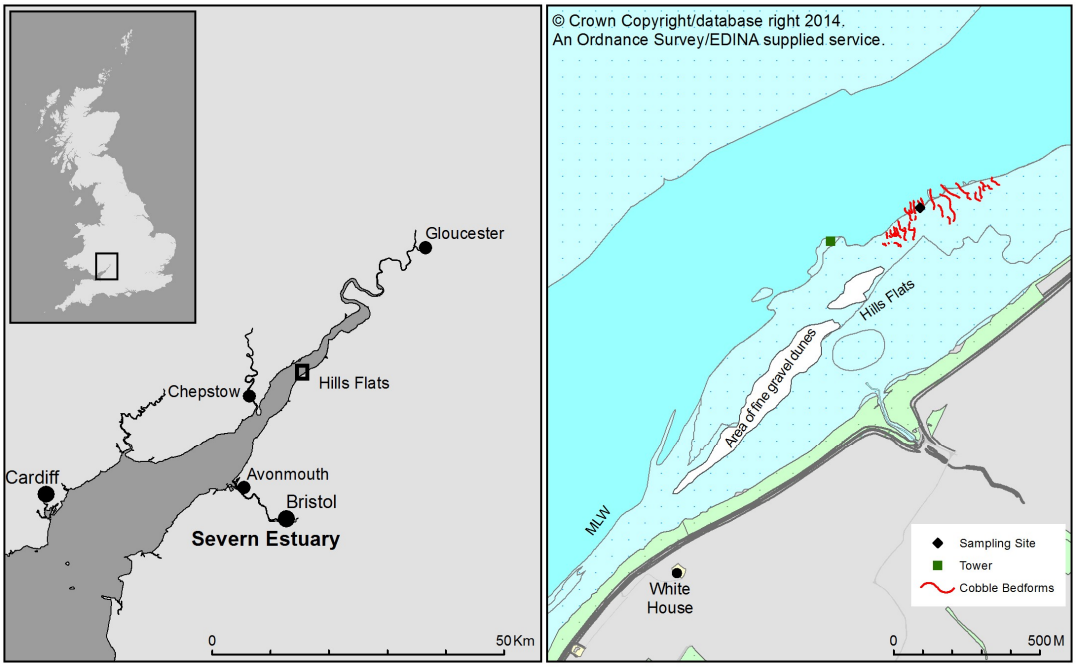

Figure 3.13 Location of study site, Hills Flats, Severn Estuary, UK.

3.2.2 Geology and sediment

Allen and Fulford (1996) provided some geological details of Hills Flats (Figure 3.14) that it is a rock platform on the left bank of the Severn Estuary. This area, lies on the Triassic Mercia Mudstone Group which is made up of parallel-bedded layers, 0.5 to 1 m thick, dipping towards the northwest (Welch and Trotter, 1961). The Flandrian Wentlooge Formation, which consists of green estuarine silt and brackish-freshwater peats, is found landward on this platform and in contact with the Triassic Mercia Mudstone group, which consists of red mudrock and muddy sandstones (Figure 3.14). Both of them are largely covered by contemporary sediments ranging from muddy-sandy gravel to mud. Apart from this, there are three other types of geological formations in the southeast of Hills Flats, with rising elevation towards the sea bank. These formations, appearing on a narrow belt of the active salt marshes along the bank, are the Rumney Formation, the Awre Formation and the Northwick Formation (Figure 3.14). On the surface of Hills Flats, a wide range of sediments occur; mud, sand, gravel, as well as cobbles and boulders could be found. They are transported during both flood and ebb tides and the residual sediment transport is downstream by the ebb tide.

While the inner part of bedrock platform is covered by a semi-permanent deposit of muddy-sandy gravel grading to mud with thickness of up to 0.4 m (Allen and Fulford, 1996), the active gravel dunes were found in the outer bedrock platform (Allen, 1993). Tidal currents are the important factor in deforming the sedimentary layer and result in a series of flow transverse fine-gravel dunes (Allen, 1993) which are two-dimensional with both straight and slightly sinuous crests. The gravel dunes, are found in the outer bed rock platform, close to the estuarine tidal channel (Figure 3.15). Dune crests are not positioned very close to each other. Their troughs are bedrock floored which may consists of large cobbles or thin mud layers. Moreover, there is also a thin covering of up to 20 cm of mud-infused fine gravel on the bedrock platform which may extend below these dunes (Carling *et al.*, 2006).

Carling *et al.* (2006) have studied the fine-gravel dunes at this site and provided some information of these dunes. The dune crests are exposed during the ebb tide, and exposed during low spring tides, while the troughs act as late-ebb drainage channels allowing water flow to the estuarine channel. The maximum dune height and length are 0.7 m and 7 m individually. Their orientations are north-west to south-east direction. The development of secondary dunes or gravel sheets were observed in the troughs and on the stoss side of the primary dunes during spring tides. The dunes seem to move in the north-east to south-west direction, parallel with the coast and channel. The variety of sediments found on the dunes

and in this area are generally from various sources: platy shale from local bedrock cliff and well-round, angular and blocky pebbles to cobble-sized clasts from gravel terraces in the estuary and a palaeosols atop the Triassic Group on Hills Flats. It is stated that mud, silt and sands, shells, and peat blocks are supplied by the reworking of Holocene sediments as ad-mixtures to the dunes. In addition, mud-drapes, formed by thin sheet of organic-rich silt and clay, are developed during high slack waters by deposition of the high suspended loads in estuary.

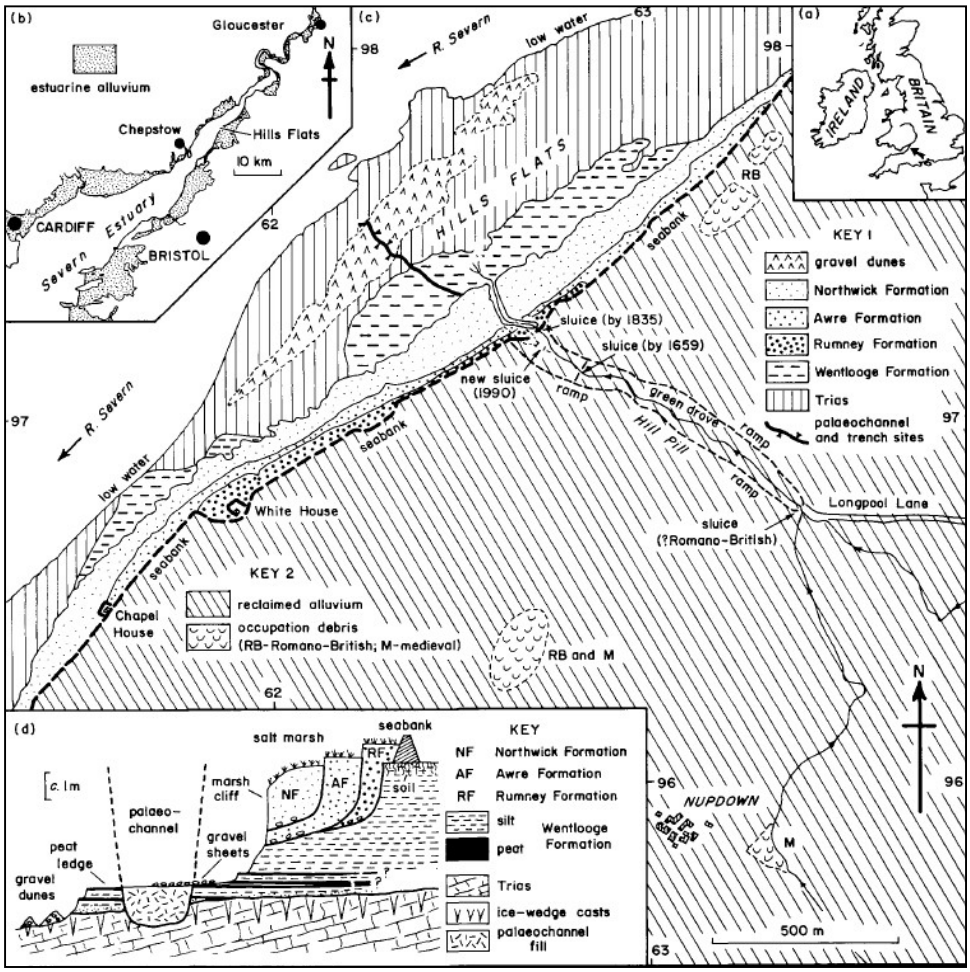

Figure 3.14 Location of Hills Flats, Severn Estuary and geology of Hills Flats and surroundings. Adapted from Allen and Fulford (1996; their Figure1)

Figure 3.15 Air photograph (900 X 1000 m) showing the coast in 1969 at Hills Flats. DF is Dunefield; S is seabank; M is active salt marshes; P is palaeochannel. Taken from Allen and Fulford (1996; their Figure2). Crown copyright reserved.

3.2.3 Tide and wave regime

Since Hills Flats is situated in the Severn Estuary, a part of the Bristol Channel, its tidal and wind-wave regime can be referenced to the general regime of the estuary and channel. Avonmouth is the nearest place to the study site which is able to provide records of the regime relevant to the site. The high tidal range recorded at Avonmouth, where the lowest elevation is -0.2m below chart datum (-6.7 m OD), could reach 14.6 m (8.1 m OD) in some years approximately. The mean of high-water spring tide (MHWST) is about 13.2 m (6.7 m OD) while the mean high-water neap tide (MHWNT) slightly declines to 9.8 m (3.3 m OD) (Allen and Duffy, 1998). However, Uncles and Jordan (1980) stated that the tidal range in the upper Severn, from Avonmouth to Tewkesbury, decrease due to lower tidal energy. In the estuary, tidal currents ranges from 1.5 m/s to 4.10 m/s which can be stronger due to storm surge conditions (Lennon *et al.*, 1963; Hamilton, 1979; Crickmore, 1982; Uncles, 1984; Carling *et al.*, 2006; Williams, Carling and Bell, 2006).

According to the studies of Carling *et al*. (2006) and Williams *et al.* (2006), the fine-gravel dunes on Hills Flats are submerged under water about 5 hours during the highest spring tides, but only 3 hours during the lowest neap tides. During spring tides, when the ebb tide duration

is 15% longer than flood, the water depth above the dunes could reach 6.5 m and current speed reached to 1.37 m/s and 1.3 m/s during the flood and ebb tides respectively. During the neap tides, which the duration of flood and ebb are similar, the water depth and current speed decreased. The water depth over the dunes reached only 1.3 m and the speed is 0.6 m/s and 0.23 m/s during flood and ebb tides respectively. Carling *et al.* (2006) stated that unevenness of these properties; flow speed and flood and ebb durations, can be related to the internal sedimentary structure development. Considering the wind-wave regime, though there was a report of waves 1 to 2 m high existing in the main channel of the mid-estuary (Allen and Duffy, 1998; Williams *et al.,* 2006), where is close to Hills Flats, the study site is protected and less effected by sizable waves (< 0.4 m). Moreover, the local wind data show no significant wave action and no significant waves existed during study periods (Carling *et al.,* 2006; Williams *et al.*, 2006).

3.2.4 Suspended sediment

The turbidity in the estuary is high with fine sediment concentrations of which the highest value is found in the winter months (Allen and Duffy, 1998) and it was considered that, in the intertidal zone, there might be large quantities of muddy sediment deposited and resuspended during individual tidal cycles. This results in silt and clay can be found in the void space of the gravel framework in a variable amount (Williams *et al.*, 2006). However, studies of suspended sediment processes in the area of Bristol Channel and Severn Estuary were largely focused on the inner channel and lower estuary as mentioned in section 3.1.2. There is limited information of the suspended sediment over Hills Flats. However, there are a few numbers of studies done in Hills Flats and the vicinity (i.e. Allen and Fulford, 1996; Carling *et al.*, 2006; Williams *et al.*, 2006; Carling, 2013). Among these studies, Carling (2013) measured and provided some background of suspended sediment in this area. The study investigated sub-tidal 'yardangs' in the same area as the cobble dune field of this study. The suspended sediment was observed in this study that during the flood tide, suspended sediment concentrations (SPM), at 0.40 m above the bed, increased from 148 mg/L to 654 mg/L just before high slack water. Carling (2013) also stated that "concentrations fell at high water, spiked on the first ebb-flow to 749 mg/L (presumably as slack-water settled sediment was resuspended from the bed) and then oscillated during the ebb flow (average ebb concentration: 145 mg/L; SE = 22 mg/L)." Moreover, this study also provide grain size of suspended sediment measuring in different heights; 35, 45, 55, 65 and 75 cm above the bed. Coarse granules were found as a significant component in suspension up to 0.45 m above the

bed, but above this level, suspended grain size distribution is uniformly similar with finer grains, from silt to 0.25 mm sand. However, there are differences in the component of coarser grains at each elevation.

3.2.5 Coarse gravel dunes on Hills Flats

Dunes in the present study consist of coarser sediments than those in the fine-gravel dunes reported by Carling *et al*. (2006) and Williams *et al*. (2006). These coarse-gravel dunes upstream on the north-east side of the fine-gravel ones and further offshore. The initial survey of coarse-gravel dunes shows that the dunes are large with straight or slightly sinuous crests, elongate into the sub-tidal water, and lie in the same direction as other dunes on Hills Flats (Figure 3.16). Differently, the dunes in the present study consists of large-size sediments, e.g. cobbles (Figure 3.16). However, the details of dune dynamics and internal structure, which are not well studied yet, will be further investigated in this research.

Figure 3.16 The view of the study site; (Top) A panoramic view of coarse-gravel dunes from near-shore towards the Severn estuary.; (Bottom left) View from landward along the crestline of a dune.; (Bottom right) Large-size cobble sediment existing on the top of the dunes.

Chapter 4: Methodology

This chapter describes the methodology for this research topic. In order to understand the processes of dune development, the important factors having effects on dune dynamics should be investigated. Data used in this study are mainly derived from fieldwork study. Several techniques were selected to collect data relating to estuarine bedform morphology and can be organised into three main sections following the theory of bedform process: form, flow and sediment (Leeder, 1982).

To study dune dynamics and changes in form, the main purpose is to investigate shape, size, position and pattern of the coarse gravel dunes existing at the field site. Current meters were deployed to collect general flow properties over the bed to explain the hydrodynamic condition of the stream flow impacting the dune form. Lastly, data related to bed sediments, bedload transport and suspended load dynamics were also collected to provide detail of the background and quantify basic sediment transportation that may relate to the development of coarse gravel dunes in the tidal flow. All fieldwork tasks are summarised in the end of this section (Table 4.4).

4.1 Form investigation

4.1.1 Morphology of dunes: shape and position

The morphology of the dunes was determined using survey equipment: a differential Global Positioning System (dGPS) and a Total Station. The dGPS is "a method of providing differential corrections to a Global Positioning System (GPS) receiver in order to improve the accuracy of the navigation solution." (Australia Maritime Safety Authority, 2015). This survey equipment provides more precise positions than normal handheld GPS. Figure 4.1 shows the principle of dGPS. The equipment is divided into two main receivers; a base station (or ground base station) and a roving GPS receiver. The ground base station (point A in Figure 4.1) is set up on the Earth surface with a precisely known location. It works by tracking signal from satellites and calculating its position. Knowing the base position and connecting to satellites, the equipment can calculate "the differences between the actual measured timings and the theoretical predicted signal timings from each satellite" (Lisle *et al.*, 2011). This procedure provides 'error correction' applied to the GPS data that are transmitted to the receiver (rover unit; point B in Figure 4.1) (Lisle *et al.*, 2011). DGPS has been used in a wide range of fields

which need high accuracy of study location, for example yield monitoring systems in agriculture (Whitney *et al.*, 2001), maritime navigation (Australia Maritime Safety Authority, 2015), and geological and geomorphology studies (van Lancker *et al.*, 2004; Knaapen *et al.*, 2005; Barnard *et al.*, 2006; Pearce *et al.*, 2006; Barrie *et al.*, 2009).

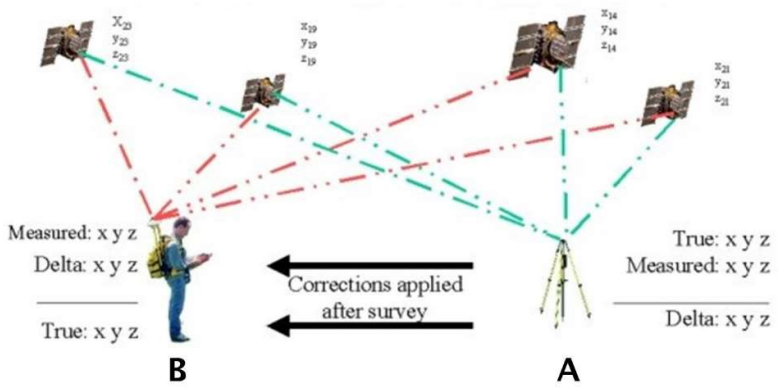

Figure 4.1 The principle of differential GPS (dGPS) systems: A) a base station which communicates with satellites and transmitted the corrected position to B) a rover receiver (image source: EO-MINERS (2015)).

A Total Station is "a modern surveying instrument that integrates an electronic theodolite with an electronic distance meter" (Jurovrich Surveying, 2015). This equipment consists of a horizontally mounted telescope that is free to rotate in both the horizontal and vertical plane (point A in Figure 4.2) measuring the angle of the telescope relative to the horizontal (θ in Figure 4.2). An electronic distance meter (EDM) is also in-built to measure the travel time of an emitted pulse of low-power infrared laser energy to a prism reflector mounted on an adjustable rover held by a second person at a survey point (point B in Figure 4.2). The prism reflects the laser energy back to the station which results in an average value for the speed of light in air and a distance with millimetre precision is calculated by the laser reflection travel time (Lisle *et al.*, 2011). A Total Station, similar to the dGPS, is widely used in many scientific fields such as engineering survey, cadastral survey, mine survey as well as geological survey (Keim *et al.*, 1999; Feng *et al.*, 2001; Nainwal *et al.*, 2008).

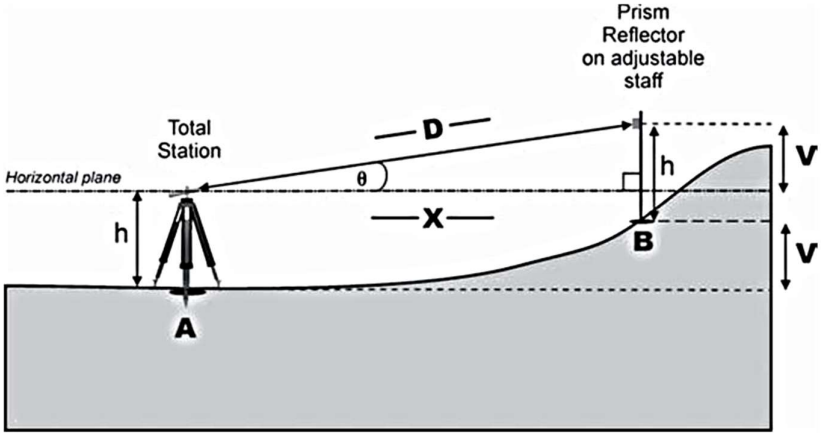

Figure 4.2 The principle of making measurements with a total station (from Lisle et al., 2011)

The dunes were surveyed 15 times from February 2013 onwards (see details in Table 4.1) during ebb spring tide periods when water level is low enough and allowed dunes to be exposed. This footwork survey could be done when the water level is lower than 1 m OD. The closest tide gauge to the site for tidal level data is at Avonmouth, approximately 20 km downstream from the site, resulting in around an hour delay of lowest tide on site (details of water level for fieldwork are shown in Table 4.5) when compared with the predicted time at Avonmouth. The duration of the low water level over the study site is about 2-3 hours, hence there is a significant time limitation in completing data collection. Twenty to thirty dunes are exposed along the edge of the rock platform, most of which align in a northwest-southeast direction (Figure 4.3A). The results of repeated surveys provided the positions and shapes of the dunes after the ebb flow such that the data may indicate any planform changes over time. The model of dGPS unit that was used consisted of a Leica GS09 and CS09 controller. The unit can measure up to a range of 2 km. The antenna has Global Satellite Navigation Surveying Systems (GNSS) technology which can provide good quality measurement with an accuracy of 1 mm for standard mode (Leica Geosystems, 2013). The antenna connects to the controller by Bluetooth connections (Leica Geosystems, 2009). For the total station, the model used is a Leica TCRP1205+ R1000 Reflectorless Robotic. This equipment has a search feature which will search and track the targeted prism automatically allowing the survey to be done by only one person. The maximum range of survey with a single prism is 3 km. There is also a remote controller for the total station which connects to the base station by Bluetooth (Leica Geosystems, 2013).

In the field, the survey unit, either dGPS or Total Station, is separated into two parts; base unit and rover unit. Firstly, the survey base unit, including the antenna, was installed on the

estuarine flood control embankment, approximately 300 m from the dunefield (Figure 4.3 and Figure 4.4A) and is located with unimpeded visibility of the survey rover equipment. The base station, for every survey, was set up at the same location to avoid errors. The estuarine embankment is the suitable location for the base station as it is high enough to avoid any physical barriers and allows it to communicate with the rover unit more easily. Moreover, this location is in the range that the rover and base station can link properly during the survey. The system was set up with the coordinate system of Ordnance Survey National Grid reference system also known as the British National Grid.

Once the base station is set up a footwork survey could be completed by using a rover with its remote controller (Figure 4.4B). At the beginning of survey, a number of control points were selected as reference locations to tie-in repeat surveys. The more control points used, generally the better the accuracy. The selected control points must be at the same positions in every survey. In this study, there were ten control points; six points on fence posts and field gates, and the other four at the base corners of a steel navigation tower next to the dune field in the estuary (Figure 4.3B and C). After all control points are recorded the dune survey begins. At this stage, the auto-survey mode was used to record X, Y and Z positions which are easting and northing, and heights of dune crest lines. The automatic mode records the data every second as the rover is moved along the dune crests which a visually determined high point with an error of ±50 cm in its lateral location, giving surveyed points every 1-1.5 m approximately.

The Total Station was used for the survey for a couple of times instead of the dGPS due to the availability of equipment. The process during fieldwork is similar for both instruments. Firstly, a survey point (base station in Figure 4.3) was set up at the same position as the dGPS base unit and the rover was used to survey locations (Figure 4.4C). Similar to the dGPS, manual mode was used to record control points while the dune crests were recorded by automatic mode for every second. The base and rover units communicate by radio signal. Normally, the measurements require two persons to operate the total station and to move the target reflector. However, it is possible for one person to make measurements with this equipment by using a remote controller which can be installed on a roving pole (Figure 4.4D). The 360° prism is used as a target in every survey with the total station which can automatically search for the rover and is controlled remotely. To measure the distance, the base station emits a red laser beam to the target which is reflected back to the station and results in the calculated distance and angle between each location and the base.

The data recorded in the field were later exported and converted into a computer system in comma-separated values (CSV) or text file format. Each dataset contains information of easting, northing, height and coordinate quality of data point showing an accuracy about ±0.01-0.02 m. These formats allowed input into ArcMap software (version 10.1) to map the dune with regards to real world coordinate positions and to illustrate dune planform shape changes. All data were plotted as points on a map such that later the data points defining the dune crests could be created as lines showing a better picture of the dune crestline planform. Apart from the planform, it is possible to measure the distance between each dune and the reference points, like the tower. Last, a series of dune survey data could be overlaid and used to compare changes through time. An example of the mapping result can be seen in Figure 4.3A.

However, the coordinate system in Total Station is set up arbitrarily on site, hence they need to be linked to the real coordinate with dGPS data by matching all control points prior to plotting a map and comparing with other datasets.

There were some problems in the footwork survey data. The main issue is related with the selection of control points. The field site is a wide and open area. There are not many fix objects close to the dune field that can be used as control points and the good quality of control points should surround the survey site as much as possible. For the initial surveys, only the four corner of the navigation tower were used and these closely spaced controls were found to be inadequate, resulting in the initial data containing errors. The errors originate from the distortion of control points at the four corners of the green tower base which should plots a square shape but instead plotted as a diamond or kite shape. These errors occurred in a number of survey data (see Table 4.1 for details). As a result, the errors need to be managed. A correction was applied by an application of LEICA Geo Office software (version 7.0.0.0), provided by Leica Company, and ArcMap (Version 10.1). A high-quality dataset surveyed in 19th September 2013 was used as a reference in order to remove errors in early survey control points. The reasons for selecting this dataset is that they show no distortion as well as containing additional control points added during the later surveys which make the data more reliable. Moreover, these data contain the lowest 3D co-ordinate quality (3DQ) value which is a measure of estimated error (≤ 0.01 m approximately) indicating that they have very good quality. The process starts from importing the dataset which need correction as well as the reference dataset into LEICA Geo Office software. The reference points, which are common, in each dataset were manually matched. The coordinate positions of corrected dataset were then automatically calculated and shifted to the right positions. Once all data were corrected, they

were saved in ASCII format which can be used in ArcMap to compare reference positions with a base map and plot a dune map. Besides, there were a few other technical issues such as low quality signal, weather limitation, as well as disconnection between base station and rover unit. These problems were managed in the field by resetting the equipment as required.

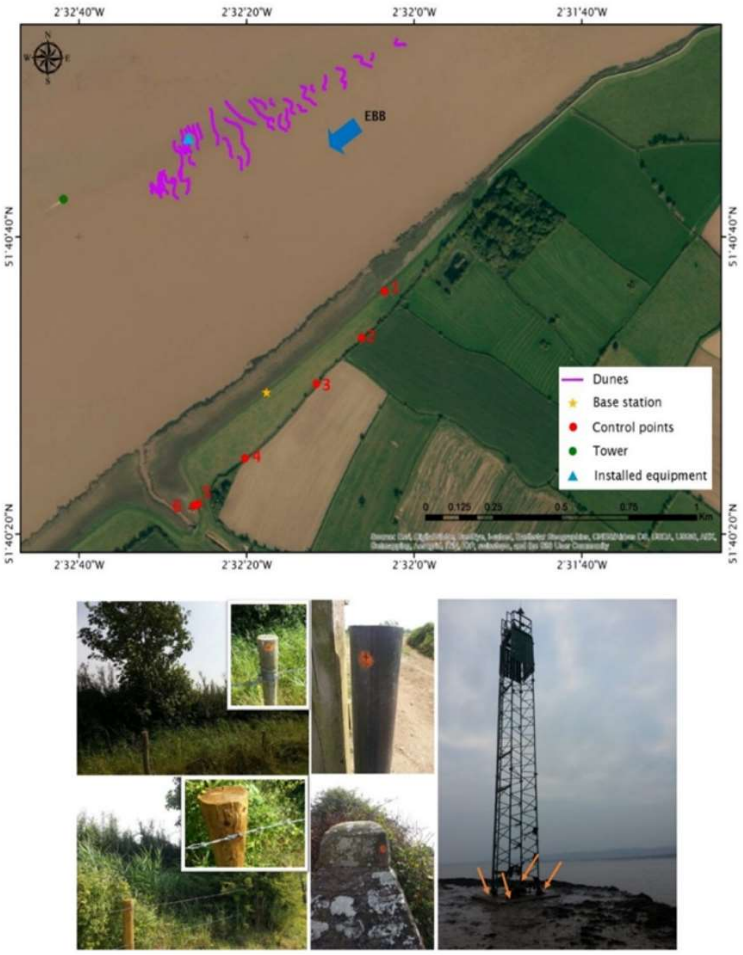

Figure 4.3 A) A map of the study site showing the location of the cobble dune field in the Severn Estuary. The Base unit of survey equipment, dGPS and Total Station, is set-up on the river bank (yellow star). The control points are along the estuarine margin; six points (red dots) are located on the fenceline landward of the sea bank while four other control points are at the navigation tower in the estuary (green dot). Equipment used to collect field data, e.g. sediment traps and current meters, are set up in the middle of dune field (blue triangle). B) Examples of control points on the fence (no. 1-6 in the map above). C) A navigation tower in the river. The arrows show positions of control points at the tower.

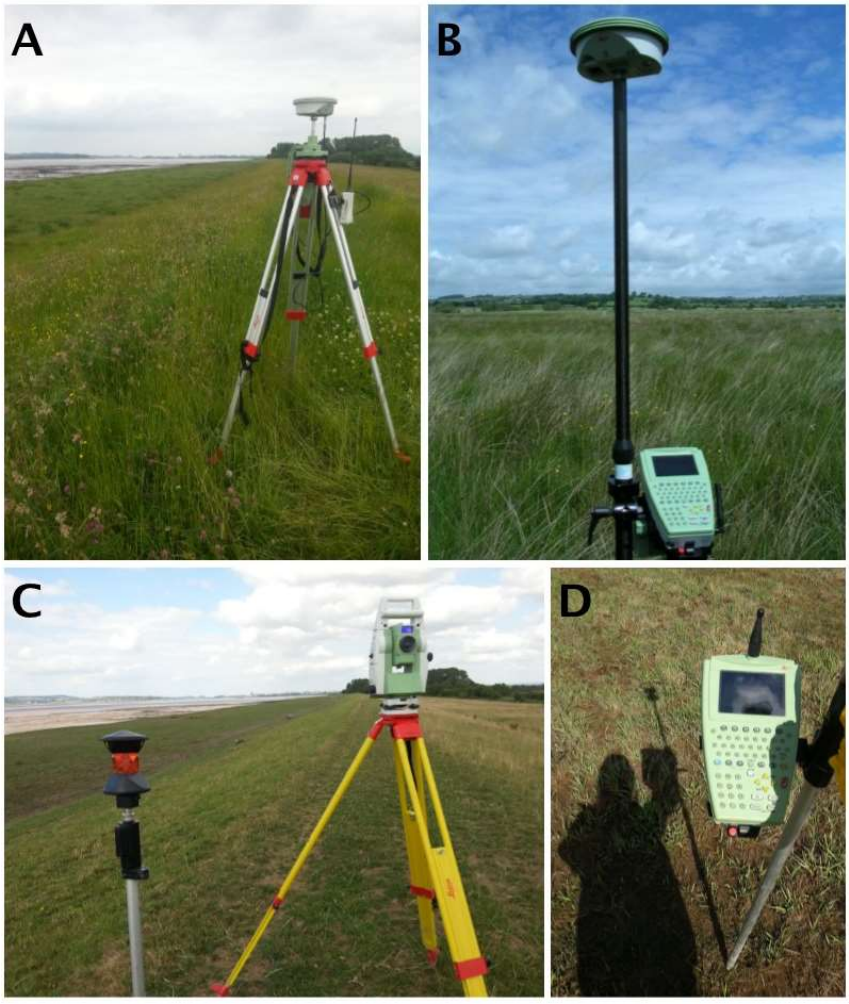

Figure 4.4 Survey equipment used in the site survey; A) The dGPS base station is set up on the estuary bank with the estuary on the left; B) The dGPS rover receiver with a controller is used to manage files, record data, and send commands to the equipment; C) Total station is set on the estuary bank at the same position as the dGPS and a 360°prism mounted on a roving pole to be used as a target in measurement; D) A total station controller is an optional device installed on a rover. It is used to control the equipment remotely in case that the survey is done by only one person.

4.1.2 Morphology of dunes: dunes surface

A survey of dune surface was done by using the Terrestrial Laser Scanner (TLS), also known as ground-based lidar. TLS provides high resolution (could be less than a centimetre) of topography of surfaces. It is widely used in many studies related to the Earth sciences and geosciences (UNAVCO, 2016). The TLS survey was done on 14th and 15th July 2014 to observe short-term change over the dune after two tidal cycles.

The scanning was done on dune number 12 where all the equipment, flow meter, impact sensor as well as brick tracers were set for this study (Figure 4.3 and 5.9). A Leica ScanStation C10 TLS, using a 532 nm visible wavelength green laser (Leica Geosystems AG, 2011), was used for this survey. Surveys were undertaken with a resolution (point spacing) of ~0.005 m at 10 m, resulting in models with a consistent resolution of 1 cm or better. In the field the station was set up on both sides of the dune and four targets were attached to tripods which were set on both bedrock and other dune crests where metal pins were fixed to the bed to indicate the reference point for the resurvey on the 15th July 2014 (Figure 4.5).

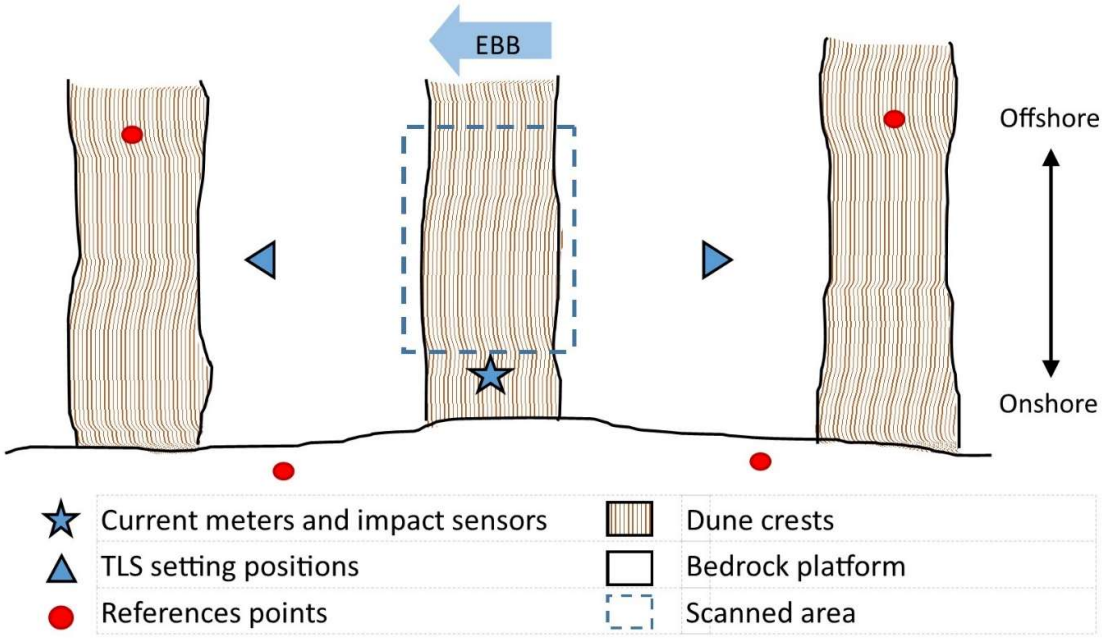

Figure 4.5 The illustration showing the approximate positions of Leica ScanStation C10 and reference points set on the bedrock platform in order to scan the surface of dune number 12 (Figure 4.3 and 5.9) between 14th and 15th July 2014

Table 4.1 Details of topographic survey with the dGPS, total station (TTS) and Terrestrial Laser Scanning (TLS) completed during fieldwork

No	Date	Equipment	Note
1	11 Feb 2013	dGPS	The positions on the map were distorted due to the error of coordinate set up and lack of control points (only the tower points were used at that time). The data then were corrected in GeoOffice software by using data collected in September 2013 as a reference.
2	12 Feb 2013	dGPS	
3	11 Mar 2013	dGPS	
4	12 Mar 2013	dGPS	
5	13 Mar 2013	dGPS	
6	27 May 2013	dGPS	
7	26 June 2013	Total Station	More control points were added in field survey. So the data have less error when they were plotted on the map. However, TPS data do not contain real coordinate positions so they have to be tied with the coordinate system in GeoOffice software by using data collected in September 2013 as a reference.
8	23 July 2013	Total Station	
9	24 July 2013	Total Station	
10	20 Aug 2013	Total Station	
11	19 Sep 2013	dGPS	Data collected on this day are the most reliable as there are enough control points and all the data are already tied with coordinate coordinate system. Hence this dataset is used as a reference for other datasets
12	20 Sep 2013	dGPS	The data contains low quality. The 3DQ during the survey was higher than 1m and could not be adjusted on site.
13	18 Mar 2014	dGPS	Survey was completely done with good quality (3DQ ≤ 0.02m).
14	19 Mar 2014	dGPS	Only control points were recorded due to time limitation.
15	16 June 2014	dGPS	All data, including control points, were shifted from the referenced data on 19 Sep 2013 (approx. 2.7 m to the south-west direction).
16	14 July 2014	TLS	Dune surface measurement, completely done
17	15 July 2014	TLS	Resurvey of dune surface, completely done
18	29 Sep 2015	dGPS	Completely surveyed with good quality (3DQ ≤ 0.02 m)

4.1.3 Morphology of dunes: longitudinal cross sections

Apart from measuring the planview shape and position of the dunes, general information of dunes in the cross-sectional profile is also need to be observed as background for further study of dune structure. The dGPS and total station were employed to create the longitudinal cross sections of dunes in order to illustrate the dune profiles. The measurement was done twice: in August 2014 (with dGPS) and September 2014 (with total station). A number of dunes were sampled for this survey; 12 in August and 6 in September. These dunes are in the middle of the dune field, including one where the hydrographic equipment was installed (Figure 4.6). The heights of dunes were measured every 50 cm across the dune surface, from the dune toe to the other side, in a down-estuary to up-estuary direction. The start of each transect was perpendicular with toe lines and extends towards the other side which was also perpendicular to the toe line (Figure 4.7).

Data from cross-section measurement were later imported to be processed in Microsoft Excel 2013. At this stage, the values of dune height were extracted from the dataset and plotted in the form of XY diagrams. The Y axis presents height while the X axis show the distance across a dune.

Results from fieldwork surveys provide the detailed information on longitudinal shape of dunes after ebb tides. Parameters of dunes (Figure 4.8) can be extracted from these transects following Carling *et al.* (2006). These parameters include; steepness (L_2/H), flatness index (L_1/L_2), lee and stoss slope angles (α, β), residual migration rate (from dGPS), flatness index (L_1; near-horizontal surface; where present), and asymmetry (L_U/L_D). However, it was suggested for the dunes with a definitive, single, crestal high point that asymmetry is the proportion of L_U and L_D on either side of H. While asymmetry of dunes with flat horizontal crest was "defined relative to the lee side termination of L_1"(Carling *et al.*, 2006).

However, this method provides only general characteristics showing the outline of dune structure. Details of the dune stratigraphy and sedimentology were investigated by trenching the dunes on 10th March 2016. Two longitudinal sections were opened and cut down to the bedrock surface through dune no.12, where the flow equipment was installed, and dune no.15 by using spades and shovels.

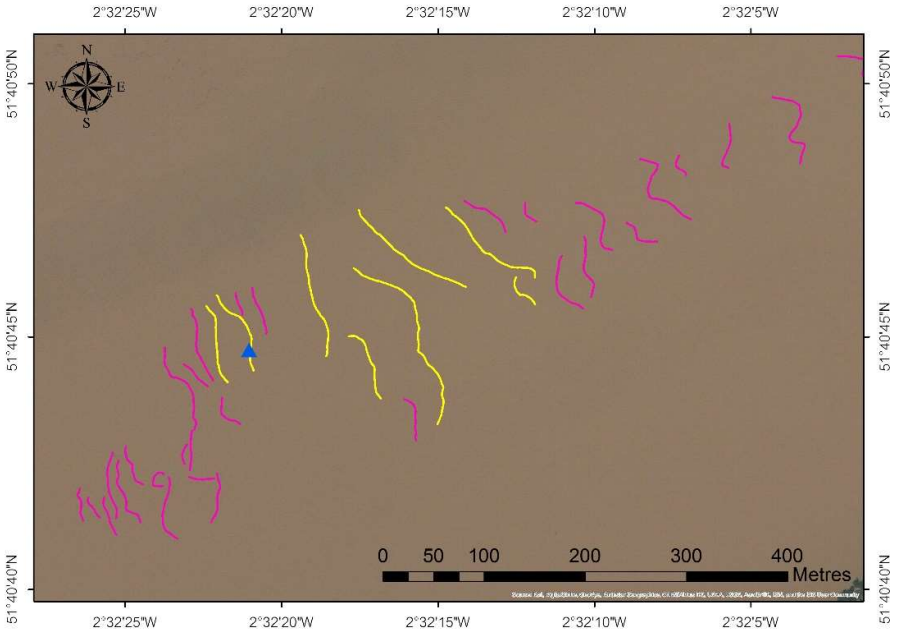

Figure 4.6 The map shows the area of dune field in September 2013. Seven dunes selected for cross-section measurement are in the middle of field and presented as yellow lines. The blue triangle is the location of flow meters.

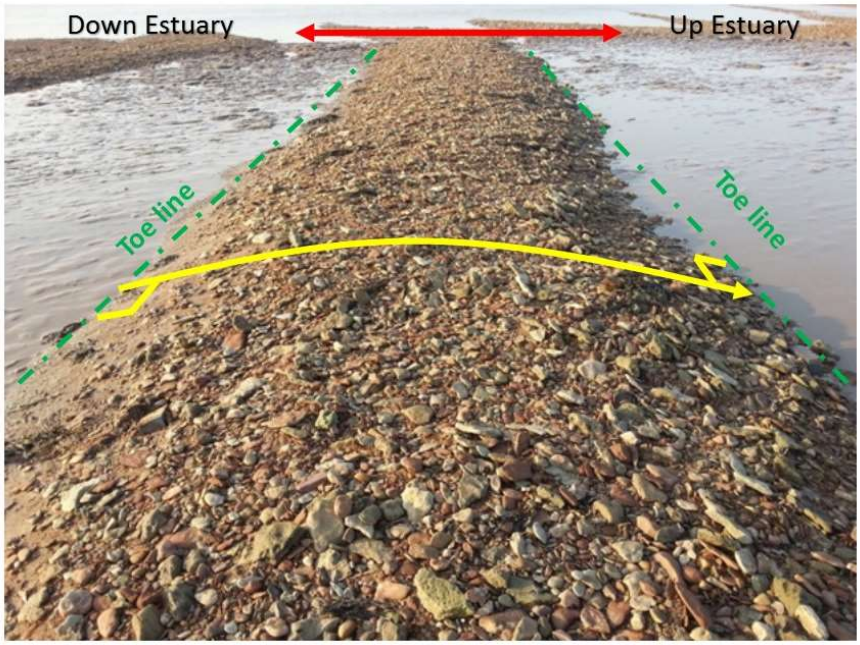

Figure 4.7 Direction of cross-section survey. The measurement starts from down estuary toe to up estuary toe for every 50 cm. The start and end points are perpendicular to toe lines.

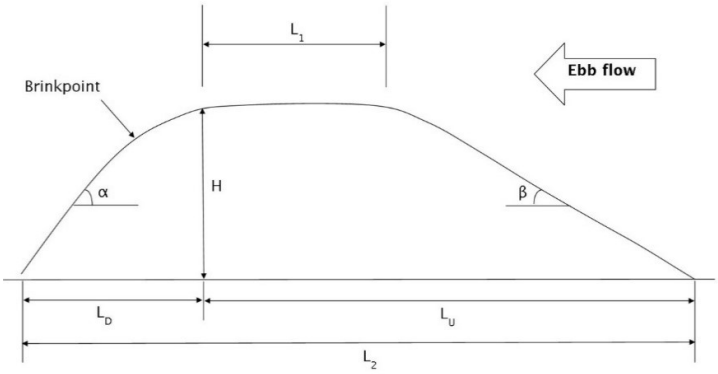

Figure 4.8 Diagram of dune transect parameters (redrawn from Carling, 2006)

4.2 Flow measurement

4.2.1 Hydrodynamic data

Valeport electromagnetic current meters, model 808, were deployed to collect the data of flow properties across the dune field. The current velocity which can be recorded by the meters ranges from 0 to 5 m/s and the accuracy is ±0.01% for reading recorded as m/s. Apart from current speed, the meters can record current direction, temperature and pressure. The pressure is important to aid calculation of water depth over the measured location which will be described later. The standard capacity of the memory is 128 kbytes which provides over 8500 records of flow conditions (60 days at 10 minute sampling). The power supply of the meters is a removable battery, Integral 8 “D” cells (alkaline) (Valeport Limited, 1998).

During the lowest water when the dunes are exposed, based on predicted tidal heights of between 0.22 m and 14.35 m at Avonmouth, they were set up initially on aluminium tripod frames fixed to flat bedrock 10 m approximately to landward of the gravel dunes selected for hydrographic survey (see blue triangle Figure 4.3 and Figure 4.6), at different heights ranging from 0.15 to 0.50 m (Figure 4.9). In 2014, an aluminium scaffold was constructed on the dune crest, replacing the tripod. The scaffold is more durable and more adjustable to fit the meters on and more convenient in terms of transportation and field deployment. The meters were programmed to record current speed, direction, pressure, turbidity and wind-wave data (if present) in burst sampling mode every 20 minutes and every 5 minutes for the last two

measurements (in July and August 2014). Burst duration lasts for 20 seconds. The study of spring tides commenced in February 2013 and finished in May 2015. During the first three months of the pilot study; February, March, and May 2013, only one current meter, set up at 0.35 m high above the bed, was deployed to recorded data for initial analysis of flow properties. Later, in July and August 2013 until the last survey in May 2015, more current meters were added to record the data in the different heights previously mentioned. The current meter deployments are summarised in Table 4.2. The data received from the meters were then exported by WaveLog programme and processed for further information of local flow characteristics such as water depth, velocity profile, shear stress, etc. in order to interpret the hydrodynamic links to the morphodynamics and internal structure of dunes.

However, before calculating all data, they needed to be edited as some parts of each dataset contains very high value of current speed which are due to the wind when the equipment is out of the water during the low water level. To remove these high values in records, a number of criteria were used. Firstly, the predicted tidal heights at Avonmouth were used to limit the time that current meters were possibly exposed to the wind rather than the water flow. Afterwards, the variation in current speed directions, turbidity, and atmospheric pressure were considered to estimate the possibility of the time that the wind run across the sensor of the equipment. The direction changed suddenly when the current meters were out of the water, while the turbidity during wind exposure would equal to zero and the pressure would be about 10.1 bar, which could be similar pressure when the water is very shallow. After all dataset were completely edited, calculation for other flow properties could be started which will be described in the next section.

Figure 4.9 Current meters set in different height in the dune field. (Top) Aluminium tripods were used to install current meters above the bedrock close to dune crest in the early deployment (2013); the left-hand meter measured flow at 15 cm above the bed and the right-hand meter measured flow at 40 cm above the bedform; (Bottom) A scaffold was set on the dune crest in 2014 to replace the tripods.

Table 4.2 Summary of Valeport current meter deployment

Period of Record	No of Current meters	Heights (m)	Burst sampling mode (seconds/minutes)	Burst sampling duration (seconds)	Wave Cycle Time (secs/minutes)	Wave Burst Duration (secs)
11 – 20 Feb 2013	1	0.35	1200/20	20	10800/180	2048
12 – 19 Mar 2013	1	0.35	1200/20	20	10800/180	2048
28 – 29 May 2013	1	0.35	780/13	20	780/13	512
23 – 24 July 2013	2	0.19, 0.35	780/13	20	780/13	512
20 – 21 Aug 2013	3	0.15, 0.30, 0.40	1200/20	20	10800/180	512
16 – 17 June 2014	2	0.15, 0.30	1200/20	20	10800/180	512
14 – 16 July 2014	3	0.15, 0.40, 0.50	300/5	20	10800/180	512
12 – 14 August 2014	2	0.15, 0.50	300/5	20	10800/180	512
18 – 19 May 2015	2	0.15, 0.35	1200/20	20	10800/180	512

The Valeport current meters also have a function to record waves. The wave sampling mode was set up as presented in Table 4.2. Wave bursts start at the same time as a Tide burst. At the end of each wave burst sampling period the system automatically records descriptive statistics and an energy spectrum; these data include mean water level, tidal slope over the burst period, significant wave height, maximum elevation above a de-trended mean level, maximum elevation below the de-trended mean level, mean period, mean zero up-crossing period, peak period, significant wave period, maximum wave height and total energy (Valeport Limited, 2003).

4.2.2 Water depth calculation

Water depth at the site could be computed using the standard formula of UNESCO (Fofonoff and Millard, 1983). This formula is based on the relationship between pressure and water depth with computation of the gravitational field at the latitude of the study location. It is defined as follows:

$$D = \frac{(C_1 * (P_b * 10) + C_2 * (P_b * 10)^2 + C_3 * (P_b * 10)^3 C_4 * (P_b * 10)^4}{(g(\emptyset) + {}^1\!/_2\, g' * P_b)} + \Delta d/9.8 \qquad (4.1)$$

where: D is depth (m)

$g\ (\emptyset)$ is 9.780318 * (1.0 + 5.2788E-3 * $\sin^2\emptyset$ +2.36E-5 * $\sin^4\emptyset$)

g' is +2.184E-5 m/s^{-2}/bar^{-1}

C_1 is +9.72659

C_2 is -2.2512E-5

C_3 is +2.279E-10

C_4 is -1.82E-15

P_b is the hydrostatic pressure (bar)

Δd is the geopotential anomaly, expressed in J/kg.

However, it is stated that the term of Δd equals zero for standard seawater, as salinity = 35 and temperature = 0°C and this term in the WaveLog programme is assumed to be zero. As a

consequence, the algorithm, called 'Simple UNESCO Depth', was selected to apply in this study as:

$$D = \frac{(C_1 * (P_b * 10) + C_2 * (P_b * 10)^2 + C_3 * (P_b * 10)^3 C_4 * (P_b * 10)^4}{(g(\emptyset) + {}^1/_2\, g' * P_b)} \quad (4.2)$$

Finally, a standard off-set value of 9.92117 was subtracted from all the calculated values of D. Afterwards, the complete results of during the period of immersion above the study site were acquired and could be used for further analysis, including initial analysis of suspended sediment concentration which will be described later.

4.2.3 Velocity profile (log profile)

After obtaining some key hydraulic parameters, including current speed, flow direction, as well as calculated water depth, these data can be further analysed by deriving calculations related to the velocity profile; these data included the bed shear stress, the bed roughness length and the derived Shields parameter. To obtain these flow parameters the structure of the vertical velocity distribution should be determined as is explained below. The theory of velocity distribution explains that the resistance of the bed and the banks in flowing water has the impact of slowing flow speed, especially in the layer of water that is very close to the solid boundary (Richards, 1982). This could be summarised in as much as the flow velocity adjacent to river bed is slower compared to the speed in the upper layer of water which increases relative to the distance above the bed (Figure 4.10). Understanding the velocity profile would lead to other findings of flow properties, such as bed roughness, shear velocity, and the size of grains can be moved by the flow. As a result, the velocity profile is initially needed to be created in this study by using velocity in different range of heights collected in a field site.

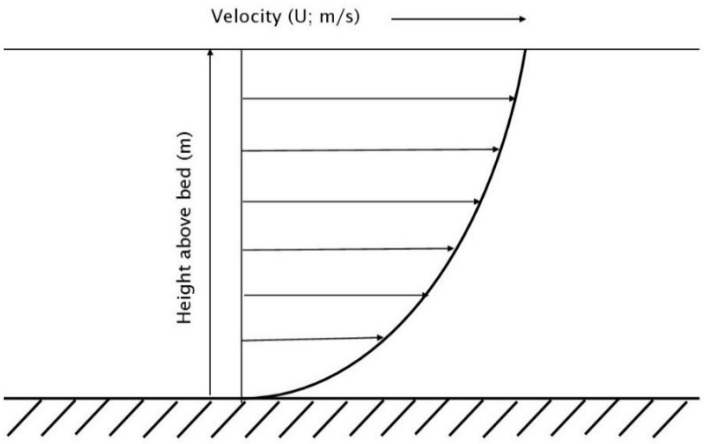

Figure 4.10 Velocity distribution in river flow (redrawn from Richards, 1982)

The data needed for creating velocity profile are current speed (m/s) and height above the bed (m). For example, plots of the time-averaged velocity U, (m/s) data, against the heights recorded above the bed, (m) from the field data are given in Fig. 4.11 for cases where there were three velocity points in the vertical; 15 cm, 40 cm and 50 cm (Figure 4.11). In steady-flow the velocity normally increases relative to the height above the bed, which conform to the velocity distribution theory (Figure 4.10). Fig. 4.11 shows that often profiles were non-logarithmic during portions of the tidal cycle. This behaviour was systematic and as expected due to the accelerating and decelerating tidal flows.

A check on calibration and the possibility of 'shadowing' of meters by the deployment frame showed no deployment errors. Rather the non-logarithmic profiles reflected the hydrodynamic flow structure above the bed. This structure is considered and explained in the Results. Suffice it to say that velocities measured at points above c. 0.4 m (e.g. at 0.5 m) above the bed tended to be considerably greater than the velocities measured below 0.4 m such that log-profiles could not be fitted. In contrast, the change in the relative flow speed between the two lower points was more moderate and consistent throughout tides. Consequently for subsequent surveys, when only two current meters were available, speeds were measured in the lower 0.4 m of the profile and the two-point data processed using equation 4.3 as following;

$$\overline{U} = (u^*)\frac{1}{\kappa}\ln(\frac{z}{z_0}) \tag{4.3}$$

where $\overline{U}$ is depth average velocity

z is height above the bed

z_0 is bed roughness length

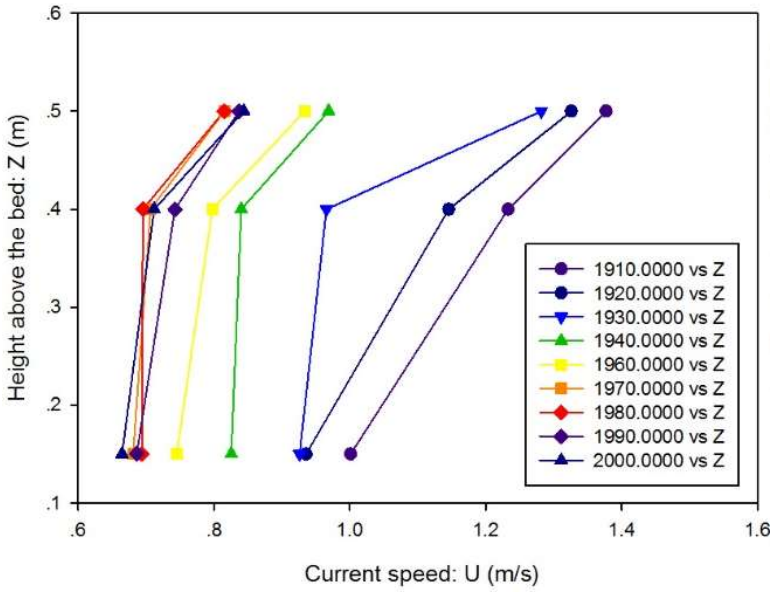

Figure 4.11 Examples of velocity data in July 2014 where there were three velocity points in the vertical plotting against the height above the bed. Data shown in different colours present the velocities measured during different periods of the tide when the flow velocity was measured at three levels of height above the bed (15 cm, 40 cm, 50 cm).

The methodology at this stage was the same as proposed by Bergeron and Abrahams, 1992). An analysis is completed using a simple linear regression to produce a best-fit least-squares curve for each dataset. Prior to application of a linear regression to the curves, it is necessary to transform the heights above the bed by applying natural logarithmic function (ln). Once the ln-function is applied to all heights, untransformed velocity (U) later were plotted against these transformed heights (lnZ) (Figure 4.12). Then a linear regression function is applied to each velocity profile which also provides a linear function of the form;

$$y = bx + a \tag{4.4}$$

where a and b depend on each log-profile and later will be used to calculated for bed roughness and shear velocity which is presented in the next section. An example of the regression equation is given in Figure 4.12. All results and detail of linear function could be found in the next chapter.

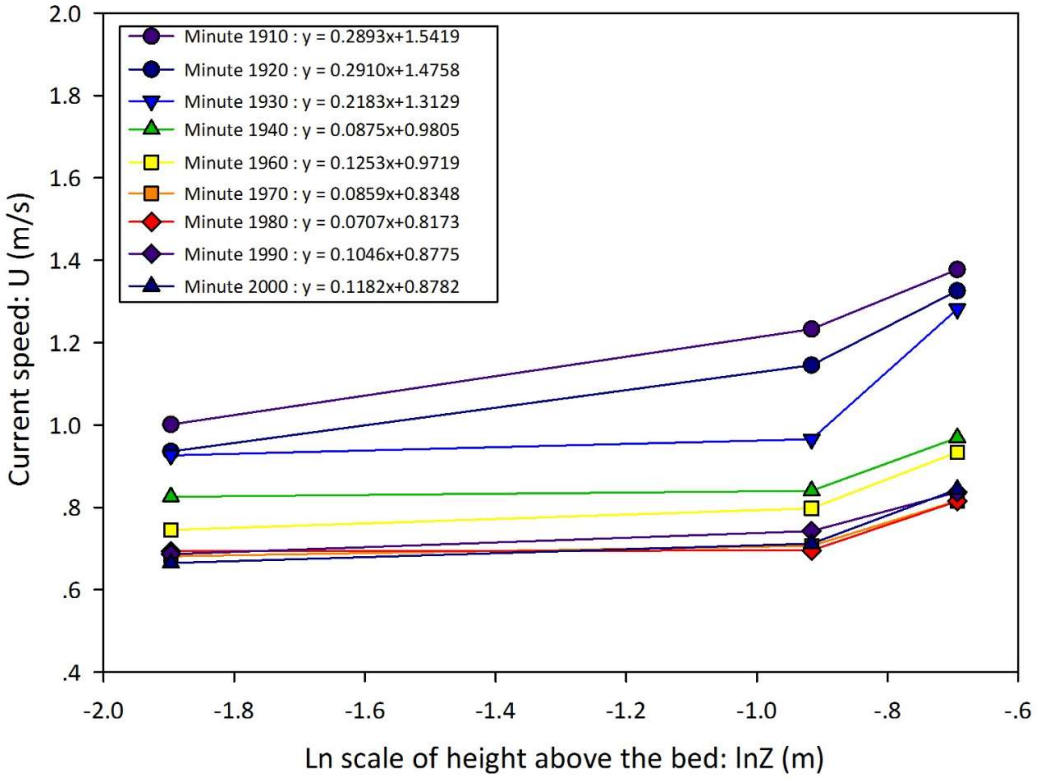

Figure 4.12 Examples of velocity profile data in July 2014. Data shown in different colours presents the velocity measured in different periods which flow velocity was measured at three levels of height above the bed (15 cm, 40 cm, 50 cm). The heights were transformed into ln scale and plotted against real current velocities. The linear regression is applied to each dataset and results in equations, $y = bx + a$, which later a and b will be used to derive shear velocity (u_*) and bed roughness length (Z_0).

4.2.4 Bed roughness and shear stress calculation

The values of a and b, the intercept and slope from the linear regression equation (Equation 4.4), are the key values which are used to determine other flow parameters, including hydraulic bed roughness (Z_0) and shear velocity (u_*). The Z_0 is a parameter in the log velocity profile equation for near-boundary conditions. It is equivalent to the height above the bed at which the water velocity theoretically becomes zero. It is called the roughness length because it is typically related to the height of bed roughness elements and has the dimensions of a length. Whilst it is not a physical length, it can be considered as a length-scale that is a representation of the roughness of the surface.

$$Z_0 = \frac{1}{30} k_s \tag{4.5}$$

where k_s is the 'equivalent sand roughness'. k_s typically equals $3.5D_{84}$ or $6.8D_{50}$ depending on the authority (Lane *et al.*, 2004).

In this study, the bed roughness length (Z_0) and the shear velocity (u_*) will be calculated from *a*- and *b*- values obtained from the linear regression mentioned above by;

$$Z_0 = anti\ (ln) of\ (-\frac{a}{b})\ \text{ or }\ Z_0 = Exponential\ of\ (-\frac{a}{b}) \tag{4.6}$$

$$u_* = \kappa b \tag{4.7}$$

where a is the intersection of the line from regression equation (Equation 4.4)

b is the slope of the line from regression equation (Equation 4.4)

Shear stress is one important parameter leading to transportation of particles underwater. The initial motion of particles starts once the shear stress is strong enough. Shear stress (τ_o) is calculated as per the arguments presented in section 2.3.1; page 35;

$$\tau_o = \rho u_*^2 \tag{4.8}$$

Once all the values above can be defined, it is possible to determined initial motion of particles over the bed by using the Shields' equation, which a non-dimensional critical shear stress (Shields' parameter: θ_c) can be written as Equation 2.18 (section 2.3.1; page 35). Shields stated that "critical bed shear (τ_{0c}) increase with particle size, but also depends on the bed roughness conditions" (Richards, 1982).

According to previous studies, there are a range of critical shear stress being reported. Buffington and Montgomery (1997) gathered the data of incipient motion from several studies as well as studying different methods to define incipient motion. The traditional Shields parameter equals 0.045 for the movement of the mean grain size in a distribution. This is an average value for rough turbulent flow reported by previous studies, such as Miller et al. (1977) as well as Yalin and Karahan (1979). However, when looking at individual values from these studies they range from 0.02 to 0.065 approximately (Buffington and Montgomery,

1997). A diagram of Shields entrainment function comparing data of Shields (1936) and modified data of Miller *et al.* (1977) is shown in Figure 2.14. Moreover, upper and lower limits for the Shields parameter for grain size coarser than 10 mm have been suggested as 0.25 and 0.01 by Williams (1983). Apart from flow conditions another factor considered to have effect on the difference in values of initial motion, is bed-material characteristics, which includes friction angle of grains (pivoting angles), grain protrusion (degree of exposure), imbrication or clustering of particles, grain shape, grain size distribution, and degree of packing (Kirchner *et al.*, 1990; Buffington and Montgomery, 1997; Knighton, 1998).

4.2.5 Wave entrainment calculation

Waves in sufficiently shallow water could produce velocity at the bed resulting in sediment entrainment. In order to confirm that the waves have no significant effects on the studied cobble dunes further investigation was warrented. Even though it was stated that wave heights in intertidal areas of the middle estuary are less than 0.4 m which result in no significant wave effects on sediment entrainment (Allen and Duffy, 1998a), wave characteristics were measured in the present study as noted above during the current meter surveys and so these data were examined to check the ascertion of Allen and Duffy (1998a).

Waves were recorded by the current meters which provide important characteristics of waves such as significant wave height (H_s), maximum wave height (H_{max}), wave period (T_1), etc. These data can also be used for further calculation of other properties. One of them is calculated wave entrainment which indicates if there is a possibility of sediment transport by wave actions. The calculation can be done by following the instruction of Soulsby (1997). Waves can produce an oscillatory velocity at the bed and have impact on sediment entrainment if the water is sufficiently shallow. In order to investigate if water is shallow enough, it can be calculated by

$$h < 0.1gT^2 \tag{4.9}$$

or, alternatively

$$h < 10H_s \tag{4.10}$$

where H_s = significant wave height,

T = wave period,

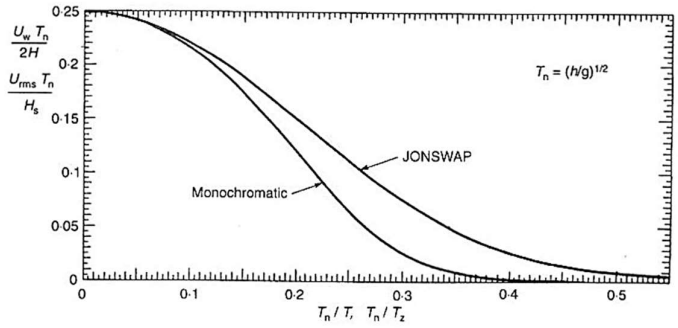

Figure 4.13 Bottom velocity for monochromatic waves ($U_w T_n/2H$ versus T_n/T) and random waves ($U_{rms} T_n/H_s$ versus T_n/T_z) (Soulsby, 1997).

After that the wave orbital velocity amplitude at the sea bed (U_w) can be found by a relationship curve showing bottom velocity (Figure 4.13). Prior to knowing a value from this diagram, the scaling period for waves (T_n) must be known which can be defined by

$$T_n = (\frac{h}{g})^{1/2} \tag{4.11}$$

With the value for the *x*-axis (T_n/T), later a value for the *y*-axis, for monochromatic or random waves, can be known which enables the calculation of U_w as follows;

$$\frac{U_w T_n}{2H} \; or \; \frac{U_{rms} T_n}{H_s} \tag{4.12}$$

where H = height of water wave,

The calculated value of U_w can be used to identify the size of bed sediment at the threshold for motion (Figure 4.14) and consequently an estimation of grain sizes likely to be entrained by a range of wave heights are obtained. Conversely the critical height of waves that do not entrain sediment can also be isolated.

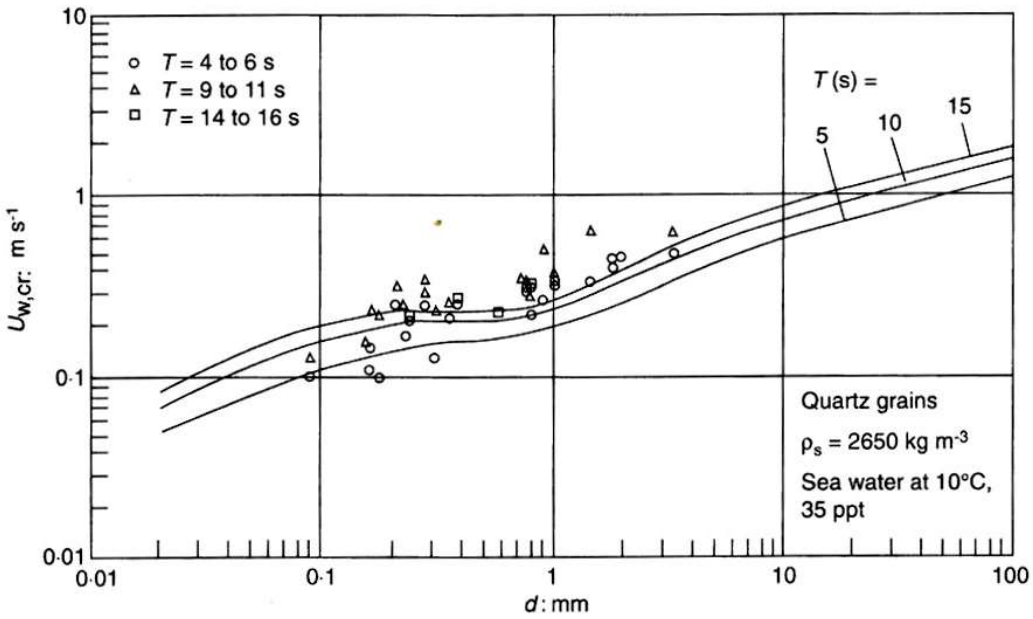

Figure 4.14 Threshold orbital velocity for motion of sediment by waves

4.3 Sediment transport measurement

The component driver of bedform development is sediment transportation once sediment has been entrained from the bed. A knowledge of the characteristics and the dynamics of the particles moving across the bed primarily as bedload is needed. There are several techniques to study sediment which are different due to types of sediment load: suspended load and bedload (Fraley, 2004) which can be classified into four main techniques; trapping, tracing, topographic monitoring/re-surveying, and modelling (Lee *et al.*, 2000; Sear *et al.*, 2000). Each technique might use different technology and has different limitations which was summarised by Sear *et al.* (2000). For the current study, the techniques applied for measuring sediment transport are trapping and tracing techniques as follows.

4.3.1 Sediment trapping

4.3.1.1 Bedload sediment

The Helley-Smith bedload sampler was originally developed by (Helley and Smith, 1971). This technique is recognised as a world-wide standard method for data collection as it has been

improved, studied and used to investigate bedload transportation in several sites over the world for many decades (e.g. Pitlick, 1988; Gaudet *et al.*, 1994; Ryan and Porth, 1999; Emmett, 2010). The ability of extensive calibration and simple operation are the important advantages in using this equipment (van Rijn, 1986). The sampler was designed regarding to pressure difference of flow and consists of two important parts; the rigid nozzle (metal frame) and sample-collection bag which is flexible. A number of factors were stated to have influence on the efficiency of the sampler which include the size and exit/entrance flair ratio of sampler nozzle as well as sample bag size, mesh opening, and filament size (Emmett, 2010).

A pair of Helley-Smith type bedload samplers were utilised for sampling coarse bedload transport over the dunes during flood and ebb tides. The traps (Figure 4.15) were made from steel with a rectangular nozzle dimension of 15 × 15 cm. The end of the frame has a slightly larger size than the nozzle with the dimension of 18 × 25.5 cm (Figure 4.15). The collection bags were securely attached at the end of the sampler traps. These sample-collection bags were made from trailing net which is abrasion-resistant and durable to be submerged under water in the tidal environment. The mesh aperture is 2 mm which allows water to flow through and is able to retain fine gravels . These bags were cone shaped, tied shut at the distal end with a plastic cup, extending 0.7 m. The capacity of each trap is about 15 litre or 36 kg. Traps were deployes to face both the flood and ebb directions and so could sample only the flood or the ebb tides on each deployment (Fig. 4.16)

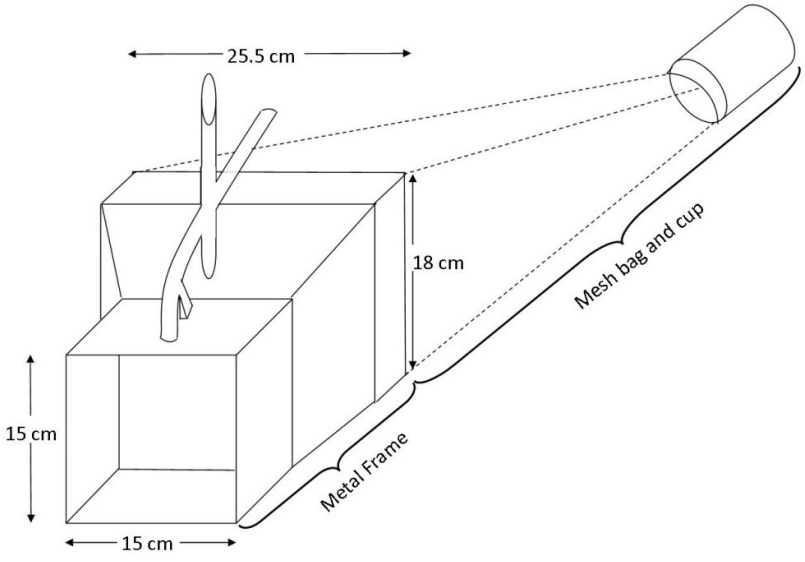

Figure 4.15 Dimension of bedload trap used in this study

In the field site, a pair of bedload samplers, including the collection nets, were installed on the crest of one of the dune ridges (Figure 4.3A) with different direction of the nozzle towards the flow. One faces the flood tide, whilst the other faces the ebb tide with the distance of 1-2 m between each other. Both traps were fixed on both sides of the trap handles by 0.30 m long metal stakes hammered into the dune and tied with plastic covered wire in order to tightly secure the trap so as not to be dislodged by the strong flows (Figure 4.16). The samplers were installed during low water level, when the dunes were exposed above water level. Both of them were left on the dune field for one night and were retrieved for collecting samples on the next day, thus they sampled over the period of two tides. It is not known if the traps fill on the first tide or if some sediment can be added on the second tide. However, diurnal pairs of tides are always very similar in terms of tidal height and discharge hydrographs so similar amounts and sizes of sediment should be in transport on both tides. A quantity of fine sediment (<2 mm) can be moving as bedload and can be caught in the traps. In similar fashion, fine sediment in suspension (<15 cm above the bed) can be trapped in the nets despite the 2 mm notional mesh size.

Figure 4.16 A pair of Helley-Smith bedload sediment traps are set up on the crest of dune (red circle). The inset shows the traps are facing the flood and ebb directions in order to sample bedload sediment being transported in opposing directions.

4.3.1.2 Suspended sediment

Three different types of samplers were used to collect suspended sediment: (A) a tower-shape McLane Phytoplankton sampler modified to collect fine suspended sediment with filter papers in March 2013 (Figure 4.17A), (B) pan-piped sampler with vertical cylindrical tubes in July 2013, August 2013, and July 2014 (Figure 4.17B), and (C) a prototype sediment sampler (KC™ Denmark) in May 2015 (Figure 4.17C). Information on suspended sediment would provide the supporting background of local conditions over the site. Unfortunately, due to technical issues, the first model of sampler rarely caught samples as most of the tubes to the filters were blocked during data collection, probably because concentrations in the Severn estuary are generally are very high in relation to the design of the sampler. So it will not be mentioned further in this section.

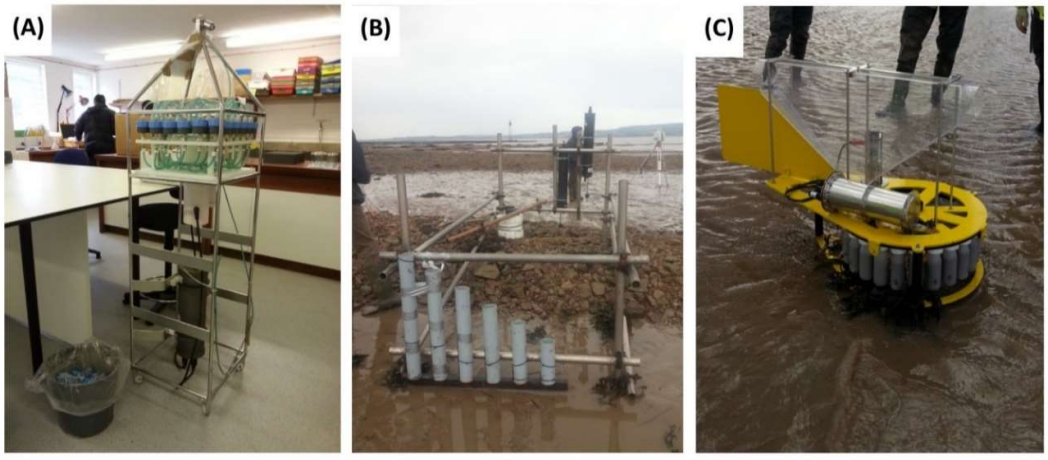

Figure 4.17 Three suspended sediment samplers used during the study; (A) McLane Phytoplankton sampler, (B) Pan's-pipes sampler and (C) a prototype sediment sampler (KC™ Denmark).

In July 2013, August 2013 and July 2014, a Pan's-pipes sampler was used. A set of six vertical tubes with 10 cm diameters, was fixed at the stoss toe of the instrumented dune with different heights above the bedrock surface; 25, 35, 45, 55, 65 and 75 cm (Figure 4.17B) to trap fine sediment settling at given heights above the bed during tidal cycles. However, the results for the tube with 25 cm height were discarded as turbulence always resuspended any settled sediment, leaving negligible sediment in the tube, giving a false sample weight retained. As

the tubes are in place throughout two tides the samples retained represent both flood and ebb tides as undifferentiated integrated samples. The advantage of the sampler is its simplicity and ability to obtained time-integrated samples from different heights above the bed to determine typical but generalized grain-size distributions. However, the sampler does not return data on sediment concentrations.

Later in May 2015, a prototype sediment sampler (KC™ Denmark) was fixed above a swivel bolted to the bedrock up-estuary of the study dune with the intake at a height of 0.75 m above the bedrock platform (Figure 4.18). The sampler had not been trialled in the field prior but had been designed to collect seston in slow currents in Scandanavian fjords and so was not ideal for the Severn estuary subject to high velocities and high sediment concentrations. However, it had the advantage of robustness, full submergence and automatic discrete sampling of large volumes of water (c. 250 ml). Water enters the sampler through a 10.5 cm diameter circular intake and exits via a 10.5 cm diameter outlet at the same height. The sampler rotates, by means of a vane, so that the intake faces into the flow with the outlet facing down flow so that the flow is largely unimpeded. The sediment entering the sampler has the possibility to settle out (horizontal length of settling chamber is about 60 – 70 cm height) in a large, gravity-focussed, funnel-shaped container at the base, which feeds into a smaller funnel that sits above the sampling bottle below. The unit was set to rotate the sample bottle every one hour, with the first sample (no.1) taken at the beginning of a flooding tide at 18:00 on 18th May 2015. The unit was retrieved at 18:00 on Sunday 19th May 2015, the following day, and the last bottle (no.24) was observed to rotate into place at 17:00 as the sampler began to emerge in the falling tide. Each bottle retained a sediment sample that was dried and weighed. Thus, basic results consist of the weight of sediment collected every hour over two tides. Later, grain size analyses were also conducted on each sample using a Saturn DigiSizerII within the Geography and Environment laboratory at Southampton. Apart from the grain size analyses, suspended sediment concentration (SSC) was calculated. The concentration (mg/L) in the KC sampler flow was estimated by dividing the trapped weight of sediment by the discharge through the sampler during one hour. The discharge was calculated from the area of the intake times the incident flow velocity recorded simultaneously to sediment sampling at the same height as the intake. However, calibration in a flume is not possible due to the large size of KC sampler. Consequently, it is required to compare the results with previous studies of suspended sediment in the estuary to ascertain if the results are reasonable, which will be explained in the Results Chapter.

Figure 4.18 A prototype sediment sampler (KC Denmark) set on the bedrock platform next to the studied dune

Several studies have reported that suspended fine sediment is present at high concentrations (c. 100 to 1000 mg/L) for all tidal states (Hydraulics Research Station, 1981; Crickmore, 1982; Kirby, 1986) with lutoclines occurring on occasion near the head of the estuary, such that surface-water sediment concentrations within the inner estuary can exceed 4000 mg/L (Crickmore, 1982) and between 500 –10,000 mg/L within the outer estuary (Manning *et al*., 2010). Carling (2013) deployed a laboratory-calibrated modified McLane Phytoplankton sampler at 0.40 m above the bed very close to the location of the present cobble dune sampling site. The sampler collected 24 1-litre samples at 20 minute intervals throughout a 12.88 m Spring tide. The concentrations increased monotonically during the flood tide from an initial value of 148 mg/L to a value of 654 mg/L just before high slack water. Concentrations fell at high water, spiked on the first ebb flow to 749 mg/L (presumably as slack-water settled sediment was resuspended from the bed) and then oscillated during the ebb flow (average ebb concentration: 145 mg/L).

From the suspended sediment samples collected by KC Denmark, the concentration of suspended sediment concentration was calculated by a relationship of the dry weight of suspended sediment being trapped, flow velocity and area of sample inlet of each hour as following;

$$SSC = \frac{TSS}{U \times A \times 3600} \tag{4.13}$$

where; SSC is suspended sediment concentration (mg/L);

TSS is total suspended solids or dry weight of suspended sample (g);

A is a surface area of the inlet of the sampler (m^2).

Note: the value of 3600 is included to convert the unit of per second to per hour.

4.3.2 Grain size analyses

Both bedload and suspended sediment samples were analysed in a research laboratory in the School of Geography and Environment, University of Southampton.

For **bedload sediment**, the samples were processed by dry sieving techniques to obtain grain size distributions. Dry sieving could be operated with sieve shaker and a set of sieves, equivalent to British standards, with decreasing aperture size from largest aperture size (45 mm) to the smallest one(< 63 μm) to sort the grain size of all samples (Figure 4.19).

As there were some coarse woody organics materials mixed in the sample, so these were initially removed from samples by hand. Samples free of coarse wood were then dried in an oven at approx. 50^{o}C, for at least 24 hours or up to 3 - 5 days, depending on the amount of samples. Once all samples were totally dried, they were put into the top sieve in a nested column of sieves arranged in decreasing order (the largest aperture on the top to the smallest aperture at the bottom). Only five sieves could be stacked on the shaker each time, so there were five sets of sieve shaking to be done (Table 4.3). Each column was shaken for 10 minutes. Sediment retained in each sieve was weighed and the results were recorded in tables for further analysis. The Wentworth size scale is used in this study (Wentworth, 1922)

Gradistat, a program written to use in grain size analysis by Blott and Pye (2001), which is integrated into a Microsoft Excel spreadsheet, was applied in this study to analyse grain size distribution and statistics of the bedload samples. It is developed by compiling the standard methods of grain size analysis which are acceptable among sedimentologists, i.e. calculation by Folk and Ward and moments methods as well as the standard world-wide units of grain size (metric unit and phi (φ)). This program helps users to analyse rapidly and allows more modification for individual requirements.

To run an analysis by this program, it requires input data from any of the standard measuring techniques, i.e. weight, volume or percentage of sediment in each size fraction from several

methods; a series of sieves, a laser granulometer etc. Results of Gradistat are provided in the form of tabular and graphical output. The statistics results of each sample include mean, mode(s), sorting (standard deviation), skewness, kurtosis, and a range of cumulative percentile values. Apart from the statistics values, the program also presents the analysis graphical outputs; the diagram of grain size distribution of particle diameter (μm) against class weight (%), diagram of gravel-sand-mud components, and diagram of sand-silt-clay. For the purpose of initial recording, that portion of the grain-size curve < 2 mm were retained as part of the bedload grain-size curves. Latterly, for consideration of the results, that portion that can be found in suspension (< 2 mm) was subtracted from the bedload curve data records.

Figure 4.19 Sieve shaker: a machine used in sorting dried sediment sample into classes. Sieves are stacked regarding to aperture size; the coarsest sieve is on the top while the finest is at the bottom of the stack.

Table 4.3 Aperture size used in sieving: The sieves are separated into five sets due to limited number of sieves which can be put on the shaker.

Set 1	**Set 2**	**Set 3**	**Set4**	**Set 5**
45 mm	8mm	1.4mm	300micron	90micron
31.5mm	5.6mm	1mm	250micron	63micron
22.4mm	4mm	710micron	212micron	<63micron
16mm	2.8mm	500micron	180micron	
11.2mm	2mm	355micron	125micron	

Alternatively, samples of **suspended sediments** consists of fine grains of which size are less than 2 mm. These fine sediment samples were analysed by Saturn DigiSizer II 5205 V1.02 (Figure 4.20). The results show the statistics of grain size distribution of the fine sediment.

Figure 4.20 Saturn DigiSizer unit (Model: II 5205 V1.02): the machine fine particle sizing instrument

4.3.3 Determining bedload movement with a portable impact sensor

A portable impact sensor was also used to determine some aspects of bedload transportation of coarse particles passing over the dune crest. Previously, a number of studies used this kind of technique (Bogen and Moen, 2003; Richardson *et al.*, 2003; Reid *et al.*, 2007; Rickenmann and McArdell, 2007; Vatne *et al.*, 2008; Raven *et al.*, 2009; Raven *et al.*, 2010; Rickenmann and Fritschi, 2010; Rickenmann *et al.*, 2012; Beylich and Laute, 2014)

The impact sensor was developed in order to improve a technique to measure initial motion and bedload transport in high-energy rivers where it is expensive and risky for the instrument being deployed in such hostile environments. Other reasons urging the development in this instrument are the limitation of using suspension cable and support frame and safety of researchers in field measurement. According to the deployment in harsh environment, an instrument needs to be robust during high-flows and can be installed safely during low-flows (Richardson *et al.*, 2003).

The instrument deployed in this study is similar to those used in the previous studies mentioned above. The device used in this technique is designed “to detect the acceleration of

a steel plate fixed to a rock riverbed upon being struck by a clast, and to count the impacts detected within fixed interval times" (Richardson *et al.*, 2003). The sensor's unit can be divided into two main parts; a data logger and a steel plate. The data logger unit being used in this study is the "Gemini Tinytag Plus Shock data logger" (Figure 4.21A) with a reading range of 0 – 100 g and a sensitivity and accuracy of 0.4 g. The logger has small size of 7.3 × 6.8 × 3.4 cm and weighs only 140 g (Tinytag, 2011). The steel plate for detecting a strike by a clast is 15 × 13 × 0.6 cm. In the field the logger is attached to the underside of this plate.

Unlike the study of Richardson and colleagues where the logger was placed into a recess chiselled into a bedrock surface and covered with a steel plate, in this study the logger has to be installed on the dune crest developed in loose grains which can be moved by flows. As a result, a rectangular concrete block with a recess in the middle was used to secure the logger from being moved away from its location. The logger was put in the recess of this block and cover by a steel plate which was secured with four screws at each corner (Figure 4.21B). The block, together with the data logger and steel plate, was carefully buried in the dune crest, minimizing disturbance, until the plate was flush with the dune surface 2 m away from the flow meter scaffold (Figure 4.21C). The battery of the data logger can be replaced and lasts for over 6 months. The logger was left in the field on 14th July 2014 and retrieved on 16th July 2014, which resulted in sampling over eight tides.

The logger works by counting the impacts on the unit. It does not provide the quantitative bedload transport rate but the intensity of contacts through time provides a qualitative indicator of bedload transport. Importantly, the initial and final impacts provide an indication of the times at which measurable transport begins and ends on each tide. These data are then compared with hydrodynamic data. The data are useful for determining the threshold of initial sediment motion and cessation as well as indicating bedload transport intensity. As designed, the impact sensor cannot record sand-sized sediment impacts but can record gravel impacts. However, no information is available on the detail of the impacting grain sizes, as the impacts recorded are a result of the momentum of the impacting particles, which is dependent on both the speed and size of the impacting particles; which two factors cannot be differentiated. The results from data logger will later be analysed by plotting the recorded bedload impacts against the shear stress on the bed. This will show the existence of a threshold for detected bedload transport.

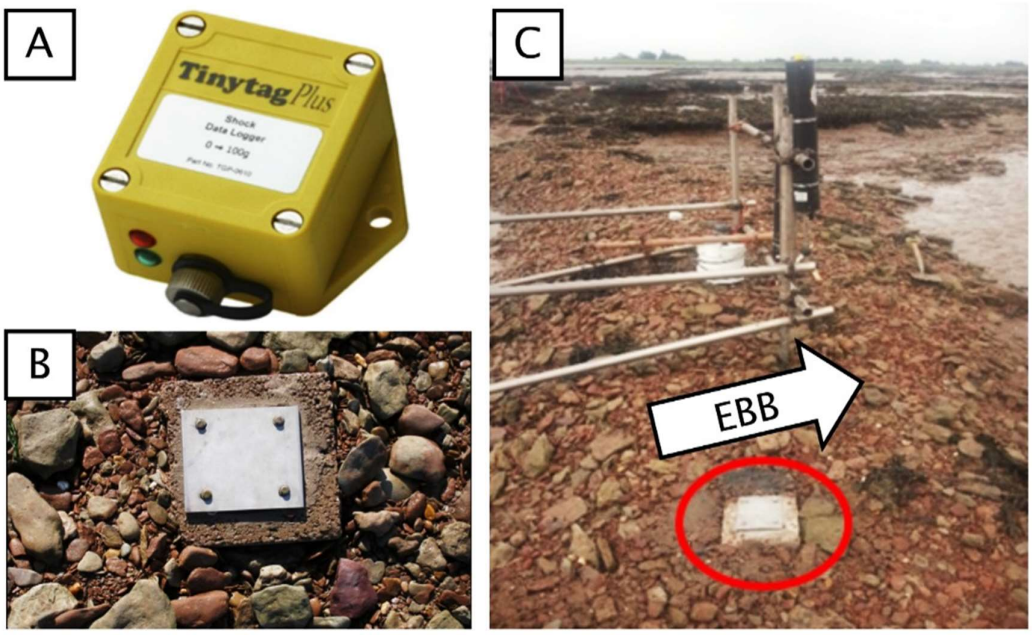

Figure 4.21 (A) A bedload tracer Tinytag Plus logger, used in this study to count coarse grains and record the time when large particles were in motion across the dune crest. (B) The logger was put inside a concrete cube, covered by a steel plate and secured by screws at the corners. (C) The logger unit was buried on the dune crest (Red circle on the right) close to the flow meters. The steel plate at the top of the cube was set flush with the surface of dune crest.

4.3.4 Tracing sediment (spray-painting)

Spray painting tracer particles is a further technique to track the movement of particles transported by flows (Carling *et al.*, 2006). However, the short period of emergence does not allow coarse gravel to dry and be painted whilst it is not feasible to take a large quantity of cobbles back to the laboratory for painting. However, a number of cobble-equivalent bricks were marked with indelible abrasion-resistant painted numbers, and placed in the study area. These painted objects were then surveyed and their locations subsequent to a series of tides were recorded to compare with the original surveyed positions.

In this study, a set of 50 bricks were used as a representative of the cobbles in the dune field. The bricks are used to represent blocky cobbles with a grain size coarser than D_{90} of the grain

size distribution of the bulk bed material. The D_{90} of the bed sediment is approximately 50 mm. The dimension of each painted brick is 20 × 10 × 6.5 cm. Moreover, a comparison between natural cobbles and the tracers in terms of their shapes using the Zingg parameters (Zingg, 1935; see Boggs, 2011) shows that the brick shape is similar to the blocky natural cobbles. The Zingg classification places the bricks at the limit of the triaxial class close to oblate whereas the blocky natural cobbles range from triaxial to oblate. The measured brick density is about 2.10 g/cm^3 (2100 kg/m^3) which is close to the density of the larger grains found in the dunes, which is 2.30 g/cm^3 (2300 kg/m^3) approximately. The density of these grains, largely supplied by the Triassic Mercia Mudstone Group, is less than quartz grains (2.65 g/cm^3 or 2650 kg/m^3) (Carling *et al.*, 2006). Each numbered brick was placed proud on the bed as part of a row on both dune crest and trough (25 bricks for each) (Figure 4.22) as such they should be readily transportable in contrast to any embedded coarse cobbles. Consequently, the tracer represents readily mobile cobbles.

All these painted bricks were left in the field and could be resurveyed only when low spring tides permitted. Footwork GPS survey shows movement (or non-movement) and direction of travel of the bricks which would help in understanding of cobble dispersion through tidal cycles.

Figure 4.22 Two rows of bricks were aligned on the crest (left) and trough (right) from onshore towards the river channel. Each row consists of 25 bricks individually identified by painted numbers.

4.4 Limitations relating with fieldwork

In order to complete the fieldwork, there are some limitations hindering the process. This section will explain issues that mainly deal with time, equipment and number of people to work in the field. Some technical issues related to the dGPS and Total station are already considered in section 4.1.1.

4.4.1 Limitation of time for fieldwork

The fieldwork can be done only when the water is low enough (< 1 m OD at Avonmouth) which allows dunes to be exposed and accessed on foot. Occasionally, if it is necessary, fieldwork can be done when water level is between 1 m OD and 1.5 m OD but the period for fieldwork is then very short and not many equipment installations and surveys can be done. However, this range of low water levels does not occur often. The low water levels are only encountered during the lowest spring tides. Boat work was ruled out as no local boatman could be identified who would work in the strong currents at the bedrock shelf edge.

However, the suitable environmental conditions for fieldwork are not dependant only on the water level but also the local weather. Fieldwork cannot be done during bad weather conditions, such as strong winds or heavy rains. These conditions obstruct the process in fieldwork. Some equipment used in this study have limitations regarding weather, i.e. rain can stop the measurement when using a laser scanner and total station, and very strong wind can restrict distance measurement of total station or hinder a drone flight to capture aerial photograph systematically. Moreover, poor weather is not suitable for the safety of the research team. During winter, weather over the site is quite harsh; wind is strong, temperature is very low, visibility might be low due to the short daytime, and is not safe to work. As a result, this season is largely avoided for fieldwork.

According to the limitations above, the time frame for fieldwork through a year is limited to March to September each year approximately. Moreover, when considering the conditions of tide levels, weather conditions as well as other limitations which will be discussed later, the selected dates for fieldwork which are available and suitable for fieldwork in the last 3 years are presented in Table 4.5.

Apart from limited time for selecting dates for fieldwork, there is also time limitation in each fieldwork. Semi-diurnal tidal system results in two flood and two ebb tides in one day which is

about 5-6 hours for one tide. The minimum water level, happening between transitions of ebb and flood tides, usually occurs in early morning and afternoon. The low water in the afternoon is selected for fieldwork allowing safe access in daylight. However, the duration of exposed dunes is only 2-3 hours, before the flood tides come back to the site. So fieldwork has to be done efficiently within the time and all the tasks have to be planned carefully and effectively.

4.4.2 Limitation of equipment and number of people working in the field

There are many types of equipment deployed in this research, provided by School of Geography and Environment and National Oceanography Centre, University of Southampton. Some of the equipment were not available for every fieldwork especially the current meters. Three meters are the maximum number of devices available for flow measurement on site and many times only two meters were deployed as the third was not available. The dGPS was also sometimes unavailable but it could be replaced by the total station.

Apart from availability of equipment, another limitation which occurred in fieldwork is related to the number of field assistants required. According to the short duration of low water and the various multiple tasks, it is not possible to complete all the measurements simultaneously on each fieldwork campaign as usually it was not possible to assemble a large enough team. The plan for collecting data had to be arranged carefully to build-up sufficient data for comparable Spring tides such that the data might be considered pseudo-synoptic and compatible.

Table 4.4 Details of data collection in fieldwork from February 2013 to May 2015

Date	Tasks									
	Shape and position measurement	Cross-section measurement	Flow measurement	Bedload sediment	Suspended sediment	Impact Sensor	Spray-painting tracing	Laser scanning	Drone flight aerial photograph	Dune trenching
11 – 12 Feb 2013	✓		✓	✓						
11 – 13 Mar 2013	✓		✓	✓	✓					
27-28 May 2013	✓		✓	✓						
25 – 26 June 2013	✓			✓						
23 – 24 July 2013	✓		✓	✓	✓					
20-21 Aug 2013	✓		✓	✓	✓					
19 – 20 Sep 2013	✓			✓						
18 – 19 Mar 2014	✓			✓						
16 – 17 June 2014	✓		✓	✓						
14 – 16 July 2014			✓	✓	✓	✓	✓	✓		
12 – 14 Aug 2014		✓	✓	✓		✓	✓	✓		
10 Sep 2014		✓					✓			
18 – 20 May 2015			✓		✓				✓	
29 Sep 2015	✓						✓			
10 Mar 2016										✓

Table 4.5 Tide table showing time of highest and lowest tides at Avonmouth during period of field study.

(Source: http://www.tides4fishing.com/uk/england/avonmouth and Tide prediction (Android application))

Date	1st tide	2nd tide	3rd tide	4th tide	Date	1st tide	2nd tide	3rd tide	4th tide
11-Feb-13	02:23h Low tide (0.76m)	07:56h High tide (13.96m)	14:47h Low tide (0.47m)	20:17h High tide (13.74m)	29-May-13	5:30h Low tide (1.1m)	11:10h High tide (12.8m)	17:45h Low tide (1.5m)	23:35h High tide (12.7m)
12-Feb-13	03:08h Low tide (0.72m)	08:38h High tide (13.98m)	15:26h Low tide (0.55m)	20:56h High tide (13.66m)	25-Jun-13	03:56h Low tide (0.69m)	09:26h High tide (13.52m)	16:20h Low tide (0.87m)	21:50h High tide (13.70m)
11-Mar-13	01:14h Low tide (1.05m)	06:56h High tide (13.49m)	13:38h Low tide (0.66m)	19:17h High tide (13.38m)	26-Jun-13	04:44h Low tide (0.66m)	10:14h High tide (13.42m)	17:05h Low tide (0.96m)	22:38h High tide (13.53m)
12-Mar-13	02:02h Low tide (0.82m)	07:38h High tide (13.72m)	14:23h Low tide (0.57m)	19:56h High tide (13.51m)	23-Jul-13	02:50h Low tide (0.85m)	08:26h High tide (13.48m)	15:17h Low tide (0.89m)	20:50h High tide (13.86m)
13-Mar-13	02:44h Low tide (0.83m)	08:17h High tide (13.73m)	15:02h Low tide (0.68m)	20:32h High tide (13.48m)	24-Jul-13	03:44h Low tide (0.52m)	09:14h High tide (13.70m)	16:08h Low tide (0.69m)	21:38h High tide (13.97m)
27-May-13	04:08h Low tide (0.81m)	09:35h High tide (13.40m)	16:32h Low tide (1.02m)	22:02h High tide (13.43m)	20-Aug-13	01:32h Low tide (1.30m)	07:20h High tide (13.00m)	14:05h Low tide (1.23m)	19:47h High tide (13.57m)
28-May-13	04:53h Low tide (0.90m)	10:23h High tide (13.16m)	17:11h Low tide (1.21m)	22:47h High tide (13.14m)	21-Aug-13	02:32h Low tide (0.74m)	08:11h High tide (13.56m)	15:02h Low tide (0.81m)	20:35h High tide (13.97m)

Table 4.5 (continue) Tide table showing time of highest and lowest tides at Avonmouth during period of field study.

Date	1st tide	2nd tide	3rd tide	4th tide	Date	1st tide	2nd tide	3rd tide	4th tide
19-Sep-13	02:11h Low tide (0.78m)	07:53h High tide (13.47m)	14:38h Low tide (0.90m)	20:14h High tide (13.84m)	16-Jul-14	05:26h Low tide (0.60m)	10:59h High tide (13.40m)	17:44h Low tide (0.96m)	23:23h High tide (13.40m)
20-Sep-13	03:02h Low tide (0.62m)	08:35h High tide (13.65m)	15:26h Low tide (0.86m)	20:56h High tide (13.88m)	12-Aug-14	03:44h Low tide (0.36m)	09:11h High tide (13.98m)	16:08h Low tide (0.50m)	21:35h High tide (14.24m)
18-Mar-14	02:44h Low tide (1.33m)	08:11h High tide (13.27m)	15:02h Low tide (1.29m)	20:29h High tide (13.13m)	13-Aug-14	04:32h Low tide (0.22m)	09:56h High tide (13.98m)	16:53h Low tide (0.49m)	22:20h High tide (14.09m)
19-Mar-14	03:17h Low tide (1.24m)	08:44h High tide (13.30m)	15:35h Low tide (1.31m)	21:02h High tide (13.04m)	14-Aug-14	05:11h Low tide (0.35m)	10:38h High tide (13.71m)	17:29h Low tide (0.75m)	23:02h High tide (13.65m)
16-Jun-14	04:53h Low tide (0.93m)	10:23h High tide (13.21m)	17:14h Low tide (1.20m)	22:50h High tide (13.26m)	10-Sep-14	03:26h Low tide (0.30m)	08:53h High tide (14.08m)	15:50h Low tide (0.46m)	21:14h High tide (14.31m)
17-Jun-14	05:35h Low tide (1.05m)	11:11h High tide (12.90m)	17:53h Low tide (1.39m)	23:38h High tide (12.89m)	18-May-15	02:32h Low tide (1.02m)	08:08h High tide (13.40m)	14:56h Low tide (0.85m)	20:29h High tide (13.37m)
14-Jul-14	03:59h Low tide (0.65m)	09:26h High tide (13.67m)	16:23h Low tide (0.80m)	21:50h High tide (13.91m)	19-May-15	03:20h Low tide (0.95m)	08:53h High tide (13.43m)	15:41h Low tide (0.91m)	21:14h High tide (13.37m)
15-Jul-14	04:44h Low tide (0.52m)	10:11h High tide (13.65m)	17:05h Low tide (0.77m)	22:38h High tide (13.77m)	29-Sep-15	03:20h Low tide (0.39m)	08:47h High tide (14.16m)	15:44h Low tide (0.52m)	21:08h High tide (14.35m)

Chapter 5: Results

This results chapter consists of four sections. The first part provides a geomorphological description over study site. The second documents the measured hydrodynamic data and calculated flow conditions whereas the third part is devoted to the sediment data collected from the field site. Last, the fourth part details sedimentary structure.

5.1 Geomorphological description over study site

5.1.1 Bathymetry

There are some reports of bathymetry data in the Bristol Channel and the Severn Estuary (i.e. Mackie *et al.*, no date; United Kingdom Hydrographic Office, no date). However, the bathymetry of the upper estuary, including Hills Flats, has not been widely reported. In this study, the bathymetry was derived from data supplied by the Gloucester Harbour Trustees. The points of surveyed data which cover the study area and the cross-section of the river are shown in Figure 5.1 and Figure 5.2 respectively. The river profiles in different sections show similar pattern of river bed. The highest elevation of the bed is on the shores of both England and Wales, ranging from 1.5 to 4 m OD Starting from the Welsh bank, the elevation decreases from above 0 m OD to the depth of 4 m below the Ordnance Datum (-4 m OD). After that, the bed become shallower and increasing depth exists again with gently slope until the deepest bed with 5-6 m below the surface (-5 to -6 m OD) closer to England's shore, where the elevation tends to have a steeper slope than shore of Wales. Moreover, the dataset no.13 and 14 provide a profile in the deep channel in the upstream to downstream direction which shows that the elevation of estuarine channel bed tends to decreases downstream (Figure 5.2: Bottom). The dune field in this study is in the elevation of -1 to 1 m OD approximately (Figure 5.2: Top). The interpolation showing the variation of bathymetry over the cobble dune field and the surrounding areas are presented in Figure 5.3.

Different bedrock surface geometries around the dunes might have effects on flow characteristics across them. In this case, the cobble dunes and the current meters are located close to the outer edge of the bedrock platform close to the main channel of the tidal River Severn. On the landward side of the dunes the bedrock platform is characterised by variable heights but with a tendency to gradually increase towards the steep slope of the marsh and the highest point at the river bank (Figure 5.4; see more details of Hills Flats in Chapter 3:

Study site). Consequently, the dune crest are aligned roughly normal to the shoreline. The onshore-off-shore difference in elevation of the bed had an effects on the changing tidal flow velocity, especially towards the end of the ebb tides. At this time the velocity curve often exhibits 'shoulder' when the velocity is sustained for a time or can rapidly increase for a short time before decreasing to zero. This shoulder is due to the ebb tidal drainage from the platform being sustained as the ebb tides drain out of the dune troughs at the end of ebb tides and accelerates over the edge of the platform into the channel. (more details will be described in section 5.2.4).

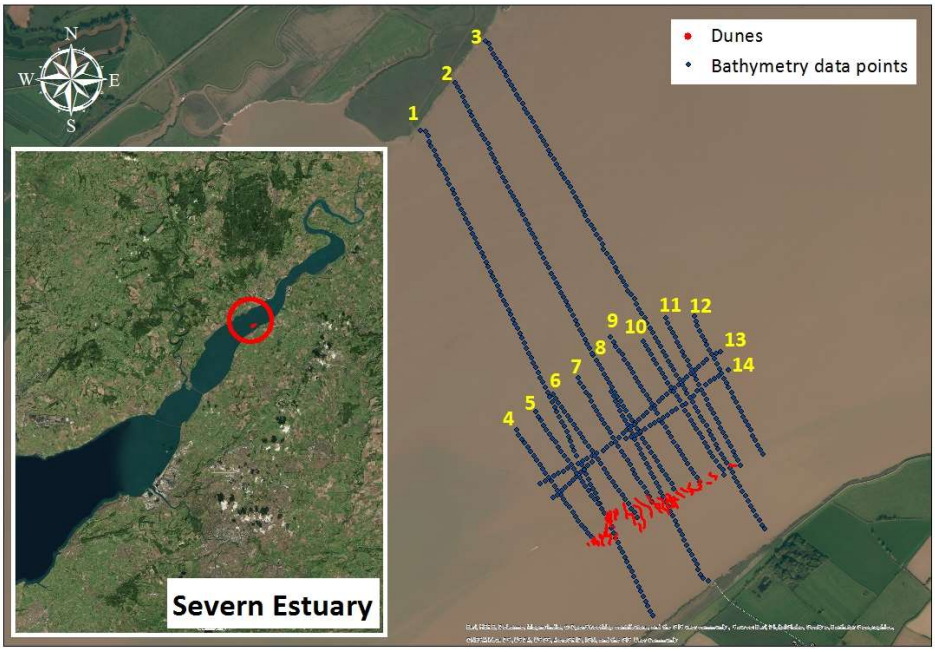

Figure 5.1 A diagram shows surveyed points of which the bathymetry data were collected. Line 1, 2 and 3 start from Wales toward England, while lines 4 to 12 start from the mid channel, and line 13 and 14 were measured from downstream to the upstream. Each point is about 20 m away from the adjacent point.

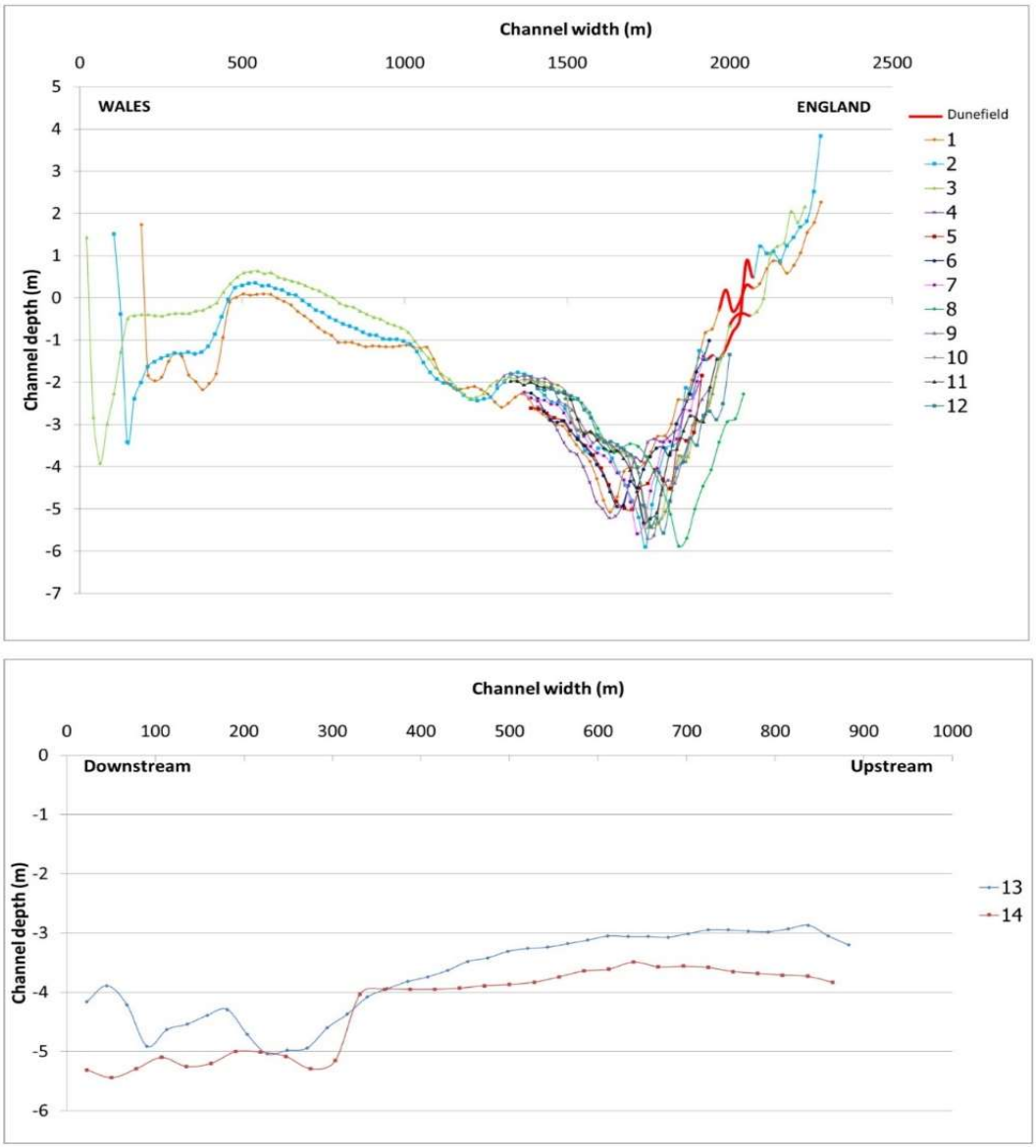

Figure 5.2 Bathymetry plots from the data collected from the surveyed points in Figure 5.1: (Top) The profile from a shore of Wales to a shore of England. On the lines 1, 2 and 3, the red thick short lines close to England side present the area where the dune field exists; (Bottom) The bathymetry from upstream to downstream the surveyed dataset 13 and 14 in Figure 5.1.

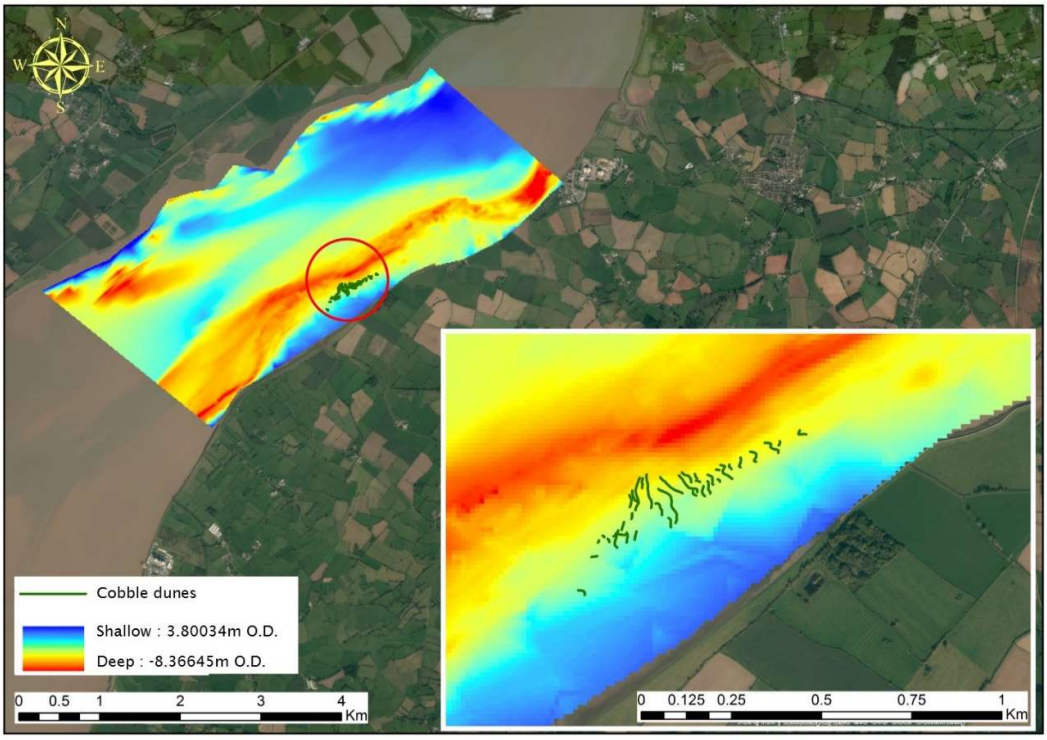

Figure 5.3 Interpolation of bathymetry of the study site and adjacent area.

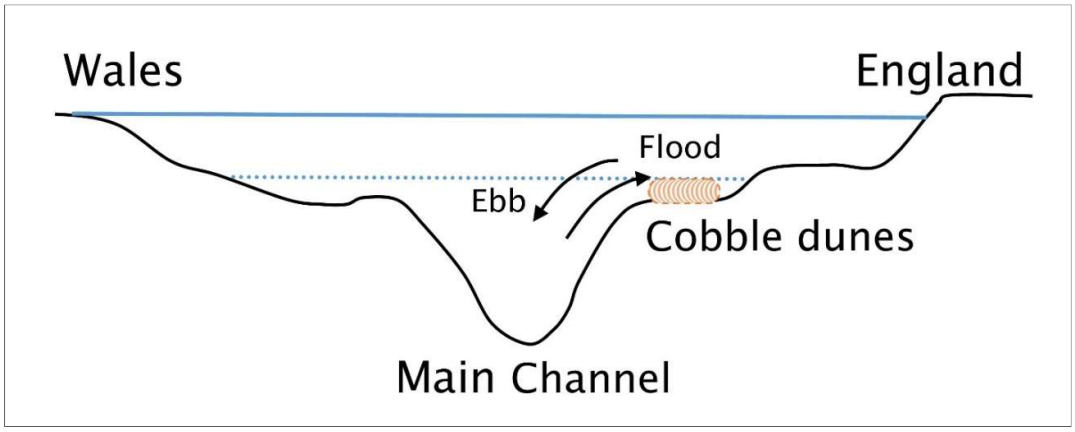

Figure 5.4 A simplified cartoon illustrates the estuary cross-section at the study location showing an area of cobble dunes on the bedrock platform (brown area). Primary ebb direction is out of the estuary toward readers. Arrows indicate the local flow direction off the platform into the tidal channel. Solid and dotted blue lines represent the high water level and lower water level before draining off the bedrock platform until the cobble dunes are exposed.

5.1.2 Changes in bedform surface

Terrestrial Laser Scanning was completed during 14th – 15th July 2014 (see section 4.1.2 for field deployment information). The scanner was set up to measure at a resolution of 0.005 m at 10 m range, resulting in a final raster model of 0.01 m resolution. The vertical error of each raster cell will be a function of the variation in elevations within that cell, but based on the grainsize of the site ($D_{50} \approx 17$ mm approximately), it was calculated that total error was likely to be below 0.01 m. The result shows that, after two tides, there were many changes on the dune surface. Erosion was mostly found on the up-estuary side while deposition was detected on the up-estuary side due to the ebb flows entrainment (Figure 5.5). However, there was no significant change greater than the average grain size ($D_{50} \approx 17$ mm approximately) over the two tidal cycles.

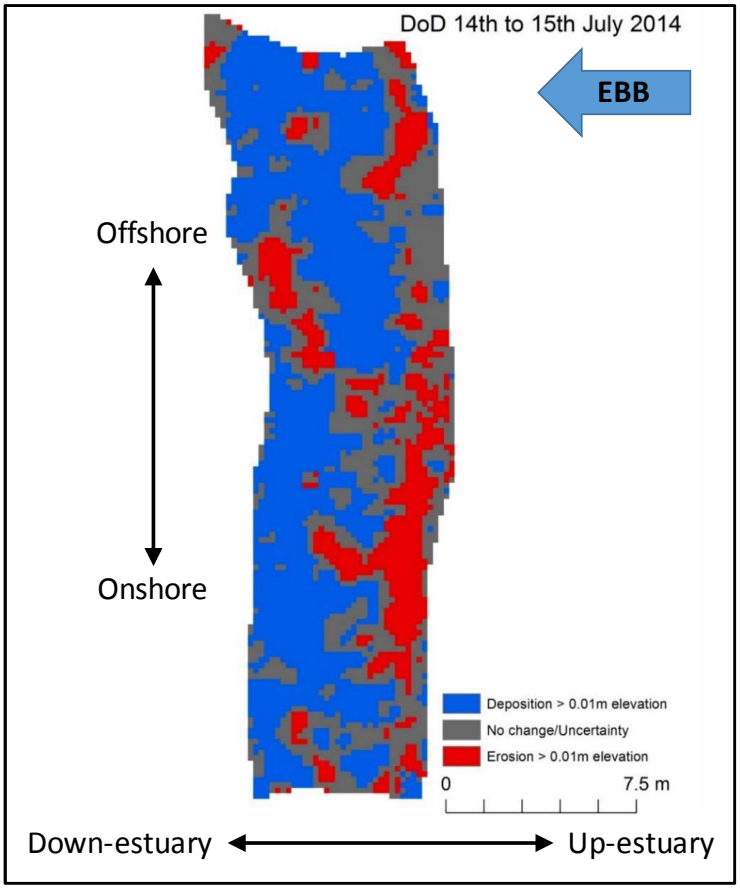

Figure 5.5 The scanning results over the dunes number 12 (Figure 4.3 and 5.9). Erosion was mostly found on the upstream side (red) while deposition was detected on the downstream side (blue). Not much change greater than the average grain size (17 mm) was observed.

5.1.3 Painted sediment tracers

A set of concrete bricks have been used for tracers. Fifty bricks were marked by numbers and left in the field for tracing their movements after tides. Tracers were separate into two sets; 25 aligned on the bedrock platform and 25 aligned on dune crests (see more details in Methods section 4.3.4). For convenience in this section, tracers on the bedrock will be called as set A, while those on the dune will be called as set B. The fifty bricks were selected at random from 100 numbered bricks, and the initial position of each numbered brick was recorded. This deployment was started on 15th July 2014 and the positions of individual tracers have been surveyed until 29th September 2015. Table 5.1 shows the dates of surveys including the details of tides and number of bricks surveyed. However, for the last period of tracing (March 2016) in this table the results are only approximate as there was limited time available to complete the survey in the field.

Table 5.1 Summary of the dates, number of tides, and number of tracers found in each surveys.

Date	Period	Number of days	Number of tides	Number of bricks found
15/07/2014 (Start date)	0	-	-	50
15/07/2014 -16/07/2014	1	1	2	50
16/07/2014 - 12/08/2014	2	27	52	41
12/08/2014 - 13/08/2014	3	1	2	45
13/08/2014 - 14/08/2014	4	1	2	38
14/08/2014 - 10/09/2014	5	27	52	39
10/09/2014 - 29/09/2015	6	384	742	8
29/09/2015 – 10/03/2016	7	163	315	16

A number of painted bricks located during each survey has been different through all the surveys (Table 5.2). In the first period of tracers, after two tides between 15th July 2014 to 16th July 2014, all the tracers were relocated around the area of dunes where they were originally deployed. Many tracers started disappearing after the second survey period. A few bricks were found in all surveys which are no. 8, 9, 18, 24 and 35. On the other hand, brick no. 40 was found in only one survey before disappearing until the last survey. Most of the bricks have been located and disappeared alternately, especially the tracers in set B (no.26-50) originally set up on a dune. The reasons of this behaviour of the bricks probably results from the impact of strong flow either moving them away from the vicinity and later moving them back or more likely, they were buried underneath the dunes surfaces and might be exposed again when the

dune migrated (Figure 5.6). Ignoring the final survey in March 2016 when the tracers were not surveyed in an entirety, the survey in September 2015, after 852 tides, only 8 tracers were relocated which has been interpreted as most tracers having been moved away from the immediate vicinity with some being buried locally. This interpretation is based on diligent search of the surface of the low-amplitude dunes which showed no, or few, partially buried tracers. Given the relatively large size of the tracers (D < 20 cm) in contrast to the small dune heights (< 1 m) it is unlikely that most tracers would be deeply buried leaving few examples partially exposed at the surface. Re-exhumation of some buried tracers did occur however as is detailed below.

Table 5.2 Existence of tracers being found in all survey periods (see Table 5.1 for the dates of each period). The green blocks presents identified tracers and the white colour presents the tracers that disappeared during the survey.

ID	Period							ID	Period							ID	Period						
	1	2	3	4	5	6	7		1	2	3	4	5	6	7		1	2	3	4	5	6	7
1								18								35							
2								19								36							
3								20								37							
4								21								38							
5								22								39							
6								23								40							
7								24								41							
8								25								42							
9								26								43							
10								27								44							
11								28								45							
12								29								46							
13								30								47							
14								31								48							
15								32								49							
16								33								50							
17								34								Total	50	41	45	38	39	8	16

The tracers were plotted as a map to identify the direction of coarse cobble movement and to generally see the distance each tracer moved. The latter observation provides information on whether tracers move from the bedrock onto the dunes, whether tracers can move from the bedrock over dunes and back onto the bedrock, and whether tracers move from dune to dune. Figure 5.7 shows the net movements of all tracers between the start of setting them up on 15th

July 2014 and the last survey on 29th September 2015. The map generally shows that the tracers both moved down-estuary and up-estuary. The majority of tracers moved down-estuary (31 tracers) rather than up-estuary (19 tracers) (Table 5.3). From this map it is clearly seen that tracers originally aligned on the smooth bedrock (set A), have moved greater distances than those on the crest of dune (set B).

Figure 5.6 Examples of tracers found during surveys from mid July 2014 to the end of September 2015. A few tracers were found lodged in clefts at the edge of bedrock platform. They could be prominent (A) or covered by weeds (B). Many of tracers were found on the bedform, both on the dune crests or at the toes (C)-(G). These tracers could be found clearly exposed or partly buried under the dune surface.

Although Figure 5.7 and the details of movements previously mentioned shows net changes of tracers between the first and the last survey, it might not be enough to describe all the movements of the tracers. Considering in detail all survey of tracers, pattern of tracer movements are various but interpretable (Figure 5.8). Most tracers migrated both down-estuary and up-estuary, except a few of them which showed only one direction: no.3, 14, 45, 49 down-estuary. Occasionally, some tracers moved along the crests and do not strongly show either up-estuary or down-estuary migration, for example tracer no. 6 in the 5th period that moved along the crest of dune no. 2.

Figure 5.8 shows more details of movements having occurred to the tracers for whole study period and for clearly visual investigation, movements of tracers are shows in two maps regarding to the sets of tracers. Initial comparison of Figure 5.7 and Figure 5.8 provides that tracers on the bedrock (set A) have moved further than those on the dune crest (set B). They moved along distance on the bedrock either toward the bedrock edge or the dune crests. Once

they reached the toe or the crest, they started moving shorter distances and stayed around the bedform. While most of these tracers remained on the crests next to the bedrock platform (dune no. 1 and 2 in Figure 5.7 and Figure 5.8), there are a few tracers that moved further than the others and crossed over to the next dunes, which are tracers no. 5, 14 and 20 moving down-estuary from dune no. 2 to dune no. 3. Moreover, a few of the tracers moved to the edge of the local bedrock step and became stuck at the edge for some period, some of which stayed there until the last survey or disappeared or moved to the bedform latterly. Unlike the tracers on the bedrock, the tracers set B, originally aligned on the dune crest no. 3, exhibited less mobility than the first set on the bedrock. Most of tracers slightly moved around their original positions with random direction toward up-estuary and down-estuary for the whole surveys, except only two tracers, no. 35 and 37, which moved much further than others and migrate toward the up-estuary dunes (dune no. 1 and 2 in Figure 5.7 and Figure 5.8).

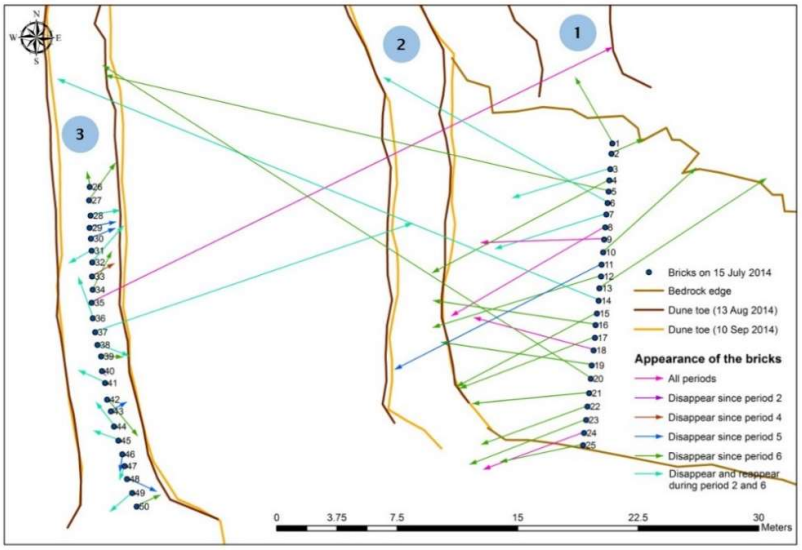

Figure 5.7 Net movements of all tracers since the initial deployment on 15th July 2014 until the last survey on 29th September 2015. Three dunes present in this area are labelled as 1, 2, 3, separated by flat bedrock areas. The arrow heads show the direction of net movement of the tracers. For the many bricks that disappeared and were latterly recovered during the study period, the movements were measured from the start in 15th July 2014 to the last position being found. The appearance of the tracers are classify into six groups: (1) the tracer(s) which appear all the survey period; (2), (3), (4) and (5) the tracer(s) which start disappearing since the 2nd, 4th, 5th and 6th periods respectively; and (6) the tracers which disappear and reappear during the 2nd period to the 6th period (see more details in Table 5.3)

Details of the distance, direction as well as information on the disappearance of some tracers are provided in Table 5.3. The net distance of tracer movement ranges from 0.45 m to 36.38 m approximately. Maximum net movements of set A and set B are 36.38 m (no. 14, to down-estuary) and 23.23 m (no. 35, to up-estuary). Both value are also the maximum net distance of tracers in terms of the direction toward down-estuary and up-estuary respectively. The minimum values of both A and B sets are 2.18 m (no. 2, to up-estuary) and 0.45 m (no. 40, to down-estuary). The migration rate of the maximum net movements of these tracers equals to 0.043 and 0.027 m/tide, while the minimum migration rate of net movements are 0.003 and 0.001 m/tide (see details inTable 5.3). More information of moving tracers including the migration rate between each survey is also provided in Table 5.3. As previously mentioned, many tracers disappeared in the study period, so they cannot being measured during some surveys only to reappear again at a later date such that they might be measured again.

The study of cobble movements was during mid July 2014 to the end of September 2015 with different sampling intervals, from two tides to several hundred tides, depending on tidal state allowing access to the site. The results from all surveys shows that the tracers moved systematically at various rates but in consistent directions. The tracers initially located on the bedform crest moved with a very low rate while on bedrock tracers were able to move longer distances. As velocities were likely greater in the shallow flow above the dune crests the difference in transport distances is readily related to the difference in bed roughness. The rough cobble surface of the dunes impeded tracer movement whilist tracers moved more freely across the smooth bedrock surface. Only a few tracers from the bedform have travelled with a great distance towards the other dunes: tracers no. 5, 14, 20, 35 and 37. While most of tracer movements show a down-estuary residual orientation, many tracers moved up-estuary as well. Moreover, many tracers disappeared over time, some of which reappeared during the study period. Although it is possible that some were transported away from the site and later transported back, most were probably buried in the bedforms around the site, notably dunes 1, 2 and 3. As a result, the movement of the tracers implies that it is possible for the tides to transport large natural particles of similar weight, including cobbles which have similar properties to the tracers. In summary most tracers on the bedrock moved rapidly to the crests or toes of the neighbouring dune 2 during the first few tides. Later, some particles passed to dunes 1 or 3. The dunes are sites of preferred accumulation of tracer, and by analogy of coarse gravel, as the tracers on dune 2 largely remained in situ and many tracers that disappeared appeared to have been buried within the dunes and later reappeared due to dune migration. Natural dispersion and burial of the tracer resulted in tracer eventually being

moved off site or buried permanently in dunes such that the number of tracers over time decreased significantly.

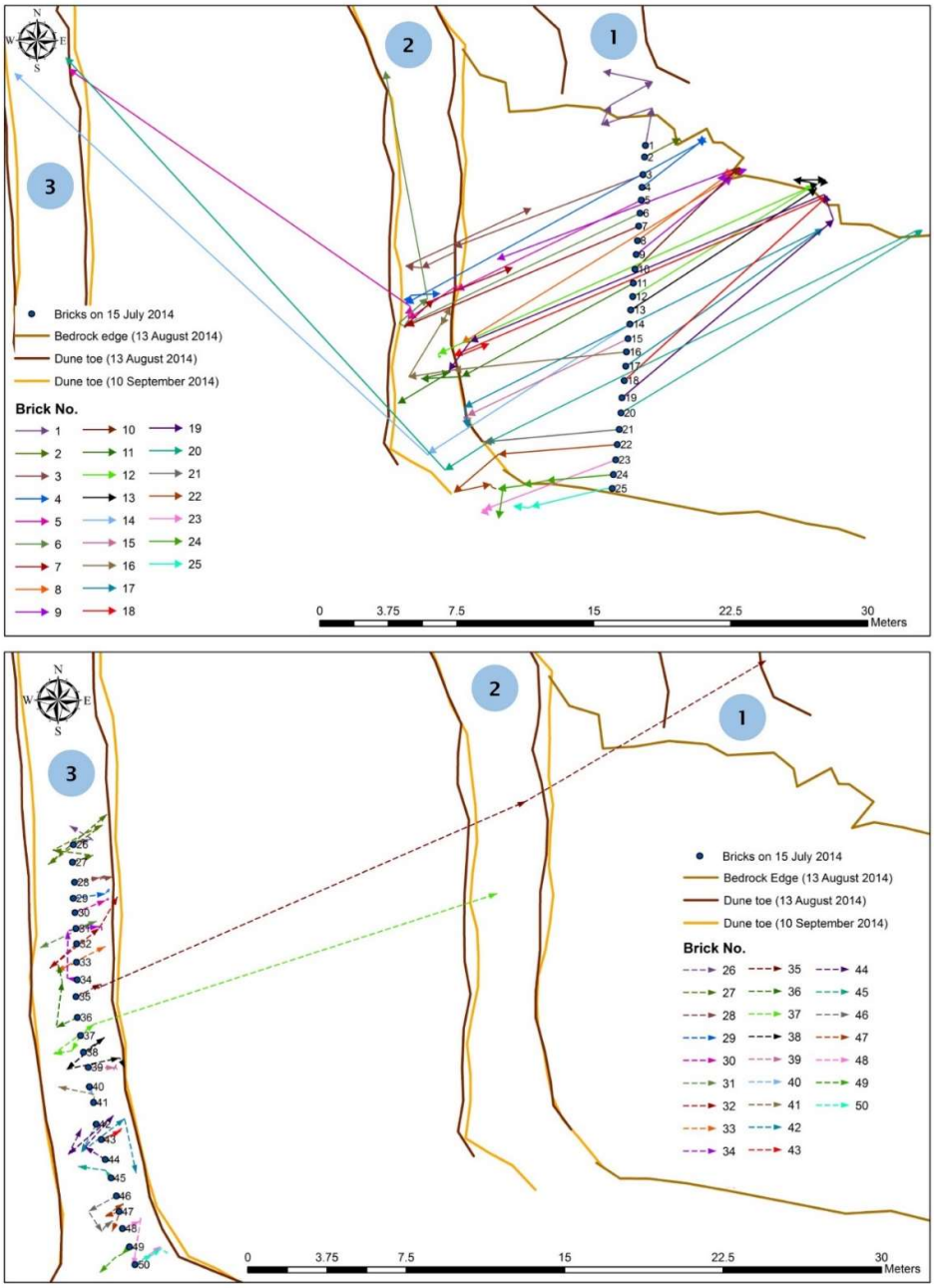

Figure 5.8 All movements of all tracers since the start of setting them up on 15th July 2014 until the last survey on 29th September 2015. (Top) A map shows all movements of tracers in set A (no. 1-25). (Bottom) A map shows all movements of tracers in set B (no.26-50)

Table 5.3 Distance and migration rate of all tracers being surveyed in each period. The white blocks are the data which have been measured regularly, the red blocks shows the tracers missing in survey, and the green blocks shows the data of tracers that reappeared after their earlier disappearance. The results of net movement comparing changes between the first and final survey, 15th July 2014 to 29th September 2015 (columns filled with light blue colour). The positive and negative values present the directions of tracers toward down-estuary and up-estuary.

ID	15July14-16July14		16July14-12Aug14		12Aug14-13Aug14		13Aug14-14Aug14		14Aug14-10Sep14		10Sep14-29Sep15		15July14-29Sep15 (Net movement)	
	Number of tides: 2		Number of tides: 52		Number of tides: 2		Number of tides: 2		Number of tides: 52		Number of tides: 742		Number of tides: 852	
	Distance (m)	Rate (m/tide)	Distance (m)	Rate (m/tide)	Distance (m)	Rate (m/tide)	Distance (m)	Rate (m/tide)	Distance (m)	Rate (m/tide)	Distance (m)	Rate (m/tide)	Distance (m)	Rate (m/tide)
1	-2.092	-1.046	2.934	0.056	-1.184	-0.592	-2.636	-1.318	2.776	0.053			4.671	0.005483
2	-2.190	-1.095	0.071	0.001	0.082	0.041	-0.089	-0.044	-0.145	-0.003			-2.182	-0.002561
3	11.070	5.535	0.290	0.006	1.973	0.987	0.877	0.439			-7.569	-0.010	13.928	0.016348
4	-4.400	-2.200	0.493	0.009	18.258	9.129	-0.525	-0.263	-1.614	-0.031			12.486	0.014655
5	11.253	5.626	-0.237	-0.005	3.205	1.602	-0.686	-0.343	22.779	0.438			32.162	0.037749
6	14.339	7.170	0.292	0.006	-2.054	-1.027			12.650	0.234			15.967	0.018741
7	13.847	6.923	0.133	0.003	0.047	0.024			-2.188	-0.041	-4.686	-0.006	11.956	0.014033
8	-6.644	-3.322	0.784	0.015	-1.239	-0.620	0.315	0.158	0.145	0.003	17.723	0.024	-6.589	-0.007733
9	-6.720	-3.360	0.785	0.015	-1.659	-0.829	0.259	0.130	0.307	0.006	14.091	0.019	-7.240	-0.008498
10	-7.974	-3.987	-0.028	-0.001	-0.049	-0.025	0.383	0.191	-0.160	-0.003			-7.784	-0.009136
11	10.684	5.342	2.240	0.043	-1.616	-0.808	3.324	1.662					14.475	0.016989
12	-11.651	-5.826	22.530	0.433	-0.200	-0.100	-0.024	-0.012	-0.128	-0.002			10.979	0.012886
13	-12.157	-6.079	0.534	0.010	0.887	0.443	-1.752	-0.876	0.431	0.008			-12.410	-0.014566
14	13.115	6.558	0.097	0.002					30.832	0.571			36.385	0.042705
15	9.735	4.867	0.508	0.010	-0.084	-0.042	-0.069	-0.034	-0.093	-0.002			9.899	0.011618
16	9.509	4.754	2.494	0.048	-4.455	-2.227	0.081	0.041	1.019	0.020			10.240	0.012019
17	-13.166	-6.583	21.920	0.422	-1.118	-0.559	-0.196	-0.098	-0.170	-0.003			9.037	0.010607

Table 5.3 (continue) Distance and migration rate of all tracers being surveyed in each period. The white blocks are the data which have been measured regularly, the red blocks shows the tracers missing in survey, and the green blocks shows the data of tracers that reappeared after their earlier disappearance. The results of net movement comparing changes between the first and final survey, 15th July 2014 to 29th September 2015 (columns filled with light blue colour). The positive and negative values present the directions of tracers toward down-estuary and up-estuary.

ID	15July14-16July14		16July14-12Aug14		12Aug14-13Aug14		13Aug14-14Aug14		14Aug14-10Sep14		10Sep14-29Sep15		15July14-29Sep15 (Net movement)	
	Number of tides: 2		Number of tides: 52		Number of tides: 2		Number of tides: 2		Number of tides: 52		Number of tides: 742		Number of tides: 852	
	Distance (m)	Rate (m/tide)	Distance (m)	Rate (m/tide)	Distance (m)	Rate (m/tide)	Distance (m)	Rate (m/tide)	Distance (m)	Rate (m/tide)	Distance (m)	Rate (m/tide)	Distance (m)	Rate (m/tide)
18	-15.036	-7.518	22.204	0.427	0.065	0.033	-0.046	-0.023	-0.209	-0.004	-1.797	-0.002	9.187	0.010783
19	-15.128	-7.564	1.483	0.029	21.000	10.500	1.956	0.978	-0.127	-0.002			9.501	0.011151
20	-19.299	-9.650	0.291	0.006	26.283	13.142	2.712	1.356	30.690	0.590			36.101	0.042372
21	7.449	3.724	-0.055	-0.001	0.066	0.033	0.111	0.056	-0.235	-0.005			7.340	0.008615
22	6.530	3.265	3.196	0.061	-2.047	-1.024	-0.174	-0.087	-0.249	-0.005			7.060	0.008287
23	7.711	3.856	-0.242	-0.005	0.329	0.164	-0.494	-0.247	0.377	0.007			7.797	0.009152
24	3.652	1.826	1.301	0.025	0.108	0.054	1.294	0.647	-0.264	-0.005	1.417	0.002	6.135	0.007200
25	0.382	0.191	4.151	0.080	0.205	0.103	0.785	0.393	-0.246	-0.005			5.303	0.006224
26	-0.823	-0.412	0.042	0.001	-0.212	-0.106	0.191	0.095	1.130	0.022			0.914	0.001073
27	-1.029	-0.514	1.927	0.037	-2.647	-1.323	3.188	1.594	-3.661	-0.070			-2.797	-0.003282
28	-1.228	-0.614	-0.280	-0.005	0.143	0.071	0.167	0.084			-0.628	-0.001	-1.226	-0.001439
29	-1.539	-0.769	-0.271	-0.005	-0.119	-0.060	0.112	0.056					-1.678	-0.001970
30	-1.551	-0.775	-0.179	-0.003	0.095	0.047	0.051	0.026					-1.620	-0.001901
31	-1.045	-0.523			2.964	0.055			-0.280	-0.005			1.653	0.001940
32	1.721	0.861			-3.013	-0.056			-1.731	-0.032			-2.957	-0.003470
33	1.045	0.522	-2.590	-0.050	-0.021	-0.011							-1.569	-0.001841
34	0.476	0.238	-2.254	-0.043	-1.466	-0.733	-0.133	-0.067	-0.205	-0.004			2.609	0.003062

Table 5.3 (continue) Distance and migration rate of all tracers being surveyed in each period. The white blocks are the data which have been measured regularly, the red blocks shows the tracers missing in survey, and the green blocks shows the data of tracers that reappeared after their earlier disappearance. The results of net movement comparing changes between the first and final survey, 15th July 2014 to 29th September 2015 (columns filled with light blue colour). The positive and negative values present the directions of tracers toward down-estuary and up-estuary.

ID	15July14-16July14		16July14-12Aug14		12Aug14-13Aug14		13Aug14-14Aug14		14Aug14-10Sep14		10Sep14-29Sep15		15July14-29Sep15 (Net movement)	
	Number of tides: 2		Number of tides: 52		Number of tides: 2		Number of tides: 2		Number of tides: 52		Number of tides: 742		Number of tides: 852	
	Distance (m)	Rate (m/tide)	Distance (m)	Rate (m/tide)	Distance (m)	Rate (m/tide)	Distance (m)	Rate (m/tide)	Distance (m)	Rate (m/tide)	Distance (m)	Rate (m/tide)	Distance (m)	Rate (m/tide)
35	-0.149	-0.074	-1.170	-0.023	-0.172	-0.086	0.218	0.109	-22.159	-0.426	-12.946	-0.017	-23.232	-0.027267
36	1.106	0.553			-2.182	-0.040	0.831	0.416					2.662	0.003124
37	0.833	0.417			0.868	0.016	-2.385	-1.192	-20.058	-0.386			-20.846	-0.024467
38	-1.217	-0.608			2.340	0.043	-2.562	-1.281	-0.542	-0.010			-2.104	-0.002470
39	-1.246	-0.623	-0.171	-0.003	0.297	0.148	-0.235	-0.118	-0.231	-0.004			-1.361	-0.001597
40	-0.448	-0.224											0.448	0.000526
41	-0.388	-0.194							1.692	0.031			1.833	0.002152
42	1.507	0.754	-2.577	-0.050	0.071	0.036	-0.123	-0.061	-2.694	-0.052			-2.998	-0.003519
43	-1.030	-0.515	0.043	0.001	0.118	0.059	-0.228	-0.114					-1.114	-0.001308
44	1.130	0.565	-2.015	-0.039	2.833	1.417			1.364	0.025			1.848	0.002169
45	0.446	0.223							1.315	0.024			1.660	0.001948
46	1.509	0.754	-1.168	-0.022	-0.229	-0.115	-0.521	-0.261					1.186	0.001392
47	0.719	0.359	-1.061	-0.020					1.413	0.026			0.998	0.001172
48	-0.896	-0.448	-0.205	-0.004	2.351	1.176	-1.627	-0.813					-2.019	-0.002370
49	0.504	0.252			0.333	0.006			1.042	0.019			1.863	0.002186
50	0.184	0.092	-1.115	-0.021	-0.516	-0.258	-0.365	-0.182	0.137	0.003			-1.624	-0.001906

5.1.4 Topographic survey of dune crests

According Table 4.1, there were 16 surveys between February 2013 and September 2015. However, some datasets contain some spatial errors created by technical issues, especially in the first few surveys of 2013. Some of these datasets were improved by the technique mentioned in the Methods chapter. Even though the data were improved, spatial errors are not acceptable for quantitative comparisons: the surveys of February and May 2013. As a result, five datasets; 11th – 12th February 2013, 12th – 13th March 2013, and 27th May 2013; were rejected for quantitative analysis as they could not be improved. However, considering the shape of dunes alone, rather than their absolute location, both datasets show a similar pattern to the referenced map of September 2013. The two data sets in 20th September 2013 and 19th March 2014 also were of limited quantitative value.

As a result, there are nine datasets being available for further quantitative analysis (Table 5.4) and the survey in 12th March 2013 will be used as the base map for comparing changes of the later surveys. The individual surveyed dunes were labelled by number, starting with 31 dunes in March 2013 and new dunes formed later were labelled with the numbers 32 to 46 (see Table 5.4 and Figure 5.9). Numbers of dunes in the survey were labelled not only as individuals but also as groups of dunes. These groups of dunes include dune number 7, 8 and 20. These grouped dunes are separated into individuals, such as 7.1, 7.2, 7.3, 8.1, 8.2, 8.3, 8.4, 20.1, and 20.2 (Figure 5.10). The number of dunes recorded during each survey are different due to a number of reasons which are; a) the water levels during the surveys are different which allow different exposure of dunes; b) decay or growth of small dunes especially in the down-estuary portion of the survey area; and c) time-limitation during survey. All these topographic surveys were done around low tide with rising and falling spring tides (Table 5.5). Nevertheless it was generally possible to identify significant changes in the number and planform of the individual dunes and their relation one to another.

Table 5.4 Summary of the available datasets of dune survey showing the number of dune being measured. The colour-filled schedule represents the dunes were measured in each survey, while the white one represents dunes were not found during each survey.

No	Date	Period	1	2	3	4	5	6	7	8	9	10	11	12	13	14	15	16	17	18	19	20	21	22	23	24
1	11-Mar-13	0																								
2	26-Jun-13	1																								
3	23-Jul-13	2																								
4	24-Jul-13	3																								
5	20-Aug-13	4																								
6	19-Sep-13	5																								
7	18-Mar-14	6																								
8	16-Jun-14	7																								
9	29-Sep-15	8																								

No	Date	Period	25	26	27	28	29	30	31	32	33	34	35	36	37	38	39	40	41	42	43	44	45	46	47	All
1	11-Mar-13	0																								31
2	26-Jun-13	1																								25
3	23-Jul-13	2																								31
4	24-Jul-13	3																								18
5	20-Aug-13	4																								24
6	19-Sep-13	5																								33
7	18-Mar-14	6																								36
8	16-Jun-14	7																								28
9	29-Sep-15	8																								31

Table 5.5 Details of period length between surveys including the number of tides during those periods, between March 2013 and September 2015

No	Start date	End Date	Number of days	Number of tides
1	11 Mar 2013	26 June 2013	108	207
2	26 June 2013	23 July 2013	28	52
3	23 July 2013	24 July 2013	1	2
4	24 July 2013	20 Aug 2013	28	52
5	20 Aug 2013	19 Sep 2013	31	58
6	19 Sep 2013	18 Mar 2014	181	348
7	18 Mar 2014	16 June 2014	91	174
8	16 June 2014	29 Sep 2015	471	908
Total			**939**	**1801**

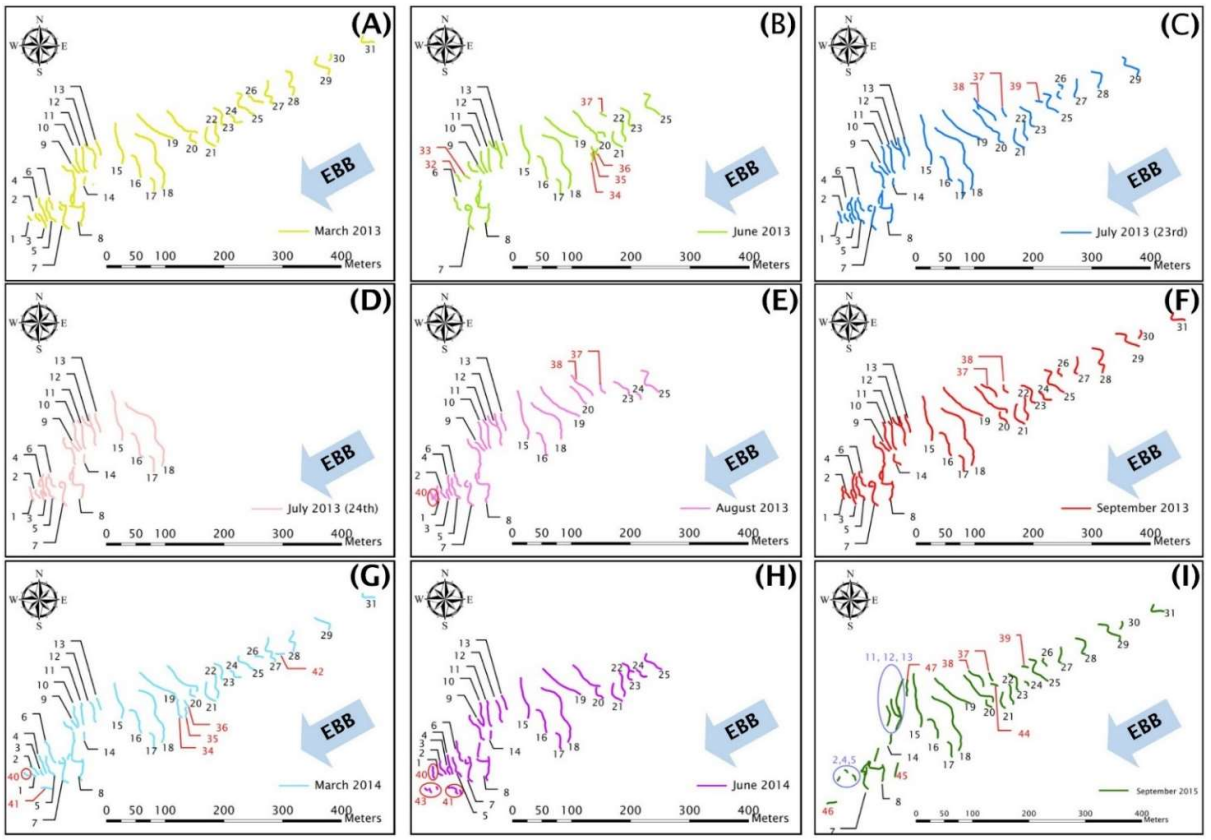

Figure 5.9 Surveyed dunes at different times during March 2013 to September 2015. The black colour numbers are the common dunes that had been identified and surveyed since the base survey in March 2013. The red numbers presents the new dunes found and measured after March 2013. The red circles in the down-estuary identify those very small dunes which were poorly developed. It is not possible to be sure if these were newly developing dunes or residual masses from fragmented dunes which had formed earlier. The light violet circles in September shows the area of dunes with significant planform changes found in the dunefield.

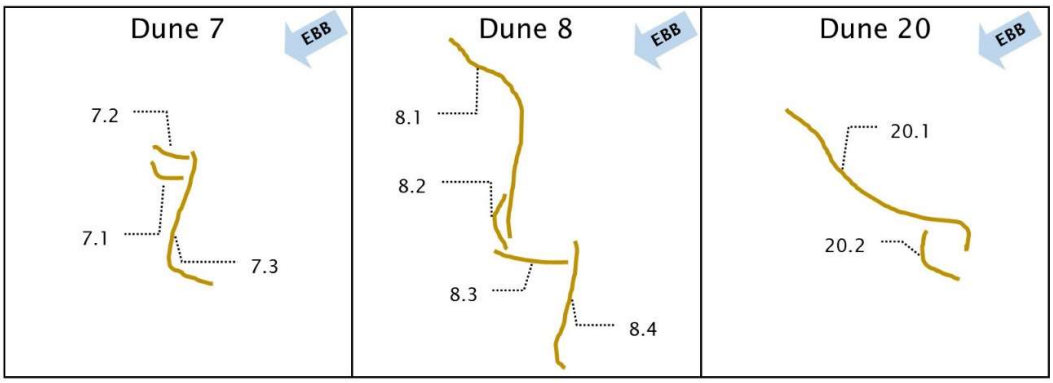

Figure 5.10 Sub-section of groups of dunes. Dune number 7, 8 and 20, from a survey on 11th – 12th March 2013.

From initial visual observation on site during all the surveys, together with subsequent investigation of the maps, dunes extend into the main channel with straight or slightly sinuous crests (Figure 5.9 and Figure 5.11). The orientations are north-west to south-east direction. The date of surveys as well as the number of tides between each survey are summarised in Table 5.5. Unlike most dunes which have crests transverse to the main flow, dune number 7.1, 7.2 and number 8.3 (Figure 5.10) have very small size and were developed in finer grains than the dunes in the up-estuary. Their crests aligned slightly in the parallel direction with the main flows, or in the north-east to south-west. There are two possible explanations which may act in concert. Firstly, more rapid residual migration of the dune crest may occur offshore where currents are stronger with slow migration or a static duneform to landward (as is seen with dune 8.1), causing the dune to bend in the intermediate area. If this process is pronounced then the dune crest in the intermediate area might become parallel to the main flow (as is seen with dune 7.1 and 8.3). An alternative explanation is that short dunes, transverse to the main dune alignments, form as late ebb runoff from the tidal flat is channelled northwards in the trough between two major dune crests. Clearly these two processes might act in concert. However, the frequent flexure of the dune crestlines down estuary further northward suggest the first processes is the major constraint on dune alignment. In the field, individual dune crestlines often consist of loose, weed-free clasts to the north (offshore), such as Figure 5.11C and D, but are consolidated and well-vegetated by seaweed to the south (onshore), Figure 5.11E and F, where they appear to be fixed in position, which supports the concept of greater mobility offshore.

Moreover, there are several very small new undulation forms that appear after the first survey, the dunes labelled with red colour in Figure 5.9. These new dunes consist of mixed-size

loose grains and are very low in height. Consequently, these new small dunes can disappear during whole study period either due to decayed by flows or on occasion they could have been too low to be exposed during some surveys.

An overlay of all topographic surveys using ArcGIS software provides a general results that the changes of dunes in terms of shape and position between each individual survey does not show significant change (Figure 5.9) and they may be considered as near-static bedforms, especially in the first year of observation of which the interval between each survey is short, the later survey have been done within a month after a previous survey. However, in longer time-scale of a year or more, there are two surveys showing evident movements of dune crests. The first significant change of dune crests is found in March 2014 and the other one in September 2015. These results are amplified below.

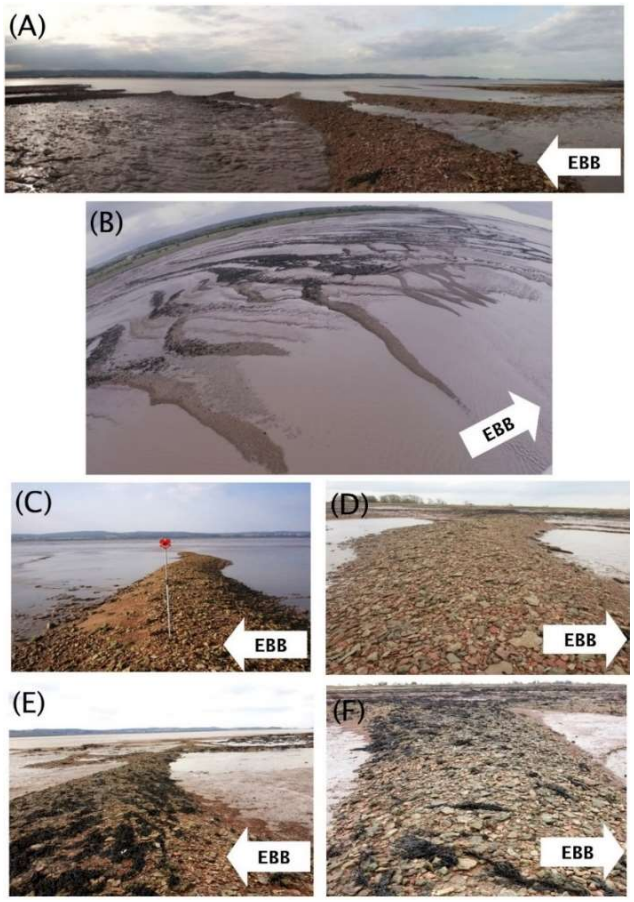

Figure 5.11 Images of dune crest; (A) panoramic view of dunes looking north toward the main channel where the crests closed to the main channel were not fully exposed due to the water level not being low enough; (B) fish-eye aerial photograph of dune field; (C) and (E) view along individual crests toward the main channel on the

offshore side, while (D) and (F) shows the other view of dune crests towards the estuarine margin on the onshore side.

March 2013 to March 2014

Since the survey in March 2013, the first apparent change of dune crests is in March 2014. After 377 days or 719 tides, the comparison of these two maps show slight changes in most dunes, whilst dunes down-estuary have changed more (see Figure 5.12). The crests of dunes number 1 to number 12 are obviously different while the others have small changes. A number of new dunes were found in this survey which are the dune numbers 34, 35, 36, 40, 41 and 42. The dunes no. 34, 35, 36 and 40 were formed within this period of comparison (after March 2013 and before March 2014), whilst number 41 and 42 were firstly found in March 2014 (Table 5.4). The visual comparisons of dune locations are supported by measuring the distances from the base survey in March 2013. The migration along the dune crests varied at different rates whilst few of the dunes show no change. The information in Table 5.6 provides the maximum and minimum of migrating distances (L_{max} and L_{min}) of all 36 dune crests, the maximum migration ratio per tide (L_{max}/tide) as well as number of data points collected along the crests and the direction of data point movement.

The distance of crest migration of 36 dunes range from no movement up to 6 m approximately. From the total maximum distance (L_{max}) on all dunes, there are 12 dunes having the L_{max} more than 2 m, while 14 and 10 crests have moved between 1-2 m and less than 1 m respectively. So the majority of L_{max} is between 1 to 2 m. On the other hand, most of the minimum movements (L_{min}) equal to zero. The highest L_{max} was found in dune number 8.2 with a distance of 6.61 m down-estuary, followed by dune number 8.1, 6, 10, and 2 with 4.58, 4.44, 3.96, and 3.73 m respectively which all move down-estuary except dune number 6 moving up-estuary. For the lower L_{max} of the other dunes, these are down-estuary, except dune numbers 1, 4, 6, 8.3, and 28 which move up-estuary. Only a few dunes for which L_{min} shows slight movement, from 0.36 to 1.48 m approximately, migrated in the same direction as their L_{max}. In this study, the migration rates of each dunes are considered by the relationship between the L_{max} and number of tides. The highest rate occurs on the dune number 8.2 with 0.0092m/tide or 0.92 cm/tide, while the lowest rate is 0.0007 m/tide or 0.07 cm/tide on the dune number 18.

Considering the direction of the maximum and minimum distance data points and the percentage of migrating direction, there are 29 dunes (80.56%) with the L_{max} occurring down-estuary and 7 dunes (19.44%) in contrast move up-estuary. Looking at the total data points on

each crest, there is a same trend with L_{max} in that most crests moved down-estuary (58.33%), followed by static dunes (27.78%) and only a few moved up-estuary (13.89%).

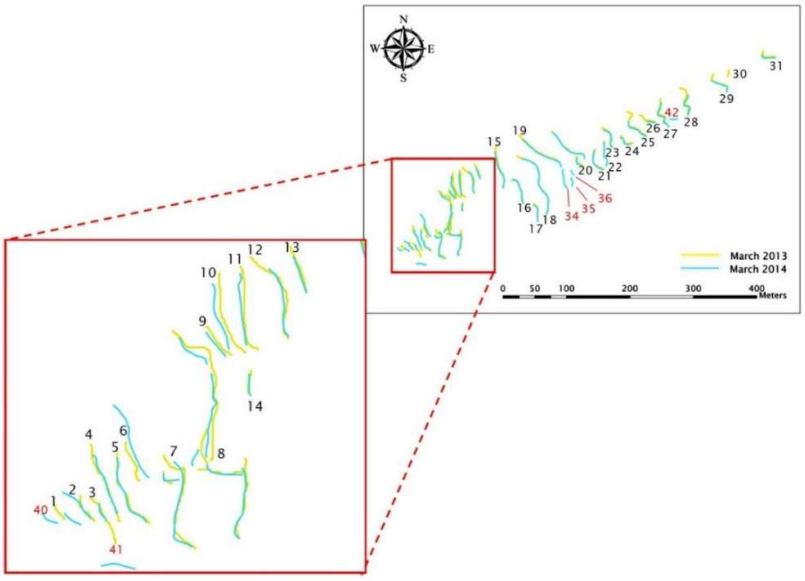

Figure 5.12 A map showing a comparison of dune crests between March 2013 and March 2014. The inset red frame is an expanded view of the down-estuary area where mobility of dune crests clearly exist.

March 2014 to September 2015

After a first significant change in March 2014, the other survey showing important details is in the latest survey, September 2015, the results show significant changes in dunes after 1,081 tides. Similar to the previous period, dunes down-estuary, number 1 to 13, have higher mobility and exhibit more changes than those up-estuary (Figure 5.13). The visual observation and distance measurement from the previous survey in March 2014 show difference in terms of shape, position, as well as distance of migration. In this comparison, a few of dune crests disappeared; these are dune number 1, 3, 6, 9, 10, and a part of 7 and 8, while dune number 44, 45 and 46 only exist after a survey in March 2014. The apparent changes in planform occurs to dune number 11, 12 and 13 where the maximum migration distance are the highest among other dunes. Moreover, dune number 7.1, 7.2 and 8.2 may have change in shape by combining together into one crest.

Details of migration in this period are provided in Table 5.7. The total surveyed crests are 27 with the range of movement from 0 to 15 m approximately. Almost half of dunes move less

than 1 m (48.15%). Apart from these dunes, the majority of dunes have L_{max} between 2 to 10 m (33.33%) while only two dunes have L_{max} between 1 and 2 m (7.41%) and L_{max} greater than 10 m are measure for three dunes (11.11%). The five highest L_{max} values were measured for dune numbers 11, 14, 12, 5 and 8.1 with approximate movements of 15.30, 14.62, 12.17, 6.29 and 5.55 m respectively. All of these L_{max} values migrate up-estuary and are similar to the trend of the total data point of dunes in this period of which the majority move up-estuary. The other dunes move in both directions, but there are two dunes showing no changes. Similar with the previous period, most dunes has no movement for minimum migration (L_{min}). Only a few dunes move down-estuary in that L_{min} is greater than 0 m, ranging from 0.25 to 7.94 m with the same direction as L_{max} on their own dunes. Migration rate (L_{max}/tide) is highest on dune number 11 with 0.014 m/tide or 1.4 cm/tide. In contrast, the minimum migration rate is 0 m/tide on dune number 24 and 28 as their L_{max} are 0m which were considered as static dunes.

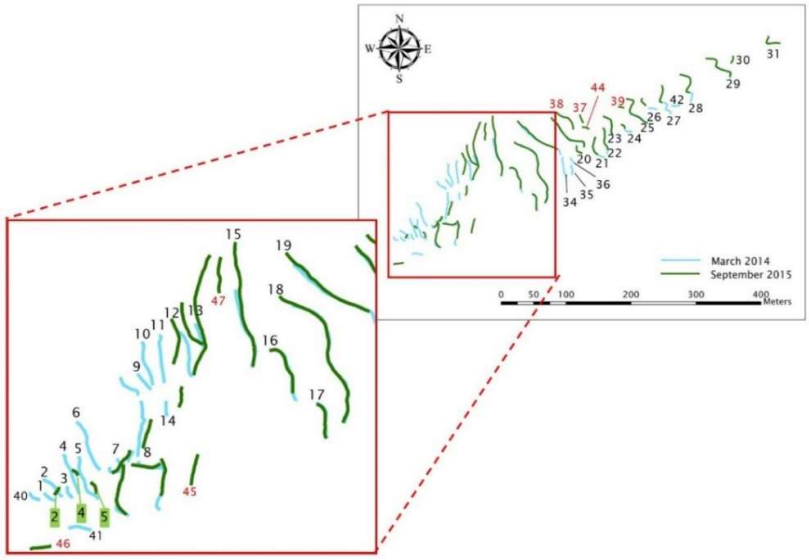

Figure 5.13 A map showing a comparison of dune crests between March 2014 and September 2015. The inset red frame is an expanded view of the down-estuary area where mobility of dune crests clearly exist.

Looking at the direction of all L_{max} data, the majority of L_{max} shows the migration toward up-estuary (59.26%), others move down-estuary (33.33%) or are static (7.41%). However, considering the direction of all data points in each dunes, most dunes are static (55.56%), up-estuary migrating (37.04%) and only few are down-estuary moving (7.41%). This is different from comparison of the first period, March 2013 to March 2014, when most dunes move down-estuary, a few move up-estuary, the static dunes slightly increase. The opposing

migrating direction of many dunes happening within these two periods might imply a near-balance in the ebb-flood flow conditions over extended time periods. Although flood tides may move dunes up-estuary and ebb tides move them down-estuary the resultant is a low residual migration rate down the estuary, demonstrating a weak ebb dominance.

March 2013 to September 2015

The comparison between two surveys in March 2013 and September 2015 is done in order to shows the net changes happening to the dunes during the study period of two and half years. After 939 days or 1801 tides from the first survey, significant changes occurs to the dune field. According to an observation of an overlayed map (Figure 5.14) and the data of movement of all surveyed dunes (Table 5.8), it can be clearly seen that most dunes in the down-estuary field, dune number 2 to 15, generally move towards up-estuary while the dune crest, number 16 to 31, in the up-estuary field mostly move down-estuary. Data of migration measurement in Table 5.8 shows that the migration distance starts from 0 to 19 m approximately. Most L_{max} are between 1 and 2 m (35.48%), and many data points of L_{max} are between 2 and 10 m (29.03%) followed by less than 1 m (22.58%) and small number of L_{max} more than 10 m (12.90%).

Considering only the maximum distance (L_{max}) measured on each dune, the movements being measured are from 0 to 19.42 m. The furthest distance of 19.42m was found on dune number 12 and the other shorter distance is found on dune number 7.1, 14, 11 and 7.2 with distance of 14.90, 13.91, 12.00 and 7.27 m. All of these L_{max} data points were found in the down-estuary area and moved up-estuary, whilst the L_{max} values in the rest of the dunes tend to move down-estuary, especially the dunes in the up-estuary area. The minimum distance (L_{min}) measured in the field equaled zero. Only a few dunes are not totally static as their minimum migration is above 0m, most of which are the down-estuary dunes. The highest L_{min} values are found in the case of dunes number 11, 12 and 14 with distance of 6.88, 2.35 and 10 m respectively. These three points moved the same direction and are found in the same dunes having the highest L_{max}. The highest migration rate (L_{max}/tide) on the dune number 12 is about 0.011 m/tide or 1.1 cm/tide and the lowest migration rate is on the dune number 26 with 0.0003 m/tide or 0.03 cm/tide which is very low rate.

The proportion of L_{max} between directions of down-estuary, up-estuary, and static is 54.84%, 45.16% and 0% respectively. For all data points of each dune, the migration trend of each crest are similar to the L_{max} data with most of dunes in the down-estuary area moving up-estuary, on the other hand, the majority of up-estuary dunes migrate down-estuary. However, there

are a few dunes which turn out to be static among the other dunes. The percentage of these two directions as well as the static state is not much different. The dunes with the most data points moving up-estuary are high as 38.71%, followed by static dunes 32.26% and down-estuary as 29.03%.

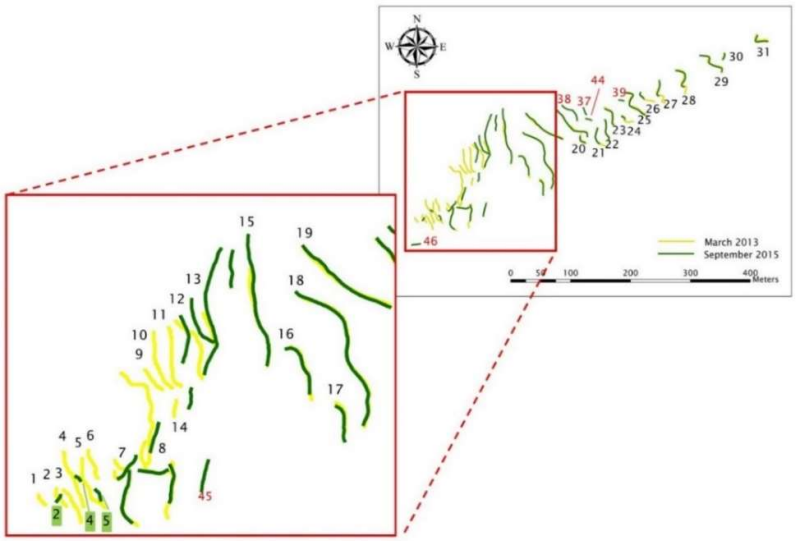

Figure 5.14 A map showing a comparison of dune crests between March 2013 and September 2015. The inset red frame is an expanded view of the down-estuary area where mobility of dune crests clearly exist.

In summary, the crests of cobble dunes migrate at different rates due to differences in the power of the tidal streams. The rate of migration is generally low, the maximum rate in the study period is only approximately 0.01 m/tide. Higher migration rates occur for the dunes in the down-estuary area, and for those portions of those crestlines further towards the main channel where tidal currents are likely to be stronger. In the first year, the results show that in terms of residual movement, most of the dunes slightly moved down-estuary while a few moved up-estuary. On the other hand, the second comparison for the period of March 2014 to September 2015 provides different results. Several dunes in the down-estuary area migrated up-estuary and some of them changed their planform shapes. Many dunes in the up-estuary area tended to be static while only a few crests moved down-estuary. However, the net changes of dune crests from the first to the last survey of the study shows that dunes moved both down-estuary and up-estuary as well as remaining static in slightly similar proportions. The migrating tendencies of dune crests are shown in Figure 5.15. Figure 5.15A, B and C are plotted by using all data points for all dunes while Figure 5.15D, E and F consider only the maximum migration distance of each dune. All histograms in Figure 5.15 show high frequency of movements close to 0 m, from which it is evident that the dunes rarely move in

all three study periods. Except for Fig. 5.15A and D which shows predominant down-estuary movement, the other histograms are skewed to include a tail of high migration distances up-estuary. The down-estuary maximum distances tend to be relatively short in contrast to the up-estuary values. In summary in the first period, March 2013 to March 2014, dunes tends to migrate down-estuary rather than move up-estuary. Later in the second period, March 2014 to September 2015, as well as the overall study period, March 2013 to September 2015, dunes are tended to move up-estuary often with a few examples of movement over considerable distances. For each dune crest the migration rate along the crestline could vary between surveys as could the direction of net migration. Significant up-estuary migration, as noted above, may be due to storm action, whilst other differences in migration rate may be due to the on-shore to off-shore alignment of the dunes into deeper and faster flowing water. The location right on the edge of the rock platform next to a deep channel will ensure complex interchange of water between the channel and the platform as was noted in the results section on tidal current strength and direction (Section 5.2).

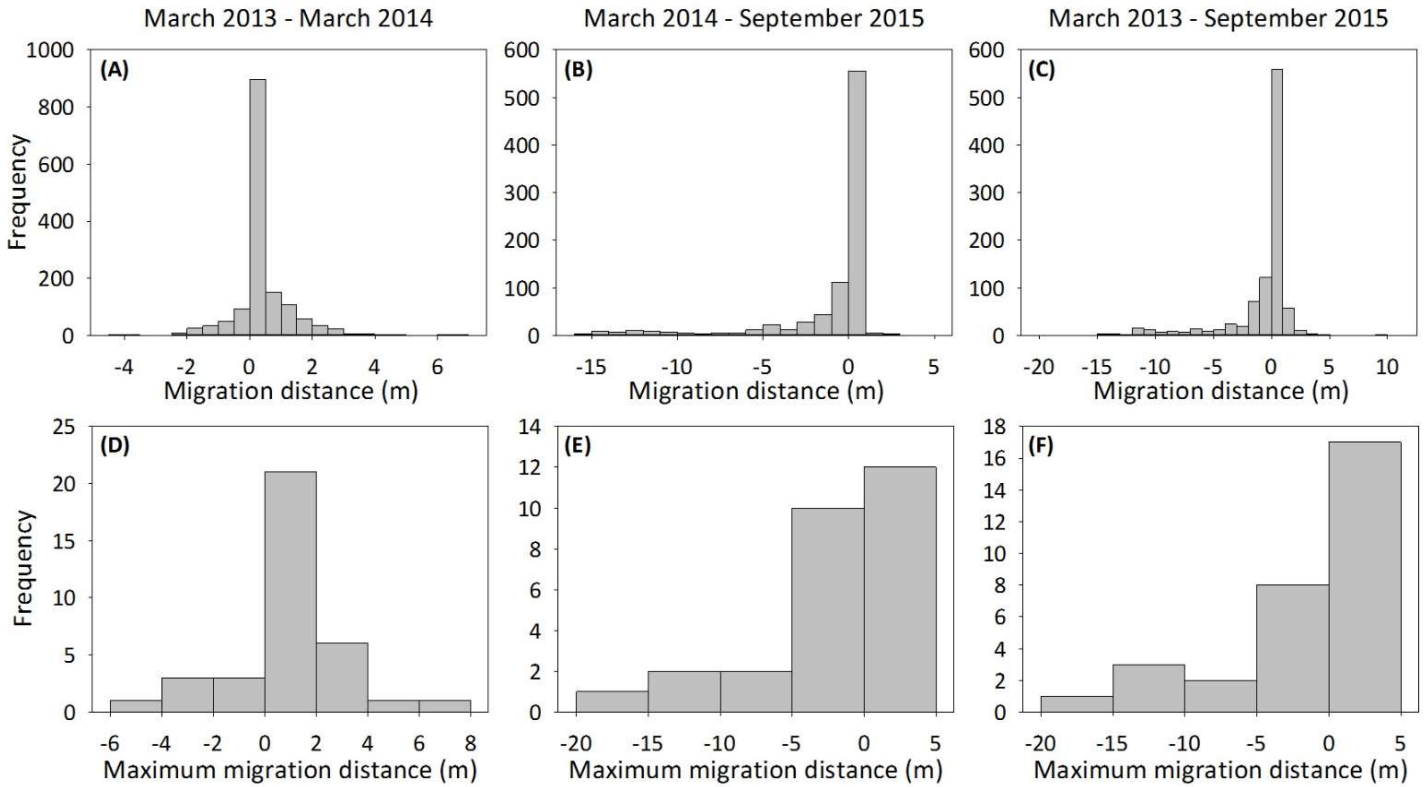

Figure 5.15 Histograms present the frequencies and trends of migration distance measured on dune crests. (A), (B) and (C) histograms are plotted by all data points of all dunes while (D), (E) and (F) are plotted by the maximum migration distance of each dune. The positive and negative values symbolize down-estuary and up-estuary migration respectively.

Table 5.6 Details of migration rates measured between March 2013 and March 2014. The direction of movement are defined as D (down-estuary), U (up-estuary), and X (no movement).

11th March 2013 – 18th March 2014									
Dune no.	Maximum movement		Minimum movement		Lmax/No. of tides (m/tides)	No. of data points collected and the direction of movements			
	Length (m)	Direction	Length (m)	Direction		Total	D	U	X
1	2.13	U	1.48	U	0.00296	6	0	6	0
2	3.73	D	0.00	X	0.00519	23	10	2	11
3	0.66	D	0.00	X	0.00091	14	5	2	7
4	1.25	U	0.00	X	0.00174	43	0	15	28
5	0.42	D	0.00	X	0.00059	53	14	6	33
6	4.44	U	0.89	U	0.00617	25	0	25	0
7.1	0.90	D	0.00	X	0.00125	12	3	1	8
7.2	2.60	U	0.00	X	0.00362	8	0	7	1
7.3	2.12	D	0.00	X	0.00295	60	36	0	24
8.1	4.58	D	0.00	X	0.00638	86	81	0	5
8.2	6.61	D	1.00	D	0.00920	15	15	0	0
8.3	1.04	U	0.00	X	0.00144	22	0	8	14
8.4	0.90	D	0.00	X	0.00125	44	25	0	19
9	2.03	D	0.62	D	0.00282	21	21	0	0
10	3.96	D	1.29	D	0.00551	45	45	0	0
11	2.42	D	0.00	X	0.00336	48	45	0	3
12	1.47	D	0.00	X	0.00205	43	21	7	15
13	0.71	D	0.00	X	0.00099	27	19	0	8
14	0.52	D	0.00	X	0.00072	13	3	1	9
15	0.77	D	0.00	X	0.00107	79	52	6	21
16	0.67	D	0.00	X	0.00093	53	22	4	27
17	1.16	D	0.00	X	0.00162	26	15	0	11
18	0.49	U	0.00	X	0.00068	131	18	6	107
19	1.10	D	0.00	X	0.00153	73	53	0	20
20.1	1.36	D	0.00	X	0.00189	84	28	1	55
20.2	1.02	D	0.00	X	0.00142	26	12	10	4
21	1.00	D	0.00	X	0.00139	46	23	4	19
22	0.43	D	0.00	X	0.00059	52	4	7	41
23	1.44	D	0.00	X	0.00200	45	23	9	13
24	1.67	D	0.00	X	0.00232	27	21	0	6
25	1.37	D	0.00	X	0.00191	51	39	4	8
26	1.65	D	0.36	D	0.00229	19	19	0	0
27	1.65	D	0.00	X	0.00230	58	19	32	7
28	2.38	U	0.00	X	0.00331	52	11	37	4
29	1.11	D	0.00	X	0.00155	44	21	7	16
31	2.30	D	0.00	X	0.00320	36	28	6	2

Table 5.7 Details of migration rates measured between March 2014 and September 2015. The direction of movement are defined as D (down-estuary), U (up-estuary), and X (no movement).

18th March 2014 – 29th September 2015									
Dune no.	**Maximum movement**		**Minimum movement**		**Lmax/No. of tides (m/tides)**	**No. of data points collected and the direction of movements**			
	Length (m)	**Direction**	**Length (m)**	**Direction**		**Total**	**D**	**U**	**X**
2	2.89	D	0.00	X	0.00267	8	3	4	1
4	3.69	U	0.25	U	0.00341	7	0	7	0
5	6.29	U	1.50	U	0.00582	11	0	11	0
7.3	2.02	U	0.00	X	0.00186	39	0	16	23
8.1	5.55	U	2.48	U	0.00513	22	0	22	0
8.3	4.02	U	0.00	X	0.00372	20	6	5	9
8.4	0.93	U	0.00	X	0.00086	25	0	8	17
11	15.30	U	7.94	U	0.01414	30	0	30	0
12	12.17	U	0.96	U	0.01125	38	0	38	0
13	2.27	U	0.54	U	0.00210	18	0	18	0
14	14.62	U	10.04	U	0.01351	15	0	15	0
15	2.50	U	0.00	X	0.00231	59	8	39	12
16	0.70	D	0.00	X	0.00064	40	12	5	23
17	0.54	D	0.00	X	0.00050	30	18	0	12
18	0.92	U	0.00	X	0.00085	105	30	5	70
19	2.33	U	0.00	X	0.00215	61	0	32	29
20.1	1.20	D	0.00	X	0.00111	67	17	22	28
20.2	0.27	D	0.00	X	0.00025	16	4	0	12
21	0.75	U	0.00	X	0.00069	27	3	6	18
22	0.56	D	0.00	X	0.00052	33	20	0	13
23	0.42	D	0.00	X	0.00039	34	6	2	26
24	0.00	X	0.00	X	0.00000	10	0	0	10
25	0.26	D	0.00	X	0.00024	37	14	7	16
26	0.59	D	0.00	X	0.00054	10	4	0	6
27	0.19	U	0.00	X	0.00018	26	2	4	20
28	0.00	X	0.00	X	0.00000	25	0	0	25
29	1.96	U	0.00	X	0.00181	31	10	4	17
31	0.77	D	0.00	X	0.00071	26	8	0	18

Table 5.8 Details of migration rates measured between March 2013 and September 2015. The direction of movement are defined as D (down-estuary), U (up-estuary), and X (no movement).

11th March 2013 – 29th September 2015									
Dune no.	**Maximum movement**		**Minimum movement**		**Lmax/No. of tides (m/tides)**	**No. of data points collected and the direction of movements**			
	Length (m)	**Direction**	**Length (m)**	**Direction**		**Total**	**D**	**U**	**X**
2	4.18	D	0.00	X	0.00232	8	3	4	1
4	3.34	U	0.83	U	0.00186	7	0	7	0
5	5.77	U	1.60	U	0.00320	11	0	11	0
7.1	14.90	U	0.00	X	0.00827	10	0	9	1
7.2	7.27	U	0.00	X	0.00404	9	0	8	1
7.3	0.69	D	0.00	X	0.00038	53	10	0	43
8.1	4.18	U	0.00	X	0.00232	22	0	21	1
8.3	1.04	D	0.00	X	0.00058	21	3	6	12
8.4	1.67	D	0.00	X	0.00093	28	13	3	12
11	12.00	U	6.88	U	0.00667	33	0	33	0
12	19.42	U	2.35	U	0.01078	54	0	54	0
13	2.72	U	0.76	U	0.00151	21	0	21	0
14	13.91	U	10.00	U	0.00772	16	0	16	0
15	2.27	U	0.00	X	0.00126	61	2	31	28
16	0.68	D	0.00	X	0.00038	37	18	2	17
17	1.68	D	0.00	X	0.00093	22	20	0	2
18	0.67	D	0.00	X	0.00037	106	42	5	59
19	1.57	U	0.00	X	0.00087	67	22	26	19
20.1	1.78	D	0.00	X	0.00099	62	24	15	23
20.2	1.02	D	0.00	X	0.00057	17	10	2	5
21	0.64	D	0.00	X	0.00035	28	5	4	19
22	0.66	D	0.00	X	0.00036	33	9	0	24
23	1.40	D	0.00	X	0.00078	35	18	6	11
24	1.41	D	0.00	X	0.00078	9	7	0	2
25	1.90	D	0.00	X	0.00105	55	31	14	10
27	1.59	D	0.00	X	0.00088	28	5	11	12
28	1.87	U	0.00	X	0.00104	38	14	20	4
29	2.10	U	0.00	X	0.00117	39	19	8	12
30	0.88	U	0.21	U	0.00049	10	0	10	0
31	2.35	D	0.00	X	0.00130	31	21	8	2

5.1.5 Cross section measurement

During the study, cross-section profiles were measured over the dunes in the middle of dunefield and close to the equipment location, dune no. 12 (Figure 5.16). Measurement were completed twice during the study: September 2014 and March 2016. Dune no.12, in the middle of the dunefield, where the flow meters were installed was surveyed, as were a number of adjacent dunes, both down-estuary and up-estuary of dune no.12. In total, 12 sections of dunes were measured in this study from the down-estuary to up-estuary. Details of measurement process is explained in the previous section (see section 4.1.3)

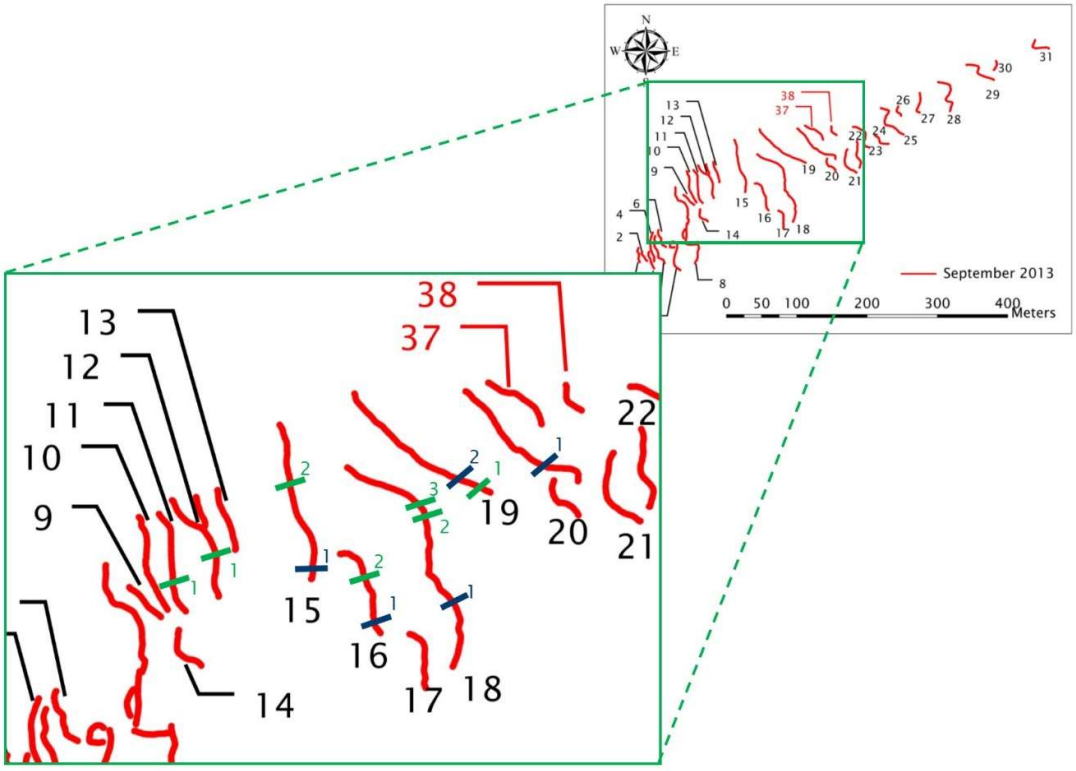

Figure 5.16 Positions of cross profile being measured in the dunefield. The overall map shows dune crestlines (red). The short lines across the crestlines show the position of measurement labelled with numbers. Different colours present the time of measurement; September 2014 in green colour and March 2016 in dark blue colour.

All longitudinal shapes of dunes and their statistics are shown in Figure 5.17 and Table 5.9. They show different size and shape even the cross-section measured in the same dunes but different position, for example sections no 15-1 and 15-2. Considering both height (H) and length (L_2) they are lower than 1 m and shorter than 12 m. Using criteria suggested by Ashley (1999), dunes have different size classification. Dunes tend to be smaller in scale in the down-estuary portion of the dunefield while the size of up-estuary dunes tend to increase (Figure 5.17). Almost half of dune profiles show that their size cannot be exactly classified into one scale with respect to both their heights and lengths considered together. For example, Dune 15-1 and 18-1 are considered as large scale in terms of their heights but medium scale in terms of their length.

Taking the highest point of a dune crest vertically down to the bed, the total dune length can be divided into two portions: the lengths on the up-estuary and down-estuary sides (L_U and L_D) (Figure 4.8). Rather than only consider the cross-sections visually to determine a degree of dune symmetry, the two length indices, L_U and L_D, are used to indicate quantitatively if the dunes are symmetric or asymmetric. Most cross-section profiles show slightly asymmetry with ebb orientation (L_U>L_D or L_U/L_D >1), except dune 16-1, 16-2, 19-2 and 20 which have slight flood orientation (L_U<L_D or L_U/L_D <1). For the ebb orientation, Dune 11 and 12 shows down-estuary asymmetry (L_U/L_D = c. 2), while the other down-estuary orientated profiles show lower asymmetric ratio, some of which are very low and their asymmetric ration is close to 1 implying they are almost symmetry, i.e. Dune 19-1. Among the group of flood orientation profiles, Dune 16-2 shows the most flood orientated asymmetry (L_U/L_D = c. 0.5), followed by Dune 16-1 (L_U/L_D = c. 0.7), while the other two profiles, Dune 19-2 and 20, in this group have higher rate close to 1, showing almost symmetry. Cross-section measurement was done after ebb flows which might be a reason that most profiles show ebb orientation. However, cross-sections after flood tides cannot be measured during this study. It is unknown if the asymmetry of dunes will be effected by the action of flood tides.

Among the dunes, only a few cross-sections have near-horizontal crests (L_1), which are dune 11, 16-1, 19-1 and 19-2, so the flatness index defined as L_1/L_2 (Carling, 1996b) of most sections are 0 as most of them do not have a crestal platform. The available flatness index are 0.22, 0.34, 0.43 and 0.48. On average the angle of repose of dune slopes are low. Specifically, the angles of lee and stoss slopes varied between 11° and 22° and between 9° and 21° respectively, which the median angles of both slopes are 15.5° and 14.5°. Both lee and stoss

slopes of each dune are often similar in angle, except dunes 15-1 and 16-2 of which the steeper slope is twice as steep as the gentler slope (Table 5.9).

According to the relationship between height and length given by Ashley (1990) as $H = 0.0677L^{0.8089}$, the estimated height from this relationship is lower than the measured height. The $H - L$ relationship from measurements is $H = 0.1249L^{0.8501}$ (Figure 5.18). Steepness values (H/L) are not higher than 0.1 with the lowest ratio being about 0.06 (Table 5.9) which falls in the range of experimental data provided by previous studies (Bridge, 2003; See Figure 2.5 in Chapter 2). Moreover, dune steepness (L_2/H), a dune index presented by Carling *et al* (2006), ranges from 7 to 16 approximately.

Water depth (h), one of the important factors on dune development, was related to dune height (H) and length (L). As flow data on the date that cross-sections were measured are not available, water depth on the survey date was calculated by using the relationship between predicted height at Avonmouth and water depth calculated from the flow meters (equation: $y = 1.1139x - 5.8527$ in Figure 5.27). Here, an average maximum water depth for the same period as when the cross-section measurements were made was 9.58 m. The h/H ratios generally fall in the range of 3 to 20 with reference to other empirical data (Bridge, 2003). Considering empirical relationships between depth and dune height as $h/H = 6$ by Yalin (1964) and $h = 11.6H^{0.84}$ (Allen, 1970), the actual water depth is higher than the estimated depths from the empirical relationships. Previous empirical studies provides the relationship between height and depth (H/h) and length (L/h) (Allen, 1984; Bridge, 2003). The typical ratio of H/h for prior studies is about 0.2, while the ratio for the present studied dunes are lower with a ratio of 0.07 which nevertheless is close to ratios of marine dunes (Allen, 1984; Figure 8-20; page 333). L/h from prior studies is typically about 4 but the observed data show a range of L/h from 0.5 to 1.1, about 0.79 on the average, which values are rare in the $L - h$ relationship and also relate more closely to dunes in the marine environment (Allen, 1984; Figure 8-18; page 333).

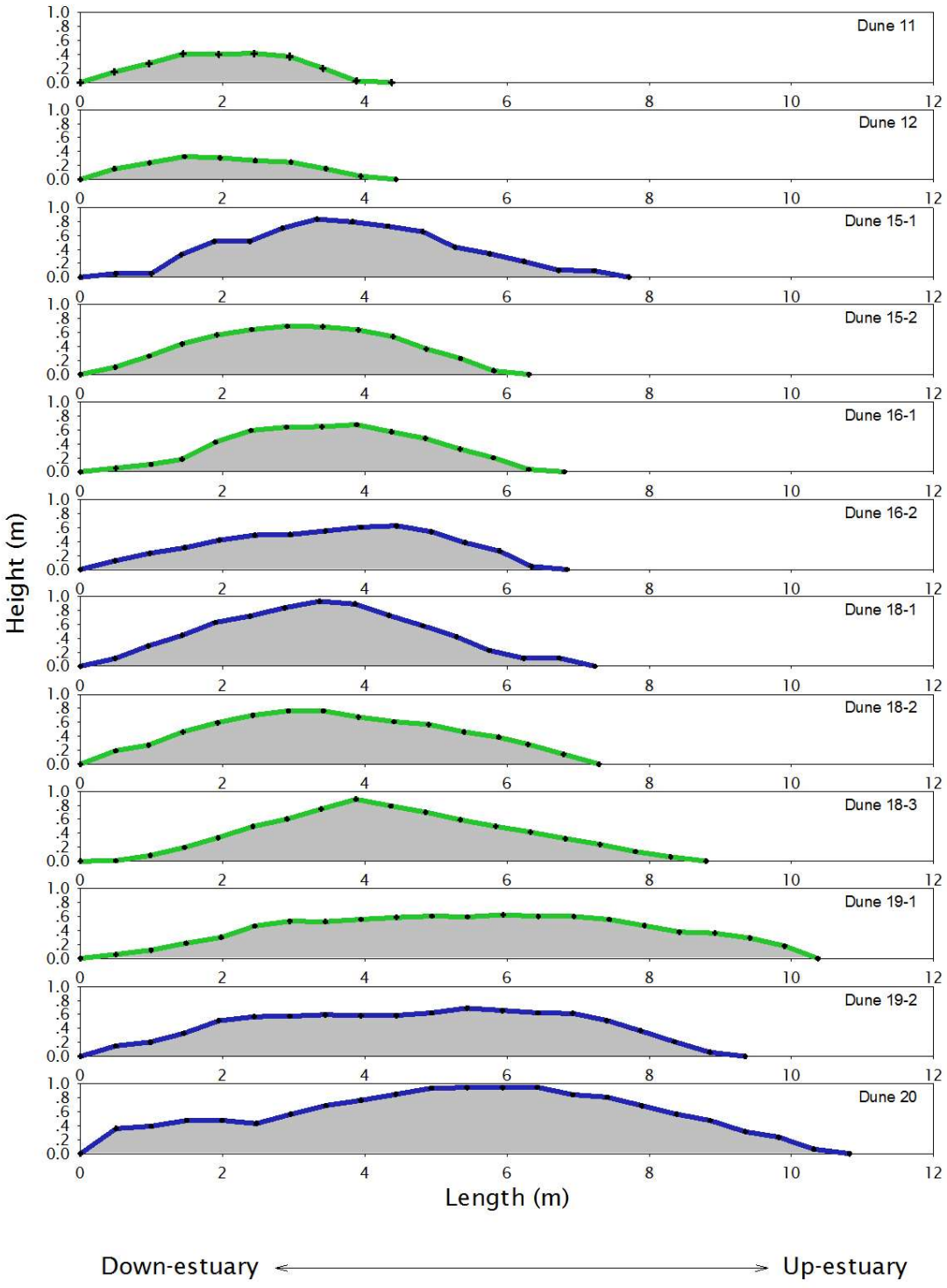

Figure 5.17 Cross-section profiles of the studied dunes. Different colours present the time of measurement; September 2014 in green colour and March 2016 in blue colour.

Table 5.9 Statistical parameters of longitudinal shape of dunes measured during study period: H = height (m); L_1 = near-horizontal surface (m); L_2 = length from the edges from lee to stoss side (m); L_D = length from the crest toward down-stream (m); L_U = length from the crest toward up-stream (m) L_2/H; = dune steepness; L_U/L_D = asymmetry; L_1/L_2 = flatness index; α = lee slope angle; β = stoss slope angle, h = water depth.

Dune sections	**11**	**12**	**15(1)**	**15(2)**	**16(1)**	**16(2)**	**18(1)**	**18(2)**	**18(3)**	**19(1)**	**19(2)**	**20**	**Average**	**Note**
Height (m): H	0.42	0.33	0.83	0.69	0.68	0.63	0.93	0.76	0.89	0.62	0.69	0.95	0.70	>0.04
Length (m): L_2	4.38	4.44	7.72	6.31	6.81	6.84	7.23	7.29	8.80	10.37	9.35	10.82	7.53	>0.6
Down estuary side length (m): L_D	1.44	1.46	3.33	2.91	3.88	4.44	3.36	2.92	3.87	4.94	5.44	5.43	3.62	
Up estuary side length (m): L_U	2.93	2.98	4.39	3.40	2.92	2.40	3.87	4.37	4.93	5.43	3.91	5.38	3.91	
Asymmetry: L_U/L_D	2.03	2.04	1.32	1.17	0.75	0.54	1.15	1.50	1.27	1.10	0.72	0.99	1.22	
Near horizontal surface: L_1	1.5	N/A	N/A	N/A	1.5	N/A	N/A	N/A	N/A	4.5	4.5	N/A		
Flatness: L_1/L_2	0.34	N/A	N/A	N/A	0.22	N/A	N/A	N/A	N/A	0.43	0.48	N/A		
Lee angle: α	15	11	36	17	22	11	18	16	13	11	14	11	16.25	
Stoss angle: β	21	9	18	20	16	20	16	15	10	11	15	13	15.33	
Scale (H and L): Ashley's criteria	M/S	S	L/M	M	M	M	L/M	L/M	L/M	M/L	M	L		
$H - L$ relationship														
Steepness: L_2/H	10.47	13.57	9.25	9.11	10.05	10.88	7.75	9.57	9.92	16.63	13.52	11.37	11.01	
H/L (Allen, 1982; Leeder 1999; Bridge 2003)	0.10	0.07	0.11	0.11	0.10	0.09	0.13	0.10	0.10	0.06	0.07	0.09	0.09	
$H = 0.0677L^{0.8089}$	0.22	0.23	0.35	0.30	0.32	0.32	0.34	0.34	0.39	0.45	0.41	0.46	0.34	
$H - h$ relationship (d = 9.58)														
H/h	0.04	0.03	0.09	0.07	0.07	0.07	0.10	0.08	0.09	0.07	0.07	0.10	0.07	
h/H (h/H = 6; Yalin, 1964)	22.92	29.31	11.49	13.84	14.14	15.23	10.26	12.58	10.80	15.36	13.85	10.07	13.64	3< h/H <20
$h = 11.6H^{0.84}$ (Allen, 1970)	5.57	4.53	9.96	8.52	8.36	7.86	10.95	9.23	10.49	7.80	8.51	11.12	8.58	0.1<h<100
$L - h$ relationship (h = 9.6m)														
L/h	0.46	0.46	0.81	0.66	0.71	0.71	0.76	0.76	0.92	1.08	0.98	1.13	0.79	

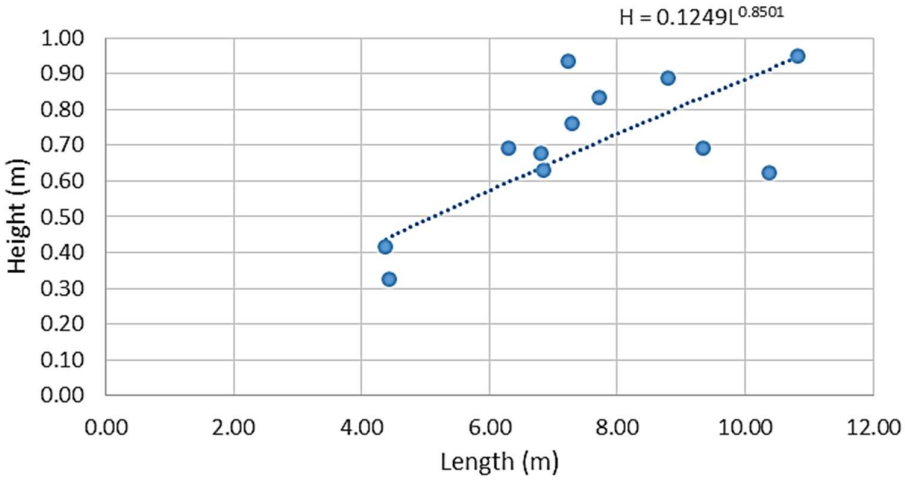

Figure 5.18 The $H - L$ relationship from all cross-section measurements.

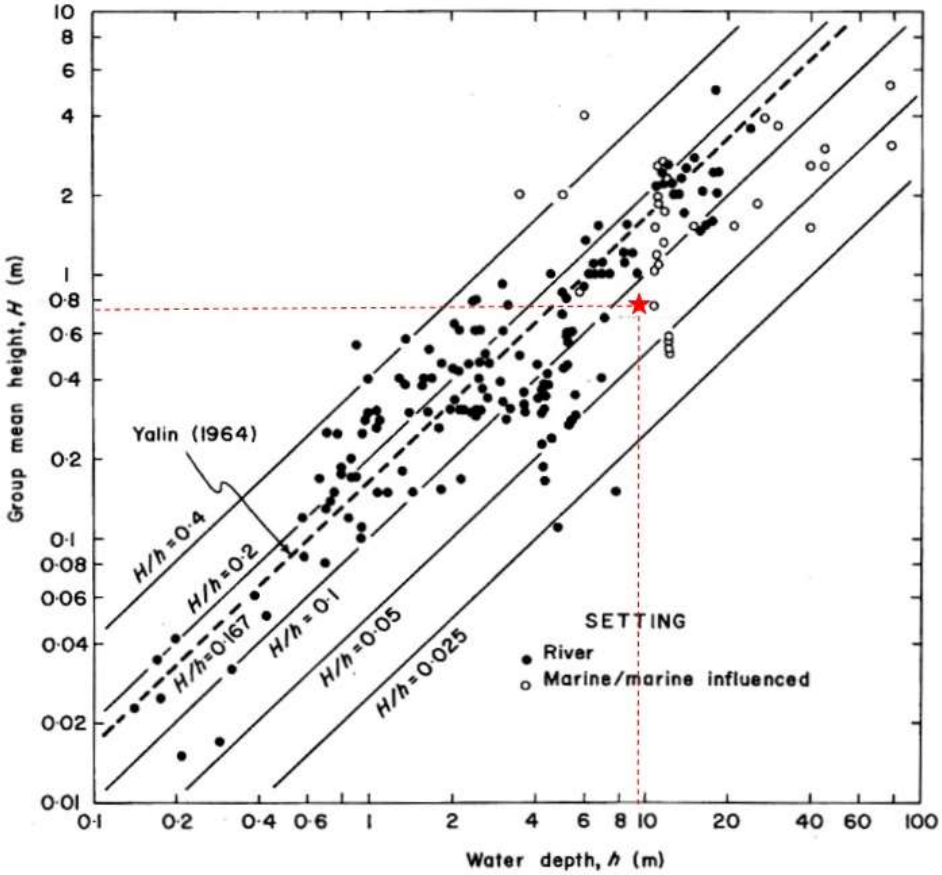

Figure 5.19 Group mean wave height and water depth for dunes in river and marine or marine-influenced settings (Allen, 1984). The red star and red-dotted lines show the water depth and group mean height observed during the study period.

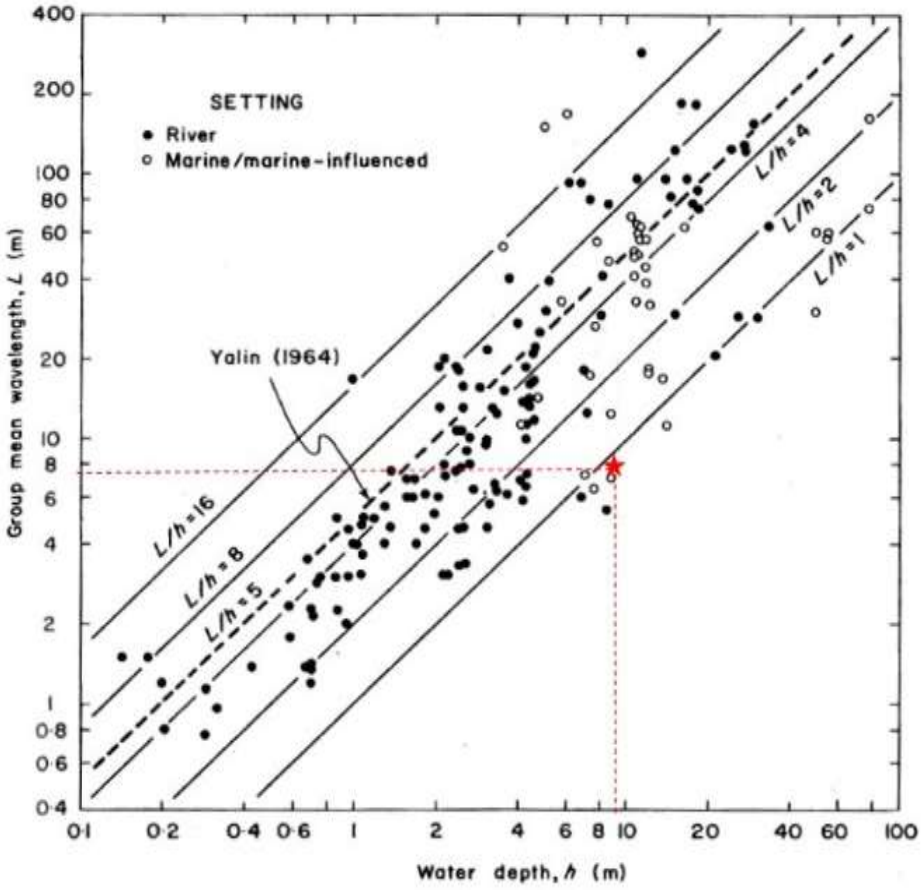

Figure 5.20 Group mean wavelength and water depth for dunes in river and marine or marine-influenced settings (Allen, 1984). The red star and red-dotted lines show the water depth and group mean height observed during the study period.

5.2 Hydrodynamics data

Apart from the previous study and published material, including predicted height of tides at Avonmouth, which was mentioned in Chapter 3; section 3.1.3, the data related to flows over the dune field were collected by a deployment of Valeport current meters from February 2013 to May 2015 (see more details in Table 4.2 and Section 4.2.1). These data are the main source of hydrodynamic data in this study, including flow direction, pressure and current velocity which can be further used to derive other flow conditions such as water depth, bed roughness, and shear stress. Furthermore, the properties of the wind-waves were also recorded by these current meters.

5.2.1 Calculated wave entrainment over the bed

Due to limited observational data concerning local conditions, including wind-wave characteristics, over the field site, this study will refer to the information from previous studies of adjacent areas (see section 3.1.4 and 3.2.3) as well as considering the data collected during the present study.

The data of wave height over the site had been recorded by the Valeport Current Meters. The wave data were recorded five times in the same period coincident with the tidal flow measurements undertaken in the study (see Table 4.2). Available mean wave periods (T_1) recorded in this study are in a range of 1-2.5 seconds which are lower than those reported by Allen and Duffy (1998a) who recorded wave periods normally about 3-4 seconds (Table 5.10). Apart from these values, there are more average wave periods (T_1) collected in February and March 2013 but they consist of very high values of 100-500 seconds which were not considered further as they represent low-amplitude 'swell' from the ocean and outer channel. The maximum local wind-wave heights and significant wave heights in each survey are summarised in Table 5.11 and Figure 5.21. Although the maximum height recorded is about 0.78m in August 2013, the average height of the combined data is otherwise lower than 0.4 m. Some wind-waves may be enhanced by the wind blowing counter to the tidal current but this effect is accounted in the measured wave heights. Considering information from previous studies the middle estuary where the study site is located, is less stormy and not affected by sizable waves in contrast to the outer estuary to the west of Avonmouth where sizable waves and swell are recorded (Hydraulics Research Station, 1979; 1980; 1981a; Shuttler, 1982; Allen and Duffy, 1998a; Carling *et al.,* 2006). Local wind calculation by Allen and Duffy (1998a) shows that the average wave heights for similar intertidal areas of the middle estuary is less than 0.4 m, which is in accord with the data recorded by the current meters. It was also reported that, on some occasions, the wave height might reach 1 – 2 m during gales and it was also predicted that storm surge can create a wind-wave up to 1.5 m high for the mean of high-water spring tides (MHWST; Allen and Duffy 1998a), but these comments were not supported by observations. Additionally, the study of Carling *et al.* (2006), concerning Hills Flats, but approximately 1 km down-estuary of the study site, suggested that this area is less affected by sizeable waves as "wave energy is low and significantly dissipated across the broad flat during calm weather" and also concluded that with all the reference data there is no significant wave action.

Moreover, the recorded waves in this study were used to calculate prospective wave entrainment of bed sediment in order to define the possibility that waves would have effect on sediment transport over dunes and this concurred with previous studies that there are no significant waves over the site. The wave entrainment calculation is explained in the Methodology chapter (*see section 4.2.5*). Firstly, the relationship between water depth and either significant wave height (H_s) or wave period (T_1) rarely shows a sufficiently shallow water for entrainment. Only few wave records are slightly sufficiently in shallow water (when water depth is lower than $0.1g(T_1)^2$ or $10H_s$ at a given recorded time). Considering these records of sufficiently shallow water, values of the orbital velocity due to waves (U_w), given by the relationship of bottom velocity for monochromatic and random waves as detailed in section 4.2.5 and Figure 4.14, are universally lower than 0.2 m/s, which is able to move grains less than 1mm (Figure 4.14; Soulsby, 1997). According to the recorded waves during this study together with the reference studies, the wave effect in this study is considered as insignificant and will not be considered further.

Table 5.10 Mean wave period (T_1) measured over the site. Unit is second (sec).

Date	No.	Mean wave period (sec)	Date	No.	Mean wave period (sec)	Date	No.	Mean wave period (sec)
28 May 13	1	1.10	29 May 13	24	1.28	29 May 13	47	1.34
	2	1.45		25	1.27		48	1.34
	3	1.60		26	1.25		49	1.32
	4	1.55		27	1.37		50	1.29
	5	1.76		28	1.47		51	1.25
	6	1.72		29	1.54		52	1.18
	7	1.67		30	1.56	16 June 14	53	1.55
	8	1.69		31	1.69	17 June 14	54	1.70
	9	1.70		32	1.71		55	1.28
	10	1.90		33	1.76		56	1.48
	11	1.70		34	1.62		57	2.12
	12	1.53		35	1.56		58	1.31
29 May 13	13	1.51		36	2.01		59	1.63
	14	1.64		37	1.67		60	1.50
	15	1.72		38	1.84		61	1.44
	16	1.58		39	1.74		62	2.11
	17	1.52		40	1.62		63	1.25
	18	1.48		41	1.54	18 May 15	64	2.47
	19	1.50		42	1.50		65	2.42
	20	1.42		43	1.54	19 May 15	66	1.54
	21	1.40		44	1.54		67	1.84
	22	1.38		45	1.48		68	1.52
	23	1.34		46	1.42		69	2.13

Table 5.11 Statistical data of wave heights recorded from February 2013 to May 2015. There were more than one dataset recorded in August 2013 and June 2014 because there were more than one meters used to collect flow data including the wave conditions. The different values from different meter in the same month is related to the short gap of logging time between each meter which is approximately 3-5 minutes different. H_s is significant wave height; H_{max} is maximum wave height.

	Maximum H_s	**Minimum H_s**	**Average H_s**	**Maximum H_{max}**	**Minimum H_{max}**	**Average H_{max}**
Feb-13 (35 cm)	0.163	0.025	0.057	0.257	0.039	0.089
Mar-13 (35 cm)	0.168	0.029	0.059	0.264	0.045	0.093
May-13 (35 cm)	0.354	0.012	0.100	0.555	0.019	0.157
Aug 13 (15 cm)	0.024	0.005	0.018	0.038	0.008	0.028
Aug13 (30 cm)	0.074	0.004	0.049	0.117	0.006	0.078
Aug13 (40 cm)	0.494	0.006	0.042	0.775	0.009	0.066
June14 (15 cm)	0.398	0.045	0.158	0.625	0.070	0.248
June14 (30 cm)	0.269	0.029	0.126	0.423	0.045	0.198
May15 (15 cm)	0.266	0.005	0.134	0.418	0.008	0.211

Overall	Maximum	Minimum	Average	Standard deviation (SD)
Hs	0.494	0.004	0.073	0.072
H_{max}	0.775	0.0064	0.114	0.113

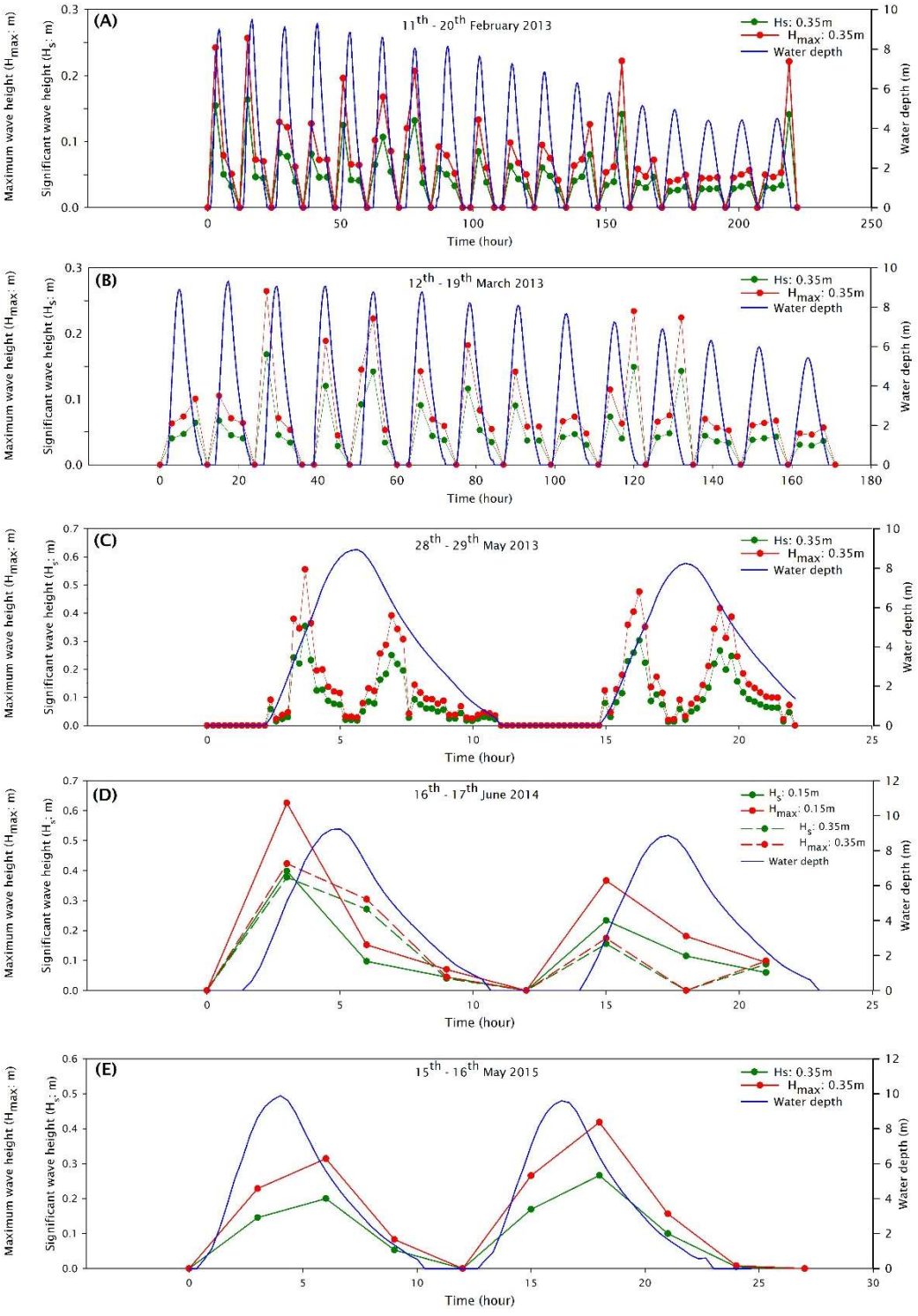

Figure 5.21 Significant heights (H_s), maximum wave heights (H_{max}) and water depth measured during the study periods.

5.2.2 Flow direction

Flow directions above dune crests were also recorded by the Valeport current meters. Figure 5.22 and Figure 5.23 shows flow direction trends that demonstrate that flows mainly run in two directions which are south-west and north-east direction during spring tides, reflecting reversing tidal flows. The first figure shows flow direction and strength, recorded in February and March 2013, from peak spring tides to a transition period for which the data were recorded for 7 – 8 days before Neap tidal cycle starts, while the latter shows only data recorded in high Spring tides during the study period. In Figure 5.22, the velocity towards each direction was classified from less than 0.2 m/s to greater than 1 m/s. Moreover, the different length and proportion of the vectors towards these two main directions in the diagram can reveal the different duration and flow strengths that exist between two directional flows. The longer ebbs in the diagram result from the fact that the duration of the ebb flow being longer than flood tides. Different flow velocity percentage of each direction implies different flow strength in flood and ebb tides.

As flow data in later months were measured for two days or three tides during peak spring tides, most of flow directions in this study are also measured for short period of three tides and are presented in Figure 5.23. The data collected in February and March 2013 (Figure 5.22) were edited for the first three tides in order to compare data in the similar spring period with other datasets. This procedure results in most velocities lower than 0.4 m/s were removed from these two datasets. Flow in the peak spring tides in these two month have the same trend as data in later months. Flow direction in Figure 5.23 mostly moves to south-west (towards WSW) or north-east direction, but there are occasionally more than one prevalent direction during flood or ebb tides. The small different angles (20° approximately) from main flow direction were found in almost every month. Ebb flows at 0.30 m above bed in June 2014 and flows at 0.15 m above the bed were orientated towards SW and flows at 0.50 above the bed in July 2014 and were directed towards W rather than WSW as with the other datasets. For flood tides, the main directions in each survey are ENE and NE. However, in August 2013, July 2014, and August 2014, various flow directions were observed. Moreover, the axis of flow direction toward ebb tides are normally longer than flood tides, but data in August 2013 shows differences with the flood axis longer. The probably related reasons to these behaviours will be explained at the end of this section.

All flow velocity at the 15 cm height above the bed measured during Spring Tides also initially can be investigated in Figure 5.23. In 2013, the first year of study, majority of flow velocity in

peak spring tides was in a range of 0.4 – 0.6 m/s and the maximum velocity is not greater than 1 m/s. Later in 2014, it is shown that flow velocity increased as the range of the majority of speeds is greater than 0.6 m/s and increases to the maximum value of 1.8 m/s approximately in August 2014 before slightly decreasing in May 2015 when the maximum is in a range of 1.2-1.4 m/s.

A number of reasons are considered to be related with changes in flow direction and various current speeds over the site as following;

(A) Changing direction between flood and ebb tides: During flood and ebb tides, the flow velocity and water depth change continuously which can result in a different flow velocity and associated water level. Once flows reach the end of flood or ebb tides, flow direction starts to change to accommodate the next tide. During this period, there might be a chance that flows run toward different directions other than the main dominant up and down estuary directions;

(B) Storm surge conditions: An increase in velocity over the site might be related to storm surges which can also have impact on different flow direction. This supposition is supported by several studies that demonstrate the tidal currents in the estuary can be stronger due to storm surge (Lennon *et al.*, 1963; Hamilton, 1979; Crickmore, 1982; Uncles, 1984; Carling *et al.*, 2006; Williams *et al.*, 2006);

(C) Wind strength; In some occasions, in principle strong wind can cause drag force over water surface, resulting in water flows similar to wind direction which could be different from the main directions;

(D) Bathymetry: the different characteristics of river bed over the site, especially the dunes are located at the edge of a bedrock platform with the current meters located on the edge of a deep main channel (see Figure 5.4: section 5.1: Bathymetry). The draining or flooding of the rock platform might have an impact on the different flow direction and speed during either falling or rising tides. One platform effect clearly seen will be explained in the next section of general flow conditions as due the bathymetric force controlled by the tidal height and 'shoulder' of sustained flow velocity;

(E) River flow discharge and tidal level: A joint variation in these two factors are possibly insignificant for direction but might have impact on flow speed as tidal current speed is depended on the range of mean Spring tidal range (MSTR); the fast currents exist with the large MSTR (Uncles, 2010). Although the trend of

maximum tidal height shows a slight increase in the second and third year of study (2014 and 2015), which probably have impact on increasing velocity, the amount of change does not seems to be a significant control.

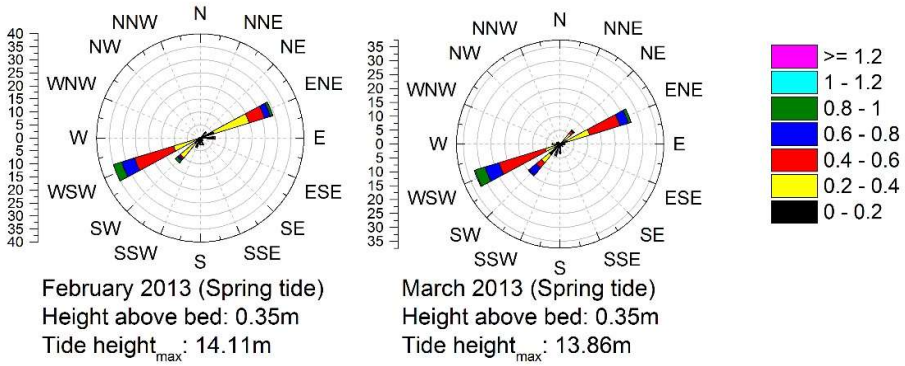

Figure 5.22 Flow direction from peak spring tides to transition period (c.8 days or 16 tides) collected in February and March 2013.

To conclude, tidal flow over the study site run towards two main directions; south-west (WSW) during ebb tides and north-east (ENE) during flood tides, and the flow velocity during peak spring tides could exceed 1 m/s. However, on occasion flow was orientated to different directions and velocity could increased to 2 m/s. This change could have resulted from the related controls mentioned above. However these change did not persist through time for long enough to be considered as significant in respect of dune dynamics to warrant further investigation for this study. Further details of flow conditions such as flow duration, velocity as well as other properties will be presented in the later sections.

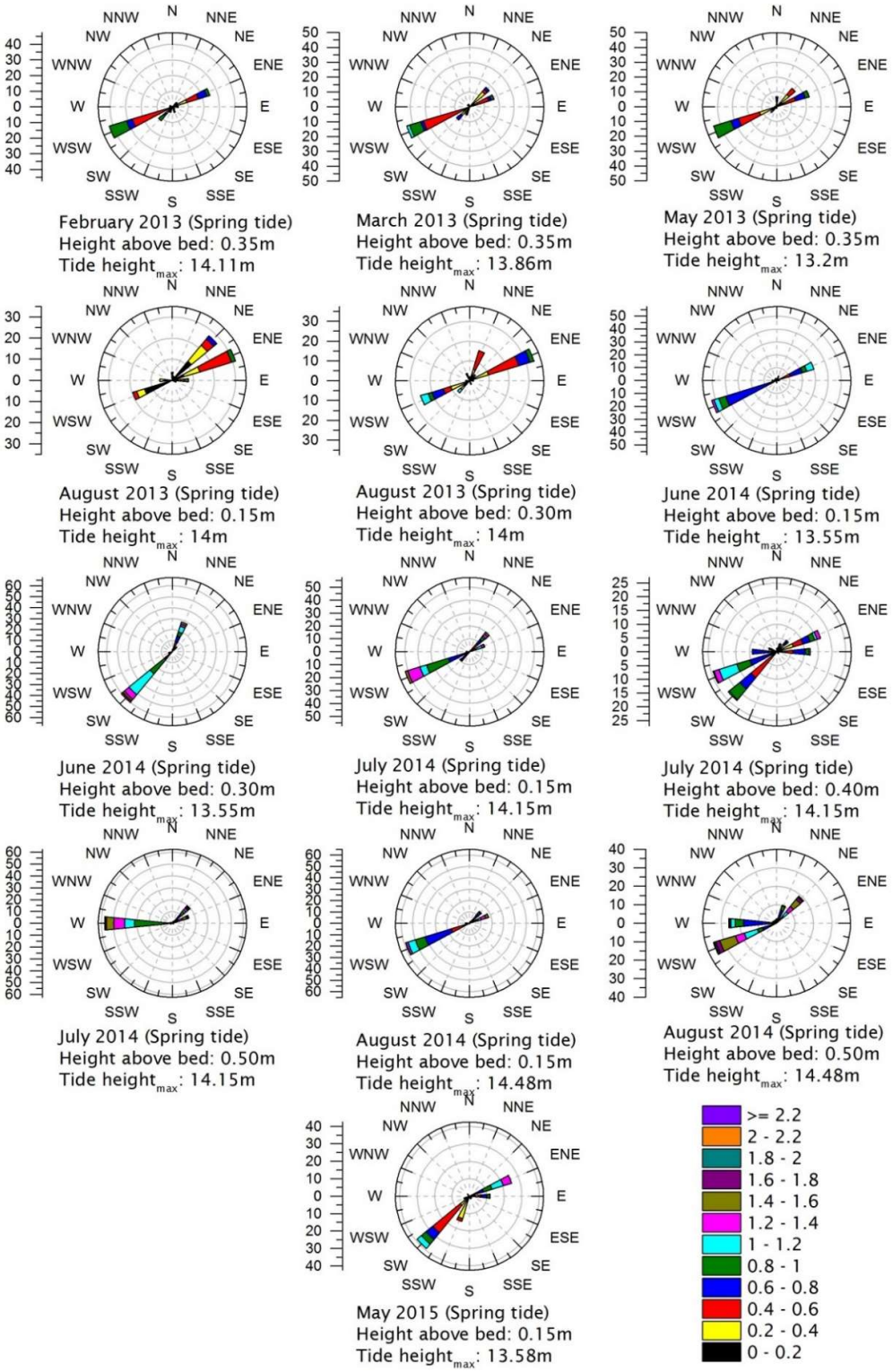

Figure 5.23 Flow direction over study site shows the frequency of stream flowing to particular directions.

5.2.3 Suspended sediment process

Suspended sediment grain size

Grain size analyses of all suspended sediment samples were automatically processed by the Saturn DigiSizerII (section 4.3.2 in Chapter 4: Methodology). Apart from samples in August 2013 which were unavailable due to the trap being dislocated, three samples collected by a pan-piped sampler in July 2013 (Figure 5.24A) and July 2014 (Figure 5.24B and C) provide grain size distributions at different heights above the bed, with all grain size distributions being less than 650 μm (0.65 mm) at the coarsest. Figure 5.24 shows the cumulative volume of grains at different heights. The median grain size (D_{50}) values of all heights and samples are in a range of clay to silt, 20 – 200 μm (0.02 – 0.2 mm The grain size distributions in July 2013 have slightly different trends to the other two samples in 2014 of which all curves of each sediment sample have similar shapes but different proportions. The sample collected on 15th – 16th July 2014 tends to have slight coarser grains than the other two samples. In July 2013, coarser sediments, greater than 400 μm (0.4 mm), were found 35 cm above the bed with small amount while in July the 65 cm samples have slight coarser particles (> 300 μm) which were not found in the other heights.

The overall grain size distributions from 25 cm to 75 cm above the bed in this study are finer than the particles observed in Carling's study (2013), which sampled the suspended sediment in the Hills Flats and close to the present study site using Pan's pipes. Carling (2013) reported that the coarse sand/granule component (> 1000 μm; > 1 mm) were observed suspended up to 0.45 m above the bed. The high variability in grain size between different pipe heights would imply considerable turbulence occurred over the site which is in agreement with the flow conditions, especially the high Reynolds numbers which could exceed 10^7. Moreover, considering the sediment at different heights above the bed, suspended sediment in the study of Carling (2013) showed that the grain size tends to be coarser near the bed, although a few samples did not follow this trend. In contrast, the three Pan's-Piped samples in this study do not show a regular progression to coarser sediment near the bed. This may be related to the considerable mixing in the water column as well as some resuspension and redeposition in the pipes over the two tidal cycles that occurred before the samples could be recovered.

The other suspended sediment sampler, KC Denmark equipment, represent grain size at 75 cm above the bed through time, at one hour intervals. The grain size curves from this sampler show more uniform shapes than the pan-piped samples which had various shapes. The

maximum grain size from KC Denmark sampler is 250 μm (0.25 mm) approximately, whereas the pan-piped sampler shows grains coarser than 300 μm (0.3 mm) at heights of 65 to 75 cm. This discrepancy may relate to the small inlet to the sampler and the backwater pressure which may prevent the coarser grains being sampled in the KC Denmark sampler, or differences in the tidal state and weather at the time of sampling when comparing the two samplers. Moreover, there is no clear pattern of increasing or decreasing grain size through time. Figure 5.25 shows the grain size distribution from the KC Denmark sample in each hour through two tidal cycles. More information of the grain size statistics of samples from both the Pan's-pipes and KC Denmark samplers is presented in Table 5.12 and Table 5.13.

Suspended sediment concentration (SSC)

The suspended sediment concentration (SSC) over the study site was calculated by the data from the KC sampler. The SSC should be similar in magnitude to those recorded elsewhere in the estuary, especially similar to those recorded by Carling (2013). However, concentrations are about 1% of those that might be expected from the work of Carling, although the trend in concentrations over a tidal cycle is similar to the tidal effects on concentration recorded by Carling (2013). Thus, it is evident that although a larger amount of sediment settled each hour in higher concentration flows within the KC Denmark sampler than in lower concentration flows, the majority of the sediment load passed through the sampler and was not trapped as it was too fine-grained to settle in the collection chamber. Thus in the results, the concentrations reported from the KC Denmark sampler are approximately 100 times too low and would need to be adjusted upwards by a similar factor to be comparable with concentrations reported by Carling (2013). If this correction were made, the concentrations would be comparable with those reported prior, whilst the trend in concentrations through a tidal cycle are as recorded by the KC Denmark sampler. The unadjusted and adjusted SSC values are presented in Figure 5.26. Although the uncorrected concentrations are low, the trends through time in the concentration range are in accordance with the results of Carling (2013) when concentrations increased to very high values when the sediment settles at high slack water and also possibly peaking at the beginning of the ebb when the sediment concentrated near the bed is resuspended early in the ebb currents. Although the flow contains high SCC (Carling, 2013), the high concentrations are not considered to have significant impact on reducing the flow turbulence as the Reynolds numbers are very high and could exceed 10^7 (Baas and Best, 2002; Best and Leeder, 1993; Wang and Larsen, 1994) and flow velocity is greater than 0.3 m/s and

Williams *et al.* (2006) stated that the turbulence damping will not occur if the velocity is greater than 0.3 m/s. Thus turbulence modulation caused by high suspended sediment concentrations are unlikely to impact the dynamic behaviour of the gravel dunes which are dominated by coarse-bedload transport.

The data of suspended sediment concentration trends through time observed in this study provides an understanding of local conditions. The suspended sediment can resuspend over the bedform during the flood tide and settle into the gravel bed at high slack water, contributing to the bed material and also being trapped in the bedload samples. As a consequence, both bulk bed and bedload samples consist of very fine particles, but they have a relatively very small proportion by weight.

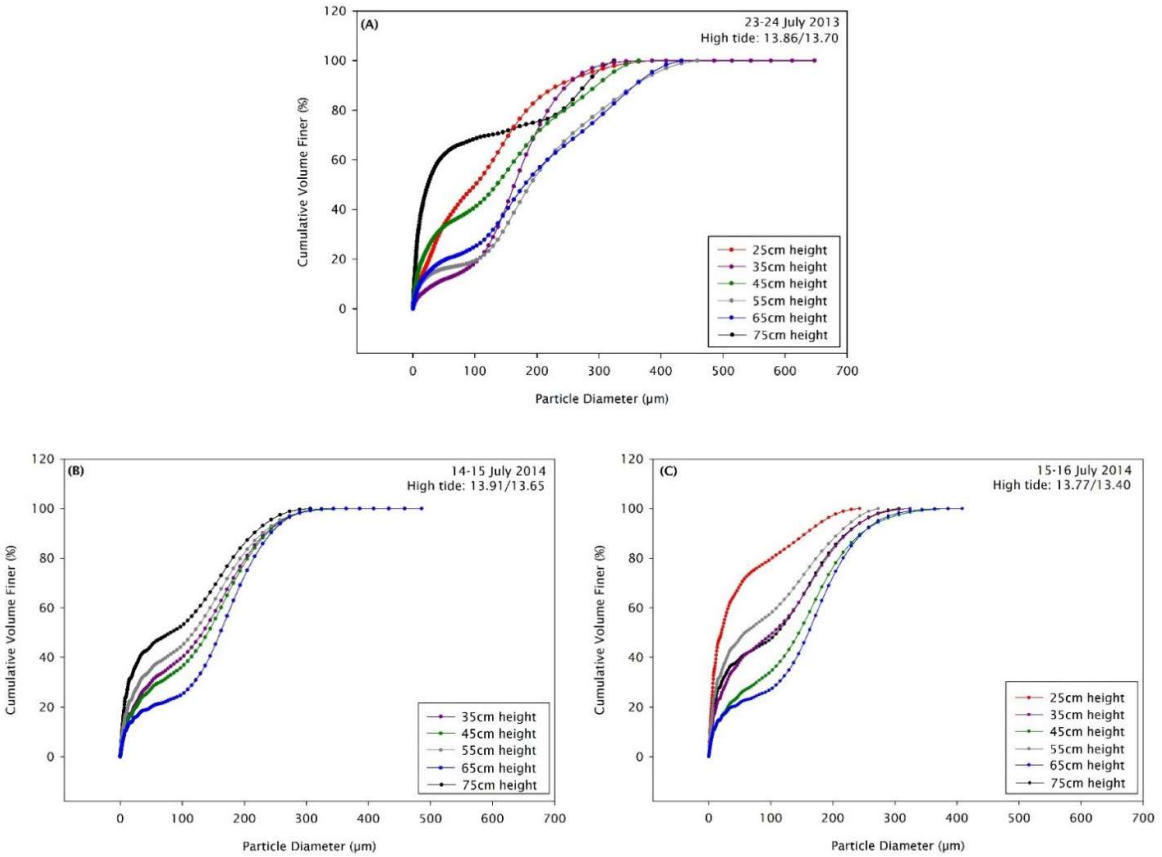

Figure 5.24 The cumulative volume finer of suspended sediment samples collected by a pan-piped sampler on 23rd – 24th July 2013 (A) and 14th – 16th July 2014 (B) and (C). Note: the sampler at 25cm above the bed on 14th – 15th July 2014 height was discarded as turbulence resuspended any settled sediment giving a false sample weight retained.

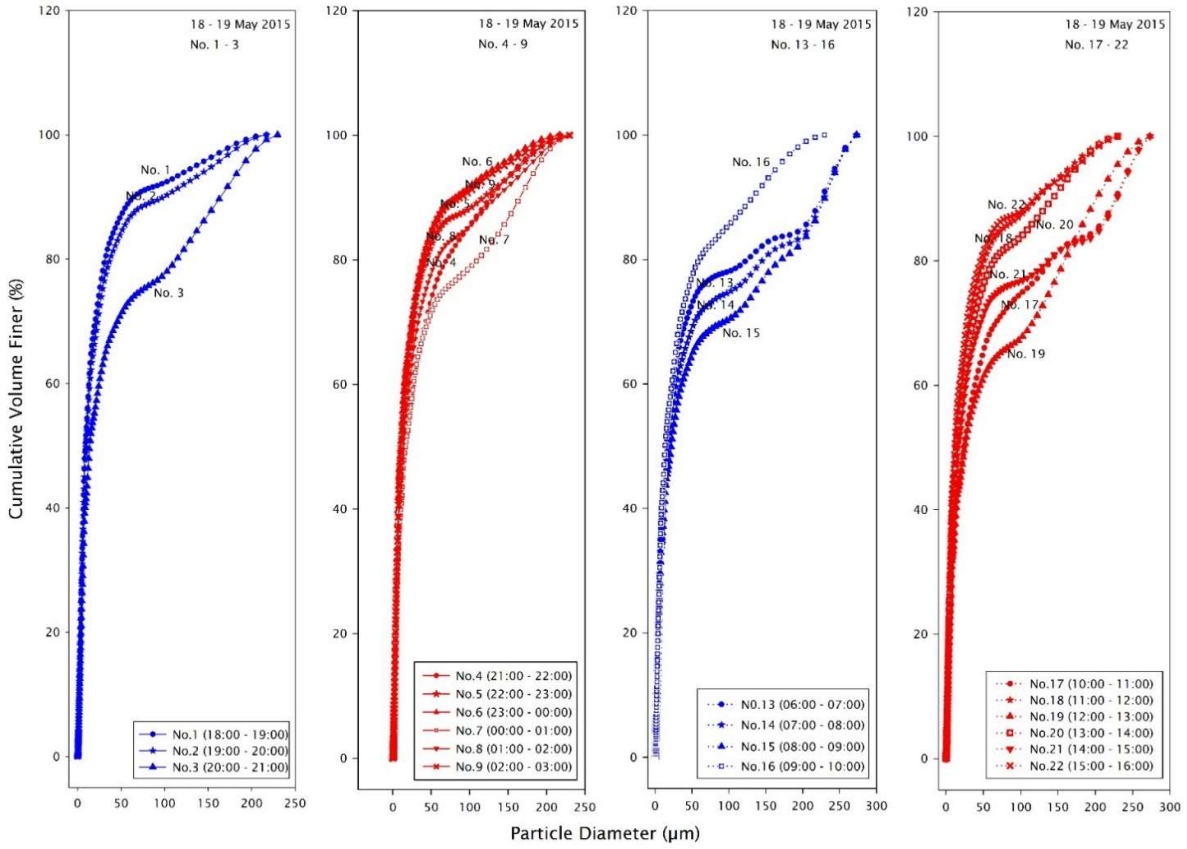

Figure 5.25 Grain size distribution from the KC Denmark sampler collected on 18th – 19th May 2016: the blue colour represents samples collected during floods and the red colour represents samples collected during ebbs.

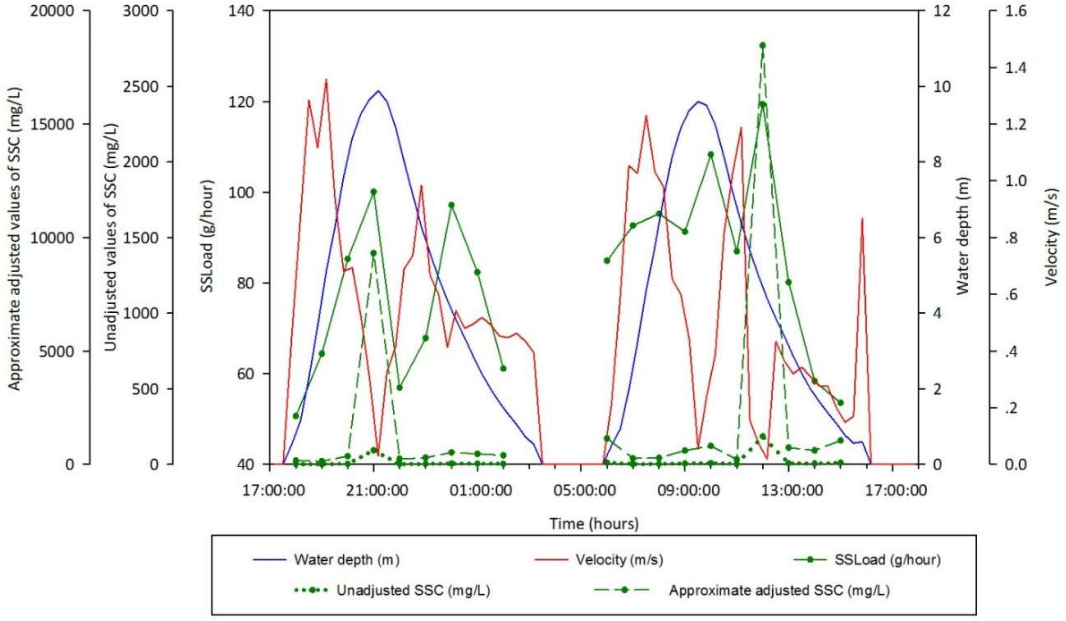

Figure 5.26 Suspended sediment load collected by the KC Denmark sampler, unadjusted suspended sediment concentration (SSC) and the approximate range of adjusted SSC against water depth (h) and flow velocity (U) through period of sample collection

Table 5.12 The grain size statistics of the pan-piped samplers. Note: the sampler at 25 cm above the bed on 14th – 15th July 2014 height was discarded as turbulence resuspended any settled sediment giving a false sample weight retained.

Date	Height above bed (cm)	D_{10} (mm)	D_{50} (mm)	D_{90} (mm)
23-24 July 2013	25	8.18	100.96	234.12
	35	36.70	163.65	248.24
	45	4.69	135.25	296.36
	55	12.62	189.00	356.85
	65	10.99	180.30	357.44
	75	2.26	24.27	277.23
14-15 July 2014	25	-	-	-
	35	5.96	132.58	233.82
	45	6.30	141.34	236.83
	55	4.19	117.97	228.85
	65	7.40	161.50	242.45
	75	3.02	81.71	215.67
15-16 July 2014	25	2.28	20.54	156.97
	35	4.12	103.52	223.88
	45	7.09	145.58	245.57
	55	3.02	59.02	209.10
	65	6.98	160.82	247.85
	75	3.50	110.63	221.70

Table 5.13 The grain size statistics of the KC Denmark sampler collected on 18th – 19th May 2016.

No.	Tide	D_{10} (mm)	D_{50} (mm)	D_{90} (mm)
1	Flood	1.90	8.94	67.56
2	Flood	1.92	9.79	98.32
3	Flood	2.14	14.00	164.17
4	Ebb	2.23	16.84	127.38
5	Ebb	1.97	10.86	117.88
6	Ebb	1.93	10.46	82.25
7	Ebb	2.24	18.63	171.80
8	Ebb	1.94	13.12	134.06
9	Ebb	1.84	11.15	86.82
13	Flood	2.08	14.50	226.17
14	Flood	2.14	18.33	229.40
15	Flood	2.20	21.83	230.41
16	Flood	2.06	13.60	132.19
17	Ebb	2.39	24.28	226.65
18	Ebb	1.94	12.77	121.23
19	Ebb	2.34	24.94	201.46
20	Ebb	1.98	13.74	142.21
21	Ebb	1.98	15.53	228.60
22	Ebb	1.90	11.96	118.53

5.2.4 General flow conditions; water depth, duration, velocity, Froude number and discharge

The site specific flow data were collected during spring tides, the first two sets of data, recorded in February 2013 and March 2013, were collected for a period in excess of one from the peak of spring tides towards transitional tides. The later six datasets were collected to represent two or four high spring tides. These flow data provide the trends of the ratio between ebb and flood duration as well as local water depth and flow velocity.

Calculated water depth from recorded data by Valeport current meters over the site generally increases during flood tides to the maximum level and start to decrease once the ebb flow starts and continue such that the dunes become fully-exposed as the rock platform drains

completely. The observed water depth data show that water depth over the site can reach 8 – 10 m during high Spring tides and can be low as 4 m in transition tides (Figure 5.27). The duration of increase and decrease of water level is related to the duration of flood and ebb tides mentioned later.

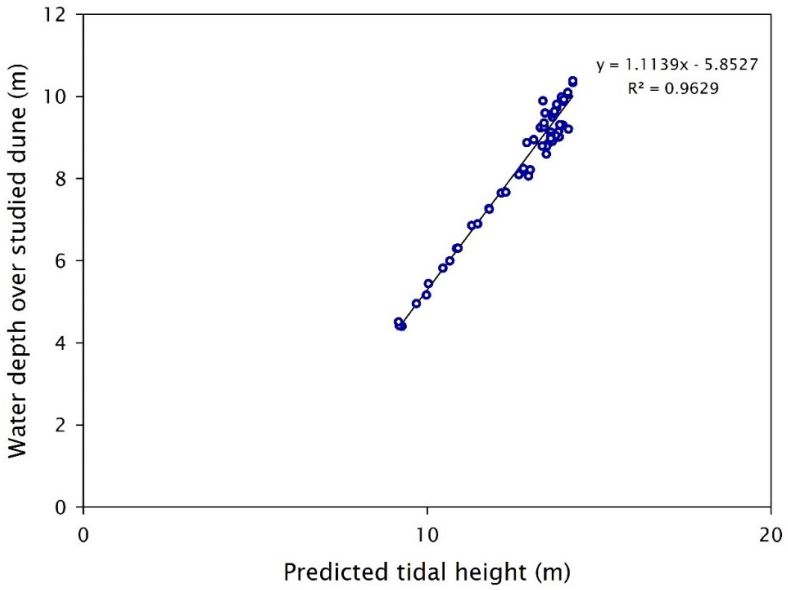

Figure 5.27 Predicted tide height at Avonmouth against water depth during Spring tides over study site

The one week recorded tide data in February and March 2013 represent the hydrodynamics of the tidal cycles over the study site (Figure 5.28 and Figure 5.29). During peak Spring tides, the studied dune crests have been submerged under water about for 8 to 10 hours per tide and this duration will reduc per tide later in the transition tidal cycle to Neap tides. Comparing the duration between flood and ebb tides, the duration between ebb and flood tides is not equal. During the high Spring tides, ebb flows have a 30% longer duration than flood tides and later ebb duration gradually decrease to the same duration during transition tides, which means duration between both flows might be symmetrical (Figure 5.28 and Figure 5.29). The duration of flood tide starts from 3 hours in the peak spring tides and slightly increases to 5 hours in transition tides. On the other hand, the duration of the ebb tide remains in a range of 5 – 6 hours approximately. The exposure period between each tide (ebb to flood), when water depth over the site is equal to zero and the dunes are exposed, is about 3- 4 hours during spring tides which slightly decreases to 2 hours in transition tides to neap tides.

Both water depth and submerged duration of theses cobble dunes are greater than the fine-gravel dunes studied by Carling *et al.* (2006) and Williams *et al.* (2006). Water depth

over the fine-gravel dunes can reach 6.5 m and they are submerged under water for about 5 hours during the highest spring tides, but only 3 hours during the lowest neap tides. This difference is due to the fact that the elevation of the fine-gravel being higher on the rock platform than the cobble dunes of this study as they are slightly closer to the estuary bank.

Apart from the two datasets in February and March 2013, the other datasets for two to four tides during spring tides also were collected during study period (Figure 5.30). These data show the same pattern of duration between flood and ebb until the data collected from July 2014 to May 2015. Data collected during this latter period show slightly longer duration of inundation in peak spring tides which increase from 8 hours to 9 - 10 hours. The flood duration has a small changes being 15 - 20 minutes longer than observed in March/February but the ebb duration increased from 5 hours to 6 hours approximately and the duration of subaerial exposed dunes decreased from 3 hours to 2 hours. These differences in durations simply reflect the increase in predicted tidal heights in 2014 - 2016. These flow data will be used for further analysis of hydrodynamic in conjunction with other types of data.

The velocities of the bi-direction flows measured over the site during big Spring tides show similar patterns for the study period. As the flood starts, the velocity rapidly increases to the maximum speed within 1.5 hours (half way to the maximum water depth) before decrease to slightly above 0 m/s when the water depth reaches the maximum level, at high water slack. After that, flow velocity increases again when the ebb tide starts. The initial velocity of the ebb flow tend to increase sharply and decrease until the water depth equals 0 m. The pattern of velocity in the ebb flow is generally similar to that observed during flood tides but during ebb flows there are short periods that the velocity slowly decreased and became sustained through time, here called a ‘shoulder’ which probably reflects a local bathymetric control. This control is probably due to friction on the rock platform impeding the ebb drainage. Moreover, sometimes just before the ebbs end, and velocity is almost down to 0 m/s, it is observed that the velocity suddenly rapidly increases (see Figure 5.28, Figure 5.29 and Figure 5.30). This is a result of shallow late-stage ebb water stored on the rock shelf draining rapidly once the water level in the main channel falls below the edge of the rock ledge. Flow data collected in August 2013, June 2014, July 2014 and August 2014 were measured at three different heights (0.15 m; 0.30 m; 0.40 m or 0.50 m). In each dataset, the temporal behaviour of the velocity at each level shows a similar pattern with the other(s). Comparing data recorded in the same time

scale, the velocity of the higher level current meter is greater than the one measured by the lower level meter which reflects the presence of the boundary layer.

The overall current velocity over the site ranges from near zero to 2 m/s. The maximum velocity recorded in each dataset during the study period ranges from 0.99 m/s in February 2013 to 2.03 m/s in August 2014. The maximum velocity during ebb tides is normally higher than during flood tides. However, there are occasions when the flood velocity is greater than the ebb velocity; especially data collected in July and August 2014 and May 2015 (Table 5.14). The greatest maximum velocity during flood and ebb tides are in July and August 2014 which are both 2 m/s approximately, whilst the smallest maximum velocity recorded 0.74 and 0.84 m/s in August 2013. The current velocity over the site might increase if there is storm surge (Lennon *et al.*, 1963; Hamilton, 1979; Crickmore, 1982; Uncles, 1984; Carling *et al.*, 2006; Williams *et al.*, 2006) but here is no evidence of such an event in the study period. The Froude number (Fr) shows a slightly different pattern as it is not only related to flow velocity but also water depth. The maximum Fr values do not have to exist at the same time as the maximum velocity or water depth. For all datasets, maximum Fr values during flood Spring tides range from 0.14 to 0.95, while those in ebb Spring tides are 0.14 to 0.57 (Table 5.14). All of these values are lower than 1, so the flow is subcritical. Even though some flood tides have higher maximum Fr value than ebbs, this is a rare occasion because most tidal cycles show that ebbs mostly have higher maximum Fr than floods. High Froude numbers only occur briefly in very shallow flows during final ebb drainage when velocities suddenly increase as noted above. Velocities and occurrences of higher Froude numbers, both tend to increase with the predicted tide height as well as water depth over the dunes. This change occurs on both flood and ebb tides and might have an impact resulting in stronger flows for both directions.

Comparing the maximum velocity in each tide, between flood and ebb flows, the asymmetry in flood and ebb flow duration and associated velocities results in different flow conditions which has an important role in driving bedform migration as well as internal structure. Apart from the flow conditions above, comparison of flood and ebb discharge is also considered here.

Table 5.15 presents the calculated ratio between the flood and ebb tide discharges ($F_Q : E_Q$). Most of ratios in each tide are lower than 1 ($F_Q : E_Q < 1$) which means ebb discharge is higher than flood discharge for a given tide. The ratios during big spring tides is lower than those in smaller spring and transition tides which are close to or equal to 1 indicating that the flood and ebb discharge are almost balance. Considering only big Spring tides of data collected in February and March 2013 together with all other datasets only collected during big Spring

tides, it can be seen that there are a few times that this ratio is greater than 1, indicating that flood discharge of that tide is higher (August 2013 and May 2015).

The asymmetry in these flow conditions, mostly showing greater values of ebb flows, might imply that there is a possibility of dunes migrating down-estuary. Such a result is consistent with the direction of residual dune movement which generally is ebb dominated as can be seen from most topographic surveys; especially the one in March 2014. However, according to the recorded data, there were many occasions during which these flow conditions in flood flows were higher than the ebb flows, especially in 2014 and 2015. As a consequence, it implies that there might be occasions when flood flows are stronger than ebb flows and might result in migration of the dunes toward up-estuary as the topographic survey shown in September 2015. Details of water depth, velocity, Froude number, and flow discharge in flood and ebb tides during the study period are shown in Table 5.14 and Table 5.15.

Table 5.14 The measured maximum depth of high water over study site for a given tidal heights at Avonmouth during study period (February 2013 to May 2015). Red and yellow highlights indicate unavailable and uncertain datasets due to technical issues of current meters.

Date		Height above bed	Max Depth	U max		Fr max		Note
Month	Year			Flood	Ebb	Flood	Ebb	
Feb	2013	0.35	9.50	0.89	0.99	0.14	0.27	
Mar	2013	0.35	9.31	0.99	1.02	0.17	0.36	
May	2013	0.35	8.95	0.93	1.00	0.14	0.14	
July	2013	0.19	N/A					Memory was full
		0.35	N/A					
Aug	2013	0.15	9.10	0.74	0.84	0.11	0.11	Rig was dislocated
		0.3	9.10	0.84	1.20	0.13	0.16	
		0.4	9.13	1.08	0.97	0.16	0.12	
June	2014	0.15	9.23	1.79	1.69	0.33	0.29	
		0.3	9.25	1.41	1.66	0.28	0.39	
July	2014	0.15	9.98	1.51	1.65	0.29	0.45	
		0.4	9.91	1.31	1.51	0.61	0.57	Direction is unusual
		0.5	9.99	2.00	1.92	0.39	0.48	
Aug	2014	0.15	10.34	1.70	1.43	0.95	0.45	
		0.5	10.38	1.91	2.02	0.41	0.46	
May	2015	0.15	9.89	1.36	1.19	0.27	0.36	
		0.35	N/A					Start plug didn't work

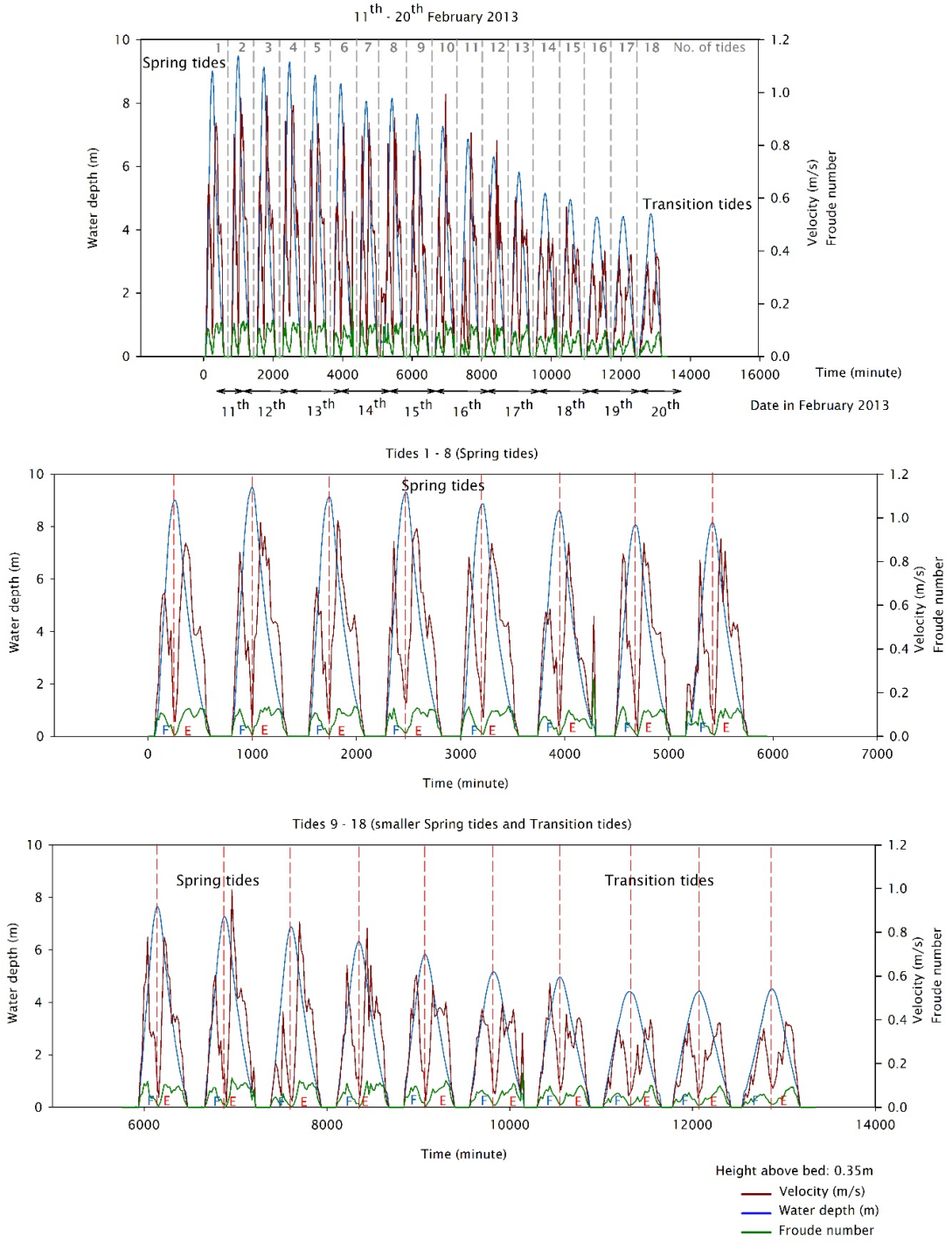

Figure 5.28 Flow conditions; velocity (red), water depth (blue) and Froude number (green), measured between the greatest Spring tide and the transition tides, from 11th to 20th February 2013.

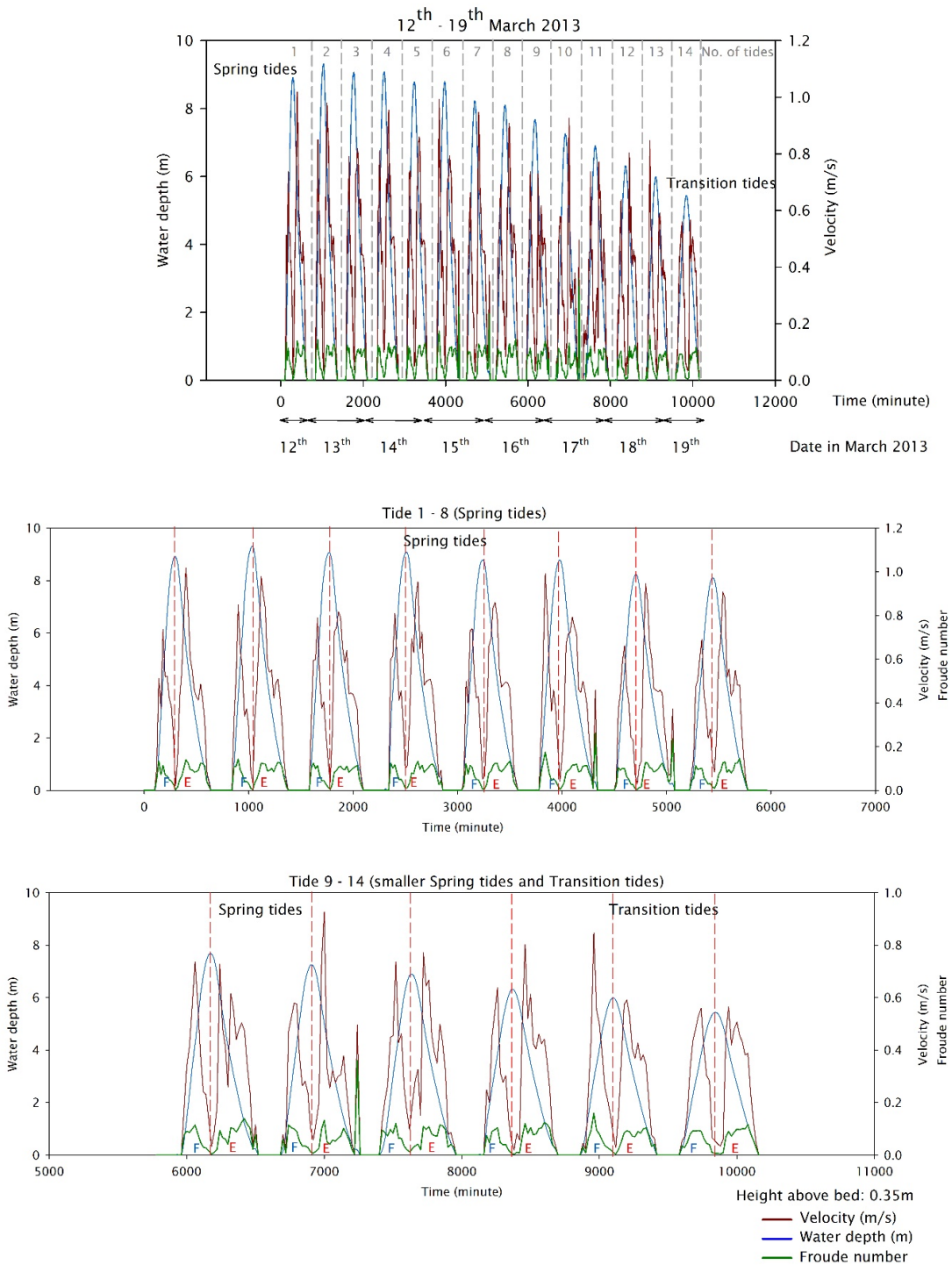

Figure 5.29 Flow conditions; velocity (red), water depth (blue) and Froude number (green), measured between the greatest Spring tide and the transition tides, from 12th to 19th March 2013.

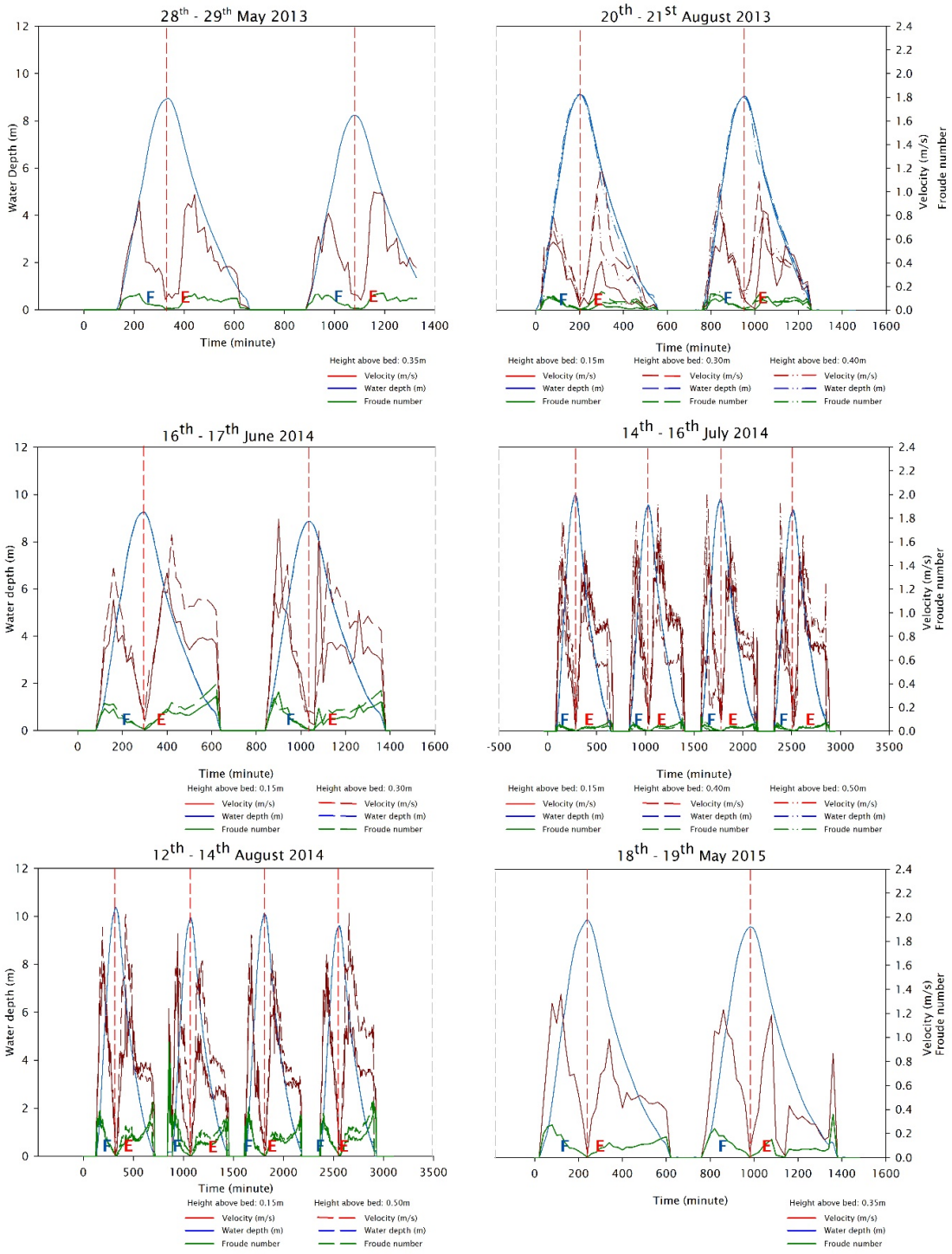

Figure 5.30 Flow conditions; velocity (red), water depth (blue) and Froude number (green), measured during spring tides from May 2013 to May 2015

Table 5.15 Discharge and velocity ratio between floods and ebbs in each tide showing asymmetry of bi-directional flows

Date	No. of tides	Total discharge (sum) F:E	Date	No. of tides	Total discharge (sum) F:E
11-20 Feb 13	1	0.57	20-21 Aug 13 (0.15m)	1	1.42
	2	0.58		2	1.01
	3	0.52	20-21 Aug 13 (0.30m)	1	0.54
	4	0.57		2	0.79
	5	0.62	20-21 Aug 13 (0.40m)	1	0.80
	6	0.65		2	0.80
	7	0.71	16-17 June 14 (0.15m)	1	0.62
	8	0.63		2	0.74
	9	0.72	16-17 June 14 (0.30m)	1	0.59
	10	0.58		2	0.61
	11	0.33	14-16 July 14 (0.15m)	1	0.56
	12	0.69		2	0.56
	13	0.87		3	0.65
	14	0.96		4	0.64
	15	0.99	14-16 July 14 (0.40m)	1	0.63
	16	1.09		2	0.68
	17	0.98		3	0.31
	18	0.97		4	0.57
12 - 19 Mar 13	1	0.63	14-16 July 14 (0.50m)	1	0.77
	2	0.55		2	0.62
	3	0.61		3	0.72
	4	0.64		4	0.73
	5	0.69	12-14 Aug 14 (0.15m)	1	0.77
	6	0.70		2	0.53
	7	0.62		3	0.52
	8	0.63		4	0.77
	9	0.83	12-14 Aug 14 (0.50m)	1	0.60
	10	0.80		2	0.66
	11	0.94		3	0.42
	12	0.71		4	0.58
	13	0.88	18-19 May 15	1	0.96
	14	0.99		2	1.11
28-29 May 13	1	0.72			
	2	0.68			

5.2.4.1 Velocity log profiles: Bed roughness and bed shear stress

The general information of water depth and current velocity measured over the bedforms were further calculated for flow conditions related to sediment entrainment especially initial motion by creating velocity log profiles (see details in section 4.2.3). Firstly, the Reynolds numbers (Re) in each dataset were calculated to know the state of flows which can be indicated by a relationship of flow depth (h), velocity (U) and kinematic viscosity (υ) ($Re = \frac{Ud}{\nu}$). The calculated Re values are very high, often exceeding 10^7, and normally higher than 2500 showing that flows over the dunes are fully rough-turbulent (Knighton, 1998). Trends of Re are similar to velocity (Figure 5.31). Values start increasing at the beginning of floods and ebbs before decreasing to near-zero during slack water after floods and to zero at low water after ebb tides when the instrument was exposed at the study site. In this section, two datasets available for these flow conditions are data collected on 14th – 16th July and 12th – 14th August 2014 (later briefly referred to as July 2014 and August 2014). The first results from velocity log profile include bed roughness length (Z_0) and shear velocity (u_*); the latter parameter is later used for estimated instantaneous bed shear stress (τ_0).

The calculated flow conditions of τ_0 and Z_0 values in July and August 2014 were plotted (Figure 5.32 and Figure 5.33) together with the grain size likely to move (D_{mobile}) and impact counts in order to compare the behaviour of these conditions through the time of data collection. The first two parameters, τ_0 and Z_0 values, will be firstly described in this section and the latter two conditions will be presented later.

The trends of calculated τ_0 values for the measured tides from these two months are different (Figure 5.32A and Figure 5.33A). τ_0 In August 2014 seems to be higher and more fluctuated than those in July 2014. Average τ_0 values are about 4.83 and 13.04 N/m^2 in July and August 2014 respectively. The maximum values can reach 51.97 N/m^2 in July while the maximum τ_0 in August reaches 85.37 N/m^2. The τ_0 values are lower and almost decrease to 0 N/m^2 during slack water when the highest water level pertained. Bed roughness values (Z_0) are shown in Figure 5.32B and Figure 5.33B which generally shows that, in both datasets, the bed under ebb flows have higher maximum roughness than the floods (max Z_0 of ebbs = 0.11 and 0.14 m and max Z_0 of floods = 0.09 and 0.12 m in July and August 2014) but the average values shows that

floods have higher values than the ebbs (average Z_0 of floods = 0.009 and 0.019 m and average Z_0 of ebbs = 0.002 and 0.014 m in July and August 2014) (Table 5.16).

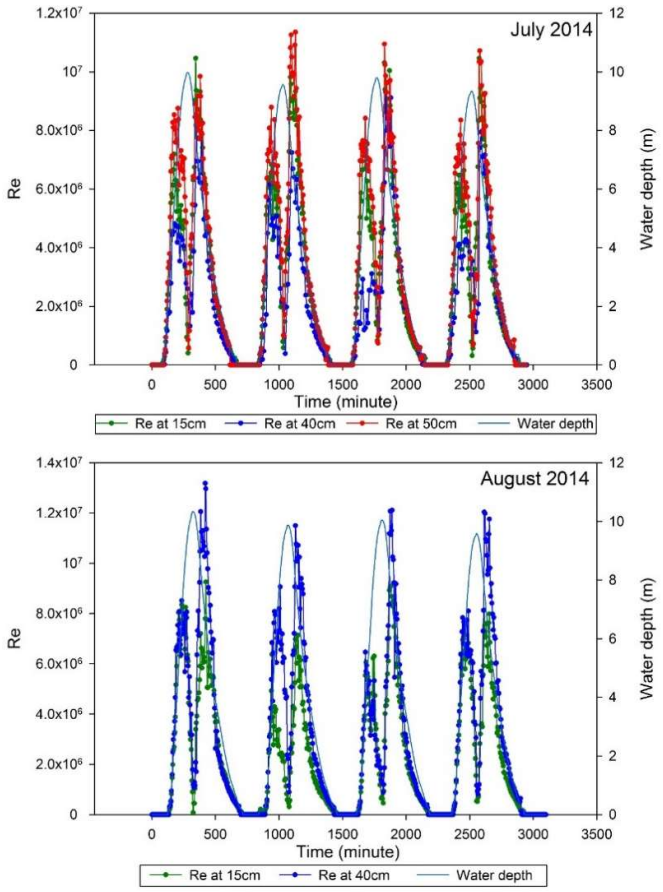

Figure 5.31 Reynolds numbers in July and August 2014

It is evident that z_o in Table 5.16 varies significantly. In steady fully-turbulent flow over a plane bed it has been found that z_o is effectively a constant function of the bed roughness: $z_o = k_s/30$ (Colebrook and White, 1937) or $z_o = D_{50}/12$ (Soulsby, 1997). Utilizing the latter relationship and D_{50} = 16.7mm indicates an average z_o value of 1.39mm and that the z_o data in Table 5.16 do not reflect this value. However, the variation in z_o actually depends on the viscosity of the water, the speed of the current and the physical size of the bed roughness. Given the high Reynolds numbers, we can assume the water is well-mixed and ignore viscosity and thus consider only velocity and the bed roughness. The tidal currents are accelerating and decelerating above an undulating dune bed, and so the flow is not steady. The flow unsteadiness is most likely responsible for the greater portion of the observed variation in z_o. In decelerating flows, there is an apparent increase in z_o and *vice versa*. Similarly the shear stress on the bed tends to decrease in decelerating flows and *vice versa* such that z_o tends to

vary with variation in u^* (Soulsby and Dyer, 1981). In Table 5.16 we note that when the average shear stress is high then z_o is also high, which variation reflects the effect of fitting a log-profile for steady-flow to unsteady flow. Values of u^* are little effected by this fitting procedure, whereas values of z_o are greatly affected (Soulsby and Dyer, 1981; Soulsby, 1997). It is also apparent that the average stress on the bed tends to be greater on the flood than the ebb tides (Table 5.16); this is likely due to greater acceleration on the short-duration flooding tide than on the longer-duration ebb. Nevertheless the dune migration data show that dunes are ebb-dominated which reflects the longer duration of competent flows on ebb tides. Despite the dominance of flow unsteadiness in mediating the range of z_o values, bed roughness might also have some influence. Given that the dunes are ebb orientated, the bedload transport rates are low and the bed is generally coarse and compacted, it is evident that the flood tide is flowing across a largely immobile dune bed with cobbles imbricated in the ebb direction. Such a bed will be rougher than if the imbrication was flood related. This increased roughness together with the flow acceleration jointly will contribute to the higher z_o values commonly observed on the flood tides. It is probable that the flood tide often does not reconfigure the bed surface significantly from that surface induced by the ebb tides.

Table 5.16 Statistical summary of bed shear stress (τ_o), bed roughness length (Z_o), D_{mobile} calculated with Shields value (θ) of 0.04, flow velocity (U) at 15 cm above the bed and the amount of impact counts which are collected during the Spring Tides in July and August 2014

Month		**14 -16 July 2014**								**12-14 August 2014**							
Tide		**1**		**2**		**3**		**4**		**1**		**2**		**3**		**4**	
Direction		**Flood**	**Ebb**	**Flood**	**Ebb**	**Flood**	**Ebb**	**Flood**	**Ebb**	**Flood**	**Ebb**	**Flood**	**Ebb**	**Flood**	**Ebb**	**Flood**	**Ebb**
Bed shear stress (τ_0; N/m2)	Average	7.58	0.47	5.71	1.99	8.09	3.84	7.93	5.84	2.85	25.29	23.79	15.90	2.26	4.18	2.75	19.37
	Max	23.66	4.51	19.19	18.81	51.97	21.87	23.48	36.94	19.46	85.37	79.96	75.98	8.64	29.44	17.86	49.88
	Min	0.23	0.00	0.16	0.00	0.00	0.01	0.58	0.00	0.04	0.01	0.02	0.18	0.02	0.00	0.05	0.02
Bed Roughness length (Z_0; mm)	Average	13.11	0.01	6.38	0.71	6.32	1.69	9.02	5.19	4.79	24.33	48.71	20.88	5.94	2.52	4.45	14.10
	Max	89.74	0.45	76.68	28.61	60.93	12.45	54.02	113.61	61.25	137.01	115.74	88.05	57.73	40.38	53.56	32.49
	Min	0.00	0.00	0.00	0.00	0.00	0.00	0.01	0.00	0.00	0.00	0.00	0.00	0.00	0.00	0.00	0.38
D_{mobile}; θ = 0.04 (mm)	Average	14.86	0.92	11.19	3.89	15.85	7.45	15.55	11.45	5.59	49.58	46.64	31.17	4.42	8.20	5.38	37.97
	Max	46.39	8.84	37.62	36.87	101.88	42.87	46.04	72.41	38.14	167.36	156.75	148.95	16.93	57.71	35.01	97.78
	Min	0.45	0.00	0.32	0.00	0.00	0.01	1.14	0.00	0.07	0.03	0.04	0.35	0.05	0.01	0.10	0.04
Velocity at 15 cm above the bed (U; m/s)	Average	0.75	0.91	0.78	0.95	0.78	0.78	0.73	0.78	0.90	0.76	0.60	0.57	0.68	0.72	0.82	0.74
	Max	1.46	1.48	1.51	1.59	1.43	1.65	1.48	1.54	1.60	1.43	1.70	1.02	1.57	1.32	1.54	1.35
	Min	0.04	0.06	0.08	0.06	0.08	0.10	0.05	0.03	0.09	0.01	0.06	0.03	0.06	0.05	0.05	0.05
Impact counts		120	136	187	144	137	209	87	177	419	140	215	182	192	125	149	137

Values of shear stress (τ_0) are useful for calculating the grain size likely to be moved (D_{mobile}) at a given time by using a function of Shields' number (θ) (Equation 2.18; section 2.3.1). However, in this function the Shields number (θ) and the grain size in motion as bedload at a given time are initially unknown. A upper and lower limit for the Shields parameter of grain size coarser than 10 mm were suggested by Williams (1983) as 0.25 and 0.01 (Knighton, 1998). Moreover, the critical Shields value (θ_c) for initial motion of gravel has been estimated as lying between 0.02 and 0.065 as provided by previous studies (Buffington and Montgomery, 1997). In order to select the best representative θ value at the time of initial motion of given grain sizes, iterating the D_{mobile} calculation with various Shields number were done, starting from 0.02 which is the lowest θ_c reported for rough beds and sequentially increasing to 0.25. The calculated D_{mobile} values for various given θ values in each tide are used to produce hypothetical grain size distributions in traction and plotted against the observed bedload sediment grain size curves from the Helley-Smith samplers. From the two periods of flow measurement available for velocity profiles, in July and August 2014, which provides calculated τ_0 values, there are six bedload samples available within the similar period, which are four samples on the 14th – 15th July 2014 (one flood and one ebb samples) and 15th – 16th July 2014 (one flood and one ebb samples) as well as two ebb samples on the 12th – 13th, 13th – 14th August 2014. In this study, these six bedload samples can be matched with available flow datasets where τ_0 has been calculated, to find the best θ values that match the observed grain size data from the traps. The iterated D_{mobile} curves with different Shields' values were plotted against the bedload sample at a given period to see which D_{mobile} curve is the best fit to the bedload sample (see Figure 5.34 for an example). However, the RMSE of the distributions of the D_{mobile} curves against the bedload samples were calculated to ensure the best θ value had been obtained to match the D_{mobile} curve with the curve for the bedload sample. According to the lowest RMSE values from the six bedload sample sets, there are five different best fitted median θ_c values, which are 0.003, 0.02, 0.05, 0.06 and 0.1 (Table 5.17). Excluding the low value of 0.003, this range closely matches results obtained in previous experimental studies (see Mueller and Pitlick 2005; and references therein). Due to the differences in Shields' values, the mean of the median values calculated for the best fitted θ_c value from the six datasets was 0.05, which value was selected as generally representative of an initial motion criterion for this study. Fitting the calculated grain size distribution curve with θ_c set as 0.05 may not fit the observed bedload curve well, as the selected value of θ provides higher or lower grain size distributions than the bedload samples and slightly higher RMSE values than the best fitted θ. This uncertainty exists, in part, due to variability of θ obtained from individual datasets: from 0.003 to 0.1. A wide range of θ may also relate to the efficiency

of Helley-Smith bedload samplers which integrate an unknown sampled proportion of the actual bedload in motion throughout two flood or two ebb tides, so that the individual integrated samples might not best represent bedload transported over the dune crest during any short period of time (e.g. of several minutes duration) or notionally instantaneous transport rates (i.e. calculated for a one second interval) during tides. This limitation inevitably results in different grain size distributions between calculated and observed samples.

Later, a combination of grain size distributions from all bedload samples collected during the complete study period (22 samples) was compared with all calculated grain sizes with θ_c set to 0.01 to 0.25 in order to assure the best representative Shields' number of overall grain size distribution and to investigate if 0.05 would be the best representative value, by fitting these calculated grain curves against the combined bedload sample. However, a plot of these curves (Figure 5.35) shows that D_{mobile} calculated with a θ of 0.04 has the best fit against the full grain size distribution of all samples. This value is slightly lower than the value initially investigated but is selected for this study because it is considered to be the value providing the best representation of calculated grain size distribution with regard to the full grain size distribution of the observed bedload. The calculated D_{mobile} size with Shields' value of 0.04 seems to agree with the sediment sizes found in bedload samples. The maximum calculated grain size of about 170 mm, is also found in the bedload samples and is close to the medium axis of the rectangular brick tracers (200*100*65 mm) which were observed to migrate during the study period. Moreover, this value fall within the limits of θ for grains coarser than 10 mm, 0.01 – 0.25 commonly proposed in the literature (Knighton, 1998) and the critical Shields number for gravels range between 0.02 to 0.065 (Buffington and Montgomery, 1997). Moreover this value is close to the median value, 0.047, often cited as representing the central tendency of θ_c data for medium-sized gravel mixtures (Meyer-Peter and Müller, 1948; Buffington and Montgomery, 1997) which is another reason to support the selection of θ of 0.04.

Once the estimated critical Shields' number was selected, the likely grain sizes being moved (D_{mobile}) were calculated (Figure 5.32C and Figure 5.33C) for observed τ_0 values. A wide range of grain sizes are found both for tides in July and August 2014, from very fine grains, less than 1 mm, to coarse grains exceeding 50 mm. The very fine grains of D_{mobile} likely dominate bedload transport when the water depth is close to the maximum level, close to slack water when tidal currents are weak but will also be mobile when coarser fractions are entrained. The average D_{mobile} size in July 2014 was about 9 mm which is lower than the mean size in August

2014 of 25 mm, approximately. Besides, the maximum D_{mobile} in July 2014 is 102 mm while it can exceed 160 mm in August 2014. As the D_{mobile} value at a given time is a function of τ_0, the time-trends of D_{mobile} are similar to τ_0. So, at a given time, the higher the τ_0 value, the coarser the size of D_{mobile} likely to be moved. Both τ_0 and D_{mobile} in July 2014 are lower than those in August 2014. Looking at the differences between tides, τ_0 and D_{mobile} during flood tides in July 2014 are greater than the ebb tides, except for the second tide which the maximum D_{mobile} is quite similar and the last tide where there were a few examples of instantaneous high values in the ebb, including the spike at the end of ebb tides, resulting in higher maximum D_{mobile} during ebb than flood. In contrast, these two values were much higher during the ebbs than floods in August 2014. However, τ_0 and D_{mobile} during flood and ebb tides in the second tide in this period are almost equal (see more details of flow conditions in Table 5.21).

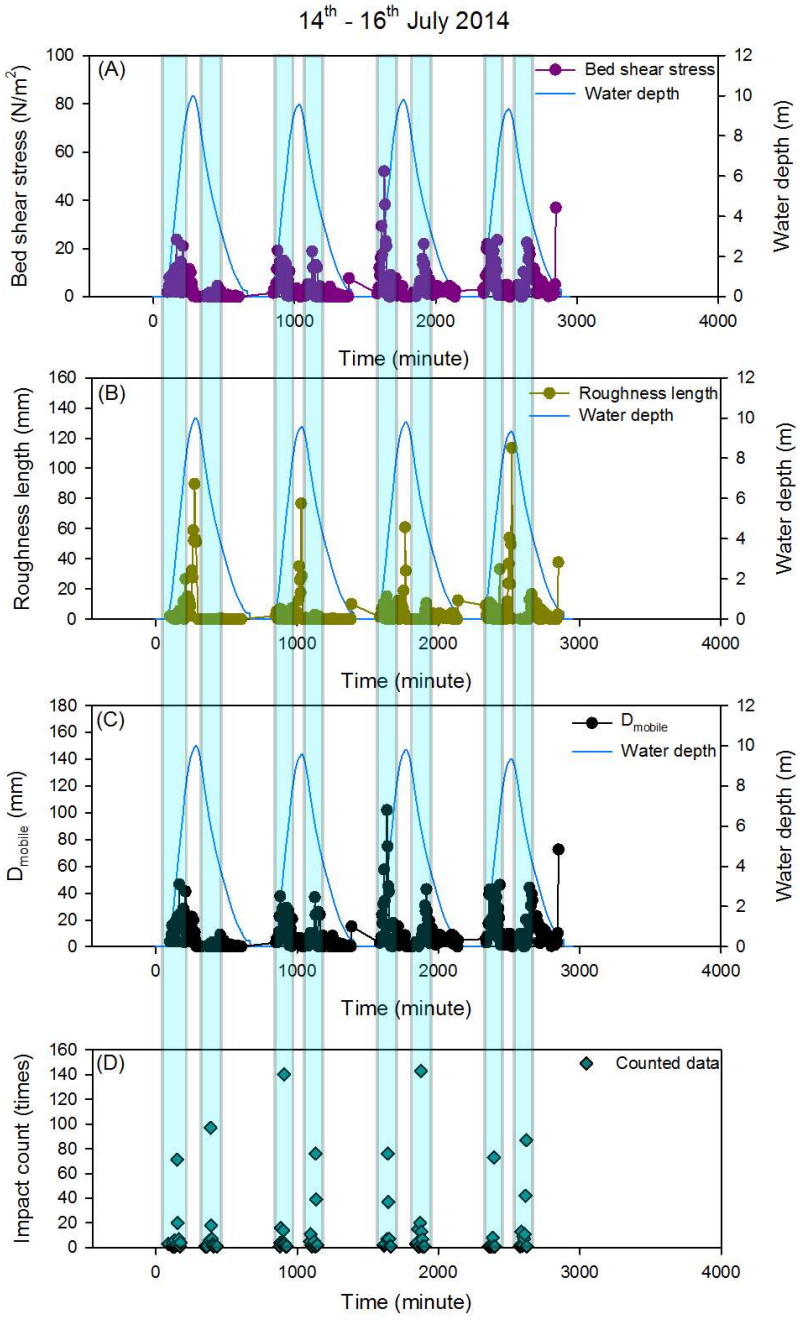

Figure 5.32 Calculated flow properties; bed shear stress (τ_0), roughness length (Z_0), predicted mobile grain size (D_{mobile}: when Shields parameter equals 0.04) against water depth (h) measured overlaid with impact sensor data (counted data) measured in July 2014. The transparent blue bands highlight the time period between first impact and last impact for flood and ebb periods.

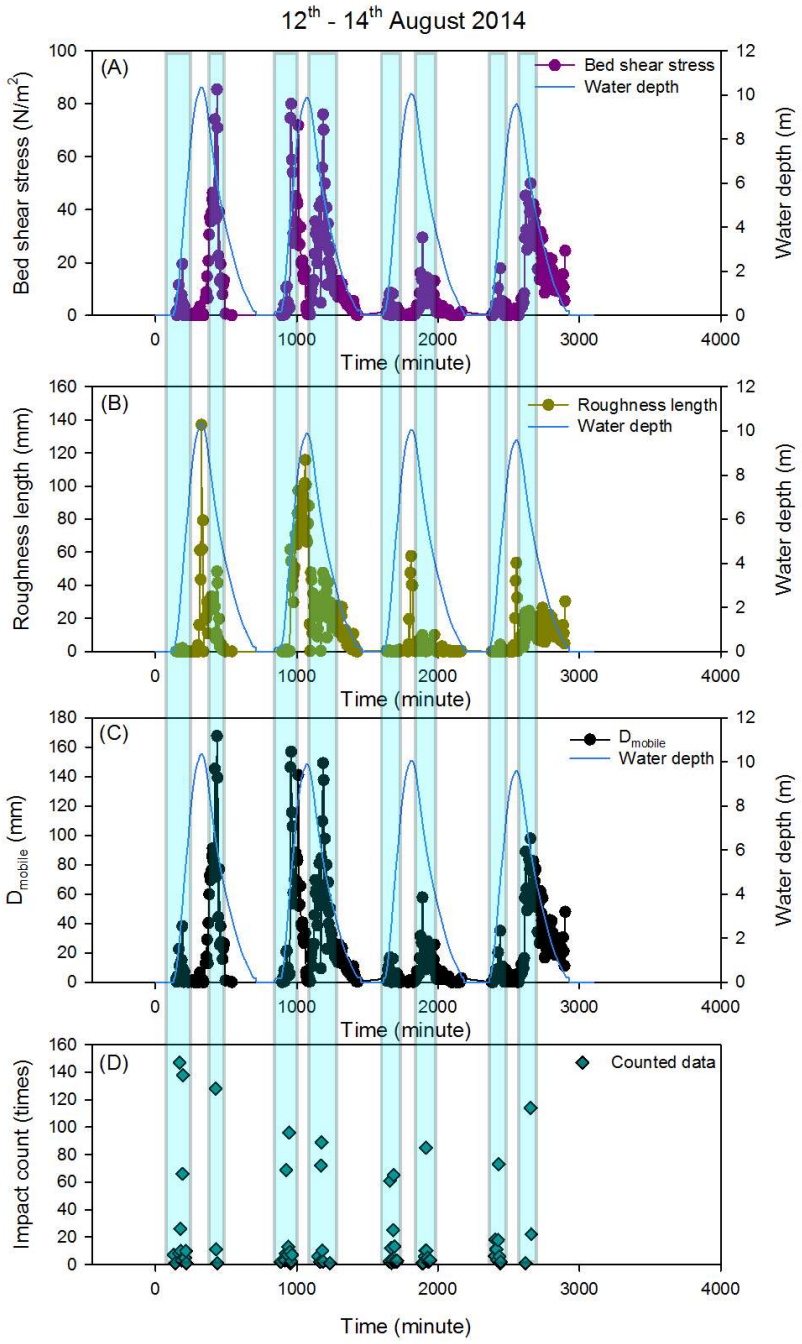

Figure 5.33 Calculated flow properties; bed shear stress (τ_0), roughness length (Z_0), predicted mobile grain size (D_{mobile}: when Shields parameter equals 0.04) against water depth (h) measured overlaid with impact sensor data (counted data) measured in August 2014. The transparent blue bands highlight the time period between first impact and last impact for flood and ebb periods.

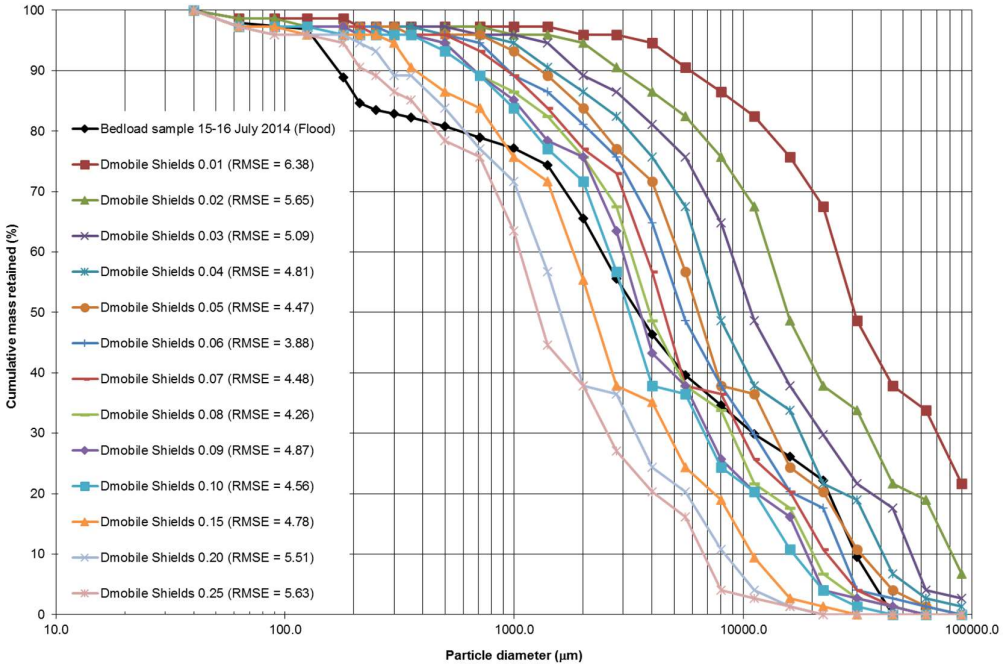

Figure 5.34 An example of fitting D_{mobile} calculated with various Shields against the bedload sample in the ebb tides 14th – 15th July 2014.

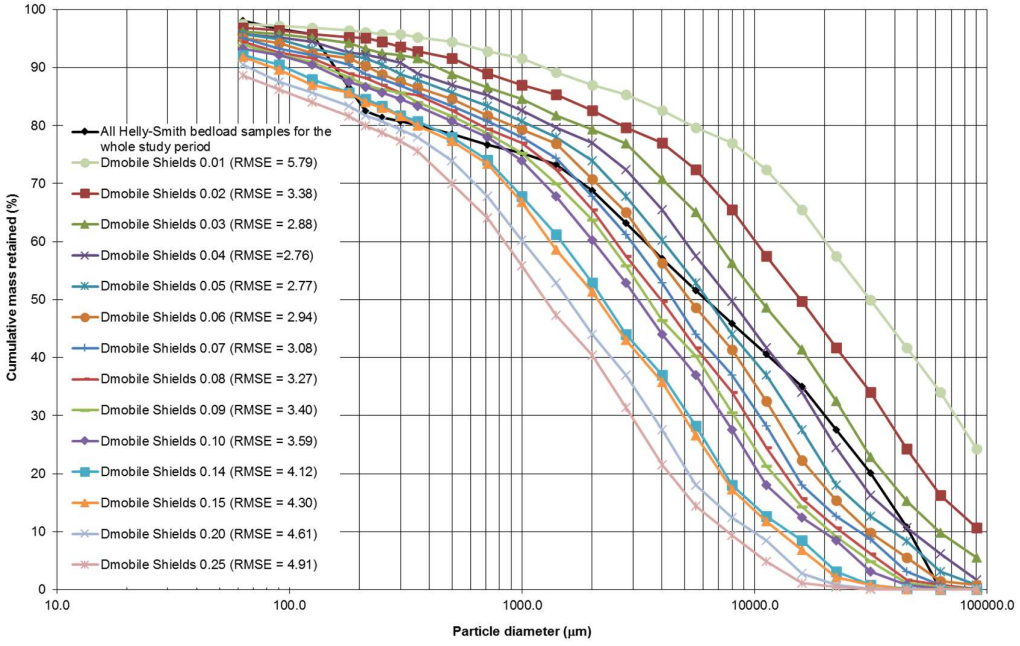

Figure 5.35 Grain size distribution plotting against D_{mobile} Curve from all six datasets collected in July 2014 and August 2014

Table 5.17 The RMSE of D_{mobile} calculated with various Shields numbers. The red font presents the lowest RMSE, best fitted curve, to the bedload sample. The green font indicates uncertainty as the selected Shields values is lower than 0.02 which is not in the range of critical Shields number for gravels suggested by previous studies (Buffington and Montgomery 1997, Knighton, 1998

Date	14 - 15 July 2014		15 - 16 July 2014		12-13 Aug 14	13-14 Aug 14
Tides	Flood	Ebb	Flood	Ebb	Ebb	Ebb
Shield no		0.002				
RMSE		4.18				
Shield no		**0.003**				
RMSE		**3.5**				
Shield no		0.004				
RMSE		3.59				
Shield no		0.005				
RMSE		4.62				
Shield no		0.006				
RMSE		4.46				
Shield no		0.007				
RMSE		4.59				
Shield no		0.008				
RMSE		4.33				
Shield no		0.009				
RMSE		4.58				
Shield no	0.01	0.01	0.01	0.01	0.01	0.01
RMSE	7.7	4.88	6.38	4.08	12.53	9.16
Shield no	0.02	0.02	0.02	**0.02**	0.02	0.02
RMSE	6.92	5.67	5.65	**4**	8.15	5.81
Shield no	0.03	0.03	0.03	0.03	0.03	0.03
RMSE	6.6	5.73	5.09	4.26	8.17	5.38
Shield no	0.04	0.04	0.04	0.04	0.04	0.04
RMSE	6.08	6.23	4.81	4.62	7.48	4.44
Shield no	0.05	0.05	0.05	0.05	0.05	**0.05**
RMSE	5.54	6.45	4.47	4.69	6.15	**4.435**
Shield no	0.06	0.06	**0.06**	0.06	**0.06**	0.06
RMSE	5.47	6.67	**3.88**	4.87	**5.92**	4.83
Shield no	0.07	0.07	0.07	0.07	0.07	0.07
RMSE	4.83	6.8	4.48	4.88	7.34	4.93
Shield no	0.08	0.08	0.08	0.08	0.08	0.08
RMSE	4.65	7.06	4.26	5.03	8.02	5.67
Shield no	0.09	0.09	0.09	0.09	0.09	0.09
RMSE	4.66	6.99	4.87	5.1	7.97	5.76
Shield no	**0.1**	0.1	0.1	0.1	0.1	0.1
RMSE	**4.33**	7.45	4.56	5.16	8.02	5.88
Shield no	0.15	0.15	0.15	0.15	0.15	0.15
RMSE	4.81	8.18	4.78	5.84	8.68	6.41
Shield no	0.2	0.2	0.2	0.2	0.2	0.2
RMSE	4.43	8.72	5.51	5.97	8.76	6.36
Shield no	0.25	0.25	0.25	0.25	0.25	0.25
RMSE	4.33	9.38	5.63	6.32	8.77	6.53
	Average RMSE		Median		SD	
	0.05		0.10		0.08	

5.2.4.2 Coarse bedload movements determined by impact sensor

The application of the portable impact sensor generally provides information on the coarse grains moving close to the bed, and probably of a minimum size of 10 mm approximately (≥ 11.3 mm according to Beylich and Laute (2014), passing over the dune crest. Even though the impact plate cannot record a given grain size, it provides the duration between when coarse grains start and stop moving (Figure 5.32D and Figure 5.33D more details about the device in section 4.3.3) and an indication of bedload intensity determined by when impacts are sparsely or closely spaced in time. An overlay of impact data against calculated τ_0, Z_0, and D_{mobile} emphasizes the times, flow conditions and the qualitative amount of gravel-sized large sediment particles transported across the dune (Figure 5.32 and Figure 5.33).

Considering each tide, which herein includes both flood and ebb directions, the total number of impact counts in August 2014 is slightly higher than in July 2014, except the first flood tide in August for which the counts increase dramatically to more than 400 counts. The increase in the number of impact counts from July to August 2014 is in agreement with an increase in τ_0 and D_{mobile} on that occasion. Considering flood and ebb flows separately, in July 2014, the ebbs tend to have more impact counts than the floods, except the second tide of which the flood flow has more counts. The maximum counts are in the ebb of the third tide, 209 counts, while the minimum of 87 counts was detected in the fourth flood tide. On the other hands, in August 2014, more impact counts were detected during floods with the highest amount in the first flood, 419 counts, while the lowest amount is 125 counts in the third ebb tide.

Comparing the relationship between impact counts and flow conditions, in terms of τ_0 and D_{mobile}, during flood and ebb separately, the data trends did not show clear patterns for any one tide. From data of eight tides in both months, it is found that the counts during the first, third and fourth tides in both months varied with the two flow conditions. The higher τ_0 and D_{mobile} during flood shows a lower amount of impact counts than those during the ebb. In contrast, the higher values of these two flow conditions during ebb have less counts than those during flood. For example, the flood flows of the first and the third tides in July 2014 have higher τ_0 and D_{mobile} but lower impact counts than the ebb flows. However, only two tides, the second tides in both July and August 2014, did not have the same behaviour as the majority. The values of τ_0, D_{mobile}, and the impact counts have the same general trend. The higher τ_0 and D_{mobile} in either flood or ebb flows, the higher counts are observed in the same flow directions. Both tides have more counts during floods which is in agreement with the higher maximum τ_0 and D_{mobile} during floods than during ebbs (Table 5.18).

Considering the start-stop period of detected impacts, there is a wide range of τ_0 values related to particle entrainments. The τ_0 values, during both floods and ebbs, at the beginning of counting are in the range: 0.16 – 45.29 N/m^2, whilst the stop τ_0 values are in a range: 0.5 – 85.37 N/m^2. The τ_0 values related to impact count in July 2014 is generally lower than those in August 2014. Looking through either flood or ebb data separately, the overall data show that half of datasets; 5 floods and 3 ebbs from 16 flows (8 tides), have the higher τ_0 values at the beginning of impact counts than when the counting stopped. This process agrees with the theory that the settling of particles or deposition occurs when the flow velocity, for any given grain size, is less than that required for entrainment; that is about two-thirds of threshold velocity for gravels (Richards, 1982 and Knighton, 1998). Moreover, a study of Reid *et al.* (1985) on bedload transport of coarse grains, which are less than 50 mm, demonstrated that the τ_0 values for initial motion are higher than those recorded for cessation of motion. On the other hand, the other half of datasets; 3 floods and 5 ebbs, have the opposite behaviour. The stop τ_0 values were higher than the start τ_0 values. The occurrences of high rates of impact counts are not directly related to high τ_0 or high U or u_*values. The maximum counts did not coincide with the timing of when the τ_0 values reach the maximum values during the duration of counting. The higher velocity might not mean that flows will move more particles. For example, the average U value for the second ebb tide in July 2014 or the third ebb in August 2014 are higher than floods but the total the counts are lower. The maximum counts occur when τ_0 is in a range of 1.12 – 49.88 N/m^2. More details of flow conditions in individual tides and start-stop τ_0, D_{mobile} and number of counts are presented in Table 5.18.

Apart from the difference in the start and stop τ_0, there is an issue of uncertainty regarding to the calculated D_{mobile}. Even though the Shields value of 0.04 seems to fit well with the bedload grain size, there is one concern to be noted in that there are a few occasions when the calculated grain sizes during the time that gravel moving was detected are very small, and could be less than 1 mm, which does not seem sensible and correct as the impact sensors are known not to respond to the impact of sand, as well as particles less 11 mm approximately. It seems unreasonable to approve those D_{mobile} values calculated with θ of 0.04, especially at the initial motion start. It can be seen that there is some variability in θ_c having impact on gravel movements over the studied dune. There are a number of reasons considered to be related to the variability of θ_c and two issues seem to be dominant. One of them is the robustness of the τ_0 derivation. The flow data were used to define velocity profiles using only two or three points in the vertical and so there is inevitably some uncertainty in the values of τ_0 derived and hence the estimates of θ. Moreover, the τ_0 values were averaged over one

minute and the timing of these samples cannot be exactly matched to the time of the detected impacts.

Table 5.18 A table presents information of bed shear stress (τ_0), amount of impact counts, and calculated D_{mobile} with a Shields number of 0.05 at the beginning and the end of impact counts during flood and ebb flows.

Month		Jul-14								Aug-14							
Tide		1		2		3		4		1		2		3		4	
Direction		Flood	Ebb	Flood	Ebb	Flood	Ebb	Flood	Ebb	Flood	Ebb	Flood	Ebb*	Flood	Ebb	Flood	Ebb**
Start detected	τ_0	7.95	0.16	11.45	1.68	16.14	1.70	8.72	4.92	11.52	37.85	0.33	28.88	8.10	29.44	1.76	45.29
	No. counts	1	1	1	5	2	3	1	2	8	128	3	6	2	1	6	1
	Calculated D_{mobile} (mm)	15.59	0.32	22.45	3.29	31.65	3.33	17.10	9.64	22.59	74.20	0.64	56.61	15.87	57.71	3.45	88.79
Stop detected	τ_0	7.47	1.56	14.84	0.77	0.64	6.19	4.46	10.10	0.50	85.37	58.88	25.69	3.03	13.02	4.62	31.35
	No. counts	4	1	1	2	1	1	1	1	1	1	7	1	3	3	1	22
	Calculated D_{mobile} (mm)	14.64	3.06	29.10	1.51	1.25	12.13	8.74	19.80	0.98	167.36	115.43	50.36	5.94	25.53	9.06	61.45
Conditions when max counts were detected	τ_0	11.01	1.12	10.95	12.13	38.20	1.48	19.50	10.26	5.75	37.85	2.52	43.15	N/A	4.48	2.19	49.88
	No. counts (max)	71	97	140	76	76	143	73	87	147	128	96	89	65	85	73	114
	Calculated D_{mobile} (mm)	21.57	2.19	21.47	23.78	74.88	2.91	38.23	20.12	11.27	74.20	4.94	84.59	N/A	8.78	4.29	97.78
Conditions when max τ_0 were observed	τ_0 (max)	23.66	1.63	19.19	18.81	51.97	6.58	21.81	10.26	19.46	85.37	79.96	75.98	8.64	29.44	17.86	49.88
	No. counts	2	3	4	1	7	1	1	87	66	1	2	2	61	1	1	114
	Calculated D_{mobile} (mm) (max)	46.39	3.20	37.62	36.87	101.88	12.90	42.75	20.12	38.14	167.36	156.75	148.95	16.93	57.71	35.01	97.78
Total counts		120	136	187	144	137	209	87	177	419	140	215	182	192	125	149	137

Note: 1) * In the 2nd ebb of August 2014, the last impact occurred after the previous count for almost an hour; ** In the 4nd ebb of August 2014, the first impact occurred before the second count for half hour.

2) The red values indicates bed shear stress contains uncertainty as it is missing during the time of impact counts due to the flow data at that time are not be able to create velocity profile.

5.3 Sediment transport processes

Sediment transport and deposition processes over the bedforms

Sediments in the study area consist of a wide range of grain sizes (Figure 3.16 in Chapter 3: Study site). The bulk bed sample collected in July 2013 generally represents the sediment sizes found within the studied dune; mostly consisting of gravels (79.4%) and sands (20.2%). This sample is classified as sandy gravel with a D_{50} of 16.7 mm (Figure 5.36, Figure 5.37 and Table 5.19). Moreover, bedload and suspended sediment samples were also collected during the study period in order to better understand the dynamics of sediment motion and deposition which related to hydraulic climate and the cobble dune development as reported later in this section.

Bedload transport process

Bedload samples were collected on most occasions of hydraulic field data collection (see Table 4.4 in Chapter 4: Methodology). The sampling was intended to quantify the grain size of bedload sediment transported and provide an indication of the minimum quantity transported over a tidal cycle. The Helley-Smith samplers trapped a lot of bedload sediment which filled the sampler bags on most sampling occasions (Figure 5.38). However, a few times unexpected issues existing in field data collection causing the Helley-Smith samplers to not catch bedload due to some reasons, i.e. blocked nozzle by seaweed, folded net bags, disjointed traps, buried net bag etc. These problems might also effect the total quantity and the grain sizes trapped in those cases where samples were trapped effectively. Problems might be related with local flow conditions around the traps, i.e. turbulence and fluid pressure outside and inside the trap etc. Apart from the standard 2 mm aperture nets used for collecting samples, a trial of finer (< 1 mm) and coarser aperture net (c. 5 mm) in the first (February 2013) and last month (August 2014) of bedload sample collection was also conducted. Apart from these latter samples in these two months, data collected in March, May, June, July 2013 as well as June and July 2014 are available for both flood and ebb tides, while the data from the other months have either flood or ebb tide data only, with missing date due to the technical issues mentioned above. Moreover, and surprisingly, the coarser net used to trap bedload sediments during flood tides in August 2014 did not trap any gravels but substantial organic matter which also entrapped very fine sediment with them (i.e. seaweed, tree branches, leaf debris, grasses or peat debris). As a consequence, two flood samples in August

2014, consisting of organic debris and fine sand, cannot be presented in this study. As a consequence, there are 22 bedload samples available in this study. Detail of bedload data collection is presented in Table 5.19. However, it is noted that the proportion of grains finer than 1 mm that occurred in bedload samples was excluded, as they are also found as suspended sediment which could have settled from suspension and may not have moved as bedload.

Twenty-two bedload samples, collected during both flood and ebb tides by coarser nets with c. 2 mm aperture size, were processed by dry sieving technique and analysed by Gradistat software as explained in the Methodology Chapter (section 4.3.2). The first sample in the ebb collected in February 2013 by fine aperture net did not trap much gravel, although the trap seemed to have functioned correctly. The sediments on this occasion are bimodal, moderately sorted and classified as slightly gravelly sand with D_{50} of 0.2 mm approximately. Only 1.6% of the sample contains gravels while the majority proportion being sand (95.6%). It is not clear if this event was dominated by sand transport or if sampling error occurred, as the tide was competent to entrain and transport gravel.

Considering all bedload samples, sediment trapped during ebb tides mostly have greater total weight than those during flood tides, possible indicating a Spring tide ebb dominance (Figure 5.39). On the other hand, a few sets of results gave a greater total weight for flood tides than total weight for the ebb tides. Moreover, the grain size distributions in Figure 5.36 and Figure 5.37 show that several ebb samples trapped coarser grains than the flood. These results might imply that the ebb flows tend mainly to have stronger flow to transport sediments than the floods which is in agreement with the topographic surveys that demonstrated most of the residual dune movements are ebb orientation and only a few times do flood orientations predominate. Moreover, the availability of sediment might be a related reason. The up-estuary area, both river bank and bedrock platform, are considered to be the source of coarse sediment nourishing the dunes. This close proximity of an up-estuary source may result in higher amount of sediment, including coarse gravels, being recorded during ebb flows than flood flows. The flood flows entrain sediment from the down-estuary within the main channel, which is known to be sandy but where otherwise the sediment characteristics are not well understood.

According to the analysis from Gradisat software, all bedload samples are very poorly sorted, most of which are polymodal (11 samples) or trimodal (8 samples) while only a few samples are bimodal (3 samples). The statistics of these samples are varied. D_{50} values range from 0.2

mm to 21 mm. The traps deployed from March 2013 onwards collected more coarse grains than the trap in February 2013 and floods tend to have finer grain size than ebbs, so the February sample does seem anomalous. The range of D_{50} of floods is between 0.2 mm and 11.8 mm, whilst ebbs have D_{50} from 0.2 mm to 20.8 mm (Figure 5.36 and Figure 5.37). The grain size distribution chart (Figure 5.36) shows the two major proportions of fine sand (0.2 - 0.3 mm) and (30 – 50 mm) coarse gravels. More details of the grain size statistics, including grain size distributions, are provided in Figure 5.36 and Figure 5.37.

Comparing the bulk bed sample and all bedload samples, it is generally shows that the bed sample consists of coarser grains than those from the bedload samplers. Moreover, the comparison of cumulative bedload curves during floods and ebbs shows that the ebb samples have similar trends and almost similar proportions of grains in different size classes as the bulk bed sample in contrast to the flood samples. This behaviour implies the ebb-dominated flow are capable of transporting the range of grain-sizes noted in the bed material sample on most Spring tides although the coarsest fractions are under-represented. Under-representation of the coarsest fractions is due to the inability of the Helley-Smith samplers to trap very large cobbles due to the size of the entrance aperture (see below), although the brick tracer data demonstrated that large clasts are mobile on most Spring tides. Consequently the interpretation advanced above is supported by the results in other sections of hydrodynamic data, topographic survey and bedload tracing. The bulk bed sample has a high percentage of gravels, almost 80%, while the bedload samples have quite similar high percentage or slightly lower percentage of gravels followed by smaller percentage of sands, except samples collected in both flood and ebb on 27th – 28th May 2013, ebb on 28th – 29th May 2013, ebb on 25th – 26th June 2013, flood on 20th – 21st August 2013, and flood on 19th – 20th September 2013, which the proportion of gravel is less than 50% and the sands become the major proportion instead. Moreover, a very small amount of mud was observed in all samples which is less than 10%, but only one sample on 27th – 28th May 2013 has slightly higher proportion as 15%.

However, it is noted that even the samplers worked properly, these samplers might have under-sampled bedload transported over the crest, in terms of both the grain size and amount of grains. It is considered that the dimension of the nozzle, 15 × 15 cm, would preclude sampling of very large clasts whereas other coarse grains where found to be moved around the dune field by visual observation and the results from brick tracing technique. The total amount of bedload moving on either flood or ebb may be also under-sampled. The reasons of this under-sampling may relate to (A) the capacity of the bag that is full too quickly resulting in

the no further movement of gravels into the bag; and (B) a back-pressures developed in the sampler due to the blocked mesh by debris.

Importantly, these bedload samples consistently show the broad range of grain sizes of sediments being transported over the dunes as integrated into the total flood or ebb samples. The short-term transportation rates (e.g. kg/m/s) over the dune crest are not able to be identified in this study, other than dividing the total load by the duration of flood or ebb which would not be a very accurate procedure. Importantly, an analysis of initial motion which was explained in previous sections was done by using the grain size distribution data of all bedload samples. All the bedload data are described in a previous section (section 5.2.4.2).

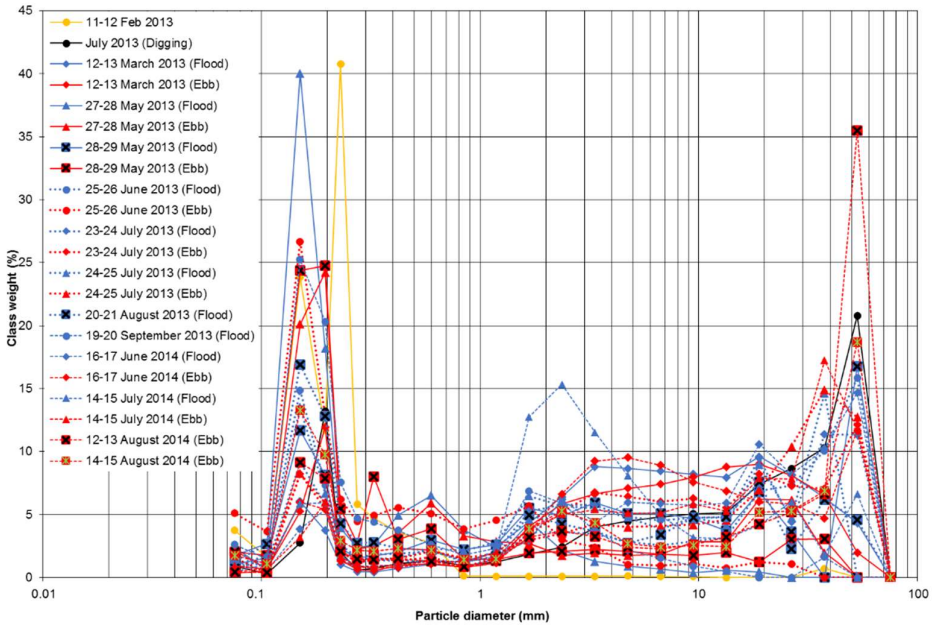

Figure 5.36 Grain size distribution of bedload samples

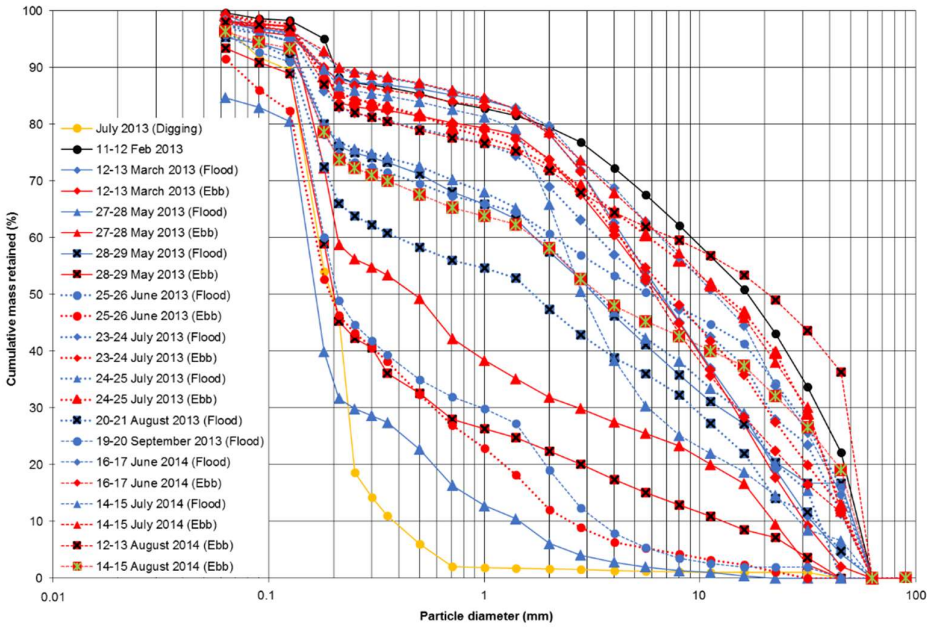

Figure 5.37 Cumulative grain size of bedload samples

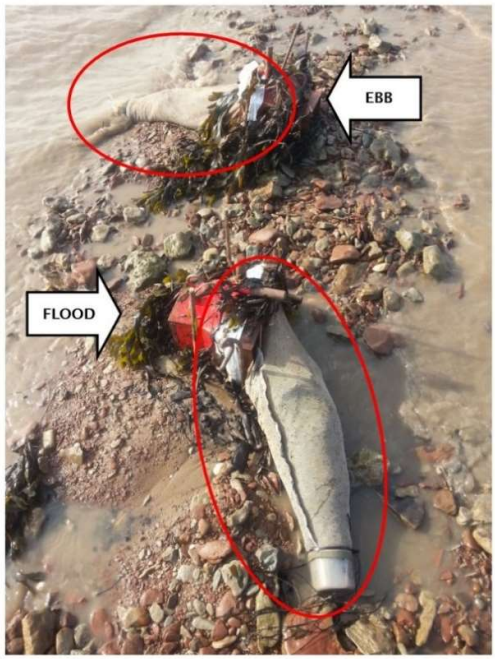

Figure 5.38 The sample bags full of bedload sediments usually trapped in both flood and ebb flows during the study period.

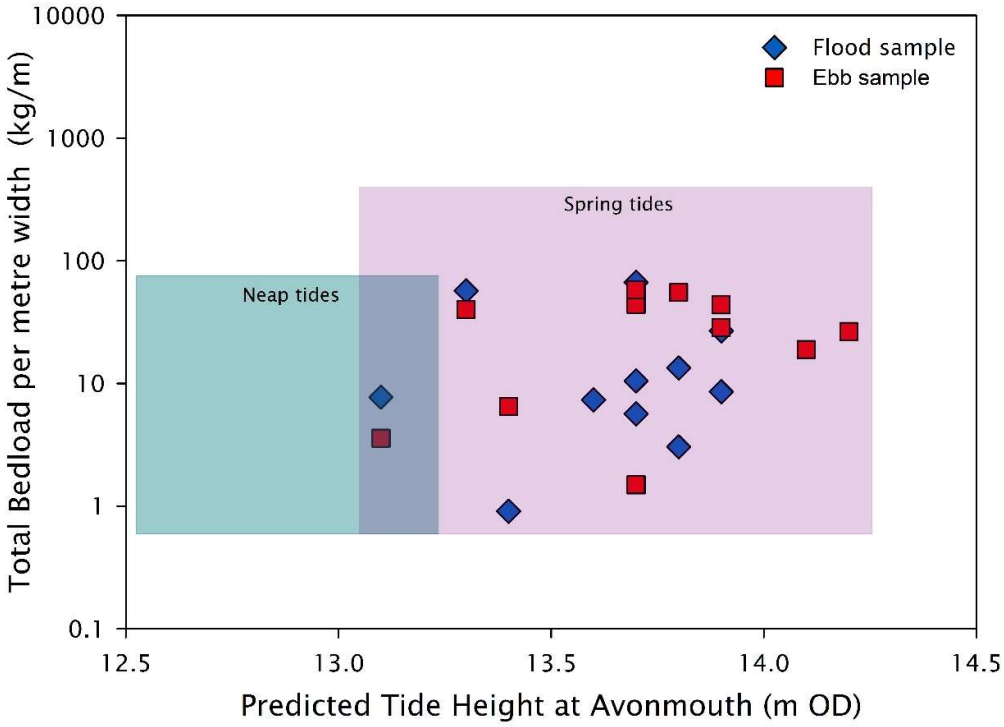

Figure 5.39 Total weight of bedload samples, ≥ 1mm, per one-metre width collected over two tidal cycles. The predicted tide height is that of the highest flood of the tidal pair at Avonmouth. Each sample necessarily was collected through two tides as the samplers had to be left out in the field for two tides before they could be retrieved.

Table 5.19 Statistics results of digging sample and bedload samples, including a trial of fine aperture net in February 2013

Date/Sample		Note	Total weight (grams)	Sample type	Textural group	Sediment name	D10 (mm)	D50 (mm)	D90 (mm)	% GRAVEL	% SAND	% MUD
23-Jul-13	-	Bed material sample collected by shovel	24967.47	Bimodal, Very Poorly Sorted	Sandy Gravel	Sandy Very Coarse Gravel	0.2	16.7	54.1	79.4	20.2	0.3
11-12 Feb 13	-	Fine aperture	3391.66	Bimodal, Moderately Sorted	Slightly Gravelly Sand	Slightly Coarse Gravelly Fine Sand	0.1	0.2	0.4	1.6	95.6	2.8
12-13 Mar 13	F		11866.87	Polymodal, Very Poorly Sorted	Sandy Gravel	Sandy Coarse Gravel	0.2	6.6	33.1	78.2	21.1	0.7
	E		8329.00	Trimodal, Very Poorly Sorted	Sandy Gravel	Sandy Coarse Gravel	0.2	6.4	30.6	73.8	24.9	1.3
27-28 May 13	F		1064.98	Bimodal, Very Poorly Sorted	Gravelly Muddy Sand	Very Fine Gravelly Coarse Silty Fine Sand	0.0	0.2	1.5	6.1	78.6	15.3
	E		2540.06	Trimodal, Very Poorly Sorted	Sandy Gravel	Sandy Coarse Gravel	0.1	0.5	21.9	31.9	66.4	1.7
28-29 May 13	F		1763.31	Polymodal, Very Poorly Sorted	Muddy Sandy Gravel	Very Coarse Silty Sandy Very Coarse Gravel	0.1	3.2	51.5	57.5	37.9	4.7
	E		2035.34	Trimodal, Very Poorly Sorted	Gravelly Sand	Coarse Gravelly Fine Sand	0.1	0.2	12.8	22.4	71.0	6.6
25-26 June 13	F		2389.22	Trimodal, Very Poorly Sorted	Sandy Gravel	Sandy Very Coarse Gravel	0.1	5.9	51.1	60.7	36.7	2.6
	E		976.93	Polymodal, Very Poorly Sorted	Gravelly Sand	Very Fine Gravelly Fine Sand	0.1	0.2	2.5	12.0	79.5	8.4

Table 5.19 Statistics results of digging sample and bedload samples, including a trial of fine aperture net in February 2013

Date/Sample		Note	Total weight (grams)	Sample type	Textural group	Sediment name	D10 (mm)	D50 (mm)	D90 (mm)	% GRAVEL	% SAND	% MUD
23-24 July 13	F		5250.44	Polymodal, Very Poorly Sorted	Sandy Gravel	Sandy Very Coarse Gravel	0.2	6.6	46.9	69.0	29.2	1.8
	E		5416.59	Polymodal, Very Poorly Sorted	Sandy Gravel	Sandy Very Coarse Gravel	0.2	7.2	48.0	73.8	25.5	0.7
24-25 July 13	F		1244.67	Polymodal, Very Poorly Sorted	Sandy Gravel	Sandy Very Coarse Gravel	0.1	3.3	35.7	58.5	38.4	3.1
	E		11146.59	Trimodal, Very Poorly Sorted	Sandy Gravel	Sandy Very Coarse Gravel	0.2	12.8	48.6	72.7	26.6	0.7
20-21 Aug 13	F		2014.73	Polymodal, Very Poorly Sorted	Sandy Gravel	Sandy Very Coarse Gravel	0.1	1.7	34.3	47.4	48.4	4.2
	E	the ebb didn't catch bedload	X									
19-20 Sep 13	F		1524.36	Bimodal, Very Poorly Sorted	Gravelly Sand	Very Fine Gravelly Fine Sand	0.1	0.2	3.4	19.0	76.8	4.2
	E	The ebb did not catch bedload	X				0.0	0.0	0.0			
18-19 March 14	F	none was trapped but	X									
	E	Clasts were found moving around the trap	X									

Table 5.19 Statistics results of digging sample and bedload samples, including a trial of fine aperture net in February 2013

Date/Sample		Note	Total weight (grams)	Sample type	Textural group	Sediment name	D10 (mm)	D50 (mm)	D90 (mm)	% GRAVEL	% SAND	% MUD
16-17 June 14	F		10124.03	Polymodal, Very Poorly Sorted	Sandy Gravel	Sandy Very Coarse Gravel	0.2	11.8	50.1	79.7	18.7	1.6
	E		7223.52	Trimodal, Very Poorly Sorted	Muddy Sandy Gravel	Very Coarse Silty Sandy Fine Gravel	0.2	6.2	47.1	78.3	19.4	2.3
14-15 July 14	F		1577.69	Polymodal, Very Poorly Sorted	Sandy Gravel	Sandy Very Fine Gravel	0.2	2.8	29.0	65.9	31.7	2.5
	E		7771.92	Polymodal, Very Poorly Sorted	Sandy Gravel	Sandy Very Coarse Gravel	0.2	12.3	47.4	78.6	19.5	1.9
15-16 July 14	F		2596.16	Polymodal, Very Poorly Sorted	Sandy Gravel	Sandy Very Fine Gravel	0.2	3.5	31.1	65.5	32.4	2.1
	E		10095.50	Trimodal, Very Poorly Sorted	Sandy Gravel	Sandy Very Coarse Gravel	0.2	8.0	47.6	73.3	25.4	1.3
12-13 Aug 14	F	very coarse aperture on flood	X									
	E		5194.96	Bimodal, Very Poorly Sorted	Sandy Gravel	Sandy Very Coarse Gravel	0.2	20.8	57.4	71.8	26.2	1.9
13-14Aug 14	F	very coarse aperture on flood	X									
	E		4451.33	Trimodal, Very Poorly Sorted	Sandy Gravel	Sandy Very Coarse Gravel	0.1	3.4	52.8	58.2	38.2	3.6

5.4 Dune stratigraphy and sedimentology

Apart from investigating topography, measuring flow conditions and the other techniques previously mentioned, longitudinal sections were opened through the dunes by using spades and shovels. The internal structure within sections of two dunes were observed on 10th March 2016. One is the dune on which the equipment was set (Dune no. 12 in Figure 5.9), herein called section A, and the other is the next upstream dune (Dune no. 15 in Figure 5.9) called section B. Although there was only time to open two sections, both showed some evidence of up-estuary dipping cross-strata. However within the small section A, which was 0.3 m high and 4.7 m long, the structures, where present, were very faint and obscured by mud (Figure 5.40). Much of this duneform exhibited no clear structure at all other than a reactivation surface separating less-compacted sediments at the surface from more compacted sediment below. So, as section B exhibited similar and additional characteristics, no further details of section A are provided here. On the other hand, the section B represented a larger dunes and clearer internal structure was visible in contrast to the first one (Figure 5.41). More detail of visible internal structure being observed in the section B is described in this section.

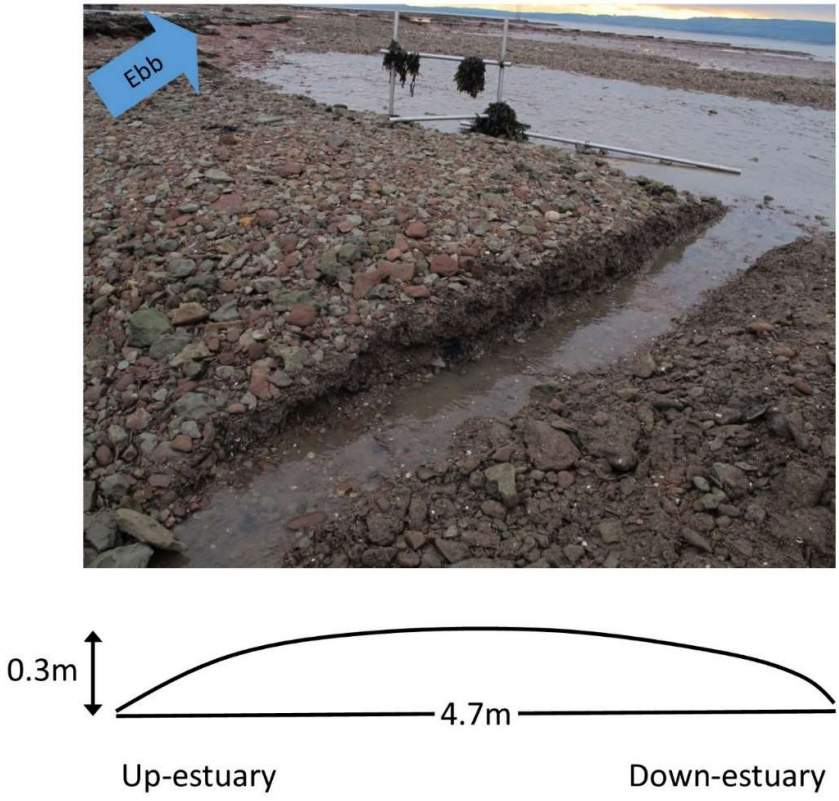

Figure 5.40 Cross-section A of pebble and cobble dunes.

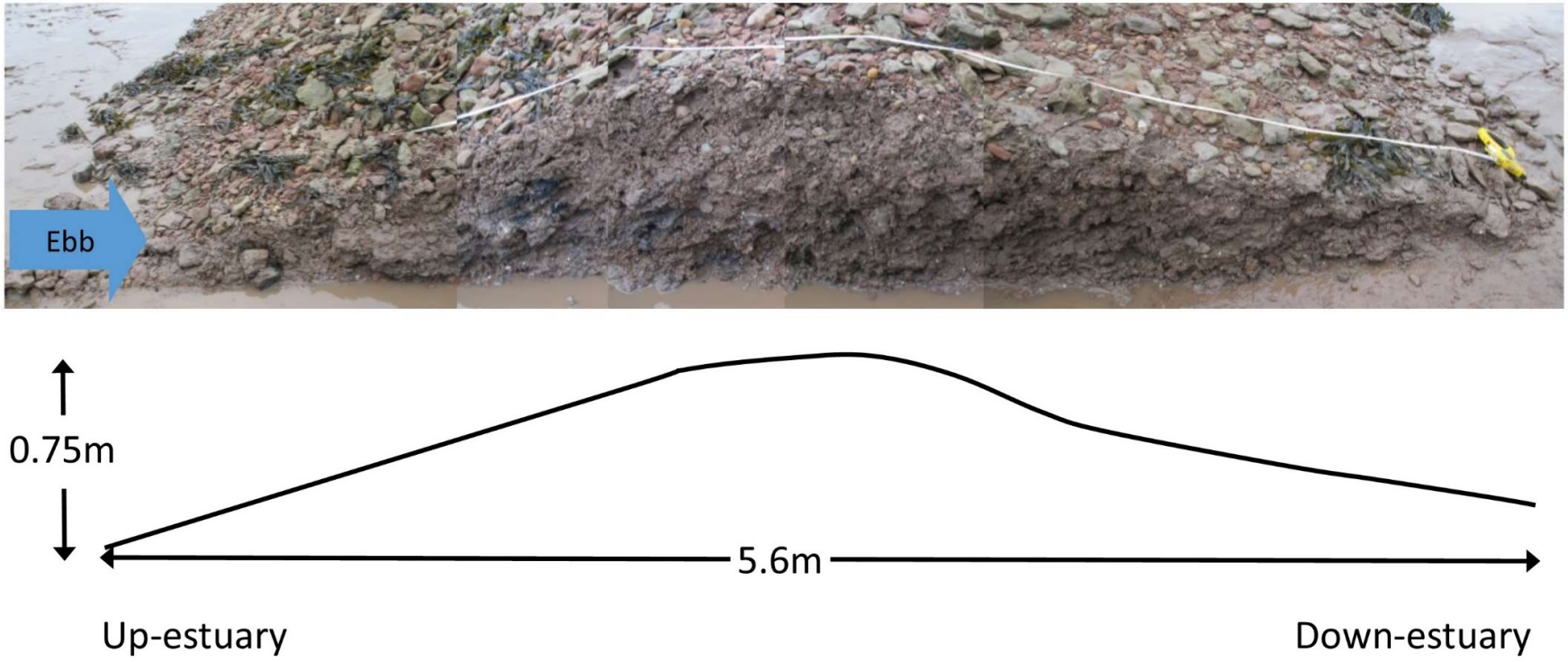

Figure 5.41 Cross-section B of pebble and cobble dunes.

Overall the section does not show clear structure. However, close observation of section B provides that there are a few parts within this section which have visible structural features. Figure 5.42 presents a general sketch of the structure. The upper portion of the dune is a little finer in grain size than the basal portion and mainly consists of angular pebbles, somewhat more loosely packed, with a little less matrix fill than the lower portion of the dune which is comprised of larger pebbles and some cobbles. The dashed line represents the approximate trend of a reactivation surface where the older coarser-grained dune has been planed-off and new finer sediment deposited above. This behaviour, whereby gravel dunes exhibit a capping deposit in reversing currents, has been described by Carling *et al.* (2006) and reflects planning-down of the dune during one tidal cycle and then rebuilding of the duneform on a later tide. Very poorly defined, flood tide cross-bedding (10 to 30^{o} inclination) is occasionally evident in the lower portion of the dune truncated by the reactivation surface. In other respects the dune lacks distinctive bedding or preferred clast orientations. The lack of distinctive bedding is largely due to the very low rates of bedload transport such that the dune sides build out laterally very slowly by accretion of just a few coarse clasts on each tide such that distinctive thick cross-sets are not formed. Subsequent tides just add a little more sediment to the depositional surface. In addition, the reversing tides cut and then refill and would be expected to form herringbone cross-bedding. Herringbone-bedding was weakly developed in the case of the fine-gravel dunes described by Carling *et al.* (2006) for Hills Flats and this cut-and-fill style of deposition would further truncate and otherwise disrupt any evidence for distinctive extensive cross-bedding migrating in one direction.

The distinctive armour layer at the top is devoid of fines. On the down estuary side of the dune the armour layer clasts tend to lie flat in the same plane as the slope of the dune side, and the surface is compact. The a-axes of the clasts tend to align with the flow direction. In contrast on the up-estuary side of the dune the clasts are disorientated and loosely deposited. This structure is interpreted as due to a local dominance of the flood tide which has caused the dune to migrate up-estuary deflating the down-estuary side of the dune whilst clasts are deposited in the up-estuary leeside in a chaotic manner. Evidently, the single ebb tide before the dune was exposed was insufficient in strength to rework, compact and align the coarse sediment on the steep up-estuary slope.

Further consideration of the internal structure of section B provided material allowing a hydrodynamic interpretation of the internal structure.(Figure 5.43, Figure 5.44 and Figure 5.45). There was no evidence of any bedding in the younger deposits above the reactivation

surface, which appears as a chaotic jumble of fine pebbles. However, bedding is poorly developed in the older deposit below the reactivation surface, but is usually only picked out by the alignment of individual flat clasts which tend to lie flat on the bedding surfaces including on the surfaces of presumed cross-beds which cannot otherwise be discerned. Occasionally, these isolated clasts are found in small groups such as strings of pebbles lying along foreset planes which pick out the bedding more effectively (Figure 5.43) or can be identified by the vague alignment of the collapse fractures along the cut face that formed as sediment was cut away from the face using a spade (Figure 5.44). Occasional buried organic-rich blocks of black mud containing sedge and seaweed fragments occur throughout the basal deposits (Figure 5.45) and probably represent riparian marsh deposits eroded from the estuarine margins. A concentration of larger cobbles at the base of the deposit (Figure 5.45) may reflect a degree of down slope sorting of coarser grains by flow and gravity such that larger grains tend to concentrate at the toes of both up-estuary and down-estuary lee sides to be over-ridden by the dune when it migrates.

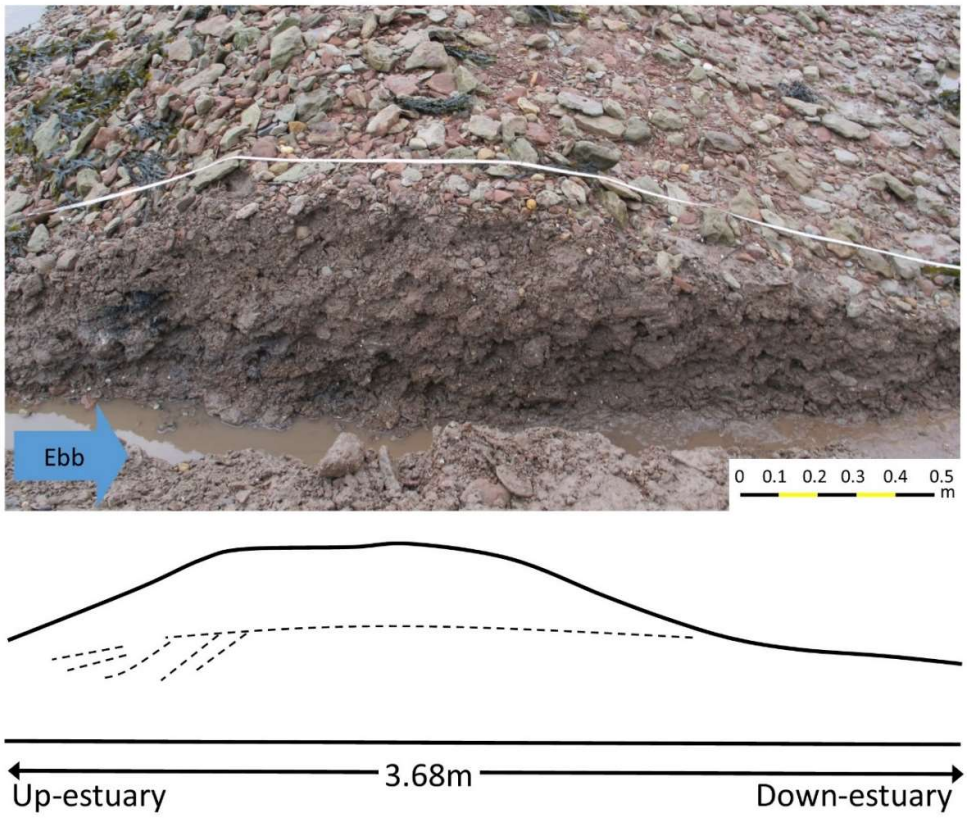

Figure 5.42 View of section cut longitudinally through a dune. The tape measure is set just back from the edge of the cut face.

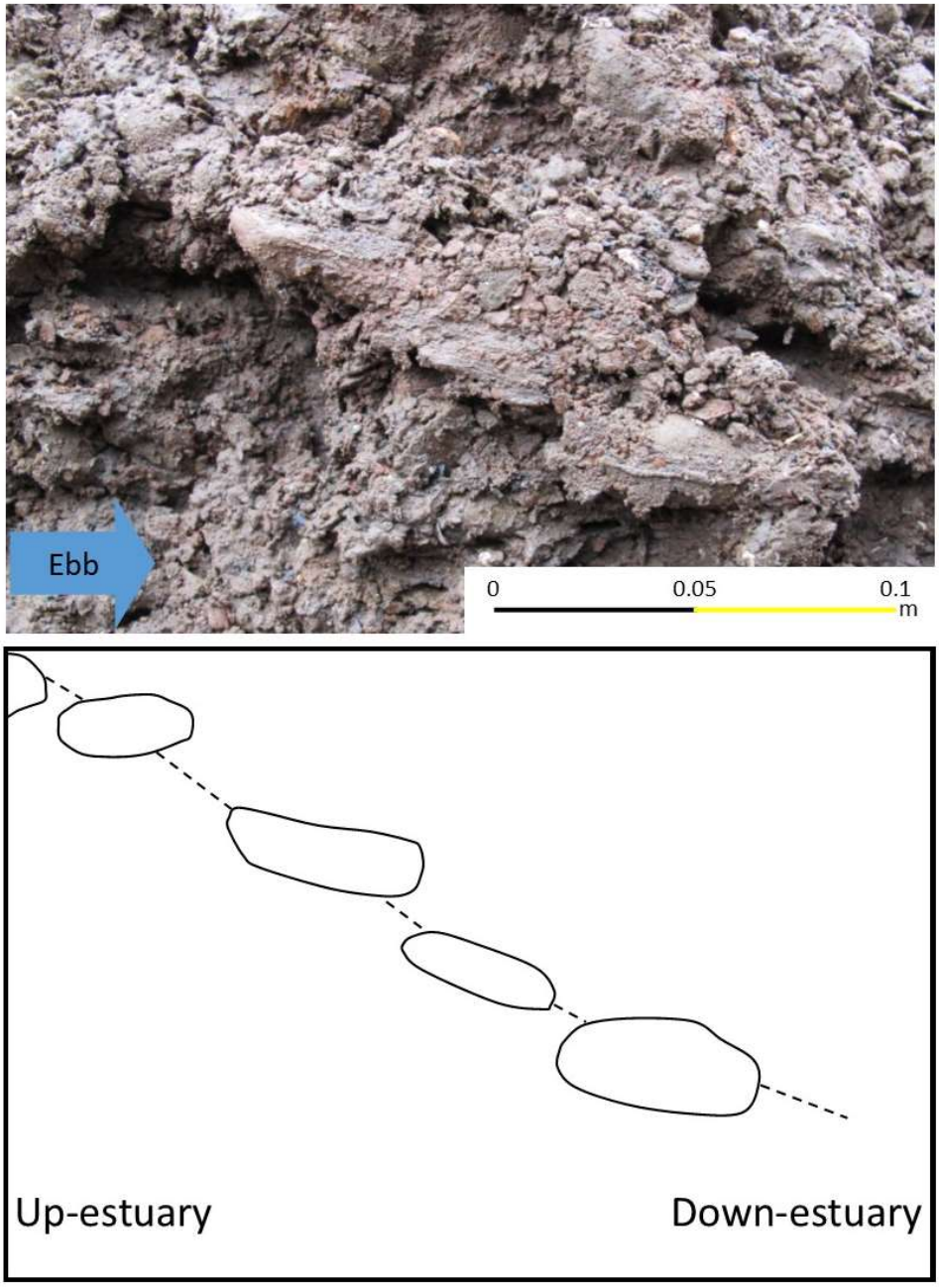

Figure 5.43 Cross-bed picked out by pebbles lying accordant with the down estuary dip 30˚of a foreset.

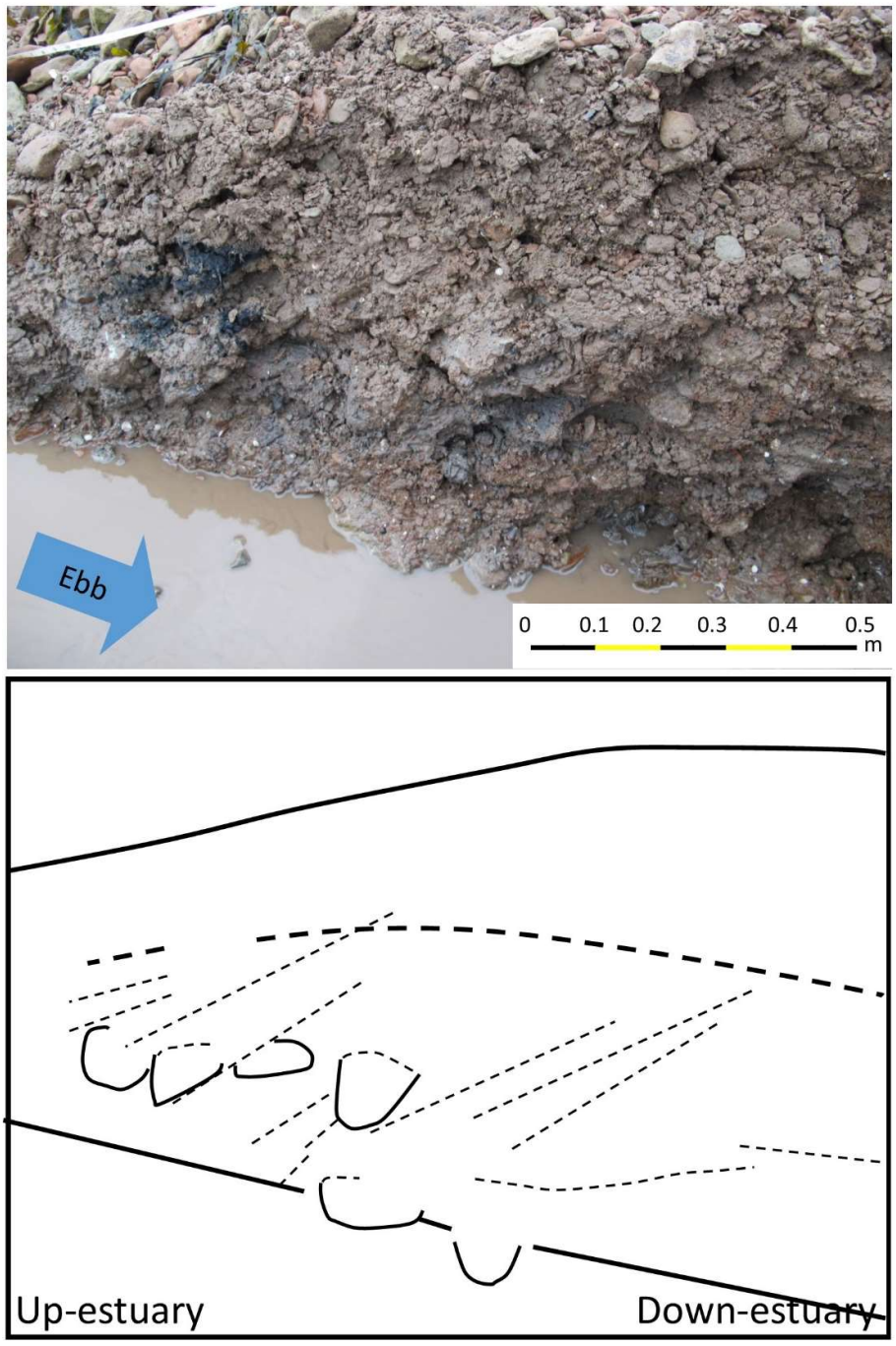

Figure 5.44 The heavy broken line depicts the position of a reactivation surface. Vague up-estuary dipping cross-bedding is evident, picked-out by clast alignment and the fracture alignment along the cut-face where sediment has fallen away during excavation. Larger pebbles tend to accumulate at the base of the dune as a lag deposit.

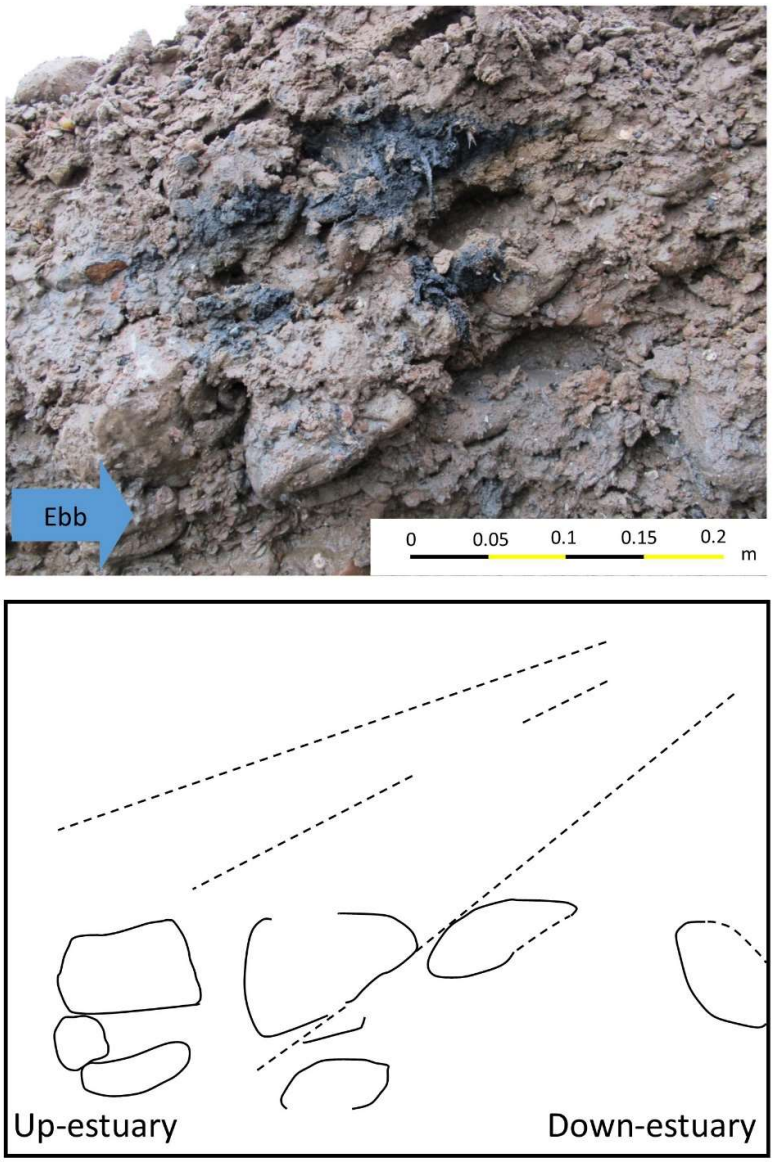

Figure 5.45 Close up of the black organic deposit visible to the left in Fig. 5.41 and in Fig. 5.43. Vague up-estuary bedding is evident together with larger lag cobbles near the base of the deposit. Fronds of decayed vegetation are evident within the black organic deposits.

Chapter 6: Discussion and conclusions

In the preceding chapters, the pebble and cobble dune development processes on Hills Flats, Severn estuary have been analysed through data obtaining from fieldwork during spring tides between 2012 and 2015. Three aspects of bedform development were considered; form, flow and sediment, as well as the interaction between these aspects. This study has been conducted in order to gain a better understanding of the behaviour of coarse-grained dunes which have rarely been reported and which may play important roles in several fields, such as navigation, engineering structure, and dredging strategies, for example (Carling *et al.*, 2006). Moreover, coarse-gravel dunes have been rarely reported from the geological record which probably is due to a lack of models detailing coarse-gravel dune stratigraphy and their hydrodynamic significance rather than a lack of dunes in the rock record. Thus a better understanding of dune dynamics might provide information on past environments more generally. This chapter will discuss the behaviour of all the data related to the dune dynamics in the following sections: (1) patterns of dune movement, (2) hydrodynamics of cobble dunes, (3) sedimentology and (4) developing an improved understanding of dune formation and evolution.

6.1 Coarse dune morphology: patterns of dune movement

In the past two years of topographic survey, February 2013 to September 2015, the individual cobble dunes have migrated with different distances in given survey periods. The migration distance of dunes in the down-estuary area is greater than those in the up-estuary. As a consequence, the dune field is generally considered to have two zones. The first one: low mobility zone (zone A), is in the down-estuary area having greater mobility than the second one: very low mobility zone (zone B), which is in the up-estuary area (Figure 6.1). The range of migration distances observed for all dunes was between 0 m and 19 m which was found in the middle of the field, dune no. 11 and 12 (Figure 6.1). In zone A, the maximum migration distance of the individual dunes ranges from 0.7 m to 19.4 m while in zone B it is between 0.6 m and 2.3 m. Apart from migrating, there were several small dune-like bedforms that developed and disappeared in zone A during the study. Moreover, the migration distance varied along each dune crest. The offshore dune terminations seem to more mobile than the onshore terminations which implies that stronger tidal currents occur towards the main channel. Even though the maximum migration of dunes could reach 19 m, however, the

majority of dune movements is in the range of 1-2 m. The maximum rate of migration is about 0.01 m per tide on dune no.12 while the other dunes migrated less than 0.01 m per tide. These dune migration rates are very low compared with previous studies of simple tidal and compound tidal sand dunes; for example, Choi and Jo (2015) where dunes migrate 1.5-2 m per day for simple dunes and 2-3 m per month for compound dunes. Fine-gravel dunes on the down-estuary but more landward area of Hill Flats migrate about 0.37 m per tide (Carling *et al.*, 2006). The comparison between the latter study and the cobble dunes demonstrates that although both studies were in the same general area and for broadly similar flow conditions, the cobble dunes despite being subject to somewhat greater flow depths and flow velocities migrated more slowly than the fine-gravel dunes. This difference implies that the grain size of sediment is one of the key factors controlling dunes movements.

Due to the dunes being controlled by bi-directional tidal flows, their materials are transported in both directions and the dunes migrate up- or down-estuary during individual tides but may also exhibit a residual direction of movement. Unlike fluvial dunes, this behaviour is typical of dunes in tidal and marine environments (Dyer, 1970b, 1971; Langhorne *et al.*, 1986; Carling *et al.*, 2006; Iacono and Guillén, 2008; Choi and Jo, 2015). An asymmetry between flood and ebb flows would cause an asymmetric geometry of dune shape and preferable migrating direction. For example, the fine-gravel dunes reported by Carling *et al.* (2006) exhibit residual movement down estuary. The overall movements in the whole study period show both flood and ebb orientation of dune shapes. In the down-estuary area, dunes no. 1 -15, mostly migrate up-estuary while many of the other up-estuary dunes also show ebb orientated movement. In the early study period it seems most of the dunes migrated down-estuary and only a few of them slightly migrated in the opposite direction. These observations initially implied ebb-dominance and down-estuary migration, which is in agreement with the fine-gravel dunes a few hundred metres down-estuary (Carling *et al.*, 2006). However, in the second year of study, several dunes migrated up-estuary, especially dunes no. 11 and 12 which changed location significantly. This behaviour would imply that flood dominated flows occurred over the site, or part of the site, resulting in the reverse migration of some dunes. This oscillating behaviour of migration, both up- and down estuary might imply that even though, in the short term, the ebb dominated flow seems to promote down-estuary migration, in the long term, flows of ebb and flood tides seem to be balanced resulting in near-static residual movement. In summary, it can be noted that the cobble dunes are temporally dynamic but spatially static as it is possibly to observe movement 'oscillating'; either down- or up-estuary with respect to the balance of tidal flow.

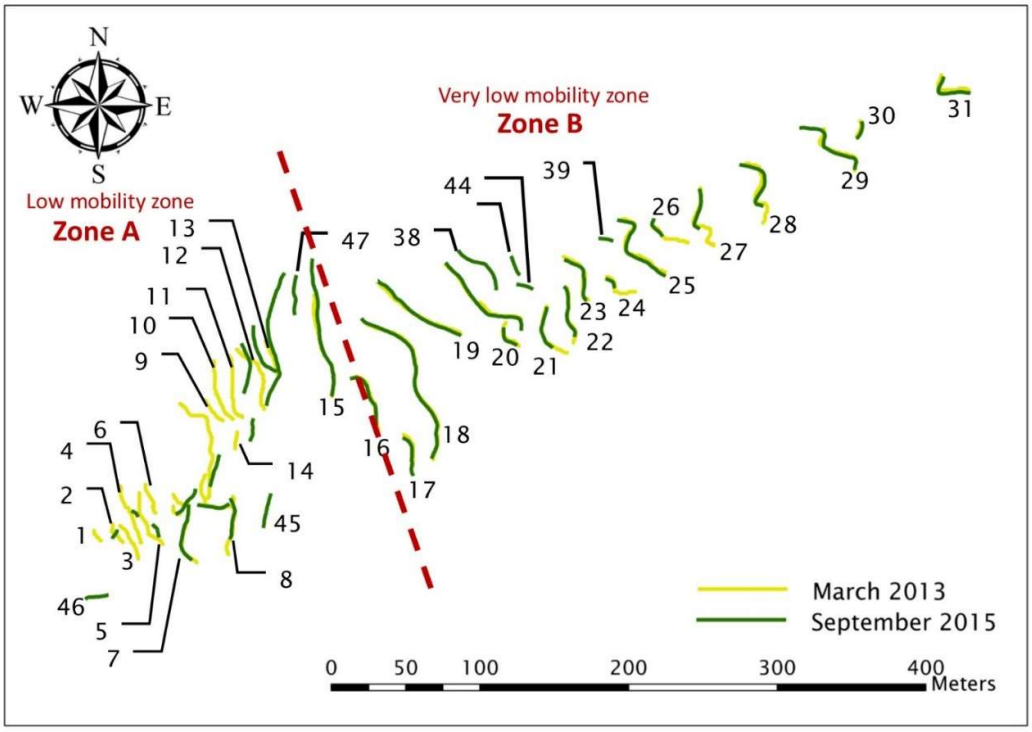

Figure 6.1 Dune crests from the first and the last survey (March 2013 and September 2015). The rea dashed line is for separating the area based on the migration rate. Zone A is for low mobility and Zone B is for very low mobility area.

The dune size in this study varies, increasing in the up-estuary direction. The height and length of representative dunes are less than 1 m and 12 m respectively or about 0.7 m and 7.53 m on average. Using Ashley's (1990) criteria, these dunes are small to large in scale. Compared to the coarse-grained dunes in previous studies, such as Dyer (1970b,1971); Langhorne *et al.* (1986) and Carling *et al.* (2006), both the wave length and height are not very different between studies; an exception is the gravelly and pebbly dunes of Iacono and Guillén (2008) that have slightly lower height and much shorter wavelength than the studies above.

However, there is an issue raised related to discrepancy of the wavelength of these dunes. Normally subaqueous dunes formed on alluvial beds, defined by crests and troughs, form continuously and are systematically spaced (for example Langhorne *et al.*, 1986; Dyer, 1971; Dyer, 1972). The wavelength or spacing can be measured either trough-to-trough (L1 in Figure 6.2A) or crest-to-crest (L2 in Figure 6.2A). The former measure provides the actual length of the alluvial bedform whilst the latter measure provides the spacing between bedform crests. For a fully alluvial bed L1 and L2 can have the same values. However, the cobble dunes in this study develop on an intertidal bedrock platform and there is a 'gap' in their wavelengths, such

that bare bedrock exists between individual dunes. Such bedforms are often termed 'starved' dunes due to the low avaibility of sediment over the site, resulting in wide spacing and short wavelength (such as the large scale dunes of Correggiari *et al.*, 1996). During geometric survey, dune wavelengths (L_{actual}) in this study were measured by stoss toe-to-leeside toe over an individual dune (L1 in Figure 6.2B) and this measurement should well present the length of the accumulated sediment forming these dunes. Alternatively, dune spacing ($L_{spacing}$) measured from crest-to-crest (L3 in Figure 6.2B), is considered to be an alternative length scale to be used in an analysis, which is considerbly longer than the actual length of the alluvial form, $L_{spacing}$ ~3 or 4 times of L_{actual} . The difference between $L_{spacing}$ and L_{actual} would result in different dune steepness values for given dune heights, and affect the relationship between geometry and hydrodynamics, which will be discussed later.

As mentioned above, the pebble and cobble dunes on Hills Flats have different scales through all the dune field, smaller in the down-estuary and larger on the up-estuary directions. The down-estuary dunes have changed more than the up-estuary ones in terms of their positions and the shape. The variability in scale of these cobble dunes is possibly due to the dunes, especially those with higher mobility down-estuary,not fully developing to equilibrium state yet. It might need to take a longer time to evolve and adjust themselves to the flows to reach equilibrium, especially in the down-estuary direction. The development to equilibrium state of cobble dunes might be hindered by sediment avaibility. Studies in the past suggested that the coarse-grain dunes, i.e. gravel dunes, have probably not grown as high as the finer dunes, sand dunes, due to the sediment size. However, if the bed is exposed to enough shear stress through a long period, coarse grains dunes can develop similar H/L ratio as equilibrium fluvial sand dunes (Carling, 1996a, 1999). Since the pebble and cobble dunes are submerged under tidal flows, during which the coarse grains are able to be entrained during spring tides, there is a possibility for dunes to grow to equillibrium state.

The steepness of dunes (H/L) is an index to indicate the equilibrium state of dunes. There are a number of methods which predict this index, such as a parabolic function for dune steepness as a function of Shields parameter (equation 2.25 and 2.26 in section 2.5.3: Chapter 2). The observed H/L, using L_{actual}, of the pebble and cobble dunes, ranging from 0.06 to 0.13 with an average of 0.09, are much higher than the calculated values from these two equations which is 0.01-0.02. On the other hand, the H/L ratio using $L_{spacing}$ provide smaller values, from 0.02 to 0.03 close to the values calculated by both equations. It is noted that, instead of using the L_{actual}, published equations (Chapter 2) might apply to closely spaced dunes, such as these two

equations, and can be applied to the spacing ($L_{spacing}$) of 'starved' dunes, such as these pebble and cobble dunes which have the bedrock regions between them. For the steepness ratio suggested by Ashley (1990), the H/L of equilibrium dunes is about 0.08. Using the $L_{spacing}$ provide low steepness values in the range 0.02 or 0.03, which is lower than the ratio suggested above. However, H/L calculated with L_{actual} provides more similar values to the observed dunes. It is not clear that the data that was included in Ashley's function includes contiguous dune trains or spaced dunes, or excluded the latter. As a result, the pebble and cobble dunes can be considered to be in equilibrium with the imposed flow conditions. They are not far from having geometries that are the steepest possible for their measured alluvial lengths and spacings and so are near-equilbrium in the sense of Ashley (1990) that equilibrium dunes have the greatest value of H for smallest possible value of L.

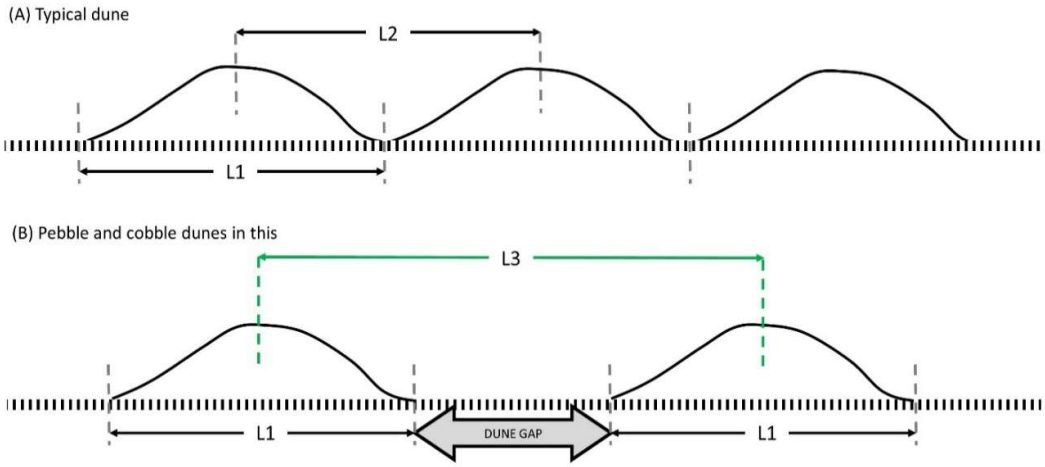

Figure 6.2 An illustration showing how to measure dune wavelength and dune spacing between (A) the typical fluvial-alluvial dunes and (B) the pebble and cobble dunes in this study. L1 represents the actual dune length and L2 represents the length of dune spacing which normally may be closely spaced, while L3 represents dune spacing in the pebble and cobble dunes which have a gap of bedrock in between consecutive dunes and thus have wider spacing than typical dunes.

6.2 Intertidal hydrodynamics of cobble dunes

The pebble and cobble dunes are situated on the bedrock platform on Hills Flats in the upper Severn estuary which is a semi-diurnal intertidal area, where the tidal range could reach 14 m

at the maximum spring tides. The channel depth varies with tidal state but the maximum depth could exceed -6 m OD (Figure 5.2). Looking at the location where these dunes are found, they form on the edge of the platform and extend towards the main channel where the bed could suddenly become deep towards the middle of the main channel flow (Figure 5.3). This change in elevation of bedrock towards the deep channel is important in controlling local changes of flow conditions which result in sudden changes in flow direction and hydrodynamic conditions as the relative depth of the water over the intertidal platform and the main subtidal channel changes during tidal cycles. Especially at the end of ebb flows, a spike in the flow velocity and the Froude number often tends to occur when the water on the platform is shallow just before it completely drains out of the edge of the platform (Figure 5.4), locally accelerating flow. However, this sudden high-energy flow conditions occur over a very short time and when the dunes were already exposed, so it is considered insignificant in relation to dune movement.

Even though the dunes are in the intertidal zone, the wave action seems to have no significant effect on the dune development (section 3.1.4, 3.2.3 and 5.2.1). The present wave records, as well as previous studies of the local wind-wave conditions (Allen and Duffy, 1998a) show that the waves on average are less than 0.4 m in height and the wave entrainment calculation predicts that the wave action is insignificant in influencing the dunes processes. So the study area as well as the neighbouring area is not affected by the sizable waves (Hydraulics Research Station, 1979, 1980, 1981; Allen and Duffy, 1998a; Carling *et al.*, 2006) noted in the deeper channels to seaward (westward). However, storm surges might be an important factor in dune dynamics as surges can increase water levels, storm wave heights and overall flow strength (Allen and Duffy, 1998a) and might in all probability result in greater migrating distances of dunes than the usual flow conditions. Although the recorded data has not included any storm surge condition over the site, it was possible that a storm surge has occurred during the study period (but outside the flow measure period) as the last year of topographic survey, especially in September 2015, shows that some dunes move up-estuary, up to 15 m, indicating exceptionally strong flood flows possibly induced by a storm surge. There are a few reports that show the possibility of storm surge occurrence in the inner zone of Severn estuary, including at Hills Flats (Allen and Duffy, 1998a; Uncles, 2010). However, as the spring tidal flows tend to be ebb-dominated, it is highly probable that the cobble dunes will slowly migrate back down-estuary towards their previous positions after storm surges. As a result, temporarily, the dunes can migrate both down-and up-estuary depend on the flow asymmetry but in a long term, these cobble dunes seem rarely to migrate and are spatially static as the

usual flows are almost balance. Storm surges might influence dune migration on occasion, especially promoting up-estuary migration with the flood tides, but there is no clear evidence in the tidal and meteorological records for any strong storm surges during the study period. This lack of evidence does not negate the possible control on dune migration by atmospheric anomalies which were not sufficient to appear in the national meteorological records.

The observed flow data shows that Fr over the cobble dunes could exceed 0.84, maximum Fr during observed floods and ebbs are 0.95 and 0.57 respectively (Table 5.14), the value of which is considered to be at the transition state at the formation of antidunes which also was suggested to decrease if the relative depths are greater than 100 (Carling, 1999). However, values of Fr greater than 0.84 rarely occurred during the study and for very short periods only as dunes became emergent at the beginning or end of tidal cycles. Otherwise, the Fr values over the cobble dunes are generally slightly above 0.1 and not higher than 0.4 (Figure 5.28, Figure 5.29, Figure 5.30). Moreover, the Fr values for the range of velocities above the threshold for motion are low, from slightly above 0.1 to 0.35 approximately (Figure 6.3). Considering the relationship between Fr and relative depth (h/D_{50}) of the pebble and cobble dunes and comparing them with previous studies of gravel bedforms, the studied dunes fall in an area close to the majority of gravel dunes described in other studies. They have greater h/D_{50} and a much lower range of Fr. The effect of Fr and h/D_{50} on the bedform existence field can further be visualised by a plot of mean flow velocity (U) and grain size for a limited range of water depth presented by Carling (1999) (Figure 6.4). This figure presents the bedform existence field with regard to mean flow velocity ($\overline{U}$) and median grain size (D_{50}) in which the fine-gravel dunes (Carling *et al.*, 2006) and the present study of pebble and cobble dunes are plotted. Unlike the fine-gravel dunes of Carling *et al.* (2006) and fine-gravel dunes more generally (less than 8 mm), the pebble and cobble dunes seem not to fall within the same area that the majority of fine-gravel dunes fall within but coarser gravels are scattered in the field under different water depths plotted in the existence field. Nevertheless the range of cobble dunes on this existence field fall close to the boundary between dunes and no movement (lower-stage plane bed; yellow dashed-line in Figure 6.4), suggesting that the cobble dunes are only weakly mobile. This conclusion is supported by the field topographic survey results and the sediment tracing which show a low rate of mobility.

Unlike fluvial dunes found in unidirectional flows, it is clearly seen that dunes in bi-directional flows in intertidal or subtidal marine environments are affected by both flows; floods and ebbs. Erosion and deposition can happen on both sides of the dunes which are transverse to

the main flows. An asymmetry of the flood and ebb tides results in unequal erosion and deposition on the dune slopes and an asymmetry in the shape of the dune profile develops. Many dunes in reversing flows in previous studies tend to be dominated by one flow direction and migrate systematically in one direction (for example, Dyer, 1971, 1972; Langhorne *et al.*, 1986; Carling *et al.*, 2006; Choi and Jo, 2015). In the case where the flow power is almost balanced for flood and ebb, the dunes might not have strong movement to either flood or ebb tides, such as the gravelly and pebbly dunes of Iacono and Guillén (2008). In the present study, the cobble dunes on Hills Flats did not show strong movement to either flood or ebb directions. This lack of preferred direction is found despite, ebbs being generally stronger and having longer duration than flood tides over the cobble dune field. Moreover, there is an asymmetry of flow discharges in which the ebb tidal discharges tend to be higher than the floods. Unequal flow conditions at Hills Flats were initially hypothesised for the studied dunes, such that it was expected that they would migrate down-estuary and probably show ebb-orientation geometries and stratigraphies (as with the neighbouring fine gravel dunes: Carling *et al.,* 2006). Later in the second year, when the tidal high water level increased, flow conditions in some datasets show that the floods become stronger and sometimes equal or are greater than those during the ebbs, but the ebb duration during spring tides then are longer. As a result, regardless of storm surges in the estuary, the total power/energy of ebb tides are not much higher than the floods (almost balanced or exhibiting a small ebb dominance) resulting in the migration down the estuary being at best slow or bedforms are essentially almost static, which is in accord with the weakly ebb-directed asymmetrical shapes of dunes or the symmetrical shapes measured in this study.

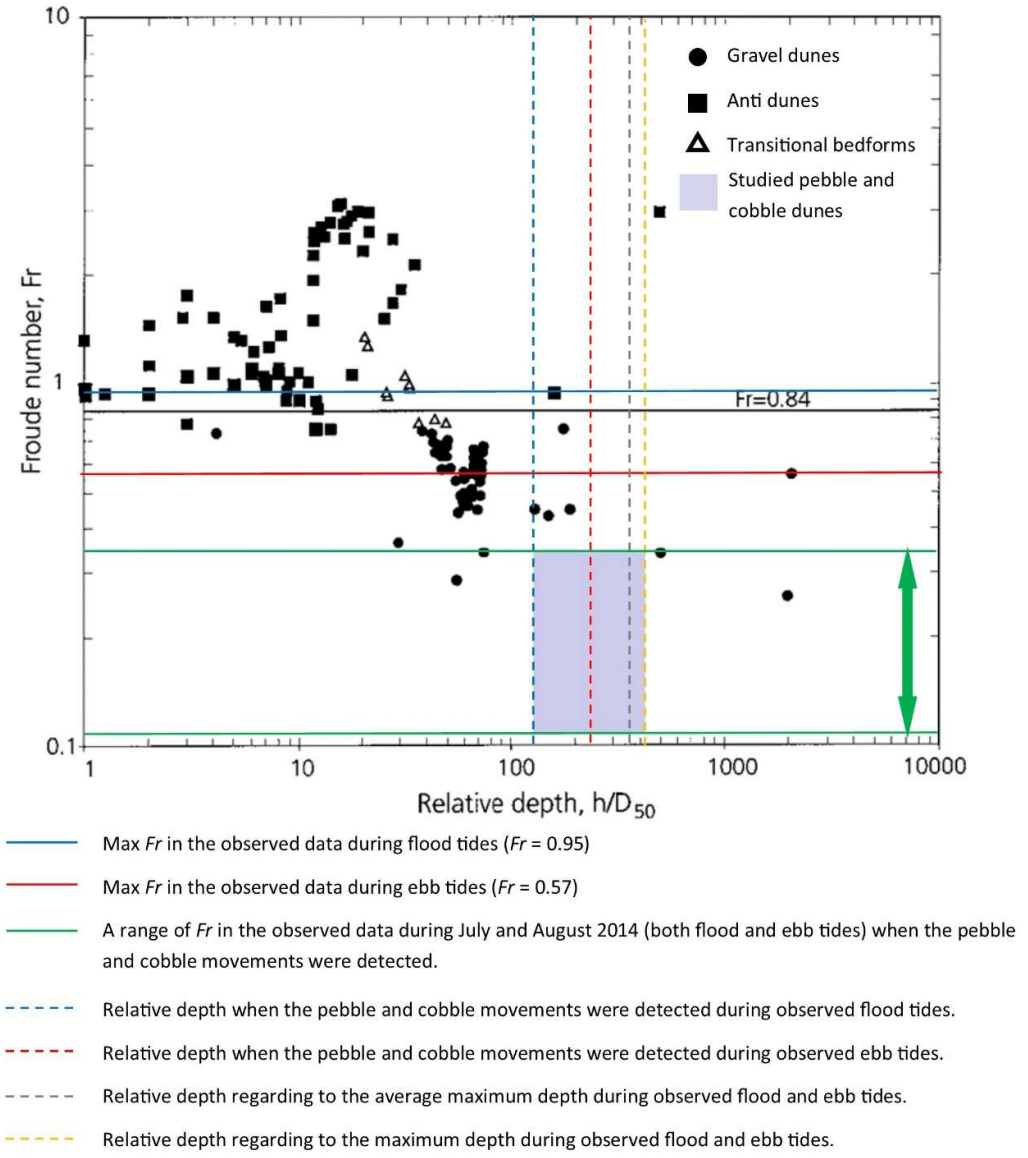

Figure 6.3 Plot of Froude number vs. relative depth for gravel dunes, taken from Carling (1999) where the data from the studies are annotated (i.e. maximum and minimum observed Froude number, the range of observed Froude number during the movements of coarse grains, relative depths as well as the area that the observed dunes fall in the diagram). The curve of Fr = 0.84 shows the theoretical discriminator.

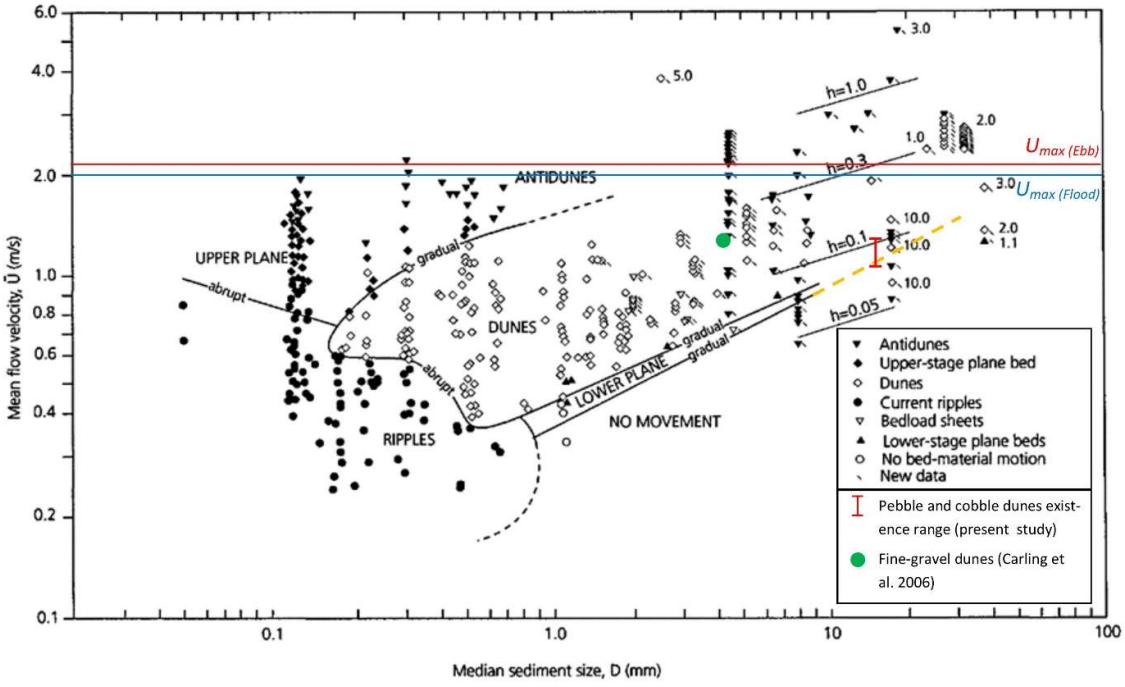

Figure 6.4 Bedform existence fields defined by velocity and grain size, taken from Carling (1999). The data of the fine-gravel dunes of Carling *et al.* (2006) and the present study are annotated to show the positions of them on the existence field. The yellow dashed line is annotated to show the extended boundary of no bed material motion movement.

In theory, the water depth is one of the key influences on subaqueous dune development, in terms of their scale (Allen, 1968; Best, 1996; Yalin, 1972; Carling, 1999; Francken *et al*., 2004). As the dunes are located in the intertidal zone, the water depth fluctuates rapidly and could exceed 10 m deep during spring tides. However, the variation in water depth does not impact greatly on the dune geometry. Even subject to the highest predicted tidal water level of 14 m, which could increase the local depth over the bed, the dunes are unlikely to respond significantly and adjust their scale with flow conditions within such a short period of a single tide as the coarse-grained dunes otherwise exhibit low mobility due to a high threshold for entrainment. Moreover, the lower water depths during neap tides are not considered in detail as calculations showed only a few of the highest neap tides might begin to mobilize the dunes. As a result, the typical flow depth over the study site is considered by looking at the typically water depth during spring tides which on average is 9.6 m. The statistics and relationship of dune length (L) and height (H) against water depth (h) are presented in section 5.1.5.

The proportional relationship between water depth and dune scale for the pebble and cobble dunes still lie within the dune fields proposed by previous studies for sandy sediment. The h/H of the studied dunes are approximately 10-29 which partially fall within a range of 3 to 20 suggested by Bridge (2003). Moreover, the relationship of mean dune height and water depth (H/h) and mean dune wavelength and water depth (L/h) of the pebble and cobble dunes have lower ratios than the empirical studies of sand dunes, for which the typical H/h and L/h are 0.2 and 4 but for gravel both are about 0.07 and 0.8. The lower values of the three ratios reflect the fact that for a given height and length, the water depth of the study area is deeper than the typically theory. The comparison of the studied dunes with previous studies in terms of height and length against water depth is shown in Figure 6.5 and Figure 6.6. In these two figures, it is generally seen that the ratios of pebble and cobble dunes are in the normal range that relate to the range for both river and marine influenced environments. Moreover, compared with the coarse-grain dunes of Dyer (1971, 1972); Langhorne *et al.* (1986) and Carling *et al.* (2006), their relationships are quite close to the studied dunes, except the gravelly and pebbly dunes of Iacono and Guillén (2008) for which the H/h and L/h are lower than the present and other studies as well as the typical sandy dunes. Differences in dune form must relate to the flow conditions and grain size. Whereas the grain size range (D_{50} ~ 2-16 mm) for the dunes presented by Iacono and Guillén (2008) are quite similar to the grain size of the cobble dunes in the present study, the water depth range is greater, affecting the lower flow intensity above the bed and thus the transport of coarse grains, leading to reduced growth of the dune scale. The fine-gravel dunes of Carling *et al.* (2006) have lower ratios than the pebble and cobble dunes, while Dyer's dunes have a wider range and the small gravelly waves of Langhorne *et al.* (1986) have the nearest values to these dunes. The L/h ratios of these coarse-grain dunes have slightly similar pattern with respect to the H/h, except the small waves of Langhorne *et al.* (1986) where the ratio is not similar to the gravel dune studies mentioned above but clearly has a lower value due to the shorter wavelength than the group mean length of the studied dunes. According to the issue about the bare bedrock 'gap' between individual and cobble dunes of this study (mentioned in the previous section), it is noted that if pebble and cobble dunes were measured crest-to-crest (to include bare bedrock within the dune length), the length of an individual section will be extended and the range and group mean length in Figure 6.6 will shift up and lie close to the typical L/h ratio of other dunes. The summary of previous studies of coarse grained dunes mentioned herein and the cobble dunes is provide in Table 6.1.

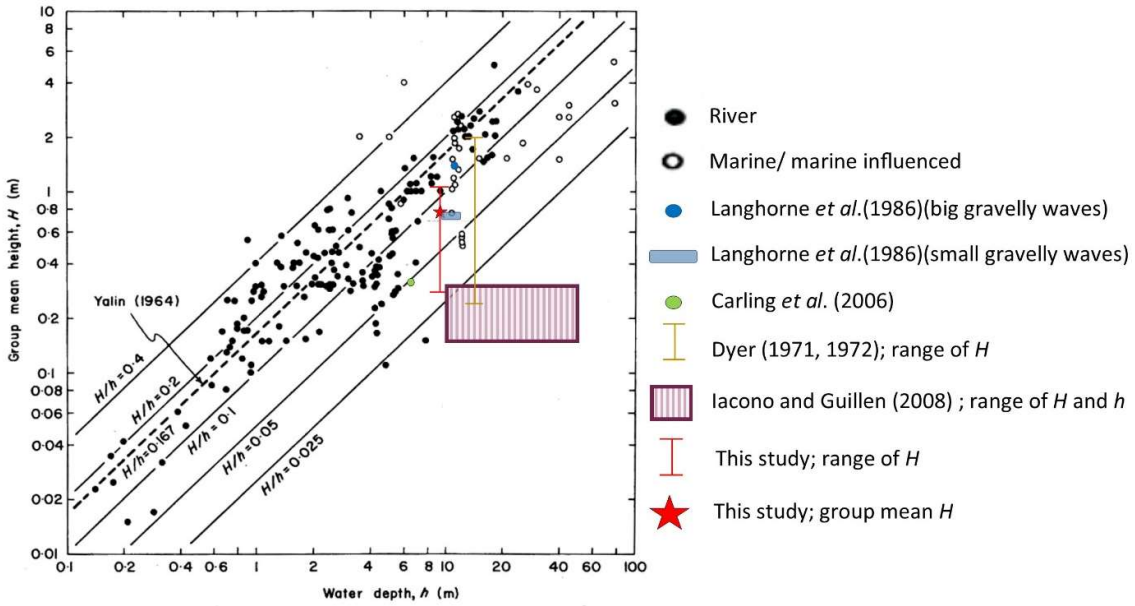

Figure 6.5 Plot of correlation between group mean height and water depth for dunes in river and marine or marine-influenced environments, taken from Allen (1984). The data for coarse-grained dunes, including the present study, are annotated.

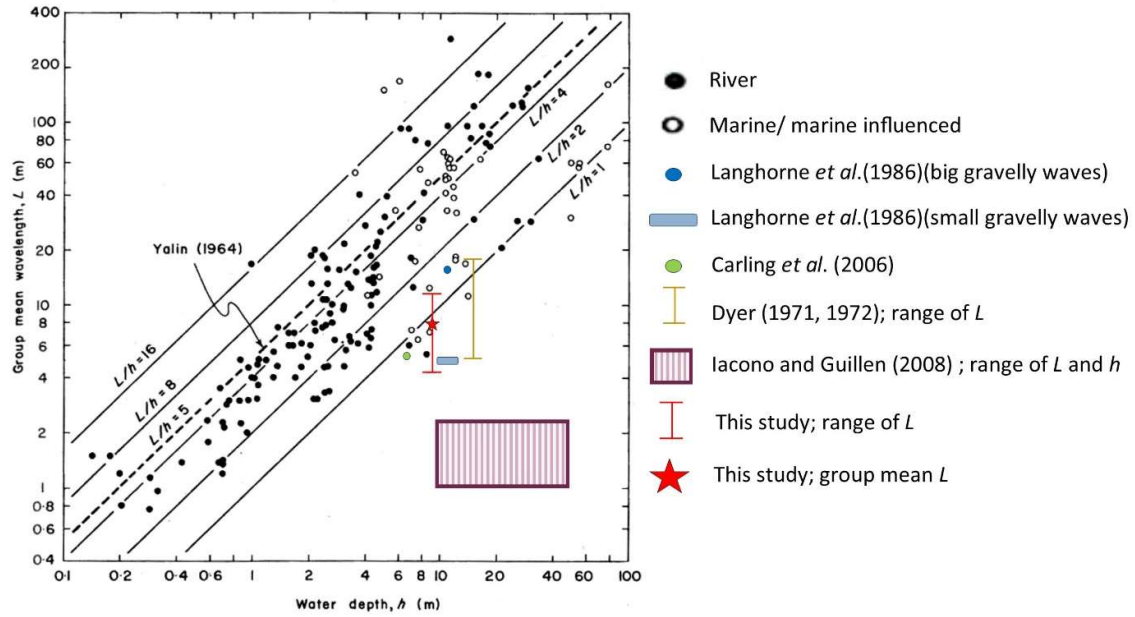

Figure 6.6 Plot of correlation between group mean wavelength and water depth for dunes in river and marine or marine-influenced environment, taken from Allen (1984), with the data of coarse-grained dunes, including the present study, annotated.

The shear stress is a fundamental flow parameter pertinent to these pebble and cobble dunes. A relatively high critical shear stress is required for initial motion due to the large grain sizes present in the dunes. Rapidly fluctuating tidal flows not only affect the water depth but also play an important role in the variability of shear stress. The flow data show that the bed shear stress can be only slightly above 0 N/m^2 to greater than 80 N/m^2. The maximum as well as average bed shear stress in July 2014, 56.5 and 5.5 N/m^2 respectively, are lower than observed in August 2014, 85.4 and 13.2 N/m^2 respectively. The difference relates to the changing flow conditions associated with different spring tidal monthly cycles. Even though the maximum velocity values of both datasets are not much different, water level had increased in the second period and affected the average flow velocity through spring tides. Moreover, the uncertainty in the measurement should be borne in mind; the shear stress data in July 2014 were calculated from velocity data from three different heights above the bed while the data in August 2014 were calculated from only two different heights. However, compared to the neighbouring fine gravel dunes, the maximum shear stress values over these pebble and cobble dunes is much higher than the maximum instantaneous bed shear stress of fine-gravel dunes slightly down-estuary, 8 N/m^2 but closer to the shore where velocities are lower (Carling *et al.*, 2006; Williams *et al*., 2006).

For the critical shear stress (τ_{0c}) of these pebble and cobble dunes, it cannot be completely determined whether flood or ebb flows have a higher critical shear stress for initial motion as values behave differently through recorded time. In July, initial motion of flood tides occurred with a higher critical shear stress than ebb flows but, in contrast, in August, ebb flows have higher critical shear stress. The pattern of shear stress (τ_{stop}) at the coarse grain cessation is slightly more complicated. According to the record, there are several times that τ_{stop} values are higher than τ_{0c} (see section 5.2.4.2 and Table 5.18). Even though the τ_{0c} values cannot be directly measured on site and it is quite complicated to define τ_{0c} precisely, the impact data help to estimate the time that the critical shear stress of the grains coarser than 11 mm was exceeded. The τ_{0c} associated with initial motion of coarse grain movements is in a wide range from 0.3 -16 N/m^2 and 0.2 – 50 N/m^2 during ebb and flood spring tides respectively. It has been reported that approximately 1 N/m^2 is predicted to move the grain size having D_{50} as 4 mm (Williams *et al.,* 2006) at the neighbouring fine-gravel dune site. Moreover, the fine-gravel dunes of Carling *et al.* (2006) and Williams *et al.* (2006) require a sustained bed shear stress of 4 N/m^2 to initiate migration of dunes of which the D_{50} is about 4 mm (9 mm of armour layer). As a consequence, the low τ_{0c} values, less than 4 N/m^2, observed over the cobble dunes, are interesting as they are lower than the threshold of finer-grain dunes but are able to move

coarser grains, up to 11 mm at least. It was initially expected that it is not often in a tidal cycle that the shear stress can reach the critical shear stress to move coarse grains, a supposition which is supported by the results of the tracer study, which represent D_{90} of dune sediment; approximately 50 mm. The tracers were not very mobile especially on the dune crests which are rough. Tracers on the flat and smooth bedrock sometimes move up- and down-estuary by the reversing tides but these also do not move very far. Furthermore, the logged impact data show not many coarse grain counts each tide which agrees with the low amount of cobbles being trapped in the bedload samples. Apart from the asymmetry of flow conditions mentioned earlier in this section, the difference between flood and ebb tides in terms of bedload sediment as well as the trend of tracer movement would also generally reflect that the hydrodynamics at the study site is ebb dominated and that shear stresses are often incompetent to entrain the coarser bed fractions. However, the amount of impact counts behave differently according to different sampled tides. The records of the impact sensors shows that the more than half of all eight tides sampled have more impact counts during the floods than the ebbs. The reason may be relate to the sediment properties. Even though the flood tides have more impact counts than the ebb tides, the grain characteristics being moved at that time are unknown. As the actual grain size of impactors on the impact plates is unknown, it must be remembered that the greater amount of counts during floods might reflect an abundance of finer grains so on occasion they may have a higher chance to be transported than those during ebbs. Moreover, the structure of dunes, including armouring, and variability tide to tide in the overall availability of sediment from source might be other related reasons which will be discussed later.

Table 6.1 Summary of coarse grained gravel dunes to compare with the present study

	Author	Year	Grain size	Location	Environment	L	H	h	U	Shape	Direction/ migration
1	Dyer	1971, 1972	16mm(gravel), 0.35mm(coarse sand), 0.17mm(medium sand)	West Solent, Southern England	Tidal marine	5-18m upto 7m	0.25-2m 120m	15m		asymmetry if gravel < 25%	
2	Langhorne *et al*.	1986	gravels mix with sand, up to 32 mm mix with sand	West Solent, Southern England	Tidal marine	5m (small waves)	0.7m (small waves)	9-13m (small waves)	could >2m/s	slight asymmetry (small waves)	Ebb orientation
						15m (large waves)	1.5m (large waves)	10-12m (large waves		more symmetrical (large waves)	
3	Dinehart	1989	coarse sand and fine gravel (D50=1.8-9.1mm)	North Fork Toutle River at Kid Valley, Washington	Fluvial		0.12-0.7m	0.8-2.2m	1.6-3.4m/s		3cm/s (fast)
4	Carling *et al.*	2006	4mm (armour layer 9mm)	Hills flats, Severn	Intertidal	5m	0.36-0.5m	6.5m	1.3-1.4 m/s	asymmetry	ebb dominate and migration with 0.74m per day (0.37m per tide max)
5	Iacono and Guillen	2008	gravelly and pebbly dunes coarse sands, gravels and pebbles (D50; 2-16mm)	Marettimo Island, Italy	Marine	1-2.5m	0.15-0.3m	10-50m		symmetrical shape + 2D crest with max extension upto 700m	Orientation occur in case of storm
6	This study	2013-present	D50 = 16.7mm	Hills flats, Severn	Intertidal	4.38-10.82m	0.33-0.95m	9.58	Up to 2m/s	almost symmetry	both flood and ebb

6.3 Sedimentology

The sediment of the pebble and cobble dunes consists of a wide range of grain sizes for which the maximum grains could exceed 45 mm. Even though the dunes develop in very coarse grains, the flows over the site are strong enough to transport all grain sizes. The suspended sediment concentration over the site is high resulting in the gravel framework being infused with deposited fines. However, the Reynolds number (Re), fluctuating through ebb and flood tides, contains high values, that could exceed 10^7, indicating high turbulence of the flow (Figure 5.31: section 5.2.4.1: Chapter 5). The suspended sediment concentration (section 5.2.3: Chapter 5) is considered as insignificant in reducing flow turbulence and strength (Best and Leeder, 1993; Wang and Larsen, 1994; Baas and Best, 2002). Calculations of the theoretical shear stresses required to entrain the coarse gravel indicate that high values would be required and sustained in order to initiate the movement. The overall results shows that the measured bed shear stress values often are high which initiates and sustains coarse grain movement. However, the record of the impact sensors reveals that there are sometimes periods during which particles are moving during periods where bed shear stresses are lower (i.e. 0.3 N/m^2) than the theoretical critical value but these flows are still able to move some coarse grains, while some periods of sustained high values of bed shear stress are required to initiate movement more generally, whereas values below critical usually do not moved any grains. This outcome is different from previous studies of coarse grains, such as Carling *et al.* (2006) and Williams *et al.*, (2006) for the case of armoured fine gravel dunes which require instantaneous bed shear stresses of 8 N/m^2 to disrupt a 9 mm armour layer and thus allow more general transport. Once the armour was broken a sustained shear stress of 4 N/m^2 was adequate to initiate fine gravel dune migration. In the case of the pebble and cobble dunes, the calculated critical shear stresses varied depending on assumptions made, but from the observed data the critical flow conditions do not demonstrate that the flood or ebb has different initial entrainment conditions which is consistent with the roughly equal ability for flood or ebb to transport coarse particles up or down the estuary (section 5.2.4.2: Chapter 5).

It is evident that the coarse grains are able to move across the bedforms as recorded by the sediment samples, whilst the recorded impacts show that the coarse grains move at a low rate. Additionally, the results from brick tracers show that coarser clasts do not move far during spring tidal cycles but migrate down- and up-estuary at different rates through the tides. All of these sediment results imply that the strength of the flow alone is not the only key parameter controlling the initiation of movement but it may be related to the availability of

loose clasts and the overall packing characteristics of the sediments over the bed at any given time. Nevertheless, the intensity of erosion and deposition of sediment in the long term have an impact on the structure and stratigraphy of bedforms. Unlike fluvial dunes in unidirectional flows, for which the cross strata are universally inclined on the surface on the lee side (Bridge, 2003) showing foreset dipping downstream (for example Carling *et al.* (2000), the herring bone structure noted in this study is one of the unique features probably found in dunes under fluvial tidal environment of other bi-directional flows (Van den Berg *et al*., 2007) more generally (Le Bot and Trentesaux, 2004; Carling *et al,.* 2006; Van den Berg *et al.*, 2007). However, for the pebble and cobble dunes, the low amount of coarse grains transported across and deposited on the dune sides during each semi-tide are not enough to create layers that are thick enough to exhibit well the distinctive cross bedding noted in herringbone structures. As a result, the patterns of dune structure and stratigraphy of the studied dunes cannot be interpreted in any great detail (*section 5.4: Chapter 5*). More preserved cross-strata features can be seen in the bottom layer below the reactivation surface showing the foreset dipping up-estuary which reflects the fact that some strong flood current transported sediment and sets migrated up-estuary even though the other results, such as overall flow conditions, tracers and bedload sediments, imply that flows are generally ebb-dominate. This assessment is in agreement with the topographic survey through all the study period, in that the dunes tend to migrate down-estuary but in some occasions the flood tides could become stronger and moved the dune up-estuary, resulting in oscillating migration.

6.4 Developing an improved understanding of cobble dune formation and evolution

The development of the dunes was affected by flow action. The majority of the literature describes dunes in the field, in the laboratory and in theory as migrating in the downstream direction. These representations relate to unidirectional flow associated with fluvial dunes. There are relatively few studies of dunes in reversing currents and these all pertain to sandy sediments. In contrast, the pebble and cobble dunes at Hills Flats develop within an intertidal environment where bi-directional flows play an important role in constraining the morphological behaviour of these dunes and their stratigraphic development. Both ebb and flood flows may have an impact on dune migration.

Regarding the behaviour and geometry of the pebble and cobble bedforms discussed above, it is reasonable to define these undulating flow-transverse bedform as dunes. The position of the

dune falls within the dune phase space on existence phase diagrams regarding either flow velocity and grain size (Figure 6.4) or heights, lengths, and water depth (Figure 6.5 and Figure 6.6). However, being on or close to the boundary of the dune and the no movement field shows that the migration rate of dunes and therefore their growth rates are very low. This conclusion is supported by the topographic survey of dune crests showing low mobility, which might result from low sediment transport rate of coarse grain size and low sediment supply. The pebble and cobble dunes migrate via foreset accretion (manifest as cross-bedding) by the actions of bi-directional flows of flood and ebb tides. The asymmetry of flow conditions as well as the sediment availability have an impact on their geometry and development which is illustrated as a conceptual model below (Figure 6.7).

Figuer 6.7A and B illustrates, in a conceptual manner, how the ebb and flood constrain the dune behaviour and geometry. The ebb tide erodes the up-estuary side, and deposits the eroded grains on the ebb-lee, down-estuary side which results in the dune migrating down-estuary (Figure 6.7A). On the other hand, the flood tide acts in the opposite way, eroding the down-estuary side whilst deposition now occurs on the flood-lee (which is now the up-estuary side), resulting in up-estuary migration (Figure 6.7B). As ebb and flood tides both have an impact on dune geometrical changes and migration, any asymmetry of ebb and flood tides would have significant impacts on dune development. In the case that stronger ebb flows occur than flood tides ($Q_E/Q_F > 1$), migration down-estuary will be dominant in the ebb direction and dunes will have an asymmetric shape with the dune slope down-estuary being shorter than up-estuary slope. In contrast, if flood tides are stronger ($Q_E/Q_F < 1$), the result will be progressive migration up-estuary with an opposite symmetry to the dune form. Here the dunes tend to migrate up-estuary and the slope of the down-estuary side will be longer than the up-estuary side (Figure 6.7B). However, in some cases such as often occurred in this study, it is found that flows between ebb and flood are rather balanced ($Q_E/Q_F \approx 1$). In this case erosion and deposition are expected to occur during both flood and ebb tides, but due to the equal energy expenditure of bi-directional flows, dune geometry is expected to be almost symmetric and the residual migration distance will be very low, and close to zero as the movements oscillate between ebb and flood tides (Figure 6.7C).

The study of the internal structure of dunes provides a stratigraphic model of dune development over the site. Correctly interpreted, the cross bed structure provides an implication of process and flow conditions over the site. Considering only one direction of flow, sediment is eroded from the upstream side (the stoss) and sediment is deposited on the

downstream, lee side, resulting in superimposed sedimentary layers dipping downstream; so-called cross-beds (or foresets) which build laterally as the dune migrates. Figure 6.7D and E generally illustrate the typical cross-bed patterns with regard to different flow directions and considering ebb and flood flows separately. The ebb dominance would results in foresets building down-estuary (Figure 6.7D). On the other hand, the up-estuary movement of dune foresets would exist under flood dominant condition (Figure 6.7E).

The upper section of more mobile sediment is sometimes referred to as a 'cap' on the dune crest which can be moved down- or up-estuary by either the ebb or flood tides. The reversing tides might be able to move it back to the other side depending upon the applied flow strength (Figure 6.7F). However, an asymmetry of tidal flows might have an impact on the reverse migration distance back towards the previous position, resulting in residual dune movement towards the stronger flow direction. This latter outcome can be seen in the present study wherein the flows were ebb dominated and low dune migration rates occurred towards ebb tides, while occasionally a flood tide might dominate. The fine-gravel dunes reported by Carling *et al.* (2006) also show the behaviour that the dunes migrate down-estuary due to ebb dominated flows, albeit in reversing tidal flow.

However, the dunes in this study consist of pebbles and cobbles which require higher flow strength than sands and granules to be entrained. The internal structure observation of representative cross-sections shows that the vertical structure can be separated into two main stratigraphic sections separated by a reactivation surface; 1) the largely immobile basal section with larger pebbles and cobbles and 2) a more mobile surface layer (Figure 5.41 in Section 5.4 and Figure 6.7G). The bottom section might be regarded as the core of the dune, which is seen conceptually to be moved at a very low rate in contrast to the upper section. The bottom section visually consists of coarser sediment and is infused with abundant mud. It might not show much structure but some weakly developed cross-bedding is evident which may be up-estuary or down-estuary such that some residual mixture of stratification type can be found. Often there is a lag of larger cobbles at the base of the dune against the bedrock surface. The upper section at the top of dune has built up with pebbles and cobbles, which is slightly loose and easy for mud infusing. This section has higher mobility which can be moved faster than the bottom section by reversing ebb and flood tides such that a herring bone structure tends to be found. This kind of internal structure requires equal currents in both directions (Allen, 1980; Nichols, 2013) and has been observed in several studies (Le Bot and Trentesaux, 2004; Van den Berg *et al.*, 2007) including for fine-gravel dunes (Carling *et al.*, 2006).

Due to the action of both flow and ebb flows, the studied dunes as well as other dunes under bi-directional flows behave differently from other fluvial dunes which are shaped by unidirectional flows. The dunes in uni-directional flows migrate downstream at various rates. In contrast, the bi-directional tidal flows might move the dunes back and forth or move them towards one preferred direction with regard to the difference in flow strength during differing tidal conditions. Moreover, given similar flow conditions, the dunes developed in finer grains have more possibility to change shape or migrate for further distances than these coarse grain sizes which require stronger flows to initiate and sustain grain movements.

According to previous studies, several factors are considered to be important in the development and dynamics of subaqueous dunes: current velocity, bed shear stress, Froude number, water depth, and grain properties (Flemming, 1978; Rubin and McCulloch, 1980; Allen, 1984; Ashley, 1990; Carling, 1999; Francken *et al.*, 2004). Similarly for sand, pebble and cobble dunes, these factors play important roles in affecting the dune dynamics. Flow velocities over the study site could exceed 2 m/s and the variation of water depth is in a range of 0 – 10 m approximately. The high current speeds due to fluctuations of flood and ebb tides in large semi-diurnal tidal range, together with the deep water channel, results in high energy flow power, especially during spring tides, which is enough to move coarse grains like cobbles over the study site but for only short distances and at a low transport rate. Apart from the factors above, the amount of sediment supplied is considered to be another important factor affecting the development of these pebble and cobble dunes. Supply from outside the dunefield was not determined but within the dunefield supply is not likely greater than the rate of bedload transport actually measured by the Helley-Smith traps. Thus the low availability of coarse sediments might be the reason that the dunes do not grow larger and have a lower relationship of height and lengths to water depth than theory suggested. Moreover, wide spacings (gaps of bare bedrock in between dunes) resulted in the issues noted between geometric measurement of the dunes, actual dune length and spacing mentioned earlier in section 6.1, which are considered to have been affected by low sediment availability.

The field observations provide the information that the studied pebble and cobble dunes are actually dynamic within the present tidal regime, and that they are not relict forms. In the long term, they seem to be static in-as-much as the dunes can be found in roughly the same location tide to tide, but, in short term (tide to tide), their migration can oscillate down- and up-estuary at various low rates. Only on rare occasions do the dunes migrate further distances, such as the up-stream migration found in the last survey which is suspected to be the result of

a storm surge. The changing in related factors controlling these dunes would have an impact on their behaviour. Future climate change might be the most important factor resulting in hydrodynamic changes which might affect these pebble and cobble dunes. Climate change has an impact on sea level rise. It is reported that the relative mean sea level around the UK is rising (Robins *et al.*, 2016), including within the Severn Estuary where the rise in mean sea level is about 2.4 mm/year (IMCORE project, no date; Uncles, 2010) and projected to be a total of 30-40 cm by 2080 (IMCORE project, no date; Phillips and Crisp, 2010). Even though projected incidences of storm surges do not show a significant rise (IMCORE project, no date; Robins *et al.*, 2016), an increase in mean sea level would increase tidal water levels and mean water depth as well as the flow velocity above these dunes. This might have an impact on longer duration and stronger flood flows moving the dunes up-estuary. If this is the case, the geometry of dunes might be changed, more asymmetric towards up-estuary as shown in the conceptual diagram in Figure 6.7B and E. In contrast, if the future dominant flows happen to be ebb-dominated, it would results in opposite direction. The dunes might show the ebb orientation and shows similar behaviour as Figure 6.7A and D. However, the internal dune structure might not change that much because the low coarse-sediment supply over the site might not allow much sediment to deposit to create thickening accreting sediment layers. Thus the stratigraphy might not change due to predicted climate change.

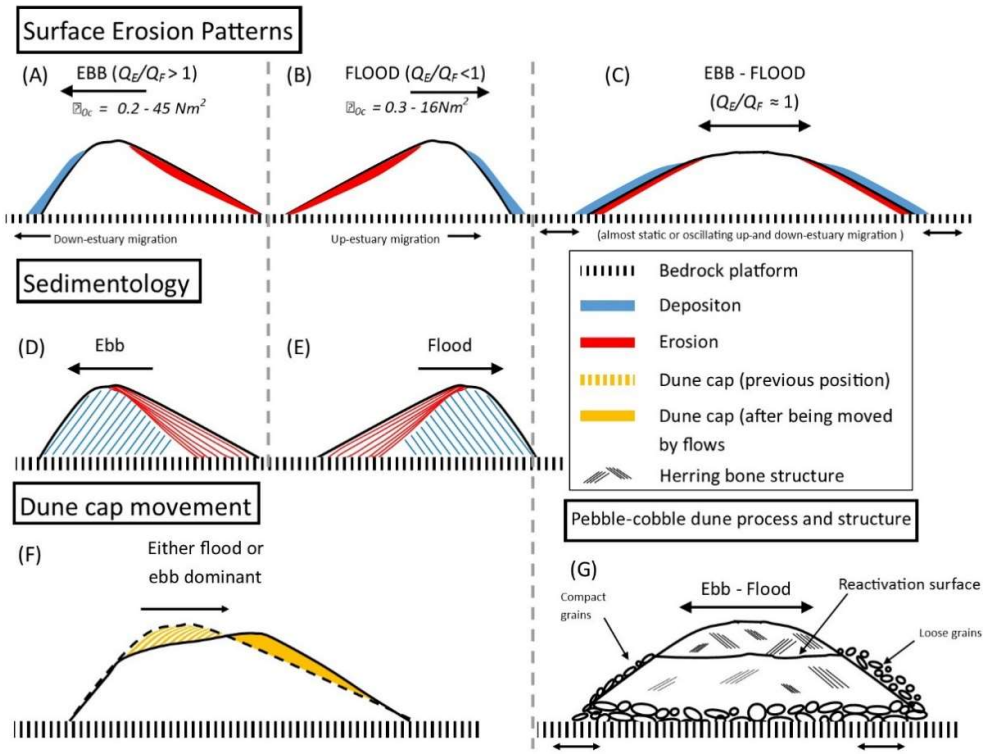

Figure 6.7 A conceptual diagram of pebble and cobble dune dynamics under intertidal flows for conditions of limited sediment supply and frequent development of surface armouring. (A), (B) and (C) illustrate the surface erosion pattern in the case of ebb dominant flows; (A) flood dominant flows; (B) balanced ebb and flood flows. Q_E/Q_F values represent discharge asymmetry. The critical bed shear stress values from observed data during ebb and flood tides are annotated in (A) and (B). (D) and (E) presents a stylized cross bedding pattern of the dunes created by either ebb flows (D) or flood flows (E). (F) cartoon showing the cap migration over the dune crest back and forth by either ebb or flood flows. (G) summary of process and generalized internal structure of pebble and cobble dunes observed over the site.

6.5 Future works

The study of pebble and cobble dune dynamics have been conducted by collecting field data covering all three aspects of flow, form and sediment. However, there are some limitations which are also mentioned in section 4.4 dealing with the time, equipment and people working in a team. The restrictions of time and weather conditions suitable for fieldwork within the study period of two and a half years have limited the number of datasets can be collected. In addition, the limitations in equipment being used might provide uncertainty. As a result, to develop further knowledge, it is suggested to collect more datasets of all aspect for longer period. The more data collected, the more reliable results for analysis and subsequent interpretation. For this study, only two dataset were used to create the velocity profiles and each were created from two or three different heights above the bed which is considered that there might be an uncertainty in an analysis of shear stress. It might be better to collect more flow velocity data with more levels of heights to reduce the possibility of uncertainty. Apart from the velocity data, the longer time-series of topographic survey, cross-section measurement, tracing painted tracers would help improving more understanding in the behaviour of these pebble and cobble dunes. Of interest would be to record dune dynamics during storm surges in particular to determine if the dunes migrate greater distances and change their morphology substantially during such events. In addition, modelling of dune behaviour using the existing data to calibrate the model would be useful to explore future scenarios such as higher seas level controls consequent upon climate change.

6.6 Conclusions

In this research, data regarding the bedform development; i.e. form, flow and sediment, of subaqueous dunes, developed by pebble and cobbles, have been measured in order to obtain an in-depth understanding of these unusual features. Specifically; (1) pebble and cobble dune movements through time; (2) hydrodynamics over the dune field; (3) sedimentology and internal structure of dunes developed in coarse sediments as well as (4) the interaction between the flows, form, and sediments have been discussed. The key new understanding of how these dunes behave are summarised thus;

- The dunes are essentially quasi-equilibrium between ebb and flood although dune size increases towards the up-estuary side. The heights of all dunes are less than 1 m, while

the wavelength ranges from 4 m to 10 m approximately. The cross-sections of dunes are most commonly found to be almost symmetrical in shape, although slight ebb-orientation and flood orientation can be observed.

- Migration rates are very low, the maximum is only 1.1 cm (0.011 m) per tide. Thus the short term surveys, within a month or a couple of months, do not show very strong movement. But in a long term, one year period for example, the dunes show slight residual movement. In the first year of survey, they slightly migrated down-estuary, showing ebb-orientation, however, in the second year, some dunes moved back up-estuary.
- The relationship of dune steepness (H/L) (or dune geometry more generally) and hydrodynamics (L/h or H/h) showed that these dunes fall within the dune phase space for bedform existence diagrams but might slightly deviate from the trend of typical sandy dunes in previous studies. However, the pebble and cobble dunes seem to fall on the boundary between dunes and no movement (Figure 6.2) indicating they are close to incipient motion and so do not move far on any competent flow. This conclusion is supported by the topographic survey of low migration rates.
- The flow conditions during high spring tides, with a range of water depth from 8 to 10 m, have high enough energy to initiate coarse grain sediment mobility, such as pebbles and cobbles exceeding 45 mm in size. Current velocity of ebb and flood tides can reach 2 m/s and decrease close to 0 m/s during high slack water when the maximum depth is reached but they are in subcritical flow as the Froude number is lower than 1. The episodes of instantaneous peak velocities at the end of ebb tides are not significant to the bedform development due to it happening when the dunes start to be subaerially exposed. In contrast, the neap tides seem not to transport these coarse grains. The wind-wave actions and suspended sediment concentrations (SSC) do not have significant impact on the entrainment conditions and do not decrease the flow turbulence over the bed.
- The bed shear stress (τ_0) over the site calculated from the data in July and August 2014 could exceed 80 N/m^2. The conditions in August 2014 present higher stress values than July 2014, which is in accord with the higher water level and the greater total counts measured from the impact sensor in August 2014. The critical shear stress (τ_{0c}) for the gravel initial movement detected by the impact sensors provide a range of 0.3-50 N/m^2 for both ebb and flood tides. There were some occasions where the τ_{0c} at the

start of motion is lower than the stop motion value which might result from the availability of coarse sediment supply.

- Dunes are developed by mixed-size grains with a D_{50} of 16.7 mm (pebbles). The Helley-Smith bedload samples show that coarse grains have been transported both by ebb and flood but the bedload transportation rate is not able to be defined exactly. Although bedload rates may not be accurate, they nevertheless indicate low rates. However, the painted tracing and impact counts are both evidence to support the measured low bedload transport rates of coarse grains like pebble and cobbles.
- Sedimentary internal structure of these cobble dunes does not show many defined features. The cut sections show coarse gravel grains filled with fine sandy sediments. The finer gravel grains were observed above the reactivation surface; whose upper layers are more mobile than the bottom largely immobile section consisting of coarser cobble grains.
- Sediment supply on the site is one issue to be considered for these pebble and cobble dunes. The low availability of coarse grains might be related to the existence of bare bedrock gaps between dunes resulting in wider spacing. Moreover, variation in sediment supply might be one reason for the varied size of dunes, especially smaller and finer-grained dunes up and down the estuary.
- The asymmetry between ebb and flood flows, in terms of longer ebb duration during high spring tides as well as higher ebb discharge and higher ebb flow velocity with rare occasions of higher flood discharge, suggested that the dunes probably migrate down-estuary and have ebb orientation even with a very low rate of migration. However, the topographic survey, the painted tracers, impact sensor counts and internal structure observation provide evidence that there is a possibility that the dunes migrate up-estuary and have flood orientation on occasion. Although, during high spring tides, the ebb tides are generally more powerful than the flood tides there is the possibility that the flow conditions between flood tides are sometimes stronger which may balance the energy of ebbs and floods in the longer term. As a result, their oscillating movements are considered to be temporally dynamic and spatially static.
- The conceptual model (Figure 6.7) for pebble and cobble dunes was developed which is useful for identifying these features and predicting changes in the future especially under the climate change conditions which seem likely to have an impact on flow conditions. The predicted sea level rise probably will increase the water level over these dunes and have an impact on dune behaviour. If present day conditions were to

change, the dunes could behave differently. For example, the increasing water level would increase the flow velocity, either ebb or flood tides, and there would be higher bedload transportation. However, the sediment supply limitation might hinder the amount of grain movement. If the asymmetry between ebb and flood tides change and the flood tides consistently become stronger, these dunes might migrate up-estuary.

Appendix A Velocity profiles

Table A 1 Data of velocity profiles at a given period collected during 14th – 16th July 2014. The grey-filled sections represent flood periods and the white-filled sections represent ebb periods.

No.	Date	Time	Minute	Z (m)	U (m/s)	u_* (m/s)	Z_0 (mm)	τ_0 (N/m²)	D_{mobile} ($\theta = 0.04$; mm)
1	14/7/2014	19:18:45 19:18:12	100	0.15 0.5	0.48 0.61	0.04	1.87	1.89	3.70
2	14/7/2014	19:23:45 19:23:12	105	0.15 0.5	0.55 0.69	0.05	1.51	2.25	4.41
3	14/7/2014	19:28:45 19:28:12	110	0.15 0.5	0.76 0.96	0.07	1.55	4.42	8.66
4	14/7/2014	19:33:45 19:33:12	115	0.15 0.5	0.94 1.21	0.09	2.23	7.95	15.59
5	14/7/2014	19:38:45 19:38:12	120	0.15 0.5	1.16 1.43	0.09	0.78	7.81	15.31
6	14/7/2014	19:43:45 19:43:12	125	0.15 0.5	1.22 1.46	0.08	0.32	6.28	12.32
7	14/7/2014	19:48:45 19:48:12	130	0.15 0.5	1.19 1.47	0.09	0.89	8.64	16.94
8	14/7/2014	19:53:45 19:53:12	135	0.15 0.5	1.06 1.35	0.10	1.77	9.12	17.88
9	14/7/2014	19:58:45 19:58:12	140	0.15 0.5	1.13 1.27	0.05	0.01	2.26	4.44
10	14/7/2014	20:03:45 20:03:12	145	0.15 0.5	1.35 1.50	0.05	1.67E-03	2.25	4.42
11	14/7/2014	20:08:45 20:08:12	150	0.15 0.5	1.46 1.77	0.10	0.58	11.01	21.57
12	14/7/2014	20:13:45 20:13:12	155	0.15 0.5	1.42 1.72	0.10	0.51	9.95	19.50
13	14/7/2014	20:18:45 20:18:12	160	0.15 0.5	1.27 1.60	0.11	1.41	11.87	23.27
14	14/7/2014	20:23:45 20:23:12	165	0.15 0.5	1.27 1.74	0.15	5.48	23.66	46.39
15	14/7/2014	20:28:45 20:28:12	170	0.15 0.5	1.29 1.58	0.10	0.73	9.39	18.41
16	14/7/2014	20:33:45 20:33:12	175	0.15 0.5	1.31 1.57	0.09	0.34	7.47	14.64
17	14/7/2014	20:38:45 20:38:12	180	0.15 0.5	1.06 1.39	0.11	3.47	12.60	24.69
18	14/7/2014	20:43:45 20:43:12	185	0.15 0.5	1.00 1.24	0.08	0.97	6.34	12.43
19	14/7/2014	20:48:45 20:48:12	190	0.15 0.5	0.98 1.30	0.11	3.77	11.33	22.22

No.	Date	Time	Minute	Z (m)	U (m/s)	u_* (m/s)	Z_0 (mm)	τ_0 (N/m²)	D_{mobile} ($\theta = 0.04$; mm)
20	14/7/2014	20:53:45 20:53:12	195	0.15 0.5	0.77 1.13	0.12	11.71	14.42	28.26
21	14/7/2014	20:58:45 20:58:12	200	0.15 0.5	0.82 0.95	0.04	0.05	1.73	3.38
22	14/7/2014	21:03:45 21:03:12	205	0.15 0.5	0.81 1.15	0.11	8.41	12.76	25.01
23	14/7/2014	21:08:45 21:08:12	210	0.15 0.5	0.63 1.06	0.14	26.55	20.99	41.15
24	14/7/2014	21:13:45 21:13:12	215	0.15 0.5	0.58 0.75	0.06	2.32	3.12	6.12
25	14/7/2014	21:18:45 21:18:12	220	0.15 0.5	0.63 0.80	0.06	1.92	3.29	6.44
26	14/7/2014	21:23:45 21:23:12	225	0.15 0.5	0.51 0.78	0.09	15.03	7.97	15.62
27	14/7/2014	21:28:45 21:28:12	230	0.15 0.5	0.61 0.83	0.07	4.50	4.92	9.65
28	14/7/2014	21:33:45 21:33:12	235	0.15 0.5	0.52 0.78	0.09	13.33	7.46	14.62
29	14/7/2014	21:38:45 21:38:12	240	0.15 0.5	0.51 0.75	0.08	10.83	6.08	11.92
30	14/7/2014	21:43:45 21:43:12	245	0.15 0.5	0.49 0.70	0.07	8.60	4.79	9.39
31	14/7/2014	21:48:45 21:48:12	250	0.15 0.5	0.52 0.67	0.05	2.37	2.49	4.88
32	14/7/2014	21:53:45 21:53:12	255	0.15 0.5	0.41 0.73	0.11	32.17	11.38	22.31
33	14/7/2014	21:58:45 21:58:12	260	0.15 0.5	0.34 0.59	0.08	27.58	6.64	13.01
34	14/7/2014	22:03:45 22:03:12	265	0.15 0.5	0.24 0.54	0.10	58.90	10.12	19.84
35	14/7/2014	22:08:45 22:10:10 22:08:12	270	0.15 0.4 0.5	0.21 0.26 0.49	0.07	52.05	5.20	10.19
36	14/7/2014	22:13:45 22:13:12	275	0.15 0.5	0.09 0.32	0.07	89.74	5.47	10.71
37	14/7/2014	22:18:45 22:20:10 22:18:12	280	0.15 0.4 0.5	0.14 0.21 0.31	0.05	52.68	2.51	4.91
38	14/7/2014	22:23:45 22:23:12	285	0.15 0.5	0.04 0.09	0.02	51.07	0.23	0.45
39	14/7/2014	22:38:45 22:38:12	300	0.15 0.5	0.32 0.35	0.01	1.78E-04	0.09	0.18
40	14/7/2014	22:43:45 22:43:12	305	0.15 0.5	0.38 0.42	0.01	1.29E-03	0.17	0.33

No.	Date	Time	Minute	Z (m)	U (m/s)	u_* (m/s)	Z_0 (mm)	τ_0 (N/m^2)	D_{mobile} ($\theta = 0.04$; mm)
41	14/7/2014	22:48:45 22:48:12	310	0.15 0.5	0.42 0.45	0.01	1.39E-04	0.14	0.28
42	14/7/2014	22:53:45 22:53:12	315	0.15 0.5	0.47 0.48	0.00	9.61E-35	0.01	0.01
43	14/7/2014	22:58:45 22:58:12	320	0.15 0.5	0.56 0.60	0.01	1.25E-06	0.15	0.29
44	14/7/2014	23:03:45 23:03:12	325	0.15 0.5	0.71 0.72	0.00	2.08E-42	0.01	0.02
45	14/7/2014	23:38:45 23:38:12	360	0.15 0.5	1.22 1.26	0.01	3.39E-15	0.16	0.32
46	14/7/2014	23:58:45 23:58:12	380	0.15 0.5	1.48 1.52	0.01	1.06E-15	0.22	0.44
47	15/7/2014	0:03:45 0:03:12	385	0.15 0.5	1.37 1.47	0.03	1.19E-05	1.12	2.19
48	15/7/2014	0:08:45 0:08:12	390	0.15 0.5	1.33 1.36	0.01	4.57E-23	0.09	0.17
49	15/7/2014	0:18:45 0:18:12	400	0.15 0.5	1.33 1.45	0.04	2.84E-04	1.63	3.20
50	15/7/2014	0:23:45 0:23:12	405	0.15 0.5	1.21 1.28	0.02	3.53E-07	0.59	1.16
51	15/7/2014	0:33:45 0:33:12	415	0.15 0.5	1.24 1.24	0.00	0.00E+00	0.0001	2.68E-04
52	15/7/2014	0:38:45 0:38:12	420	0.15 0.5	1.23 1.23	0.00	2.06E-124	0.003	0.01
53	15/7/2014	0:48:45 0:48:12	430	0.15 0.5	1.14 1.26	0.04	1.45E-03	1.56	3.06
54	15/7/2014	0:53:45 0:53:12	435	0.15 0.5	1.02 1.13	0.03	1.18E-03	1.21	2.37
55	15/7/2014	0:58:45 0:58:12	440	0.15 0.5	1.07 1.15	0.03	5.70E-05	0.83	1.63
56	15/7/2014	1:03:45 1:03:12	445	0.15 0.5	1.09 1.12	0.01	1.89E-19	0.08	0.16
57	15/7/2014	1:08:45 1:08:12	450	0.15 0.5	1.13 1.15	0.01	3.53E-28	0.04	0.09
58	15/7/2014	1:13:45 1:13:12	455	0.15 0.5	0.97 1.18	0.07	0.45	4.51	8.84
59	15/7/2014	1:18:45 1:18:12	460	0.15 0.5	1.08 1.11	0.01	1.38E-23	0.06	0.11
60	15/7/2014	1:23:45 1:23:12	465	0.15 0.5	1.00 1.01	0.00	1.19E-49	0.01	0.02
61	15/7/2014	1:28:45 1:28:12	470	0.15 0.5	0.96 1.02	0.02	3.01E-06	0.47	0.92
62	15/7/2014	1:33:45 1:33:12	475	0.15 0.5	0.90 0.95	0.02	4.59E-08	0.27	0.53
63	15/7/2014	1:38:45 1:38:12	480	0.15 0.5	0.90 1.05	0.05	0.09	2.38	4.67

No.	Date	Time	Minute	Z (m)	U (m/s)	u_* (m/s)	Z_0 (mm)	τ_0 (N/m²)	D_{mobile} ($\theta = 0.04$; mm)
64	15/7/2014	1:43:45 1:43:12	485	0.15 0.5	0.85 0.94	0.03	1.63E-03	0.89	1.74
65	15/7/2014	1:48:45 1:48:12	490	0.15 0.5	0.85 0.88	0.01	1.00E-15	0.07	0.15
66	15/7/2014	1:53:45 1:53:12	495	0.15 0.5	0.82 0.88	0.02	7.55E-05	0.51	0.99
67	15/7/2014	2:18:45 2:18:12	520	0.15 0.5	0.83 0.84	0.00	1.04E-42	0.01	0.02
68	15/7/2014	2:23:45 2:23:12	525	0.15 0.5	0.82 0.89	0.02	5.06E-05	0.49	0.96
69	15/7/2014	2:28:45 2:28:12	530	0.15 0.5	0.86 0.94	0.03	7.30E-04	0.79	1.54
70	15/7/2014	2:38:45 2:38:12	540	0.15 0.5	0.86 0.88	0.01	8.65E-21	0.04	0.09
71	15/7/2014	2:43:45 2:43:12	545	0.15 0.5	0.89 0.89	0.00	2.23E-256	0.0004	7.07E-04
72	15/7/2014	2:53:45 2:53:12	555	0.15 0.5	0.84 0.87	0.01	7.15E-11	0.14	0.27
73	15/7/2014	2:58:45 2:58:12	560	0.15 0.5	0.86 0.90	0.02	2.13E-08	0.23	0.45
74	15/7/2014	3:08:45 3:08:12	570	0.15 0.5	0.89 0.90	0.00	2.71E-155	0.001	1.93E-03
75	15/7/2014	3:13:45 3:13:12	575	0.15 0.5	0.89 0.93	0.01	4.05E-10	0.18	0.35
76	15/7/2014	3:18:45 3:18:12	580	0.15 0.5	0.86 0.93	0.02	9.78E-06	0.43	0.85
77	15/7/2014	3:23:45 3:23:12	585	0.15 0.5	0.88 0.90	0.01	5.08E-28	0.03	0.05
78	15/7/2014	3:28:45 3:28:12	590	0.15 0.5	0.85 0.85	0.00	3.30E-96	0.002	0.00
79	15/7/2014	3:38:45 3:38:12	600	0.15 0.5	0.88 0.90	0.01	1.25E-16	0.07	0.14
80	15/7/2014	3:43:45 3:43:12	605	0.15 0.5	0.91 0.91	0.00	1.74E-84	0.003	0.01
81	15/7/2014	7:48:45 7:48:12	850	0.15 0.5	0.42 0.54	0.04	2.24	1.58	3.09
82	15/7/2014	7:53:45 7:53:12	855	0.15 0.5	0.46 0.63	0.05	4.98	2.95	5.78
83	15/7/2014	7:58:45 7:58:12	860	0.15 0.5	0.57 0.69	0.04	0.53	1.63	3.20
84	15/7/2014	8:03:45 8:03:12	865	0.15 0.5	0.86 1.02	0.05	0.25	2.85	5.59
85	15/7/2014	8:08:45 8:08:12	870	0.15 0.5	0.94 1.17	0.07	0.96	5.59	10.95
86	15/7/2014	8:13:45 8:13:12	875	0.15 0.5	1.14 1.46	0.11	2.11	11.45	22.45

No.	Date	Time	Minute	Z (m)	U (m/s)	u_* (m/s)	Z_0 (mm)	τ_0 (N/m²)	D_{mobile} ($\theta = 0.04$; mm)
87	15/7/2014	8:18:45 8:18:12	880	0.15 0.5	1.07 1.48	0.14	6.89	19.19	37.62
88	15/7/2014	8:23:45 8:23:12	885	0.15 0.5	1.07 1.29	0.07	0.51	5.61	11.00
89	15/7/2014	8:28:45 8:28:12	890	0.15 0.5	1.00 1.34	0.11	4.17	12.57	24.65
90	15/7/2014	8:33:45 8:33:12	895	0.15 0.5	0.96 1.33	0.12	6.07	14.44	28.31
91	15/7/2014	8:38:45 8:38:12	900	0.15 0.5	1.46 1.71	0.08	0.12	6.72	13.17
92	15/7/2014	8:43:45 8:43:12	905	0.15 0.5	1.39 1.70	0.10	0.75	10.95	21.47
93	15/7/2014	8:48:45 8:48:12	910	0.15 0.5	1.51 1.77	0.09	0.13	7.34	14.40
94	15/7/2014	8:53:45 8:53:12	915	0.15 0.5	1.38 1.56	0.06	0.02	3.68	7.22
95	15/7/2014	8:58:45 8:58:12	920	0.15 0.5	1.24 1.53	0.10	0.85	9.26	18.14
96	15/7/2014	9:03:45 9:03:12	925	0.15 0.5	1.22 1.58	0.12	2.75	14.84	29.10
97	15/7/2014	9:08:45 9:08:12	930	0.15 0.5	1.09 1.34	0.08	0.83	7.03	13.77
98	15/7/2014	9:13:45 9:13:12	935	0.15 0.5	1.12 1.33	0.07	0.19	4.53	8.88
99	15/7/2014	9:18:45 9:18:12	940	0.15 0.5	1.11 1.46	0.12	3.24	13.49	26.45
100	15/7/2014	9:23:45 9:23:12	945	0.15 0.5	0.96 1.03	0.02	1.14E-05	0.55	1.08
101	15/7/2014	9:28:45 9:30:10 9:28:12	950	0.15 0.4 0.5	0.62 0.63 0.91	0.07	5.07	4.92	9.65
102	15/7/2014	9:33:45 9:33:12	955	0.15 0.5	0.70 0.95	0.08	5.22	6.97	13.65
103	15/7/2014	9:38:45 9:38:12	960	0.15 0.5	0.91 0.94	0.01	7.82E-11	0.16	0.32
104	15/7/2014	9:43:45 9:43:12	965	0.15 0.5	0.77 1.08	0.10	7.36	10.54	20.67
105	15/7/2014	9:48:45 9:48:12	970	0.15 0.5	0.70 0.89	0.06	1.53	3.76	7.36
106	15/7/2014	9:53:45 9:53:12	975	0.15 0.5	0.70 0.88	0.06	1.44	3.59	7.03
107	15/7/2014	9:58:45 9:58:12	980	0.15 0.5	0.60 0.77	0.06	2.29	3.31	6.49
108	15/7/2014	10:03:45 10:03:12	985	0.15 0.5	0.62 0.71	0.03	0.08	1.08	2.12
109	15/7/2014	10:08:45 10:08:12	990	0.15 0.5	0.67 0.77	0.03	0.05	1.08	2.13

No.	Date	Time	Minute	Z (m)	U (m/s)	u_* (m/s)	Z_0 (mm)	τ_0 (N/m²)	D_{mobile} ($\theta = 0.04$; mm)
110	15/7/2014	10:13:45 10:13:12	995	0.15 0.5	0.56 0.67	0.04	0.39	1.42	2.78
111	15/7/2014	10:18:45 10:18:12	1000	0.15 0.5	0.47 0.62	0.05	3.02	2.35	4.61
112	15/7/2014	10:23:45 10:23:12	1005	0.15 0.5	0.45 0.60	0.05	4.03	2.49	4.89
113	15/7/2014	10:28:45 10:28:12	1010	0.15 0.5	0.35 0.53	0.06	12.53	3.26	6.39
114	15/7/2014	10:33:45 10:33:12	1015	0.15 0.5	0.21 0.38	0.06	35.14	3.35	6.56
115	15/7/2014	10:38:45 10:40:10 10:38:12	1020	0.15 0.4 0.5	0.22 0.23 0.42	0.05	26.02	2.18	4.27
116	15/7/2014	10:43:45 10:43:12	1025	0.15 0.5	0.24 0.37	0.04	17.48	1.92	3.76
117	15/7/2014	10:48:45 10:50:10 10:48:12	1030	0.15 0.4 0.5	0.08 0.21 0.23	0.05	76.68	2.53	4.96
118	15/7/2014	10:53:45 10:53:12	1035	0.15 0.5	0.06 0.11	0.01	28.61	0.22	0.43
119	15/7/2014	10:58:45 10:58:12	1040	0.15 0.5	0.10 0.10	0.00	1.81E-06	0.005	0.01
120	15/7/2014	11:03:45 11:03:12	1045	0.15 0.5	0.16 0.18	0.01	0.07	0.07	0.13
121	15/7/2014	11:08:45 11:08:12	1050	0.15 0.5	0.29 0.34	0.02	0.12	0.27	0.53
122	15/7/2014	11:13:45 11:13:12	1055	0.15 0.5	0.39 0.45	0.02	0.05	0.39	0.76
123	15/7/2014	11:18:45 11:18:12	1060	0.15 0.5	0.43 0.48	0.02	0.02	0.37	0.73
124	15/7/2014	11:23:45 11:23:12	1065	0.15 0.5	0.48 0.60	0.04	0.91	1.44	2.82
125	15/7/2014	11:28:45 11:28:12	1070	0.15 0.5	0.46 0.52	0.02	0.03	0.47	0.92
126	15/7/2014	11:33:45 11:33:12	1075	0.15 0.5	0.68 0.73	0.02	1.88E-05	0.29	0.58
127	15/7/2014	11:38:45 11:38:12	1080	0.15 0.5	0.90 1.03	0.04	0.05	1.95	3.83
128	15/7/2014	11:43:45 11:43:12	1085	0.15 0.5	1.09 1.28	0.06	0.17	4.11	8.05
129	15/7/2014	11:48:45 11:48:12	1090	0.15 0.5	1.29 1.41	0.04	5.18E-04	1.68	3.29
130	15/7/2014	11:53:45 11:53:12	1095	0.15 0.5	1.29 1.51	0.07	0.12	5.26	10.31

No.	Date	Time	Minute	Z (m)	U (m/s)	u_* (m/s)	Z_0 (mm)	τ_0 (N/m^2)	D_{mobile} ($\theta = 0.04$; mm)
131	15/7/2014	11:58:45	1100	0.15	1.27	0.06	0.05	4.00	7.84
		11:58:12		0.5	1.46				
132	15/7/2014	12:03:45	1105	0.15	1.29	0.04	9.32E-04	1.87	3.66
		12:03:12		0.5	1.42				
133	15/7/2014	12:08:45	1110	0.15	1.25	0.07	0.10	4.67	9.15
		12:08:12		0.5	1.46				
134	15/7/2014	12:13:45	1115	0.15	1.39	0.04	1.66E-04	1.65	3.24
		12:13:12		0.5	1.52				
135	15/7/2014	12:18:45	1120	0.15	1.33	0.04	1.38E-04	1.47	2.88
		12:18:12		0.5	1.45				
136	15/7/2014	12:23:45	1125	0.15	1.37	0.14	2.74	18.81	36.87
		12:23:12		0.5	1.78				
137	15/7/2014	12:28:45	1130	0.15	1.59	0.11	0.47	12.13	23.78
		12:28:12		0.5	1.92				
138	15/7/2014	12:33:45	1135	0.15	1.52	0.04	3.57E-05	1.59	3.12
		12:33:12		0.5	1.64				
139	15/7/2014	12:38:45	1140	0.15	1.48	0.03	8.67E-08	0.77	1.51
		12:38:12		0.5	1.56				
140	15/7/2014	12:43:45	1145	0.15	1.30	0.01	5.56E-16	0.17	0.33
		12:43:12		0.5	1.34				
141	15/7/2014	12:48:45	1150	0.15	1.25	0.12	1.95	13.24	25.95
		12:48:12		0.5	1.60				
142	15/7/2014	12:58:45	1160	0.15	1.40	0.11	0.95	12.18	23.88
		12:58:12		0.5	1.73				
143	15/7/2014	13:03:45	1165	0.15	1.37	0.02	7.28E-09	0.53	1.04
		13:03:12		0.5	1.44				
144	15/7/2014	13:08:45	1170	0.15	1.35	0.00	4.38E-157	0.00	0.00
		13:08:12		0.5	1.35				
145	15/7/2014	13:13:45	1175	0.15	1.37	0.04	1.09E-04	1.50	2.95
		13:13:12		0.5	1.49				
146	15/7/2014	13:18:45	1180	0.15	1.21	0.07	0.09	4.28	8.40
		13:18:12		0.5	1.41				
147	15/7/2014	13:23:45	1185	0.15	1.31	0.00	5.72E-45	0.02	0.05
		13:23:12		0.5	1.33				
148	15/7/2014	13:28:45	1190	0.15	1.30	0.05	2.41E-03	2.21	4.34
		13:28:12		0.5	1.44				
149	15/7/2014	13:33:45	1195	0.15	1.17	0.04	2.74E-04	1.25	2.46
		13:33:12		0.5	1.28				
150	15/7/2014	13:38:45	1200	0.15	1.12	0.03	1.75E-04	1.08	2.12
		13:38:12		0.5	1.22				
151	15/7/2014	13:43:45	1205	0.15	1.12	0.05	0.02	2.50	4.90
		13:43:12		0.5	1.27				
152	15/7/2014	13:48:45	1210	0.15	1.05	0.03	5.07E-05	0.80	1.56
		13:48:12		0.5	1.14				
153	15/7/2014	13:53:45	1215	0.15	0.94	0.04	0.02	1.73	3.39
		13:53:12		0.5	1.06				

No.	Date	Time	Minute	Z (m)	U (m/s)	u_* (m/s)	Z_0 (mm)	τ_0 (N/m²)	D_{mobile} ($\theta = 0.04$; mm)
154	15/7/2014	13:58:45	1220	0.15	0.99	0.04	0.01	1.66	3.25
		13:58:12		0.5	1.11				
155	15/7/2014	14:03:45	1225	0.15	0.95	0.01	1.21E-12	0.14	0.27
		14:03:12		0.5	0.99				
156	15/7/2014	14:08:45	1230	0.15	0.96	0.01	2.06E-23	0.05	0.09
		14:08:12		0.5	0.98				
157	15/7/2014	14:13:45	1235	0.15	0.84	0.03	2.29E-03	0.92	1.81
		14:13:12		0.5	0.93				
158	15/7/2014	14:23:45	1245	0.15	0.93	0.04	0.03	1.95	3.83
		14:23:12		0.5	1.06				
159	15/7/2014	14:28:45	1250	0.15	0.89	0.06	0.57	4.10	8.04
		14:28:12		0.5	1.09				
160	15/7/2014	14:33:45	1255	0.15	0.92	0.00	1.80E-33	0.02	0.04
		14:33:12		0.5	0.94				
161	15/7/2014	14:38:45	1260	0.15	1.00	0.02	3.26E-06	0.51	1.00
		14:38:12		0.5	1.07				
162	15/7/2014	14:43:45	1265	0.15	0.95	0.02	2.23E-05	0.58	1.14
		14:43:12		0.5	1.02				
163	15/7/2014	14:48:45	1270	0.15	0.92	0.02	1.03E-07	0.30	0.60
		14:48:12		0.5	0.97				
164	15/7/2014	14:53:45	1275	0.15	0.94	0.04	0.01	1.51	2.97
		14:53:12		0.5	1.05				
165	15/7/2014	14:58:45	1280	0.15	0.96	0.01	9.36E-31	0.03	0.05
		14:58:12		0.5	0.98				
166	15/7/2014	15:03:45	1285	0.15	0.92	0.02	1.82E-08	0.26	0.51
		15:03:12		0.5	0.97				
167	15/7/2014	15:08:45	1290	0.15	0.87	0.04	0.02	1.43	2.81
		15:08:12		0.5	0.98				
168	15/7/2014	15:13:45	1295	0.15	0.91	0.03	2.39E-03	1.08	2.11
		15:13:12		0.5	1.00				
169	15/7/2014	15:18:45	1300	0.15	0.89	0.02	1.31E-08	0.24	0.47
		15:18:12		0.5	0.94				
170	15/7/2014	15:23:45	1305	0.15	0.93	0.02	5.39E-08	0.29	0.57
		15:23:12		0.5	0.98				
171	15/7/2014	15:28:45	1310	0.15	0.95	0.01	1.27E-15	0.09	0.18
		15:28:12		0.5	0.98				
172	15/7/2014	15:33:45	1315	0.15	0.93	0.02	1.18E-05	0.52	1.01
		15:33:12		0.5	1.00				
173	15/7/2014	15:38:45	1320	0.15	0.94	0.02	3.10E-07	0.35	0.69
		15:38:12		0.5	1.00				
174	15/7/2014	15:43:45	1325	0.15	0.85	0.03	1.06E-03	0.82	1.60
		15:43:12		0.5	0.93				
175	15/7/2014	15:48:45	1330	0.15	0.88	0.01	3.25E-10	0.17	0.34
		15:48:12		0.5	0.92				
176	15/7/2014	15:53:45	1335	0.15	0.94	0.02	3.00E-08	0.29	0.56
		15:53:12		0.5	0.99				

No.	Date	Time	Minute	Z (m)	U (m/s)	u_* (m/s)	Z_0 (mm)	τ_0 (N/m²)	D_{mobile} ($\theta = 0.04$; mm)
177	15/7/2014	15:58:45 15:58:12	1340	0.15 0.5	0.95 0.98	0.01	4.03E-17	0.08	0.15
178	15/7/2014	16:03:45 16:03:12	1345	0.15 0.5	0.94 0.98	0.01	1.67E-10	0.19	0.37
179	15/7/2014	16:08:45 16:08:12	1350	0.15 0.5	0.89 0.94	0.02	1.15E-08	0.24	0.46
180	15/7/2014	16:13:45 16:13:12	1355	0.15 0.5	0.94 0.96	0.01	8.69E-17	0.08	0.16
181	15/7/2014	16:23:45 16:23:12	1365	0.15 0.5	0.86 0.92	0.02	2.01E-06	0.36	0.71
182	15/7/2014	16:38:45 16:38:12	1380	0.15 0.5	0.76 0.79	0.01	4.48E-11	0.11	0.22
183	15/7/2014	16:43:45 16:43:12	1385	0.15 0.5	0.60 0.86	0.09	9.95	7.71	15.11
184	15/7/2014	20:03:45 20:03:12	1585	0.15 0.5	0.43 0.55	0.04	1.58	1.45	2.84
185	15/7/2014	20:08:45 20:10:10 20:08:12	1590	0.15 0.4 0.5	0.46 0.47 0.64	0.04	1.73	1.62	3.18
186	15/7/2014	20:13:45 20:13:12	1595	0.15 0.5	0.57 0.75	0.06	3.67	3.73	7.31
187	15/7/2014	20:18:45 20:18:12	1600	0.15 0.5	0.84 1.17	0.11	7.09	12.11	23.74
188	15/7/2014	20:23:45 20:23:12	1605	0.15 0.5	1.02 1.31	0.09	1.92	8.85	17.35
189	15/7/2014	20:28:45 20:28:12	1610	0.15 0.5	1.16 1.54	0.13	3.93	16.14	31.65
190	15/7/2014	20:33:45 20:33:12	1615	0.15 0.5	1.13 1.64	0.17	10.82	29.35	57.53
191	15/7/2014	20:38:45 20:38:12	1620	0.15 0.5	1.14 1.54	0.13	4.71	17.46	34.23
192	15/7/2014	20:43:45 20:43:12	1625	0.15 0.5	1.12 1.32	0.07	0.18	4.41	8.64
193	15/7/2014	20:48:45 20:48:12	1630	0.15 0.5	1.07 1.34	0.09	1.45	8.44	16.55
194	15/7/2014	20:53:45 20:53:12	1635	0.15 0.5	1.31 2.00	0.23	15.07	51.97	101.88
195	15/7/2014	20:58:45 20:58:12	1640	0.15 0.5	1.31 1.90	0.20	10.24	38.20	74.88
196	15/7/2014	21:03:45 21:03:12	1645	0.15 0.5	1.41 1.87	0.15	3.60	23.01	45.11
197	15/7/2014	21:08:45 21:08:12	1650	0.15 0.5	1.24 1.67	0.14	4.86	20.89	40.95
198	15/7/2014	21:13:45 21:13:12	1655	0.15 0.5	1.37 1.46	0.03	1.90E-06	0.91	1.78
199	15/7/2014	21:18:45 21:18:12	1660	0.15 0.5	1.43 1.51	0.03	2.26E-08	0.64	1.25

No.	Date	Time	Minute	Z (m)	U (m/s)	u_* (m/s)	Z_0 (mm)	τ_0 (N/m²)	D_{mobile} ($\theta = 0.04$; mm)
200	15/7/2014	21:23:45 21:23:12	1665	0.15 0.5	1.30 1.34	0.01	3.62E-14	0.21	0.41
201	15/7/2014	21:33:45 21:33:12	1675	0.15 0.5	1.25 1.26	0.00	3.49E-43	0.02	0.05
202	15/7/2014	21:38:45 21:38:12	1680	0.15 0.5	1.04 1.32	0.09	1.86	8.98	17.60
203	15/7/2014	21:48:45 21:48:12	1690	0.15 0.5	0.69 0.95	0.09	5.97	7.31	14.33
204	15/7/2014	21:53:45 21:53:12	1695	0.15 0.5	0.83 1.00	0.06	0.45	3.28	6.42
205	15/7/2014	21:58:45 21:58:12	1700	0.15 0.5	0.72 0.90	0.06	1.17	3.56	6.97
206	15/7/2014	22:03:45 22:03:12	1705	0.15 0.5	0.65 0.82	0.06	1.51	3.18	6.23
207	15/7/2014	22:08:45 22:08:12	1710	0.15 0.5	0.69 0.85	0.05	0.76	2.72	5.33
208	15/7/2014	22:13:45 22:13:12	1715	0.15 0.5	0.55 0.82	0.09	12.14	7.70	15.10
209	15/7/2014	22:18:45 22:18:12	1720	0.15 0.5	0.52 0.68	0.05	2.76	2.74	5.37
210	15/7/2014	22:23:45 22:23:12	1725	0.15 0.5	0.58 0.65	0.02	4.20E-03	0.49	0.96
211	15/7/2014	22:28:45 22:28:12	1730	0.15 0.5	0.48 0.63	0.05	3.36	2.54	4.99
212	15/7/2014	22:33:45 22:33:12	1735	0.15 0.5	0.46 0.61	0.05	3.43	2.41	4.73
213	15/7/2014	22:38:45 22:38:12	1740	0.15 0.5	0.46 0.57	0.04	1.03	1.37	2.69
214	15/7/2014	22:43:45 22:43:12	1745	0.15 0.5	0.36 0.49	0.04	5.35	1.84	3.60
215	15/7/2014	22:48:45 22:48:12	1750	0.15 0.5	0.36 0.50	0.05	7.56	2.31	4.52
216	15/7/2014	22:53:45 22:53:12	1755	0.15 0.5	0.30 0.47	0.06	18.82	3.24	6.36
217	15/7/2014	22:58:45 23:00:10 22:58:12	1760	0.15 0.4 0.5	0.25 0.25 0.36	0.03	3.73	0.67	1.32
218	15/7/2014	23:03:45 23:03:12	1765	0.15 0.5	0.15 0.35	0.07	60.93	4.34	8.51
219	15/7/2014	23:08:45 23:10:10 23:08:12	1770	0.15 0.4 0.5	0.14 0.17 0.27	0.03	32.15	1.16	2.27
220	15/7/2014	23:13:45 23:13:12	1775	0.15 0.5	0.08 0.08	0.00	1.50E-16	0.0006	1.24E-03
221	15/7/2014	23:48:45 23:48:12	1810	0.15 0.5	0.50 0.53	0.01	4.18E-10	0.06	0.11

No.	Date	Time	Minute	Z (m)	U (m/s)	u_* (m/s)	Z_0 (mm)	τ_0 (N/m^2)	D_{mobile} ($\theta = 0.04$; mm)
222	15/7/2014	23:53:45	1815	0.15	0.69	0.00	1.09E-47	0.01	0.01
		23:53:12		0.5	0.69				
223	16/7/2014	0:08:45	1830	0.15	1.31	0.02	1.21E-09	0.42	0.82
		0:08:12		0.5	1.37				
224	16/7/2014	0:13:45	1835	0.15	1.23	0.03	1.77E-05	0.95	1.86
		0:13:12		0.5	1.32				
225	16/7/2014	0:18:45	1840	0.15	1.18	0.04	1.53E-03	1.70	3.33
		0:18:12		0.5	1.31				
226	16/7/2014	0:23:45	1845	0.15	1.20	0.03	1.69E-06	0.68	1.34
		0:23:12		0.5	1.27				
227	16/7/2014	0:28:45	1850	0.15	1.30	0.02	4.24E-10	0.38	0.75
		0:28:12		0.5	1.36				
228	16/7/2014	0:38:45	1860	0.15	1.24	0.01	2.90E-15	0.17	0.33
		0:38:12		0.5	1.28				
229	16/7/2014	0:53:45	1875	0.15	1.49	0.04	2.72E-05	1.48	2.91
		0:53:12		0.5	1.61				
230	16/7/2014	0:58:45	1880	0.15	1.30	0.05	3.11E-03	2.27	4.44
		1:00:10		0.4	1.33				
		0:58:12		0.5	1.48				
231	16/7/2014	1:03:45	1885	0.15	1.18	0.07	0.14	4.60	9.02
		1:03:12		0.5	1.39				
232	16/7/2014	1:08:45	1890	0.15	1.13	0.08	0.56	6.58	12.90
		1:08:12		0.5	1.38				
233	16/7/2014	1:13:45	1895	0.15	1.23	0.08	0.29	6.13	12.01
		1:13:12		0.5	1.46				
234	16/7/2014	1:18:45	1900	0.15	1.27	0.08	0.23	6.19	12.13
		1:18:12		0.5	1.51				
235	16/7/2014	1:23:45	1905	0.15	1.01	0.13	6.03	15.69	30.76
		1:23:12		0.5	1.38				
236	16/7/2014	1:28:45	1910	0.15	1.00	0.12	4.85	13.39	26.26
		1:30:10		0.4	1.23				
		1:28:12		0.5	1.38				
237	16/7/2014	1:33:45	1915	0.15	0.98	0.15	10.66	21.87	42.87
		1:33:12		0.5	1.42				
238	16/7/2014	1:38:45	1920	0.15	0.94	0.12	6.27	13.55	26.56
		1:40:10		0.4	1.15				
		1:38:12		0.5	1.33				
239	16/7/2014	1:43:45	1925	0.15	0.87	0.10	5.04	10.40	20.39
		1:43:12		0.5	1.17				
240	16/7/2014	1:48:45	1930	0.15	0.93	0.09	2.44	7.63	14.95
		1:50:10		0.4	0.97				
		1:48:12		0.5	1.28				
241	16/7/2014	1:53:45	1935	0.15	0.92	0.10	3.64	9.87	19.34
		1:53:12		0.5	1.22				
242	16/7/2014	1:58:45	1940	0.15	0.83	0.04	0.01	1.23	2.40
		2:00:10		0.4	0.84				
		1:58:12		0.5	0.97				

No.	Date	Time	Minute	Z (m)	U (m/s)	u_* (m/s)	Z_0 (mm)	τ_0 (N/m²)	D_{mobile} ($\theta = 0.04$; mm)
243	16/7/2014	2:03:45	1945	0.15	0.75	0.07	1.61	4.42	8.66
		2:03:12		0.5	0.95				
244	16/7/2014	2:08:45	1950	0.15	0.71	0.07	1.98	4.34	8.51
		2:08:12		0.5	0.91				
245	16/7/2014	2:13:45	1955	0.15	0.75	0.08	4.05	6.89	13.51
		2:13:12		0.5	1.00				
246	16/7/2014	2:18:45	1960	0.15	0.75	0.05	0.43	2.51	4.92
		2:20:10		0.4	0.80				
		2:18:12		0.5	0.93				
247	16/7/2014	2:23:45	1965	0.15	0.74	0.04	0.12	1.73	3.39
		2:23:12		0.5	0.87				
248	16/7/2014	2:28:45	1970	0.15	0.68	0.03	0.06	1.18	2.31
		2:30:10		0.4	0.71				
		2:28:12		0.5	0.82				
249	16/7/2014	2:33:45	1975	0.15	0.71	0.05	0.50	2.50	4.91
		2:33:12		0.5	0.86				
250	16/7/2014	2:38:45	1980	0.15	0.69	0.03	0.01	0.80	1.57
		2:40:10		0.4	0.70				
		2:38:12		0.5	0.81				
251	16/7/2014	2:43:45	1985	0.15	0.69	0.04	0.11	1.48	2.90
		2:43:12		0.5	0.81				
252	16/7/2014	2:48:45	1990	0.15	0.69	0.04	0.23	1.75	3.43
		2:50:10		0.4	0.74				
		2:48:12		0.5	0.84				
253	16/7/2014	2:53:45	1995	0.15	0.72	0.04	0.05	1.31	2.56
		2:53:12		0.5	0.83				
254	16/7/2014	2:58:45	2000	0.15	0.66	0.05	0.59	2.23	4.38
		3:00:10		0.4	0.71				
		2:58:12		0.5	0.84				
255	16/7/2014	3:03:45	2005	0.15	0.64	0.06	1.53	3.10	6.08
		3:03:12		0.5	0.81				
256	16/7/2014	3:08:45	2010	0.15	0.62	0.07	3.81	4.42	8.66
		3:10:10		0.4	0.73				
		3:08:12		0.5	0.85				
257	16/7/2014	3:13:45	2015	0.15	0.64	0.06	2.79	4.13	8.10
		3:13:12		0.5	0.83				
258	16/7/2014	3:18:45	2020	0.15	0.64	0.06	1.78	3.31	6.49
		3:20:10		0.4	0.76				
		3:18:12		0.5	0.83				
259	16/7/2014	3:23:45	2025	0.15	0.63	0.06	2.22	3.55	6.96
		3:23:12		0.5	0.81				
260	16/7/2014	3:28:45	2030	0.15	0.63	0.05	1.12	2.63	5.15
		3:30:10		0.4	0.73				
		3:28:12		0.5	0.80				

No.	Date	Time	Minute	Z (m)	U (m/s)	u_* (m/s)	Z_0 (mm)	τ_0 (N/m²)	D_{mobile} ($\theta = 0.04$; mm)
261	16/7/2014	3:33:45	2035	0.15	0.62	0.05	1.24	2.68	5.24
		3:33:12		0.5	0.78				
262	16/7/2014	3:38:45	2040	0.15	0.63	0.05	1.08	2.55	4.99
		3:40:10		0.4	0.73				
		3:38:12		0.5	0.79				
263	16/7/2014	3:43:45	2045	0.15	0.63	0.05	0.88	2.39	4.69
		3:43:12		0.5	0.78				
264	16/7/2014	3:48:45	2050	0.15	0.67	0.04	0.39	2.00	3.93
		3:50:10		0.4	0.74				
		3:48:12		0.5	0.83				
265	16/7/2014	3:53:45	2055	0.15	0.62	0.05	1.21	2.68	5.25
		3:53:12		0.5	0.78				
266	16/7/2014	3:58:45	2060	0.15	0.62	0.06	1.73	3.06	5.99
		4:00:10		0.4	0.75				
		3:58:12		0.5	0.79				
267	16/7/2014	4:03:45	2065	0.15	0.61	0.06	2.28	3.36	6.59
		4:03:12		0.5	0.78				
268	16/7/2014	4:08:45	2070	0.15	0.60	0.05	1.91	2.98	5.84
		4:10:10		0.4	0.72				
		4:08:12		0.5	0.77				
269	16/7/2014	4:13:45	2075	0.15	0.64	0.04	0.52	2.01	3.94
		4:13:12		0.5	0.77				
270	16/7/2014	4:18:45	2080	0.15	0.63	0.05	0.95	2.48	4.86
		4:20:10		0.4	0.76				
		4:18:12		0.5	0.77				
271	16/7/2014	4:23:45	2085	0.15	0.64	0.06	1.49	3.04	5.96
		4:23:12		0.5	0.80				
272	16/7/2014	4:28:45	2090	0.15	0.65	0.04	0.47	2.00	3.92
		4:30:10		0.4	0.73				
		4:28:12		0.5	0.80				
273	16/7/2014	4:33:45	2095	0.15	0.61	0.07	3.96	4.47	8.77
		4:33:12		0.5	0.81				
274	16/7/2014	4:38:45	2100	0.15	0.63	0.04	0.46	1.86	3.65
		4:40:10		0.4	0.69				
		4:38:12		0.5	0.79				
275	16/7/2014	4:43:45	2105	0.15	0.64	0.03	0.08	1.15	2.25
		4:43:12		0.5	0.74				
276	16/7/2014	4:48:45	2110	0.15	0.60	0.06	3.98	4.00	7.85
		4:50:10		0.4	0.60				
		4:48:12		0.5	0.87				
277	16/7/2014	5:13:45	2135	0.15	0.38	0.01	5.29E-07	0.06	0.12
		5:13:12		0.5	0.40				
278	16/7/2014	5:18:45	2140	0.15	0.31	0.05	12.45	2.42	4.75
		5:18:12		0.5	0.45				
279	16/7/2014	8:33:45	2335	0.15	0.39	0.05	8.97	3.00	5.88
		8:33:12		0.5	0.55				

No.	Date	Time	Minute	Z (m)	U (m/s)	u_* (m/s)	Z_0 (mm)	τ_0 (N/m²)	D_{mobile} ($\theta = 0.04$; mm)
280	16/7/2014	8:38:45	2340	0.15	0.41	0.04	2.68	1.56	3.06
		8:40:10		0.4	0.41				
		8:38:12		0.5	0.58				
281	16/7/2014	8:43:45	2345	0.15	0.71	0.06	1.52	3.83	7.50
		8:43:12		0.5	0.90				
282	16/7/2014	8:48:45	2350	0.15	0.93	0.06	0.37	3.85	7.55
		8:48:12		0.5	1.12				
283	16/7/2014	8:53:45	2355	0.15	1.06	0.09	1.63	8.72	17.10
		8:53:12		0.5	1.34				
284	16/7/2014	8:58:45	2360	0.15	0.91	0.14	11.16	19.84	38.89
		8:58:12		0.5	1.34				
285	16/7/2014	9:03:45	2365	0.15	0.99	0.15	10.21	21.81	42.75
		9:03:12		0.5	1.44				
286	16/7/2014	9:08:45	2370	0.15	1.02	0.10	2.65	10.13	19.86
		9:08:12		0.5	1.32				
287	16/7/2014	9:13:45	2375	0.15	0.94	0.14	9.97	19.40	38.02
		9:13:12		0.5	1.36				
288	16/7/2014	9:18:45	2380	0.15	1.05	0.10	2.64	10.87	21.31
		9:18:12		0.5	1.37				
289	16/7/2014	9:23:45	2385	0.15	1.48	0.15	2.65	21.61	42.36
		9:23:12		0.5	1.93				
290	16/7/2014	9:28:45	2390	0.15	1.32	0.14	3.46	19.50	38.23
		9:28:12		0.5	1.74				
291	16/7/2014	9:33:45	2395	0.15	1.46	0.08	0.14	7.06	13.83
		9:33:12		0.5	1.71				
292	16/7/2014	9:38:45	2400	0.15	1.31	0.07	0.06	4.46	8.74
		9:38:12		0.5	1.51				
293	16/7/2014	9:43:45	2405	0.15	1.19	0.09	0.86	8.45	16.56
		9:43:12		0.5	1.46				
294	16/7/2014	9:48:45	2410	0.15	1.06	0.14	6.83	18.85	36.96
		9:48:12		0.5	1.47				
295	16/7/2014	9:53:45	2415	0.15	1.18	0.06	0.08	3.92	7.68
		9:53:12		0.5	1.37				
296	16/7/2014	9:58:45	2420	0.15	0.93	0.09	2.46	8.22	16.10
		9:58:12		0.5	1.20				
297	16/7/2014	10:03:45	2425	0.15	0.95	0.12	6.48	14.55	28.52
		10:03:12		0.5	1.31				
298	16/7/2014	10:08:45	2430	0.15	1.02	0.10	3.11	11.00	21.56
		10:08:12		0.5	1.33				
299	16/7/2014	10:13:45	2435	0.15	0.58	0.15	33.05	23.48	46.04
		10:13:12		0.5	1.04				
300	16/7/2014	10:18:45	2440	0.15	0.66	0.03	0.01	0.72	1.42
		10:18:12		0.5	0.74				
301	16/7/2014	10:23:45	2445	0.15	0.66	0.06	2.27	4.01	7.86
		10:23:12		0.5	0.85				
302	16/7/2014	10:28:45	2450	0.15	0.71	0.07	2.74	4.99	9.78
		10:28:12		0.5	0.92				

No.	Date	Time	Minute	Z (m)	U (m/s)	u_* (m/s)	Z_0 (mm)	τ_0 (N/m²)	D_{mobile} ($\theta = 0.04$; mm)
303	16/7/2014	10:33:45 10:33:12	2455	0.15 0.5	0.84 0.96	0.04	0.03	1.59	3.12
304	16/7/2014	10:38:45 10:38:12	2460	0.15 0.5	0.67 0.87	0.07	2.85	4.57	8.96
305	16/7/2014	10:43:45 10:43:12	2465	0.15 0.5	0.60 0.70	0.03	0.11	1.11	2.17
306	16/7/2014	10:48:45 10:48:12	2470	0.15 0.5	0.55 0.73	0.06	3.52	3.49	6.83
307	16/7/2014	10:53:45 10:53:12	2475	0.15 0.5	0.58 0.66	0.02	0.01	0.58	1.14
308	16/7/2014	10:58:45 10:58:12	2480	0.15 0.5	0.51 0.68	0.06	4.05	3.22	6.31
309	16/7/2014	11:03:45 11:03:12	2485	0.15 0.5	0.45 0.64	0.06	8.25	3.88	7.60
310	16/7/2014	11:08:45 11:10:10 11:08:12	2490	0.15 0.4 0.5	0.36 0.43 0.56	0.05	11.69	3.02	5.92
311	16/7/2014	11:13:45 11:13:12	2495	0.15 0.5	0.32 0.53	0.07	23.68	4.82	9.45
312	16/7/2014	11:18:45 11:20:10 11:18:12	2500	0.15 0.4 0.5	0.26 0.34 0.52	0.07	36.75	4.84	9.49
313	16/7/2014	11:23:45 11:23:12	2505	0.15 0.5	0.18 0.39	0.07	54.02	4.92	9.64
314	16/7/2014	11:28:45 11:30:10 11:28:12	2510	0.15 0.4 0.5	0.24 0.38 0.39	0.05	23.30	2.72	5.34
315	16/7/2014	11:33:45 11:33:12	2515	0.15 0.5	0.08 0.18	0.03	49.57	0.94	1.84
316	16/7/2014	11:38:45 11:38:12	2520	0.15 0.5	0.03 0.18	0.05	113.61	2.47	4.85
317	16/7/2014	11:43:45 11:43:12	2525	0.15 0.5	0.06 0.07	0.00	0.29	0.02	0.03
318	16/7/2014	12:38:45 12:38:12	2580	0.15 0.5	1.26 1.47	0.07	0.11	4.92	9.64
319	16/7/2014	12:43:45 12:43:12	2585	0.15 0.5	1.35 1.46	0.04	4.67E-05	1.30	2.54
320	16/7/2014	12:48:45 12:48:12	2590	0.15 0.5	1.33 1.51	0.06	0.03	3.81	7.46
321	16/7/2014	12:53:45 12:53:12	2595	0.15 0.5	1.28 1.44	0.05	0.01	2.76	5.42
322	16/7/2014	12:58:45 12:58:12	2600	0.15 0.5	1.26 1.30	0.02	7.08E-13	0.23	0.46
323	16/7/2014	13:03:45 13:03:12	2605	0.15 0.5	1.27 1.27	0.00	0.00E+00	0.00	8.46E-04

No.	Date	Time	Minute	Z (m)	U (m/s)	u_* (m/s)	Z_0 (mm)	τ_0 (N/m²)	D_{mobile} ($\theta = 0.04$; mm)
324	16/7/2014	13:08:45	2610	0.15	1.30	0.01	9.07E-21	0.10	0.20
		13:08:12		0.5	1.33				
325	16/7/2014	13:13:45	2615	0.15	1.54	0.02	1.80E-14	0.28	0.55
		13:13:12		0.5	1.59				
326	16/7/2014	13:18:45	2620	0.15	1.35	0.10	0.74	10.26	20.12
		13:18:12		0.5	1.65				
327	16/7/2014	13:23:45	2625	0.15	1.19	0.10	1.34	10.10	19.80
		13:23:12		0.5	1.49				
328	16/7/2014	13:28:45	2630	0.15	1.09	0.07	0.35	5.20	10.20
		13:28:12		0.5	1.31				
329	16/7/2014	13:33:45	2635	0.15	1.07	0.05	0.02	2.26	4.43
		13:33:12		0.5	1.21				
330	16/7/2014	13:38:45	2640	0.15	1.09	0.09	1.40	8.78	17.20
		13:38:12		0.5	1.38				
331	16/7/2014	13:43:45	2645	0.15	0.92	0.15	12.94	22.43	43.98
		13:43:12		0.5	1.37				
332	16/7/2014	13:48:45	2650	0.15	0.97	0.09	2.12	7.95	15.59
		13:50:10		0.4	1.06				
		13:48:12		0.5	1.31				
333	16/7/2014	13:53:45	2655	0.15	0.92	0.12	7.73	15.53	30.44
		13:53:12		0.5	1.30				
334	16/7/2014	13:58:45	2660	0.15	0.81	0.14	16.63	19.94	39.10
		14:00:10		0.4	0.92				
		13:58:12		0.5	1.37				
335	16/7/2014	14:03:45	2665	0.15	0.80	0.13	13.47	17.62	34.53
		14:03:12		0.5	1.20				
336	16/7/2014	14:08:45	2670	0.15	0.91	0.10	3.87	9.17	17.98
		14:10:10		0.4	0.93				
		14:08:12		0.5	1.31				
337	16/7/2014	14:13:45	2675	0.15	0.84	0.09	3.43	7.98	15.65
		14:13:12		0.5	1.11				
338	16/7/2014	14:18:45	2680	0.15	0.78	0.10	6.68	9.38	18.39
		14:20:10		0.4	0.87				
		14:18:12		0.5	1.14				
339	16/7/2014	14:23:45	2685	0.15	0.79	0.10	6.22	9.81	19.23
		14:23:12		0.5	1.09				
340	16/7/2014	14:28:45	2690	0.15	0.83	0.10	4.78	9.32	18.27
		14:28:12		0.5	1.12				
341	16/7/2014	14:33:45	2695	0.15	0.71	0.11	10.65	11.66	22.85
		14:33:12		0.5	1.04				
342	16/7/2014	14:38:45	2700	0.15	0.73	0.10	7.91	9.74	19.09
		14:38:12		0.5	1.02				
343	16/7/2014	14:43:45	2705	0.15	0.73	0.08	4.39	6.75	13.24
		14:43:12		0.5	0.97				

No.	Date	Time	Minute	Z (m)	U (m/s)	u_* (m/s)	Z_0 (mm)	τ_0 (N/m²)	D_{mobile} ($\theta = 0.04$; mm)
344	16/7/2014	14:48:45	2710	0.15	0.71	0.04	0.18	1.74	3.40
		14:50:10		0.4	0.73				
		14:48:12		0.5	0.88				
345	16/7/2014	14:53:45	2715	0.15	0.69	0.08	5.80	7.13	13.98
		14:53:12		0.5	0.94				
346	16/7/2014	14:58:45	2720	0.15	0.72	0.04	0.08	1.40	2.74
		15:00:10		0.4	0.72				
		14:58:12		0.5	0.88				
347	16/7/2014	15:03:45	2725	0.15	0.68	0.09	6.44	7.40	14.50
		15:03:12		0.5	0.94				
348	16/7/2014	15:08:45	2730	0.15	0.70	0.07	2.35	4.27	8.37
		15:10:10		0.4	0.74				
		15:08:12		0.5	0.96				
349	16/7/2014	15:13:45	2735	0.15	0.76	0.06	1.02	3.67	7.20
		15:13:12		0.5	0.94				
350	16/7/2014	15:18:45	2740	0.15	0.72	0.04	0.20	1.82	3.57
		15:20:10		0.4	0.74				
		15:18:12		0.5	0.89				
351	16/7/2014	15:23:45	2745	0.15	0.74	0.07	2.57	5.30	10.38
		15:23:12		0.5	0.96				
352	16/7/2014	15:28:45	2750	0.15	0.71	0.08	4.27	6.42	12.58
		15:28:12		0.5	0.95				
353	16/7/2014	15:33:45	2755	0.15	0.73	0.08	3.19	5.68	11.13
		15:33:12		0.5	0.95				
354	16/7/2014	15:38:45	2760	0.15	0.71	0.06	0.94	3.04	5.96
		15:40:10		0.4	0.76				
		15:38:12		0.5	0.93				
355	16/7/2014	15:43:45	2765	0.15	0.73	0.07	2.42	4.97	9.75
		15:43:12		0.5	0.94				
356	16/7/2014	15:48:45	2770	0.15	0.71	0.05	0.60	2.56	5.02
		15:50:10		0.4	0.74				
		15:48:12		0.5	0.92				
357	16/7/2014	15:53:45	2775	0.15	0.67	0.06	2.23	4.07	7.98
		15:53:12		0.5	0.86				
358	16/7/2014	15:58:45	2780	0.15	0.72	0.05	0.55	2.60	5.10
		15:58:12		0.5	0.87				
359	16/7/2014	16:03:45	2785	0.15	0.70	0.05	0.69	2.68	5.25
		16:03:12		0.5	0.85				
360	16/7/2014	16:08:45	2790	0.15	0.71	0.05	0.28	2.05	4.01
		16:08:12		0.5	0.85				
361	16/7/2014	16:13:45	2795	0.15	0.72	0.03	0.01	0.87	1.70
		16:13:12		0.5	0.81				
362	16/7/2014	16:18:45	2800	0.15	0.74	0.01	1.66E-07	0.20	0.40
		16:18:12		0.5	0.78				
363	16/7/2014	16:23:45	2805	0.15	0.72	0.02	5.03E-04	0.52	1.02
		16:23:12		0.5	0.79				

No.	Date	Time	Minute	Z (m)	U (m/s)	u_* (m/s)	Z_0 (mm)	τ_0 (N/m²)	D_{mobile} ($\theta = 0.04$; mm)
364	16/7/2014	16:28:45	2810	0.15	0.70	0.02	1.83E-03	0.59	1.16
		16:30:10		0.4	0.70				
		16:28:12		0.5	0.80				
365	16/7/2014	16:33:45	2815	0.15	0.70	0.05	0.65	2.69	5.27
		16:33:12		0.5	0.86				
366	16/7/2014	16:38:45	2820	0.15	0.70	0.04	0.26	1.94	3.81
		16:38:12		0.5	0.83				
367	16/7/2014	16:43:45	2825	0.15	0.75	0.03	1.19E-03	0.66	1.30
		16:43:12		0.5	0.83				
368	16/7/2014	16:48:45	2830	0.15	0.69	0.06	1.51	3.65	7.16
		16:48:12		0.5	0.88				
369	16/7/2014	16:53:45	2835	0.15	0.73	0.04	0.08	1.49	2.91
		16:53:12		0.5	0.85				
370	16/7/2014	16:58:45	2840	0.15	0.72	0.04	0.12	1.66	3.26
		16:58:12		0.5	0.85				
371	16/7/2014	17:03:45	2845	0.15	0.70	0.07	3.02	5.15	10.09
		17:03:12		0.5	0.92				
372	16/7/2014	17:08:45	2850	0.15	0.66	0.19	37.65	36.94	72.41
		17:08:12		0.5	1.24				

Table A 2 Data of velocity profiles at a given period collected during 12th – 14th August 2014. The grey-filled sections represent flood periods and the white-filled sections represent ebb periods.

No.	Date	Time	Minute	Z (m)	U (m/s)	u_* (m/s)	Z_0 (mm)	τ_0 (N/m^2)	D_{mobile} ($\theta = 0.04$; mm)
1	12/08/2014	19:05:36 19:05:04	145	0.15 0.5	0.56 0.65	0.03	0.11	0.96	1.88
2	12/08/2014	19:10:36 19:10:04	150	0.15 0.5	0.69 0.73	0.01	1.32E-07	0.18	0.35
3	12/08/2014	19:15:36 19:15:04	155	0.15 0.5	0.84 0.98	0.05	0.08	2.04	3.99
4	12/08/2014	19:20:36 19:20:04	160	0.15 0.5	1.17 1.29	0.04	9.43E-04	1.52	2.98
5	12/08/2014	19:25:36 19:25:04	165	0.15 0.5	1.25 1.58	0.11	1.40	11.52	22.59
6	12/08/2014	19:30:36 19:30:04	170	0.15 0.5	1.33 1.56	0.08	0.14	5.75	11.27
7	12/08/2014	19:35:36 19:35:04	175	0.15 0.5	1.17 1.40	0.07	0.28	5.57	10.93
8	12/08/2014	19:40:36 19:40:04	180	0.15 0.5	1.23 1.40	0.05	0.02	2.97	5.83
9	12/08/2014	19:45:36 19:45:04	185	0.15 0.5	1.27 1.53	0.09	0.46	7.71	15.12
10	12/08/2014	19:50:36 19:50:04	190	0.15 0.5	1.49 1.91	0.14	2.10	19.46	38.14
11	12/08/2014	19:55:36 19:55:04	195	0.15 0.5	1.52 1.72	0.07	0.02	4.57	8.96
12	12/08/2014	20:00:36 20:00:04	200	0.15 0.5	1.52 1.55	0.01	1.22E-28	0.08	0.15
13	12/08/2014	20:05:36 20:05:04	205	0.15 0.5	1.44 1.62	0.06	0.01	3.68	7.21
14	12/08/2014	20:15:36 20:15:04	215	0.15 0.5	1.43 1.50	0.02	1.74E-08	0.62	1.22
15	12/08/2014	20:20:36 20:20:04	220	0.15 0.5	1.15 1.21	0.02	1.88E-07	0.50	0.98
16	12/08/2014	20:25:36 20:25:04	225	0.15 0.5	1.04 1.12	0.03	8.31E-06	0.63	1.23
17	12/08/2014	20:35:36 20:35:04	235	0.15 0.5	1.24 1.27	0.01	1.42E-21	0.09	0.17
18	12/08/2014	20:55:36 20:55:04	255	0.15 0.5	0.94 0.97	0.01	1.35E-14	0.10	0.20
19	12/08/2014	21:10:36 21:10:04	270	0.15 0.5	0.78 0.87	0.03	3.39E-03	0.85	1.66
20	12/08/2014	21:15:36 21:15:04	275	0.15 0.5	0.85 0.87	0.01	1.32E-16	0.07	0.13
21	12/08/2014	21:30:36 21:30:04	290	0.15 0.5	0.45 0.48	0.01	1.75E-09	0.05	0.10

No.	Date	Time	Minute	Z (m)	U (m/s)	u_* (m/s)	Z_0 (mm)	τ_0 (N/m^2)	D_{mobile} ($\theta = 0.04$; mm)
22	12/08/2014	21:35:36	295	0.15	0.49	0.02	0.01	0.40	0.78
		21:35:04		0.5	0.55				
23	12/08/2014	21:40:36	300	0.15	0.33	0.04	3.85	1.28	2.50
		21:40:04		0.5	0.43				
24	12/08/2014	21:45:36	305	0.15	0.30	0.01	3.59E-07	0.04	0.07
		21:45:04		0.5	0.32				
25	12/08/2014	21:50:36	310	0.15	0.25	0.05	16.13	2.08	4.07
		21:50:04		0.5	0.39				
26	12/08/2014	21:55:36	315	0.15	0.13	0.06	61.25	3.43	6.73
		21:55:04		0.5	0.31				
27	12/08/2014	22:00:36	320	0.15	0.09	0.03	43.54	0.80	1.57
		22:00:04		0.5	0.17				
28	12/08/2014	22:05:36	325	0.15	0.01	0.04	137.01	1.25	2.45
		22:05:04		0.5	0.11				
29	12/08/2014	22:10:36	330	0.15	0.04	0.02	61.76	0.39	0.76
		22:10:04		0.5	0.10				
30	12/08/2014	22:15:36	335	0.15	0.04	0.03	79.28	0.73	1.43
		22:15:04		0.5	0.12				
31	12/08/2014	22:20:36	340	0.15	0.10	3.64E-03	2.02E-03	0.01	0.03
		22:20:04		0.5	0.11				
32	12/08/2014	22:35:36	355	0.15	0.40	0.08	21.03	6.63	12.99
		22:35:04		0.5	0.64				
33	12/08/2014	22:40:36	360	0.15	0.47	0.09	20.09	8.87	17.39
		22:40:04		0.5	0.76				
34	12/08/2014	22:45:36	365	0.15	0.49	0.12	29.78	14.80	29.01
		22:45:04		0.5	0.86				
35	12/08/2014	22:50:36	370	0.15	0.53	0.08	11.13	6.63	12.99
		22:50:04		0.5	0.77				
36	12/08/2014	22:55:36	375	0.15	0.60	0.14	27.82	20.59	40.37
		22:55:04		0.5	1.04				
37	12/08/2014	23:00:36	380	0.15	0.69	0.17	31.19	30.58	59.95
		23:00:04		0.5	1.21				
38	12/08/2014	23:05:36	385	0.15	0.86	0.19	25.00	37.08	72.69
		23:05:04		0.5	1.44				
39	12/08/2014	23:10:36	390	0.15	0.82	0.19	26.53	35.52	69.64
		23:10:04		0.5	1.38				
40	12/08/2014	23:15:36	395	0.15	0.74	0.20	33.29	38.71	75.88
		23:15:04		0.5	1.33				
41	12/08/2014	23:20:36	400	0.15	0.85	0.21	29.57	43.84	85.93
		23:20:04		0.5	1.48				
42	12/08/2014	23:25:36	405	0.15	0.82	0.22	32.77	46.40	90.95
		23:25:04		0.5	1.47				
43	12/08/2014	23:30:36	410	0.15	0.87	0.21	27.34	42.09	82.50
		23:30:04		0.5	1.49				

No.	Date	Time	Minute	Z (m)	U (m/s)	u_* (m/s)	Z_0 (mm)	τ_0 (N/m^2)	D_{mobile} ($\theta = 0.04$; mm)
44	12/08/2014	23:35:36 23:35:04	415	0.15 0.5	0.88 1.48	0.20	25.95	39.97	78.35
45	12/08/2014	23:40:36 23:40:04	420	0.15 0.5	1.17 1.98	0.27	27.06	74.10	145.25
46	12/08/2014	23:45:36 23:45:04	425	0.15 0.5	1.43 2.01	0.19	7.95	37.85	74.20
47	12/08/2014	23:50:36 23:50:04	430	0.15 0.5	1.24 1.81	0.19	11.38	36.78	72.10
48	12/08/2014	23:55:36 23:55:04	435	0.15 0.5	0.83 1.71	0.29	48.28	85.37	167.36
49	13/8/2014	0:00:36 0:00:04	440	0.15 0.5	0.86 1.66	0.27	41.50	70.96	139.11
50	13/8/2014	0:05:36 0:05:04	445	0.15 0.5	1.13 1.58	0.15	7.36	22.58	44.26
51	13/8/2014	0:10:36 0:10:04	450	0.15 0.5	1.00 1.60	0.20	19.75	39.21	76.87
52	13/8/2014	0:15:36 0:15:04	455	0.15 0.5	1.10 1.44	0.11	3.18	13.06	25.60
53	13/8/2014	0:20:36 0:20:04	460	0.15 0.5	1.20 1.62	0.14	4.81	19.51	38.26
54	13/8/2014	0:25:36 0:25:04	465	0.15 0.5	1.10 1.45	0.12	3.62	13.93	27.30
55	13/8/2014	0:30:36 0:30:04	470	0.15 0.5	1.06 1.41	0.12	3.74	13.30	26.07
56	13/8/2014	0:35:36 0:35:04	475	0.15 0.5	1.10 1.37	0.09	1.10	8.00	15.68
57	13/8/2014	0:40:36 0:40:04	480	0.15 0.5	1.22 1.54	0.11	1.68	11.76	23.05
58	13/8/2014	0:45:36 0:45:04	485	0.15 0.5	1.25 1.60	0.12	2.00	13.39	26.25
59	13/8/2014	0:55:36 0:55:04	495	0.15 0.5	0.96 1.04	0.03	3.90E-05	0.64	1.26
60	13/8/2014	1:40:36 1:40:04	540	0.15 0.5	0.68 0.71	0.01	5.79E-14	0.06	0.12
61	13/8/2014	7:35:36 7:35:04	895	0.15 0.5	0.62 0.63	4.48E-03	1.57E-22	0.02	0.04
62	13/8/2014	7:40:36 7:40:04	900	0.15 0.5	0.51 0.63	0.04	0.67	1.43	2.81
63	13/8/2014	7:45:36 7:45:04	905	0.15 0.5	0.68 0.77	0.03	0.01	0.86	1.68
64	13/8/2014	7:50:36 7:50:04	910	0.15 0.5	0.88 1.07	0.06	0.61	4.11	8.06
65	13/8/2014	7:55:36 7:55:04	915	0.15 0.5	1.23 1.28	0.02	2.42E-10	0.33	0.64
66	13/8/2014	8:00:36 8:00:04	920	0.15 0.5	1.43 1.56	0.04	4.32E-04	2.01	3.94
67	13/8/2014	8:05:36 8:05:04	925	0.15 0.5	1.21 1.52	0.10	1.33	10.55	20.68

No.	Date	Time	Minute	Z (m)	U (m/s)	u_* (m/s)	Z_0 (mm)	τ_0 (N/m^2)	D_{mobile} ($\theta = 0.04$; mm)
68	13/8/2014	8:10:36	930	0.15	1.28	0.10	1.14	10.97	21.50
		8:10:04		0.5	1.59				
69	13/8/2014	8:15:36	935	0.15	1.28	0.07	0.11	5.02	9.85
		8:15:04		0.5	1.50				
70	13/8/2014	8:20:36	940	0.15	1.48	0.06	0.01	3.45	6.77
		8:20:04		0.5	1.66				
71	13/8/2014	8:25:36	945	0.15	1.70	0.05	1.95E-04	2.52	4.94
		8:25:04		0.5	1.85				
72	13/8/2014	8:30:36	950	0.15	0.93	0.05	0.16	2.96	5.81
		8:30:04		0.5	1.10				
73	13/8/2014	8:35:36	955	0.15	0.61	0.27	61.58	74.60	146.23
		8:35:04		0.5	1.43				
74	13/8/2014	8:40:36	960	0.15	0.71	0.28	54.58	79.96	156.75
		8:40:04		0.5	1.57				
75	13/8/2014	8:45:36	965	0.15	0.82	0.24	39.12	58.88	115.43
		8:45:04		0.5	1.55				
76	13/8/2014	8:50:36	970	0.15	0.73	0.23	42.58	54.11	106.08
		8:50:04		0.5	1.43				
77	13/8/2014	8:55:36	975	0.15	0.71	0.18	29.68	31.03	60.83
		8:55:04		0.5	1.24				
78	13/8/2014	9:00:36	980	0.15	0.48	0.17	47.06	27.30	53.52
		9:00:04		0.5	0.98				
79	13/8/2014	9:05:36	985	0.15	0.51	0.19	50.84	35.46	69.51
		9:05:04		0.5	1.08				
80	13/8/2014	9:10:36	990	0.15	0.40	0.21	70.68	45.08	88.36
		9:10:04		0.5	1.04				
81	13/8/2014	9:15:36	995	0.15	0.37	0.19	68.43	35.27	69.14
		9:15:04		0.5	0.93				
82	13/8/2014	9:20:36	1000	0.15	0.44	0.21	64.60	43.26	84.80
		9:20:04		0.5	1.06				
83	13/8/2014	9:25:36	1005	0.15	0.30	0.21	83.54	42.19	82.71
		9:25:04		0.5	0.92				
84	13/8/2014	9:30:36	1010	0.15	0.29	0.27	97.22	71.89	140.93
		9:30:04		0.5	1.10				
85	13/8/2014	9:35:36	1015	0.15	0.28	0.16	75.53	26.53	52.00
		9:35:04		0.5	0.77				
86	13/8/2014	9:40:36	1020	0.15	0.28	0.16	75.67	26.98	52.89
		9:40:04		0.5	0.78				
87	13/8/2014	9:45:36	1025	0.15	0.25	0.18	85.88	33.41	65.49
		9:45:04		0.5	0.80				
88	13/8/2014	9:50:36	1030	0.15	0.23	0.14	77.81	20.04	39.28
		9:50:04		0.5	0.66				
89	13/8/2014	9:55:36	1035	0.15	0.25	0.14	73.00	19.43	38.09
		9:55:04		0.5	0.67				
90	13/8/2014	10:00:36	1040	0.15	0.22	0.14	80.60	20.77	40.72
		10:00:04		0.5	0.66				

No.	Date	Time	Minute	Z (m)	U (m/s)	u_* (m/s)	Z_0 (mm)	τ_0 (N/m^2)	D_{mobile} ($\theta = 0.04$; mm)
91	13/8/2014	10:05:36 10:05:04	1045	0.15 0.5	0.14 0.52	0.12	94.63	15.45	30.29
92	13/8/2014	10:10:36 10:10:04	1050	0.15 0.5	0.15 0.50	0.12	90.66	13.69	26.84
93	13/8/2014	10:15:36 10:15:04	1055	0.15 0.5	0.12 0.48	0.12	101.72	14.26	27.96
94	13/8/2014	10:20:36 10:20:04	1060	0.15 0.5	0.08 0.48	0.13	115.74	17.12	33.56
95	13/8/2014	10:25:36 10:25:04	1065	0.15 0.5	0.06 0.24	0.06	100.80	3.59	7.04
96	13/8/2014	10:30:36 10:30:04	1070	0.15 0.5	0.09 0.22	0.04	67.67	2.02	3.95
97	13/8/2014	10:35:36 10:35:04	1075	0.15 0.5	0.05 0.12	0.02	66.18	0.53	1.03
98	13/8/2014	10:40:36 10:40:04	1080	0.15 0.5	0.03 0.09	0.02	77.32	0.38	0.74
99	13/8/2014	10:45:36 10:45:04	1085	0.15 0.5	0.06 0.19	0.04	88.05	1.91	3.73
100	13/8/2014	10:50:36 10:50:04	1090	0.15 0.5	0.17 0.27	0.03	16.51	0.99	1.95
101	13/8/2014	10:55:36 10:55:04	1095	0.15 0.5	0.28 0.34	0.02	0.38	0.35	0.69
102	13/8/2014	11:00:36 11:00:04	1100	0.15 0.5	0.26 0.54	0.09	47.80	8.34	16.36
103	13/8/2014	11:05:36 11:05:04	1105	0.15 0.5	0.31 0.61	0.10	43.42	9.84	19.28
104	13/8/2014	11:10:36 11:10:04	1110	0.15 0.5	0.48 0.70	0.07	11.42	5.55	10.89
105	13/8/2014	11:15:36 11:15:04	1115	0.15 0.5	0.41 0.74	0.11	35.06	12.44	24.39
106	13/8/2014	11:20:36 11:20:04	1120	0.15 0.5	0.50 0.84	0.12	27.06	13.40	26.26
107	13/8/2014	11:25:36 11:25:04	1125	0.15 0.5	0.64 1.10	0.15	28.26	23.33	45.73
108	13/8/2014	11:30:36 11:30:04	1130	0.15 0.5	0.88 1.44	0.19	23.31	35.51	69.62
109	13/8/2014	11:35:36 11:35:04	1135	0.15 0.5	0.87 1.39	0.18	20.95	30.91	60.60
110	13/8/2014	11:40:36 11:40:04	1140	0.15 0.5	0.80 1.35	0.18	25.05	32.31	63.33
111	13/8/2014	11:45:36 11:45:04	1145	0.15 0.5	0.98 1.41	0.14	9.14	19.77	38.76
112	13/8/2014	11:50:36 11:50:04	1150	0.15 0.5	1.02 1.53	0.17	13.60	28.88	56.61
113	13/8/2014	11:55:36 11:55:04	1155	0.15 0.5	0.79 1.33	0.18	26.41	32.75	64.20

No.	Date	Time	Minute	Z (m)	U (m/s)	u_* (m/s)	Z_0 (mm)	τ_0 (N/m^2)	D_{mobile} ($\theta = 0.04$; mm)
114	13/8/2014	12:00:36 12:00:04	1160	0.15 0.5	0.96 1.57	0.20	22.84	41.31	80.97
115	13/8/2014	12:05:36 12:05:04	1165	0.15 0.5	0.80 1.29	0.16	20.95	26.60	52.15
116	13/8/2014	12:10:36 12:10:04	1170	0.15 0.5	1.01 1.21	0.07	0.44	4.77	9.36
117	13/8/2014	12:15:36 12:15:04	1175	0.15 0.5	0.97 1.59	0.21	23.28	43.15	84.59
118	13/8/2014	12:20:36 12:20:04	1180	0.15 0.5	0.89 1.60	0.24	33.39	55.88	109.54
119	13/8/2014	12:25:36 12:25:04	1185	0.15 0.5	0.79 1.62	0.28	47.63	75.98	148.95
120	13/8/2014	12:30:36 12:30:04	1190	0.15 0.5	0.83 1.63	0.26	42.68	70.16	137.53
121	13/8/2014	12:35:36 12:35:04	1195	0.15 0.5	0.79 1.32	0.17	23.94	29.99	58.80
122	13/8/2014	12:40:36 12:40:04	1200	0.15 0.5	0.68 1.35	0.22	44.51	49.82	97.66
123	13/8/2014	12:45:36 12:45:04	1205	0.15 0.5	0.75 1.26	0.17	26.47	29.57	57.96
124	13/8/2014	12:50:36 12:50:04	1210	0.15 0.5	0.72 1.32	0.20	36.25	40.76	79.89
125	13/8/2014	12:55:36 12:55:04	1215	0.15 0.5	0.77 1.10	0.11	8.51	11.65	22.83
126	13/8/2014	13:00:36 13:00:04	1220	0.15 0.5	0.60 1.16	0.19	41.58	34.71	68.04
127	13/8/2014	13:05:36 13:05:04	1225	0.15 0.5	0.72 1.14	0.14	20.20	20.37	39.93
128	13/8/2014	13:10:36 13:10:04	1230	0.15 0.5	0.69 1.16	0.16	25.68	24.33	47.69
129	13/8/2014	13:15:36 13:15:04	1235	0.15 0.5	0.65 1.13	0.16	29.60	25.69	50.36
130	13/8/2014	13:20:36 13:20:04	1240	0.15 0.5	0.69 1.09	0.13	19.24	17.89	35.07
131	13/8/2014	13:25:36 13:25:04	1245	0.15 0.5	0.58 0.96	0.13	25.12	16.61	32.56
132	13/8/2014	13:30:36 13:30:04	1250	0.15 0.5	0.62 0.94	0.11	14.59	11.39	22.33
133	13/8/2014	13:35:36 13:35:04	1255	0.15 0.5	0.59 0.94	0.12	20.05	13.63	26.73
134	13/8/2014	13:40:36 13:40:04	1260	0.15 0.5	0.58 0.93	0.12	19.90	13.26	26.00
135	13/8/2014	13:45:36 13:45:04	1265	0.15 0.5	0.53 0.88	0.12	24.20	13.38	26.22
136	13/8/2014	13:50:36 13:50:04	1270	0.15 0.5	0.49 0.77	0.09	18.81	8.86	17.36

No.	Date	Time	Minute	Z (m)	U (m/s)	u_* (m/s)	Z_0 (mm)	τ_0 (N/m^2)	D_{mobile} ($\theta = 0.04$; mm)
137	13/8/2014	13:55:36	1275	0.15	0.52	0.09	15.90	8.49	16.64
		13:55:04		0.5	0.79				
138	13/8/2014	14:00:36	1280	0.15	0.50	0.09	16.42	8.20	16.07
		14:00:04		0.5	0.77				
139	13/8/2014	14:05:36	1285	0.15	0.47	0.11	27.48	12.53	24.56
		14:05:04		0.5	0.81				
140	13/8/2014	14:10:36	1290	0.15	0.53	0.08	12.10	7.05	13.82
		14:10:04		0.5	0.78				
141	13/8/2014	14:15:36	1295	0.15	0.52	0.10	20.39	10.66	20.90
		14:15:04		0.5	0.83				
142	13/8/2014	14:20:36	1300	0.15	0.50	0.11	26.41	13.08	25.64
		14:20:04		0.5	0.84				
143	13/8/2014	14:25:36	1305	0.15	0.48	0.10	22.13	9.90	19.41
		14:25:04		0.5	0.78				
144	13/8/2014	14:30:36	1310	0.15	0.50	0.11	23.65	11.72	22.98
		14:30:04		0.5	0.83				
145	13/8/2014	14:35:36	1315	0.15	0.51	0.10	21.40	10.79	21.15
		14:35:04		0.5	0.82				
146	13/8/2014	14:40:36	1320	0.15	0.47	0.11	26.90	11.97	23.46
		14:40:04		0.5	0.80				
147	13/8/2014	14:45:36	1325	0.15	0.57	0.08	8.61	6.47	12.69
		14:45:04		0.5	0.82				
148	13/8/2014	14:50:36	1330	0.15	0.54	0.08	11.22	6.83	13.39
		14:50:04		0.5	0.78				
149	13/8/2014	14:55:36	1335	0.15	0.55	0.08	10.22	6.64	13.02
		14:55:04		0.5	0.79				
150	13/8/2014	15:00:36	1340	0.15	0.50	0.08	12.70	6.62	12.98
		15:00:04		0.5	0.75				
151	13/8/2014	15:05:36	1345	0.15	0.51	0.08	12.87	7.03	13.78
		15:05:04		0.5	0.77				
152	13/8/2014	15:10:36	1350	0.15	0.55	0.07	7.84	5.59	10.97
		15:10:04		0.5	0.78				
153	13/8/2014	15:15:36	1355	0.15	0.59	0.06	3.88	4.11	8.05
		15:15:04		0.5	0.78				
154	13/8/2014	15:20:36	1360	0.15	0.57	0.07	4.79	4.34	8.50
		15:20:04		0.5	0.77				
155	13/8/2014	15:25:36	1365	0.15	0.58	0.07	5.94	5.10	10.00
		15:25:04		0.5	0.79				
156	13/8/2014	15:30:36	1370	0.15	0.57	0.06	3.06	3.40	6.66
		15:30:04		0.5	0.74				
157	13/8/2014	15:35:36	1375	0.15	0.54	0.06	3.60	3.31	6.48
		15:35:04		0.5	0.71				
158	13/8/2014	15:40:36	1380	0.15	0.51	0.07	6.55	4.24	8.30
		15:40:04		0.5	0.71				
159	13/8/2014	15:45:36	1385	0.15	0.55	0.07	6.30	4.76	9.34
		15:45:04		0.5	0.75				

No.	Date	Time	Minute	Z (m)	U (m/s)	u_* (m/s)	Z_0 (mm)	τ_0 (N/m²)	D_{mobile} ($\theta = 0.04$; mm)
160	13/8/2014	15:50:36	1390	0.15	0.55	0.05	1.26	2.11	4.13
		15:50:04		0.5	0.69				
161	13/8/2014	15:55:36	1395	0.15	0.54	0.06	4.26	3.72	7.29
		15:55:04		0.5	0.73				
162	13/8/2014	16:00:36	1400	0.15	0.49	0.07	10.68	5.55	10.88
		16:00:04		0.5	0.72				
163	13/8/2014	16:05:36	1405	0.15	0.54	0.06	3.56	3.39	6.64
		16:05:04		0.5	0.72				
164	13/8/2014	16:10:36	1410	0.15	0.54	0.05	2.00	2.47	4.83
		16:10:04		0.5	0.69				
165	13/8/2014	16:15:36	1415	0.15	0.53	0.04	0.38	1.23	2.42
		16:15:04		0.5	0.63				
166	13/8/2014	16:20:36	1420	0.15	0.49	0.02	4.72E-03	0.36	0.71
		16:20:04		0.5	0.55				
167	13/8/2014	16:30:36	1430	0.15	0.47	0.01	1.11E-04	0.18	0.35
		16:30:04		0.5	0.51				
168	13/8/2014	19:55:36	1635	0.15	0.51	0.04	0.55	1.33	2.61
		19:55:04		0.5	0.62				
169	13/8/2014	20:00:36	1640	0.15	0.65	0.02	3.18E-04	0.40	0.77
		20:00:04		0.5	0.71				
170	13/8/2014	20:05:36	1645	0.15	0.92	0.07	0.57	4.37	8.57
		20:05:04		0.5	1.12				
171	13/8/2014	20:10:36	1650	0.15	1.05	0.07	0.51	5.48	10.75
		20:10:04		0.5	1.27				
172	13/8/2014	20:15:36	1655	0.15	1.34	0.09	0.39	8.10	15.87
		20:15:04		0.5	1.61				
173	13/8/2014	20:20:36	1660	0.15	1.30	0.09	0.56	8.64	16.93
		20:20:04		0.5	1.58				
174	13/8/2014	20:25:36	1665	0.15	1.27	0.06	0.04	3.77	7.38
		20:25:04		0.5	1.45				
175	13/8/2014	20:30:36	1670	0.15	1.38	0.01	5.04E-27	0.07	0.14
		20:30:04		0.5	1.41				
176	13/8/2014	20:35:36	1675	0.15	1.26	0.04	1.03E-03	1.80	3.52
		20:35:04		0.5	1.39				
177	13/8/2014	20:40:36	1680	0.15	1.57	0.09	0.14	8.20	16.07
		20:40:04		0.5	1.85				
178	13/8/2014	20:50:36	1690	0.15	1.29	0.03	0.00	1.03	2.02
		20:50:04		0.5	1.38				
179	13/8/2014	20:55:36	1695	0.15	1.13	0.02	5.54E-09	0.36	0.70
		20:55:04		0.5	1.19				
180	13/8/2014	21:05:36	1705	0.15	0.86	0.03	2.95E-03	1.01	1.97
		21:05:04		0.5	0.95				
181	13/8/2014	21:10:36	1710	0.15	0.77	0.06	0.57	3.03	5.94
		21:10:04		0.5	0.93				
182	13/8/2014	21:15:36	1715	0.15	0.62	0.01	0.00	0.20	0.40
		21:15:04		0.5	0.66				

No.	Date	Time	Minute	Z (m)	U (m/s)	u_* (m/s)	Z_0 (mm)	τ_0 (N/m^2)	D_{mobile} ($\theta = 0.04$; mm)
183	13/8/2014	21:25:36 21:25:04	1725	0.15 0.5	0.49 0.61	0.04	1.08	1.60	3.14
184	13/8/2014	21:30:36 21:30:04	1730	0.15 0.5	0.54 0.56	0.01	3.70E-16	0.03	0.06
185	13/8/2014	22:25:36 22:25:04	1785	0.15 0.5	0.21 0.22	0.00	5.25E-06	0.02	0.05
186	13/8/2014	22:30:36 22:30:04	1790	0.15 0.5	0.16 0.22	0.02	4.30	0.34	0.66
187	13/8/2014	22:35:36 22:35:04	1795	0.15 0.5	0.12 0.19	0.02	19.64	0.55	1.09
188	13/8/2014	22:40:36 22:40:04	1800	0.15 0.5	0.14 0.18	0.01	2.86	0.20	0.40
189	13/8/2014	22:45:36 22:45:04	1805	0.15 0.5	0.06 0.13	0.02	47.60	0.51	1.00
190	13/8/2014	22:50:36 22:50:04	1810	0.15 0.5	0.07 0.16	0.03	57.73	0.84	1.65
191	13/8/2014	22:55:36 22:55:04	1815	0.15 0.5	0.06 0.12	0.02	40.38	0.36	0.71
192	13/8/2014	23:00:36 23:00:04	1820	0.15 0.5	0.05 0.09	0.01	39.93	0.19	0.38
193	13/8/2014	23:05:36 23:05:04	1825	0.15 0.5	0.09 0.12	0.01	1.78	0.07	0.14
194	13/8/2014	23:20:36 23:20:04	1840	0.15 0.5	0.45 0.53	0.03	0.12	0.64	1.26
195	13/8/2014	23:25:36 23:25:04	1845	0.15 0.5	0.46 0.56	0.03	0.52	1.07	2.09
196	13/8/2014	23:30:36 23:30:04	1850	0.15 0.5	0.49 0.68	0.06	6.20	3.85	7.54
197	13/8/2014	23:35:36 23:35:04	1855	0.15 0.5	0.62 0.78	0.05	1.07	2.55	5.01
198	13/8/2014	23:40:36 23:40:04	1860	0.15 0.5	0.70 0.86	0.05	0.70	2.72	5.32
199	13/8/2014	23:45:36 23:45:04	1865	0.15 0.5	0.83 0.98	0.05	0.24	2.66	5.22
200	13/8/2014	23:50:36 23:50:04	1870	0.15 0.5	1.09 1.36	0.09	1.31	8.43	16.53
201	13/8/2014	23:55:36 23:55:04	1875	0.15 0.5	1.14 1.52	0.13	4.12	16.09	31.53
202	14/8/2014	0:00:36 0:00:04	1880	0.15 0.5	1.18 1.45	0.09	0.76	7.97	15.63
203	14/8/2014	0:05:36 0:05:04	1885	0.15 0.5	1.16 1.52	0.12	2.81	13.69	26.83
204	14/8/2014	0:10:36 0:10:04	1890	0.15 0.5	1.17 1.69	0.17	9.83	29.44	57.71
205	14/8/2014	0:15:36 0:15:04	1895	0.15 0.5	1.18 1.47	0.09	0.94	8.72	17.09
206	14/8/2014	0:20:36 0:20:04	1900	0.15 0.5	1.26 1.50	0.08	0.30	6.52	12.78

No.	Date	Time	Minute	Z (m)	U (m/s)	u_* (m/s)	Z_0 (mm)	τ_0 (N/m²)	D_{mobile} ($\theta = 0.04$; mm)
207	14/8/2014	0:25:36 0:25:04	1905	0.15 0.5	1.14 1.41	0.09	0.91	7.97	15.62
208	14/8/2014	0:35:36 0:35:04	1915	0.15 0.5	1.30 1.50	0.07	0.06	4.48	8.78
209	14/8/2014	0:40:36 0:40:04	1920	0.15 0.5	1.19 1.54	0.12	2.70	13.98	27.41
210	14/8/2014	0:45:36 0:45:04	1925	0.15 0.5	1.02 1.38	0.12	4.89	14.21	27.86
211	14/8/2014	0:50:36 0:50:04	1930	0.15 0.5	1.08 1.39	0.10	2.28	10.66	20.90
212	14/8/2014	0:55:36 0:55:04	1935	0.15 0.5	0.96 1.20	0.08	1.22	6.34	12.42
213	14/8/2014	1:00:36 1:00:04	1940	0.15 0.5	1.05 1.31	0.08	1.02	7.14	14.00
214	14/8/2014	1:05:36 1:05:04	1945	0.15 0.5	0.93 1.28	0.11	5.68	13.02	25.53
215	14/8/2014	1:10:36 1:10:04	1950	0.15 0.5	0.93 1.22	0.10	3.51	9.74	19.09
216	14/8/2014	1:15:36 1:15:04	1955	0.15 0.5	0.95 1.20	0.08	1.39	6.62	12.97
217	14/8/2014	1:25:36 1:25:04	1965	0.15 0.5	0.88 1.13	0.08	2.04	6.72	13.17
218	14/8/2014	1:30:36 1:30:04	1970	0.15 0.5	0.93 1.20	0.09	2.31	8.03	15.74
219	14/8/2014	1:35:36 1:35:04	1975	0.15 0.5	0.77 1.12	0.11	9.97	13.07	25.62
220	14/8/2014	1:40:36 1:40:04	1980	0.15 0.5	0.79 0.96	0.06	0.64	3.34	6.55
221	14/8/2014	1:45:36 1:45:04	1985	0.15 0.5	0.76 0.97	0.07	1.88	4.87	9.54
222	14/8/2014	1:50:36 1:50:04	1990	0.15 0.5	0.75 0.86	0.04	0.03	1.29	2.52
223	14/8/2014	1:55:36 1:55:04	1995	0.15 0.5	0.78 0.88	0.03	0.01	1.11	2.18
224	14/8/2014	2:00:36 2:00:04	2000	0.15 0.5	0.73 0.88	0.05	0.39	2.42	4.74
225	14/8/2014	2:05:36 2:05:04	2005	0.15 0.5	0.67 0.86	0.06	2.09	3.97	7.78
226	14/8/2014	2:10:36 2:10:04	2010	0.15 0.5	0.61 0.77	0.05	1.22	2.59	5.08
227	14/8/2014	2:15:36 2:15:04	2015	0.15 0.5	0.61 0.79	0.06	2.25	3.38	6.63
228	14/8/2014	2:20:36 2:20:04	2020	0.15 0.5	0.62 0.77	0.05	0.99	2.45	4.81
229	14/8/2014	2:25:36 2:25:04	2025	0.15 0.5	0.58 0.69	0.04	0.32	1.42	2.78

No.	Date	Time	Minute	Z (m)	U (m/s)	u_* (m/s)	Z_0 (mm)	τ_0 (N/m^2)	D_{mobile} ($\theta = 0.04$; mm)
230	14/8/2014	2:30:36	2030	0.15	0.59	0.06	3.08	3.66	7.17
		2:30:04		0.5	0.77				
231	14/8/2014	2:35:36	2035	0.15	0.61	0.03	0.07	1.02	1.99
		2:35:04		0.5	0.71				
232	14/8/2014	2:40:36	2040	0.15	0.60	0.05	1.27	2.49	4.88
		2:40:04		0.5	0.75				
233	14/8/2014	2:45:36	2045	0.15	0.60	0.03	0.11	1.11	2.17
		2:45:04		0.5	0.70				
234	14/8/2014	2:50:36	2050	0.15	0.62	0.03	0.10	1.14	2.24
		2:50:04		0.5	0.72				
235	14/8/2014	2:55:36	2055	0.15	0.58	0.05	0.89	2.08	4.08
		2:55:04		0.5	0.72				
236	14/8/2014	3:00:36	2060	0.15	0.60	0.04	0.18	1.27	2.50
		3:00:04		0.5	0.71				
237	14/8/2014	3:05:36	2065	0.15	0.62	0.04	0.23	1.47	2.88
		3:05:04		0.5	0.74				
238	14/8/2014	3:10:36	2070	0.15	0.61	0.04	0.20	1.38	2.70
		3:10:04		0.5	0.73				
239	14/8/2014	3:15:36	2075	0.15	0.61	0.04	0.65	2.00	3.92
		3:15:04		0.5	0.74				
240	14/8/2014	3:20:36	2080	0.15	0.62	0.02	0.01	0.61	1.20
		3:20:04		0.5	0.69				
241	14/8/2014	3:25:36	2085	0.15	0.57	0.03	0.03	0.69	1.35
		3:25:04		0.5	0.64				
242	14/8/2014	3:30:36	2090	0.15	0.57	0.02	2.34E-03	0.43	0.84
		3:30:04		0.5	0.63				
243	14/8/2014	3:35:36	2095	0.15	0.62	0.01	1.45E-07	0.14	0.28
		3:35:04		0.5	0.65				
244	14/8/2014	3:40:36	2100	0.15	0.64	0.00	3.90E-22	0.02	0.04
		3:40:04		0.5	0.65				
245	14/8/2014	3:45:36	2105	0.15	0.61	0.01	4.33E-08	0.12	0.24
		3:45:04		0.5	0.65				
246	14/8/2014	3:50:36	2110	0.15	0.60	0.01	7.14E-07	0.16	0.31
		3:50:04		0.5	0.64				
247	14/8/2014	3:55:36	2115	0.15	0.60	0.01	7.14E-07	0.16	0.30
		3:55:04		0.5	0.63				
248	14/8/2014	4:00:36	2120	0.15	0.58	0.01	3.28E-06	0.17	0.34
		4:00:04		0.5	0.62				
249	14/8/2014	4:05:36	2125	0.15	0.58	0.01	2.66E-10	0.07	0.14
		4:05:04		0.5	0.60				
250	14/8/2014	4:10:36	2130	0.15	0.60	0.01	4.33E-08	0.12	0.23
		4:10:04		0.5	0.63				
251	14/8/2014	4:15:36	2135	0.15	0.61	0.00	2.94E-51	0.00	0.01
		4:15:04		0.5	0.61				
252	14/8/2014	4:20:36	2140	0.15	0.59	0.01	2.66E-13	0.05	0.09
		4:20:04		0.5	0.61				

No.	Date	Time	Minute	Z (m)	U (m/s)	u_* (m/s)	Z_0 (mm)	τ_0 (N/m²)	D_{mobile} ($\theta = 0.04$; mm)
253	14/8/2014	4:25:36 4:25:04	2145	0.15 0.5	0.61 0.62	0.00	8.43E-59	0.00	0.01
254	14/8/2014	4:30:36 4:30:04	2150	0.15 0.5	0.57 0.63	0.02	2.04E-03	0.41	0.80
255	14/8/2014	4:35:36 4:35:04	2155	0.15 0.5	0.56 0.59	0.01	1.65E-07	0.12	0.23
256	14/8/2014	4:45:36 4:45:04	2165	0.15 0.5	0.55 0.67	0.04	0.40	1.40	2.74
257	14/8/2014	8:20:36 8:20:04	2380	0.15 0.5	0.58 0.60	0.01	4.75E-10	0.08	0.15
258	14/8/2014	8:25:36 8:25:04	2385	0.15 0.5	0.59 0.63	0.01	1.20E-06	0.16	0.31
259	14/8/2014	8:30:36 8:30:04	2390	0.15 0.5	0.90 0.92	0.01	7.59E-21	0.05	0.10
260	14/8/2014	8:35:36 8:35:04	2395	0.15 0.5	1.02 1.11	0.03	2.03E-04	0.92	1.80
261	14/8/2014	8:40:36 8:40:04	2400	0.15 0.5	1.26 1.39	0.04	8.79E-04	1.76	3.45
262	14/8/2014	8:45:36 8:45:04	2405	0.15 0.5	1.29 1.41	0.04	3.59E-04	1.59	3.11
263	14/8/2014	8:50:36 8:50:04	2410	0.15 0.5	1.10 1.30	0.07	0.20	4.40	8.63
264	14/8/2014	8:55:36 8:55:04	2415	0.15 0.5	1.18 1.36	0.06	0.04	3.37	6.60
265	14/8/2014	9:00:36 9:00:04	2420	0.15 0.5	1.21 1.37	0.05	0.02	2.81	5.51
266	14/8/2014	9:05:36 9:05:04	2425	0.15 0.5	1.25 1.56	0.10	1.09	10.37	20.34
267	14/8/2014	9:10:36 9:10:04	2430	0.15 0.5	1.54 1.68	0.05	0.00	2.19	4.29
268	14/8/2014	9:20:36 9:20:04	2440	0.15 0.5	1.20 1.60	0.13	4.12	17.86	35.01
269	14/8/2014	9:25:36 9:25:04	2445	0.15 0.5	1.41 1.62	0.07	0.04	4.62	9.06
270	14/8/2014	9:35:36 9:35:04	2455	0.15 0.5	1.16 1.38	0.07	0.28	5.45	10.69
271	14/8/2014	9:40:36 9:40:04	2460	0.15 0.5	1.22 1.31	0.03	0.00	0.93	1.82
272	14/8/2014	9:45:36 9:45:04	2465	0.15 0.5	0.94 1.10	0.05	0.15	2.97	5.82
273	14/8/2014	9:50:36 9:50:04	2470	0.15 0.5	0.95 0.98	0.01	0.00	0.13	0.26
274	14/8/2014	10:00:36 10:00:04	2480	0.15 0.5	0.87 1.07	0.07	0.80	4.40	8.62
275	14/8/2014	10:10:36 10:10:04	2490	0.15 0.5	0.87 1.03	0.05	0.24	2.92	5.73

No.	Date	Time	Minute	Z (m)	U (m/s)	u_* (m/s)	Z_0 (mm)	τ_0 (N/m²)	D_{mobile} ($\theta = 0.04$; mm)
276	14/8/2014	10:25:36 10:25:04	2505	0.15 0.5	0.71 0.74	0.01	0.00	0.16	0.31
277	14/8/2014	10:30:36 10:30:04	2510	0.15 0.5	0.61 0.74	0.04	0.57	1.93	3.78
278	14/8/2014	10:35:36 10:35:04	2515	0.15 0.5	0.56 0.68	0.04	0.45	1.50	2.93
279	14/8/2014	10:40:36 10:40:04	2520	0.15 0.5	0.51 0.62	0.04	0.63	1.37	2.69
280	14/8/2014	10:45:36 10:45:04	2525	0.15 0.5	0.52 0.65	0.04	1.44	1.99	3.91
281	14/8/2014	10:50:36 10:50:04	2530	0.15 0.5	0.40 0.45	0.02	0.03	0.35	0.69
282	14/8/2014	10:55:36 10:55:04	2535	0.15 0.5	0.39 0.52	0.04	3.72	1.79	3.51
283	14/8/2014	11:00:36 11:00:04	2540	0.15 0.5	0.29 0.39	0.03	3.20	0.94	1.84
284	14/8/2014	11:05:36 11:05:04	2545	0.15 0.5	0.23 0.38	0.05	20.27	2.20	4.32
285	14/8/2014	11:10:36 11:10:04	2550	0.15 0.5	0.16 0.32	0.05	42.73	2.68	5.25
286	14/8/2014	11:15:36 11:15:04	2555	0.15 0.5	0.06 0.12	0.02	53.56	0.47	0.92
287	14/8/2014	11:20:36 11:20:04	2560	0.15 0.5	0.05 0.10	0.01	32.49	0.20	0.39
288	14/8/2014	11:25:36 11:25:04	2565	0.15 0.5	0.07 0.08	0.00	0.38	0.02	0.04
289	14/8/2014	11:30:36 11:30:04	2570	0.15 0.5	0.08 0.11	0.01	5.85	0.09	0.18
290	14/8/2014	11:45:36 11:45:04	2585	0.15 0.5	0.35 0.51	0.05	9.39	2.62	5.14
291	14/8/2014	11:50:36 11:50:04	2590	0.15 0.5	0.40 0.64	0.08	19.67	6.27	12.29
292	14/8/2014	11:55:36 11:55:04	2595	0.15 0.5	0.42 0.59	0.06	8.44	3.39	6.64
293	14/8/2014	12:00:36 12:00:04	2600	0.15 0.5	0.41 0.65	0.08	17.96	6.12	11.99
294	14/8/2014	12:05:36 12:05:04	2605	0.15 0.5	0.68 0.89	0.07	2.94	4.82	9.44
295	14/8/2014	12:10:36 12:10:04	2610	0.15 0.5	0.75 1.02	0.09	5.69	8.32	16.32
296	14/8/2014	12:15:36 12:15:04	2615	0.15 0.5	1.06 1.58	0.17	12.57	29.38	57.60
297	14/8/2014	12:20:36 12:20:04	2620	0.15 0.5	0.98 1.62	0.21	23.81	45.29	88.79
298	14/8/2014	12:25:36 12:25:04	2625	0.15 0.5	0.98 1.52	0.18	16.92	32.44	63.60

No.	Date	Time	Minute	Z (m)	U (m/s)	u_* (m/s)	Z_0 (mm)	τ_0 (N/m^2)	D_{mobile} ($\theta = 0.04$; mm)
299	14/8/2014	12:30:36	2630	0.15	1.09	0.16	9.47	24.93	48.88
		12:30:04		0.5	1.57				
300	14/8/2014	12:35:36	2635	0.15	1.00	0.18	15.79	31.48	61.71
		12:35:04		0.5	1.53				
301	14/8/2014	12:40:36	2640	0.15	0.96	0.17	15.17	28.19	55.25
		12:40:04		0.5	1.47				
302	14/8/2014	12:45:36	2645	0.15	0.93	0.21	24.52	42.47	83.25
		12:45:04		0.5	1.55				
303	14/8/2014	12:50:36	2650	0.15	1.25	0.20	11.89	39.17	76.79
		12:50:04		0.5	1.85				
304	14/8/2014	12:55:36	2655	0.15	1.35	0.22	13.33	49.88	97.78
		12:55:04		0.5	2.02				
305	14/8/2014	13:00:36	2660	0.15	1.19	0.18	10.10	31.35	61.45
		13:00:04		0.5	1.73				
306	14/8/2014	13:05:36	2665	0.15	1.03	0.18	15.52	32.89	64.47
		13:05:04		0.5	1.57				
307	14/8/2014	13:10:36	2670	0.15	1.12	0.20	16.32	40.55	79.48
		13:10:04		0.5	1.72				
308	14/8/2014	13:15:36	2675	0.15	1.00	0.20	21.38	42.01	82.36
		13:15:04		0.5	1.62				
309	14/8/2014	13:20:36	2680	0.15	1.00	0.20	19.43	38.26	75.00
		13:20:04		0.5	1.59				
310	14/8/2014	13:25:36	2685	0.15	0.94	0.19	20.20	35.06	68.73
		13:25:04		0.5	1.50				
311	14/8/2014	13:30:36	2690	0.15	1.07	0.20	17.26	39.23	76.91
		13:30:04		0.5	1.67				
312	14/8/2014	13:35:36	2695	0.15	1.06	0.16	10.83	26.17	51.29
		13:35:04		0.5	1.55				
313	14/8/2014	13:40:36	2700	0.15	1.07	0.17	12.33	29.56	57.95
		13:40:04		0.5	1.59				
314	14/8/2014	13:45:36	2705	0.15	1.00	0.13	7.22	17.50	34.30
		13:45:04		0.5	1.40				
315	14/8/2014	13:50:36	2710	0.15	0.95	0.17	15.72	28.66	56.18
		13:50:04		0.5	1.46				
316	14/8/2014	13:55:36	2715	0.15	0.81	0.17	21.25	27.80	54.49
		13:55:04		0.5	1.32				
317	14/8/2014	14:00:36	2720	0.15	0.90	0.12	6.76	13.61	26.69
		14:00:04		0.5	1.26				
318	14/8/2014	14:05:36	2725	0.15	0.90	0.18	19.68	31.56	61.87
		14:05:04		0.5	1.44				
319	14/8/2014	14:10:36	2730	0.15	0.88	0.15	15.65	24.01	47.06
		14:10:04		0.5	1.34				
320	14/8/2014	14:15:36	2735	0.15	0.79	0.15	17.57	21.54	42.23
		14:15:04		0.5	1.23				
321	14/8/2014	14:20:36	2740	0.15	0.74	0.17	26.42	29.27	57.37
		14:20:04		0.5	1.26				

No.	Date	Time	Minute	Z (m)	U (m/s)	u_* (m/s)	Z_0 (mm)	τ_0 (N/m²)	D_{mobile} ($\theta = 0.04$; mm)
322	14/8/2014	14:25:36 14:25:04	2745	0.15 0.5	0.76 1.18	0.14	16.72	19.15	37.54
323	14/8/2014	14:30:36 14:30:04	2750	0.15 0.5	0.74 1.13	0.13	14.69	16.29	31.94
324	14/8/2014	14:35:36 14:35:04	2755	0.15 0.5	0.75 1.03	0.09	5.75	8.57	16.80
325	14/8/2014	14:40:36 14:40:04	2760	0.15 0.5	0.74 1.03	0.09	6.66	9.02	17.69
326	14/8/2014	14:45:36 14:45:04	2765	0.15 0.5	0.72 1.05	0.11	10.51	11.79	23.12
327	14/8/2014	14:50:36 14:50:04	2770	0.15 0.5	0.66 1.04	0.13	18.49	15.90	31.18
328	14/8/2014	14:55:36 14:55:04	2775	0.15 0.5	0.68 1.08	0.13	18.78	17.17	33.66
329	14/8/2014	15:00:36 15:00:04	2780	0.15 0.5	0.72 1.05	0.11	10.86	11.98	23.48
330	14/8/2014	15:05:36 15:05:04	2785	0.15 0.5	0.67 1.06	0.13	18.60	16.44	32.23
331	14/8/2014	15:10:36 15:10:04	2790	0.15 0.5	0.70 1.14	0.15	22.23	21.58	42.31
332	14/8/2014	15:15:36 15:15:04	2795	0.15 0.5	0.72 1.10	0.12	14.62	15.46	30.31
333	14/8/2014	15:20:36 15:20:04	2800	0.15 0.5	0.72 1.12	0.13	17.36	17.82	34.94
334	14/8/2014	15:25:36 15:25:04	2805	0.15 0.5	0.72 1.16	0.15	20.75	21.22	41.60
335	14/8/2014	15:30:36 15:30:04	2810	0.15 0.5	0.71 1.10	0.13	17.33	17.28	33.88
336	14/8/2014	15:35:36 15:35:04	2815	0.15 0.5	0.71 1.05	0.12	13.03	13.34	26.15
337	14/8/2014	15:40:36 15:40:04	2820	0.15 0.5	0.69 1.07	0.13	17.04	16.01	31.39
338	14/8/2014	15:45:36 15:45:04	2825	0.15 0.5	0.67 1.00	0.11	13.53	12.37	24.25
339	14/8/2014	15:50:36 15:50:04	2830	0.15 0.5	0.69 0.98	0.10	8.77	9.45	18.53
340	14/8/2014	15:55:36 15:55:04	2835	0.15 0.5	0.70 1.01	0.10	10.27	10.88	21.34
341	14/8/2014	16:00:36 16:00:04	2840	0.15 0.5	0.70 1.01	0.10	10.12	10.67	20.92
342	14/8/2014	16:05:36 16:05:04	2845	0.15 0.5	0.70 1.02	0.11	10.83	11.36	22.27
343	14/8/2014	16:10:36 16:10:04	2850	0.15 0.5	0.73 1.03	0.10	8.27	10.10	19.80
344	14/8/2014	16:15:36 16:15:04	2855	0.15 0.5	0.70 1.00	0.10	9.00	9.87	19.35

No.	Date	Time	Minute	Z (m)	U (m/s)	u_* (m/s)	Z_0 (mm)	τ_0 (N/m^2)	D_{mobile} ($\theta = 0.04$; mm)
345	14/8/2014	16:20:36 16:20:04	2860	0.15 0.5	0.72 1.04	0.11	9.85	11.19	21.93
346	14/8/2014	16:25:36 16:25:04	2865	0.15 0.5	0.73 1.01	0.09	6.94	8.96	17.56
347	14/8/2014	16:30:36 16:30:04	2870	0.15 0.5	0.72 1.02	0.10	8.46	9.97	19.55
348	14/8/2014	16:35:36 16:35:04	2875	0.15 0.5	0.71 1.04	0.11	11.46	12.03	23.58
349	14/8/2014	16:40:36 16:40:04	2880	0.15 0.5	0.68 1.00	0.11	11.34	11.14	21.85
350	14/8/2014	16:45:36 16:45:04	2885	0.15 0.5	0.70 1.07	0.12	16.01	15.61	30.60
351	14/8/2014	16:50:36 16:50:04	2890	0.15 0.5	0.68 0.99	0.10	11.04	10.73	21.02
352	14/8/2014	16:55:36 16:55:04	2895	0.15 0.5	0.65 0.87	0.08	4.84	5.65	11.07
353	14/8/2014	17:00:36 17:00:04	2900	0.15 0.5	0.63 1.10	0.16	30.31	24.45	47.93

Appendix B Grain size distribution for the bulk sediment

Table B 1 Grain size distribution of the bed and bedload samples collected during the study period.

	Date and sample	14 July 13	11-12 Feb 13	12-13 Mar 13		27-28 May 13	
		Bed sample	Flood (invalid)	Flood	Ebb	Flood	Ebb
Cumulative percentile values (μm)	D_{10}	203.6	116.9	177.4	177.7	24.04	139.0
	D_{50}	16663.4	195.6	6589.3	6408.5	164.4	472.4
	D_{90}	54113.8	381.2	33134.0	30574.1	1458.5	21926.3
	D_{90} / D_{10}	265.8	3.260	186.7	172.0	60.67	157.8
	$D_{90} - D_{10}$	53910.2	264.2	32956.6	30396.4	1434.4	21787.3
	D_{75} / D_{25}	12.71	1.658	7.667	9.515	3.230	35.38
	$D_{75} - D_{25}$	37964.4	95.52	15831.2	15431.5	292.9	5948.1
Cumulative percentile values (ϕ)	D_{10}	-5.758	1.392	-5.050	-4.934	-0.544	-4.455
	D_{50}	-4.059	2.354	-2.720	-2.680	2.604	1.082
	D_{90}	2.296	3.096	2.495	2.492	5.379	2.847
	D_{90} / D_{10}	-0.399	2.225	-0.494	-0.505	-9.879	-0.639
	$D_{90} - D_{10}$	8.054	1.705	7.545	7.427	5.923	7.302
	D_{75} / D_{25}	0.316	1.355	0.298	0.209	2.367	-0.968
	$D_{75} - D_{25}$	3.668	0.730	2.939	3.250	1.691	5.145
% Gravel		79.4%	1.6%	78.2%	73.8%	6.1%	31.9%
% Sand		20.2%	95.6%	21.1%	24.9%	78.6%	66.4%
% Mud		0.3%	2.8%	0.7%	1.3%	15.3%	1.7%
% Very coarse gravel		33.2%	0.0%	10.6%	8.9%	0.0%	2.3%
% Coarse gravel		17.7%	1.0%	18.0%	18.1%	0.4%	14.4%
% Medium gravel		11.2%	0.1%	16.5%	17.9%	0.9%	6.7%
% Fine gravel		10.2%	0.3%	17.5%	15.5%	1.5%	4.2%
% Very fine gravel		7.1%	0.3%	15.6%	13.4%	3.3%	4.4%
% Very coarse sand		3.4%	0.2%	6.0%	5.6%	6.7%	6.5%
% Coarse sand		2.5%	4.1%	2.0%	2.1%	10.0%	10.9%
% Medium sand		1.9%	12.6%	1.2%	1.6%	7.1%	7.0%
% Fine sand		11.1%	70.9%	8.8%	12.6%	50.7%	41.0%
% Very fine sand		1.4%	7.6%	3.1%	3.0%	4.2%	1.0%
% Very coarse silt		0.1%	0.5%	0.1%	0.2%	2.5%	0.3%
% Coarse silt		0.1%	0.5%	0.1%	0.2%	2.5%	0.3%
% Medium silt		0.1%	0.5%	0.1%	0.2%	2.5%	0.3%
% Fine silt		0.1%	0.5%	0.1%	0.2%	2.5%	0.3%
% Very fine silt		0.1%	0.5%	0.1%	0.2%	2.5%	0.3%
% Clay		0.1%	0.5%	0.1%	0.2%	2.5%	0.3%

	Date and sample	28-29 May 13		25-26 June 13		23-24 July 13	
		Flood	Ebb	Flood	Ebb	Flood	Ebb
Cumulative percentile values (μm)	**D_{10}**	135.3	104.7	138.4	69.71	154.5	167.5
	D_{50}	3236.5	200.4	5920.3	192.8	6585.6	7247.9
	D_{90}	51529.0	12828.6	51081.6	2501.7	46893.8	47996.5
	D_{90} / D_{10}	381.0	122.5	369.0	35.89	303.5	286.6
	D_{90} - D_{10}	51393.7	12723.9	50943.1	2432.0	46739.2	47829.0
	D_{75} / D_{25}	70.91	8.966	160.4	6.106	21.59	14.10
	D_{75} - D_{25}	17599.2	1179.8	33273.8	698.8	26804.7	23306.5
Cumulative percentile values (ϕ)	**D_{10}**	-5.687	-3.681	-5.675	-1.323	-5.551	-5.585
	D_{50}	-1.694	2.319	-2.566	2.374	-2.719	-2.858
	D_{90}	2.886	3.256	2.853	3.842	2.694	2.578
	D_{90} / D_{10}	-0.507	-0.884	-0.503	-2.905	-0.485	-0.462
	D_{90} - D_{10}	8.573	6.937	8.527	5.165	8.245	8.163
	D_{75} / D_{25}	-0.479	-6.734	-0.446	11.08	0.079	0.179
	D_{75} - D_{25}	6.148	3.164	7.326	2.610	4.432	3.817
% Gravel		57.5%	22.4%	60.7%	12.0%	69.0%	73.8%
% Sand		37.9%	71.0%	36.7%	79.5%	29.2%	25.5%
% Mud		4.7%	6.6%	2.6%	8.4%	1.8%	0.7%
% Very coarse gravel		16.7%	3.5%	26.4%	0.0%	23.0%	19.6%
% Coarse gravel		10.5%	5.0%	15.0%	2.3%	14.5%	16.2%
% Medium gravel		8.6%	4.3%	6.3%	1.9%	9.9%	12.3%
% Fine gravel		10.5%	4.5%	5.6%	2.1%	9.7%	13.0%
% Very fine gravel		11.2%	5.0%	7.4%	5.7%	11.9%	12.6%
% Very coarse sand		8.4%	3.9%	5.3%	10.8%	7.7%	5.2%
% Coarse sand		5.4%	6.3%	3.6%	9.5%	2.6%	2.6%
% Medium sand		3.8%	9.7%	3.8%	10.8%	2.7%	2.8%
% Fine sand		17.7%	46.7%	21.2%	39.2%	13.8%	12.9%
% Very fine sand		2.6%	4.4%	2.8%	9.2%	2.4%	2.0%
% Very coarse silt		0.8%	1.1%	0.4%	1.4%	0.3%	0.1%
% Coarse silt		0.8%	1.1%	0.4%	1.4%	0.3%	0.1%
% Medium silt		0.8%	1.1%	0.4%	1.4%	0.3%	0.1%
% Fine silt		0.8%	1.1%	0.4%	1.4%	0.3%	0.1%
% Very fine silt		0.8%	1.1%	0.4%	1.4%	0.3%	0.1%
% Clay		0.8%	1.1%	0.4%	1.4%	0.3%	0.1%

	Date and sample	24-25 July 13		20-21 Aug 13	19-20 Sep 13	16-17 June 14	
		Flood	Ebb	Flood	Flood	Flood	Ebb
Cumulative percentile values (μm)	D_{10}	140.4	169.8	129.1	126.5	209.1	180.9
	D_{50}	3332.2	12767.6	1689.8	208.6	11755.5	6157.9
	D_{90}	35706.5	48589.9	34319.7	3376.8	50134.8	47105.3
	D_{90} / D_{10}	254.3	286.2	265.9	26.69	239.8	260.4
	D_{90} - D_{10}	35566.2	48420.2	34190.7	3250.3	49925.8	46924.4
	D_{75} / D_{25}	63.38	22.28	76.09	10.23	12.46	8.194
	D_{75} - D_{25}	18369.8	32917.5	12897.0	1393.2	29561.6	17002.1
Cumulative percentile values (ϕ)	D_{10}	-5.158	-5.603	-5.101	-1.756	-5.648	-5.558
	D_{50}	-1.736	-3.674	-0.757	2.261	-3.555	-2.622
	D_{90}	2.832	2.558	2.954	2.983	2.258	2.467
	D_{90} / D_{10}	-0.549	-0.457	-0.579	-1.699	-0.400	-0.444
	D_{90} - D_{10}	7.991	8.161	8.054	4.738	7.906	8.025
	D_{75} / D_{25}	-0.418	0.123	-0.685	-4.351	0.273	0.290
	D_{75} - D_{25}	5.986	4.478	6.250	3.354	3.640	3.035
% Gravel		58.5%	72.7%	47.4%	19.0%	79.7%	78.3%
% Sand		38.4%	26.6%	48.4%	76.8%	18.7%	19.4%
% Mud		3.1%	0.7%	4.2%	4.2%	1.6%	2.3%
% Very coarse gravel		14.7%	28.4%	11.3%	1.9%	25.1%	16.3%
% Coarse gravel		14.3%	18.5%	10.6%	0.1%	19.4%	12.1%
% Medium gravel		9.2%	9.2%	10.3%	1.6%	12.1%	14.7%
% Fine gravel		8.8%	8.5%	6.6%	4.3%	12.2%	18.8%
% Very fine gravel		11.5%	8.1%	8.5%	11.2%	10.9%	16.3%
% Very coarse sand		9.6%	5.1%	7.2%	10.9%	4.8%	4.9%
% Coarse sand		4.6%	3.8%	3.7%	5.2%	2.7%	2.0%
% Medium sand		3.1%	2.9%	5.5%	9.7%	1.9%	1.7%
% Fine sand		19.0%	13.1%	27.9%	46.3%	7.5%	9.7%
% Very fine sand		2.2%	1.6%	4.1%	4.8%	1.8%	1.2%
% Very coarse silt		0.5%	0.1%	0.7%	0.7%	0.3%	0.4%
% Coarse silt		0.5%	0.1%	0.7%	0.7%	0.3%	0.4%
% Medium silt		0.5%	0.1%	0.7%	0.7%	0.3%	0.4%
% Fine silt		0.5%	0.1%	0.7%	0.7%	0.3%	0.4%
% Very fine silt		0.5%	0.1%	0.7%	0.7%	0.3%	0.4%
% Clay		0.5%	0.1%	0.7%	0.7%	0.3%	0.4%

	Date and sample	14-15 July 14		15-16 July 14		12-13 Aug 14	13-14 Aug 14
		Flood	Ebb	Flood	Ebb	Ebb	Ebb
Cumulative percentile values (μm)	**D_{10}**	176.7	215.4	171.3	207.6	161.7	135.9
	D_{50}	2848.3	12340.0	3474.4	8026.4	20771.8	3449.9
	D_{90}	28995.0	47374.3	31115.9	47577.2	57434.8	52834.9
	D_{90} / D_{10}	164.1	219.9	181.6	229.2	355.1	388.7
	D_{90} - D_{10}	28818.3	47158.9	30944.6	47369.6	57273.1	52698.9
	D_{75} / D_{25}	5.201	13.62	13.55	16.18	34.63	167.0
	D_{75} - D_{25}	6593.5	32240.7	16373.6	27436.1	48551.6	33784.8
Cumulative percentile values (ϕ)	**D_{10}**	-4.858	-5.566	-4.960	-5.572	-5.844	-5.723
	D_{50}	-1.510	-3.625	-1.797	-3.005	-4.377	-1.787
	D_{90}	2.500	2.215	2.545	2.268	2.628	2.879
	D_{90} / D_{10}	-0.515	-0.398	-0.513	-0.407	-0.450	-0.503
	D_{90} - D_{10}	7.358	7.781	7.505	7.840	8.472	8.603
	D_{75} / D_{25}	0.215	0.264	0.093	0.175	0.094	-0.451
	D_{75} - D_{25}	2.379	3.768	3.760	4.017	5.114	7.384
% Gravel		65.9%	78.6%	65.5%	73.3%	71.8%	58.2%
% Sand		31.7%	19.5%	32.4%	25.4%	26.2%	38.2%
% Mud		2.5%	1.9%	2.1%	1.3%	1.9%	3.6%
% Very coarse gravel		8.4%	29.3%	9.1%	22.3%	43.3%	26.3%
% Coarse gravel		10.3%	16.6%	17.1%	17.7%	10.1%	11.1%
% Medium gravel		6.5%	11.4%	8.5%	10.0%	6.2%	5.3%
% Fine gravel		13.2%	10.6%	11.8%	10.7%	4.9%	5.4%
% Very fine gravel		27.4%	10.7%	19.2%	12.5%	7.3%	10.1%
% Very coarse sand		15.5%	6.1%	11.6%	9.1%	4.8%	5.7%
% Coarse sand		2.6%	2.6%	3.7%	4.2%	2.3%	3.8%
% Medium sand		2.0%	1.9%	2.7%	2.0%	3.1%	4.7%
% Fine sand		10.1%	7.2%	13.3%	8.5%	15.1%	21.1%
% Very fine sand		1.5%	1.6%	1.1%	1.6%	0.9%	3.0%
% Very coarse silt		0.4%	0.3%	0.3%	0.2%	0.3%	0.6%
% Coarse silt		0.4%	0.3%	0.3%	0.2%	0.3%	0.6%
% Medium silt		0.4%	0.3%	0.3%	0.2%	0.3%	0.6%
% Fine silt		0.4%	0.3%	0.3%	0.2%	0.3%	0.6%
% Very fine silt		0.4%	0.3%	0.3%	0.2%	0.3%	0.6%
% Clay		0.4%	0.3%	0.3%	0.2%	0.3%	0.6%

Table B 2 The dry weight of all bed and bedload samples collected during the study period.

Date and sample	14 July 13	11-12 Feb 13	12-13 Mar 13		27-28 May 13		28-29 May 13		25-26 June 13		23-24 July 13	
Grain size (μm)	Bed sample	Flood (invalid)	Flood	Ebb	Flood	Ebb	Flood	Ebb	Flood	Ebb	Flood	Ebb
> 90000	0	0	0	0	0	0	0	0	0	0	0	0
90000 - 63000	0	0	0	0	0	0	0	0	0	0	0	0
63000 - 45000	5525.25	0	510.04	171.14	0	0	295.19	0	383.34	0	598.35	670.03
45000 - 31500	2901.84	0	788.44	599.8	0	60.63	0	74.73	258.14	0	635.71	411.74
31500 - 22400	2332.97	35.4	971.55	708.02	0	181.89	65.15	70.62	179.44	10.66	234.93	407.87
22400 - 16000	1960.36	0	1130.69	775.91	4.34	180.8	119.3	28.43	166.86	12.28	499.57	452.35
16000 - 11200	1449.66	0	993.45	801.42	6.07	86.82	69.32	48.04	81.46	8.04	266.74	322.67
11200 - 8000	1341.74	2.9	966.55	686.54	3.82	82.32	82.51	40.06	70.16	11.01	251.92	346.1
8000 - 5600	1353.95	3.4	1053	678.04	6.91	56.7	94.53	44.83	65.41	9.96	253	352.37
5600 - 4000	1190.2	5.11	1019.6	610.78	8.88	50.29	89.81	47.49	68.53	10.3	254.11	354
4000 - 2800	1135.85	4.55	1098.44	606.47	13.49	60.33	110.88	53.8	88.39	25.4	321.1	395.02
2800 - 2000	642.78	4.37	752.18	505.8	21.69	50.36	86.53	48.2	88.31	30	305.34	285.61
2000 - 1400	516.13	4.13	542.1	371.98	46.65	82.97	102.81	47.51	91.45	60.25	293.46	197.58
1400 - 1000	330.31	3.82	174.85	98.36	24.24	82.82	45.69	32.62	34.89	45.63	109.1	82.93
1000 - 710	257.76	5.93	103.94	73.15	38.37	97.76	40.16	34.4	33.35	39.49	64.38	48.21
710 - 500	375.62	133.9	130.49	97.72	67.7	179.02	54.34	93.12	52.84	53.19	74.2	93.04
500 - 355	296.18	171.2	86.13	81.47	50.19	104.32	36.83	70.57	46.98	56.64	72.55	75.2
355 - 300	92.4	110.08	24.75	23.25	12.9	36.39	15.01	92.41	22.12	24.67	36.42	42.86
300 - 250	84.45	147.25	29.24	29.74	12.78	36.05	14.99	33.97	20.69	24.21	34.71	35.37
250 - 212	262.49	933.25	60.11	59.41	19.2	63.97	20	61.69	31.4	30.5	52.17	57.96
212 - 180	1704.41	266.12	214.45	499.94	88.05	342.57	69.64	277.81	86.15	62.61	148.22	146.5
180 - 125	793.72	1205.97	770.14	490.89	432.25	634.09	222.41	610.03	389.53	289.94	524.31	492.59
125 - 90	81.43	74.41	71.91	57.35	26.16	14.68	26.54	39.82	40.17	35.68	46.75	21.17
90 - 63	259.69	184.85	294.53	194.25	18.32	10.82	19.5	50.29	26.76	54.14	76.61	89.79
< 63	78.28	95.02	80.29	107.57	162.97	44.46	82.17	134.9	62.85	82.33	96.79	35.63
All	24967.47	3391.66	11866.87	8329	1064.98	2540.06	1763.31	2035.34	2389.22	976.93	5250.44	5416.59

Date and sample	24-25 July 13		20-21 Aug 13	19-20 Sep 13	16-17 June 14		14-15 July 14		15-16 July 14		12-13 Aug 14	13-14Aug 14
Grain size (μm)	Flood	Ebb	Flood	Flood	Flood	Ebb	Flood	Ebb	Flood	Ebb	Ebb	Ebb
> 90000	0	0	0	0	0	0	0	0	0	0	0	0
90000 - 63000	0	0	0	0	0	0	0	0	0	0	0	0
63000 - 45000	0	1444.07	96.34	0	1491.32	835.95	104.32	917.38	0	1209.79	1890.02	851.17
45000 - 31500	191.91	1795.27	138.4	29.78	1101.84	358.01	30.15	1422.34	247.78	1094.45	376.52	332.55
31500 - 22400	59.2	1196.62	48.12	0	842.91	425.32	95.86	617.67	328.91	1007.12	280.08	243.92
22400 - 16000	110.76	789.57	160.04	0	1075.54	431.3	65.13	612.55	102.84	727.88	226.77	237.12
16000 - 11200	54.79	549.63	107.13	8.99	636.83	522.01	51.91	433.96	94.91	550.2	182.03	119.64
11200 - 8000	59.14	474.72	100.2	15.52	583.14	542.81	50.05	453.18	124.57	462.85	137.51	115.96
8000 - 5600	50.65	492.99	75.56	27.94	630.45	676.5	81.44	423.76	129.68	524.97	127.43	115.54
5600 - 4000	59.03	454.2	57.29	37.69	606.38	683.08	127.33	397.74	175.51	553.81	129.57	122.61
4000 - 2800	71.96	508.92	82.25	68.48	470.79	702.78	191.85	444.14	237.7	625.85	185.09	210.12
2800 - 2000	70.56	396.78	89.87	101.62	628.16	476	240.97	389.25	259.58	639.94	195.72	240.59
2000 - 1400	84.67	357.06	110.38	125.59	319.02	271.98	212.2	314.75	230.61	613.72	181.03	186.6
1400 - 1000	34.39	212.48	35.52	39.93	166.74	82.5	31.87	156.09	71.84	305.99	70.33	66.07
1000 - 710	27.03	179.13	26.87	31.75	129.15	58.84	20.32	97.32	46.1	210.28	46.48	65.91
710 - 500	29.97	245.53	48	46.82	141.62	86.05	21.1	106.95	48.97	213.63	71.9	103.34
500 - 355	19.22	173.22	49.49	65.74	101.24	59.01	16.32	78.55	36.27	116.59	82.06	106.82
355 - 300	9.26	78.58	29.19	37.91	45.92	27.7	7.28	35.06	15.34	40.87	37.98	47.39
300 - 250	9.49	71.68	31.19	43.95	45.3	33.22	7.7	36.18	17.91	41.75	42.11	53.67
250 - 212	14.3	119.6	44.54	63.74	72.6	45.3	13.57	64.06	30.07	82.22	54.16	65.66
212 - 180	40.24	328.62	131.01	170.48	266.19	188.45	45.56	227.27	110.1	498.2	204.33	216.16
180 - 125	181.39	1016.24	385.96	471.62	424.69	463.67	99.62	270.63	205.3	282.02	526.45	655.93
125 - 90	17.81	74.97	54.04	24.98	50.26	53.68	15.72	50.22	15.68	58.98	20.81	49.28
90 - 63	9.66	106.46	28.97	47.67	131.47	32.49	8.28	75.3	11.89	98.77	25.37	84.39
< 63	39.24	80.25	84.37	64.16	162.47	166.87	39.14	147.57	54.6	135.62	101.21	160.89
All	1244.67	11146.59	2014.73	1524.36	10124.03	7223.52	1577.69	7771.92	2596.16	10095.5	5194.96	4451.33

Appendix C Migration data for individual dunes

Table C 1 The migration distance of individual dunes from all topography surveys during the study period. There are totally eight periods for the one-to-one survey comparisons. The direction of movement are defined as D (Down-estuary), U (Up-estuary, and X (no movement). For more details of measurements, please see http://doi.org/10.5258/SOTON/D0231.

Period 1: 11th March 2013 – 26th June 2013									
Dune no.	Maximum movement		Minimum movement		Lmax/No. of tides (m/tides)	No. of data points collected and the direction of movements			
	Length (m)	Direction	Length (m)	Direction		Total	D	U	X
6	0.84	U	0.00	X	0.00406	12	1	6	5
7.1	0.00	X	0.00	X	0.00000	5	0	0	5
7.2	0.73	U	0.00	X	0.00353	3	0	3	0
7.3	0.81	D	0.00	X	0.00391	25	6	0	19
8.1	0.78	D	0.00	X	0.00377	40	19	0	21
8.2	0.00	X	0.00	X	0.00000	11	0	0	11
8.3	0.19	D	0.00	X	0.00092	8	3	0	5
8.4	1.05	D	0.00	X	0.00507	25	16	0	9
9	0.94	D	0.00	X	0.00454	11	5	0	6
10	1.19	D	0.00	X	0.00575	24	23	0	1
11	0.01	D	0.00	X	0.00005	23	2	0	21
12	0.65	U	0.00	X	0.00314	41	0	16	25
13	0.30	D	0.00	X	0.00145	12	5	0	7
15	0.75	D	0.00	X	0.00362	39	15	0	24
16	0.96	D	0.00	X	0.00464	23	15	0	8
17	0.86	D	0.00	X	0.00415	13	8	0	5
18	0.78	D	0.00	X	0.00377	64	11	3	50
19	1.00	D	0.00	X	0.00483	40	22	0	18
20.1	1.32	D	0.00	X	0.00638	34	14	0	20
20.2	0.44	D	0.00	X	0.00213	11	5	0	6
21	0.68	U	0.00	X	0.00329	19	7	6	6
22	0.31	D	0.00	X	0.00150	23	2	1	20
23	1.60	U	0.00	X	0.00773	23	3	9	11
25	1.63	U	0.00	X	0.00787	33	15	9	9

Appendix C

Period 2: 26th June 2013 - 23rd July 2013									
Dune no.	Maximum movement		Minimum movement		Lmax/No. of tides (m/tides)	No. of data points collected and the direction of movements			
	Length (m)	Direction	Length (m)	Direction		Total	D	U	X
6	0.10	D	0.00	X	0.00190	13	2	0	11
7.1	0.77	D	0.00	X	0.01472	8	6	0	2
7.2	0.00	X	0.00	X	0.00000	5	0	0	5
7.3	0.63	D	0.00	X	0.01221	38	19	1	18
8.1	0.73	D	0.00	X	0.01404	50	32	0	18
8.2	1.52	D	0.00	X	0.02924	12	11	0	1
8.3	0.59	D	0.00	X	0.01144	11	5	0	6
8.4	0.37	D	0.00	X	0.00703	27	3	2	22
9	1.17	D	0.00	X	0.02253	17	16	0	1
10	0.42	D	0.00	X	0.00812	23	18	0	5
11	0.94	D	0.11	D	0.01798	25	25	0	0
12	0.86	D	0.00	X	0.01652	47	45	0	2
13	1.03	D	0.00	X	0.01988	14	8	0	6
15	0.94	D	0.00	X	0.01808	44	37	0	7
16	0.88	D	0.00	X	0.01692	32	26	0	6
17	0.67	D	0.00	X	0.01279	20	15	0	5
18	0.82	D	0.00	X	0.01568	68	41	0	27
19	0.88	D	0.00	X	0.01701	35	15	0	20
20.1	1.84	U	0.00	X	0.03536	35	26	5	4
20.2	0.42	D	0.00	X	0.00811	12	5	0	7
21	0.90	D	0.00	X	0.01735	21	19	0	2
22	0.63	D	0.00	X	0.01218	20	18	0	2
23	1.89	D	0.00	X	0.03635	27	22	0	5
25	1.42	D	0.00	X	0.02726	29	14	0	15
37	1.01	U	0.00	X	0.01935	6	2	3	1

Period 3: 23rd July 2013 -24th July 2013									
Dune no.	Maximum movement		Minimum movement		Lmax/No. of tides (m/tides)	No. of data points collected and the direction of movements			
	Length (m)	Direction	Length (m)	Direction		Total	D	U	X
1	1.90	U	0.00	X	0.95171	18	0	17	1
2	0.69	U	0.00	X	0.34271	20	0	17	3
3	0.40	U	0.00	X	0.19893	18	0	15	3
4	1.29	U	0.00	X	0.64371	43	0	42	1
5	0.51	U	0.00	X	0.25730	42	0	22	20
6	0.57	U	0.00	X	0.28290	27	0	17	10
7.1	0.38	U	0.00	X	0.19147	11	0	7	4
7.2	1.67	U	0.00	X	0.83459	6	0	5	1
7.3	0.62	U	0.00	X	0.31036	37	2	12	23
8.1	2.00	U	0.00	X	1.00204	60	0	48	12
8.2	0.66	U	0.00	X	0.33151	17	0	11	6
8.3	0.70	U	0.00	X	0.34905	14	0	2	12
8.4	0.24	U	0.00	X	0.12209	32	0	8	24
9	1.46	U	0.27	U	0.73194	15	0	15	0
10	0.97	U	0.16	U	0.48657	39	0	39	0
11	0.85	U	0.08	U	0.42534	42	0	42	0
12	0.57	U	0.00	X	0.28696	54	0	37	17
13	0.60	U	0.00	X	0.30240	24	0	23	1
14	0.38	U	0.00	X	0.18929	15	0	13	2
15	0.49	U	0.00	X	0.24649	57	0	34	23
16	0.50	U	0.00	X	0.24934	29	0	21	8
17	0.27	U	0.00	X	0.13706	20	0	12	8
18	0.65	U	0.00	X	0.32583	84	0	33	51

Appendix C

Period 4: 24th July 2013 – 20th August 2013									
Dune no.	**Maximum movement**		**Minimum movement**		**Lmax/No. of tides (m/tides)**	**No. of data points collected and the direction of movements**			
	Length (m)	**Direction**	**Length (m)**	**Direction**		**Total**	**D**	**U**	**X**
1	3.56	U	0.00	X	0.06838	19	0	15	4
2	0.02	U	0.00	X	0.00039	18	0	1	17
3	0.00	X	0.00	X	0.00000	13	0	0	13
4	0.61	U	0.00	X	0.01164	28	0	7	21
5	0.20	U	0.00	X	0.00392	37	0	2	35
6	0.43	U	0.00	X	0.00824	27	0	18	9
7.1	0.18	D	0.00	X	0.00343	9	2	1	6
7.2	0.30	D	0.00	X	0.00579	3	2	0	1
7.3	0.58	D	0.00	X	0.01112	29	12	0	17
8.1	1.92	D	0.00	X	0.03694	51	11	2	38
8.2	0.00	X	0.00	X	0.00000	8	0	0	8
8.3	0.00	X	0.00	X	0.00000	14	0	0	14
8.4	0.37	D	0.00	X	0.00706	21	3	0	18
9	0.92	D	0.00	X	0.01761	15	2	0	13
10	0.18	D	0.00	X	0.00340	34	5	0	29
11	0.33	D	0.00	X	0.00628	35	4	0	31
12	0.00	X	0.00	X	0.00000	74	0	0	74
13	0.08	D	0.00	X	0.00155	22	1	0	21
15	0.19	D	0.00	X	0.00363	58	2	2	54
16	0.00	X	0.00	X	0.00000	33	0	0	33
18	0.79	U	0.00	X	0.01523	56	3	4	49

Period 5: 20th August 2013 -19th September 2013									
Dune no.	Maximum movement		Minimum movement		Lmax/No. of tides (m/tides)	No. of data points collected and the direction of movements			
	Length (m)	Direction	Length (m)	Direction		Total	D	U	X
1	1.51	U	0.37	U	0.02595	29	0	29	0
2	0.27	U	0.00	X	0.00471	20	0	4	16
3	0.14	U	0.00	X	0.00237	18	0	1	17
4	1.94	U	0.00	X	0.03340	34	7	7	20
5	0.02	D	0.00	X	0.00028	43	1	0	42
6	0.95	U	0.00	X	0.01638	38	0	20	18
7.1	0.11	D	0.00	X	0.00189	20	1	0	19
7.2	0.56	U	0.00	X	0.00974	3	0	2	1
7.3	0.51	U	0.00	X	0.00877	58	0	30	28
8.1	2.46	U	0.00	X	0.04242	81	7	9	65
8.2	0.01	D	0.00	X	0.00013	12	1	0	11
8.3	0.23	U	0.00	X	0.00394	21	1	1	19
8.4	0.19	D	0.00	X	0.00336	36	4	0	32
9	0.13	D	0.00	X	0.00230	20	3	0	17
10	0.21	U	0.00	X	0.00356	58	0	9	49
11	0.00	X	0.00	X	0.00000	48	0	0	48
12	0.05	U	0.00	X	0.00089	85	2	1	82
13	0.45	U	0.00	X	0.00768	34	0	2	32
15	0.59	U	0.00	X	0.01013	89	0	3	86
16	0.00	X	0.00	X	0.00000	50	0	0	50
18	0.35	D	0.00	X	0.00612	80	14	1	65
19	2.01	D	0.00	X	0.03463	86	20	0	66
20.1	0.06	D	0.00	X	0.00103	49	3	0	46
23	2.50	D	0.00	X	0.04304	33	4	1	28
24	0.04	U	0.00	X	0.00064	15	0	1	14
25	0.35	U	0.00	X	0.00602	72	0	22	50
37	2.45	D	0.00	X	0.04217	32	14	6	12
38	0.91	D	0.00	X	0.01573	20	18	0	2

Appendix C

Period 6: 19th September 2013 – 18th March 2014									
Dune no.	**Maximum movement**		**Minimum movement**		**Lmax/No. of tides (m/tides)**	**No. of data points collected and the direction of movements**			
	Length (m)	**Direction**	**Length (m)**	**Direction**		**Total**	**D**	**U**	**X**
1	3.11	D	0.00	X	0.00893	11	9	1	1
2	5.45	D	0.54	D	0.01566	24	24	0	0
3	1.39	D	0.00	X	0.00399	15	10	0	5
4	7.51	D	0.00	X	0.02158	42	26	0	16
5	0.69	D	0.00	X	0.00200	50	23	1	26
6	1.34	U	0.00	X	0.00384	34	4	15	15
7.1	0.15	D	0.00	X	0.00044	14	4	1	9
7.2	1.10	U	0.59	U	0.00315	6	0	6	0
7.3	1.54	D	0.00	X	0.00444	60	15	3	42
8.1	2.77	D	0.00	X	0.00797	86	71	0	15
8.2	3.09	D	0.55	D	0.00889	7	7	0	0
8.3	0.58	U	0.00	X	0.00168	21	1	7	13
8.4	0.13	U	0.00	X	0.00037	37	0	3	34
9	0.79	D	0.00	X	0.00226	22	12	0	10
10	3.21	D	0.86	D	0.00923	45	45	0	0
11	1.52	D	0.00	X	0.00436	48	45	0	3
12	1.35	D	0.00	X	0.00389	43	30	1	12
13	0.43	D	0.00	X	0.00124	29	15	1	13
14	0.10	D	0.00	X	0.00029	17	1	0	16
15	0.57	U	0.00	X	0.00164	80	19	12	49
16	0.13	U	0.00	X	0.00037	58	0	7	51
17	0.13	D	0.00	X	0.00036	34	5	0	29
18	0.73	U	0.00	X	0.00210	127	16	10	101
19	0.00	X	0.00	X	0.00000	72	0	0	72
20.1	0.91	D	0.00	X	0.00263	88	9	2	77
20.2	0.33	D	0.00	X	0.00096	21	4	1	16
21	0.49	D	0.00	X	0.00140	45	2	2	41
22	0.00	X	0.00	X	0.00000	51	0	0	51
23	1.14	D	0.00	X	0.00329	47	15	2	30
24	0.39	D	0.00	X	0.00112	28	12	0	16
25	0.47	D	0.00	X	0.00134	49	24	0	25
27	0.19	D	0.00	X	0.00054	31	3	0	28
28	0.71	D	0.00	X	0.00203	51	9	2	40
29	1.64	D	0.00	X	0.00473	32	16	0	16
31	0.72	D	0.00	X	0.00206	38	9	0	29

Period 7: 18th March 2014 – 16th June 2014									
Dune no.	Maximum movement		Minimum movement		Lmax/No. of tides (m/tides)	No. of data points collected and the direction of movements			
	Length (m)	Direction	Length (m)	Direction		Total	D	U	X
1	1.67	U	1.09	U	0.00957	12	0	12	0
2	8.51	U	1.24	U	0.04890	27	0	27	0
3	2.24	U	0.22	U	0.01285	12	0	12	0
4	4.06	U	0.22	U	0.02331	32	0	32	0
5	3.06	U	0.00	X	0.01757	36	0	33	3
6	6.65	U	1.95	U	0.03821	46	0	46	0
7.1	0.07	U	0.00	X	0.00042	12	0	3	9
7.3	2.07	U	0.00	X	0.01190	54	4	17	33
8.1	5.84	U	0.00	X	0.03358	78	0	63	15
8.3	1.04	D	0.00	X	0.00600	27	8	0	19
8.4	0.75	U	0.00	X	0.00430	45	0	6	39
9	1.58	U	0.24	U	0.00908	18	0	18	0
10	2.26	U	0.00	X	0.01297	35	0	28	7
11	0.30	U	0.00	X	0.00171	39	0	8	31
12	1.08	U	0.00	X	0.00620	48	0	5	43
13	0.25	U	0.00	X	0.00144	23	0	11	12
14	0.77	U	0.00	X	0.00441	13	0	12	1
15	0.68	D	0.00	X	0.00390	71	7	21	43
16	0.85	D	0.00	X	0.00491	52	33	0	19
17	0.26	D	0.00	X	0.00150	37	5	0	32
18	0.40	U	0.00	X	0.00230	116	6	7	103
19	0.91	D	0.00	X	0.00523	67	17	1	49
20.1	0.33	D	0.00	X	0.00190	58	12	3	43
20.2	1.50	D	0.00	X	0.00865	21	9	0	12
21	0.54	U	0.00	X	0.00313	40	0	11	29
22	0.71	D	0.00	X	0.00408	38	18	0	20
23	0.69	U	0.00	X	0.00395	35	6	17	12
24	0.51	U	0.00	X	0.00292	23	0	7	16
25	0.11	U	0.00	X	0.00061	41	0	3	38
40	5.07	U	0.23	D	0.02911	15	5	10	0
41	1.80	D	0.00	X	0.01037	18	4	0	14

Appendix C

Period 8: 16th June 2014 – 29th September 2015									
Dune no.	Maximum movement		Minimum movement		Lmax/No. of tides (m/tides)	No. of data points collected and the direction of movements			
	Length (m)	Direction	Length (m)	Direction		Total	D	U	X
2	7.41	D	0.00	X	0.00816	8	6	0	2
4	2.65	U	0.00	X	0.00291	7	0	5	2
5	5.31	U	0.80	U	0.00585	11	0	11	0
7.1	0.26	U	0.00	X	0.00028	7	2	1	4
7.3	8.89	U	0.00	X	0.00979	47	0	23	24
8.1	5.10	U	2.40	U	0.00562	17	0	17	0
8.3	2.32	U	0.00	X	0.00256	20	4	5	11
8.4	0.73	U	0.00	X	0.00081	29	4	6	19
11	14.88	U	8.03	U	0.01639	33	0	33	0
12	12.88	U	0.69	U	0.01418	43	0	43	0
13	2.77	U	0.58	U	0.00305	23	0	23	0
14	13.63	U	10.25	U	0.01502	16	0	16	0
15	2.49	U	0.00	X	0.00274	66	0	39	27
16	0.75	U	0.00	X	0.00082	37	0	18	19
17	0.22	D	0.00	X	0.00024	28	4	0	24
18	0.69	D	0.00	X	0.00076	105	20	8	77
19	2.04	U	0.00	X	0.00225	68	0	46	22
20.1	1.10	U	0.00	X	0.00121	56	12	29	15
20.2	0.54	U	0.00	X	0.00060	17	1	5	11
21	0.56	D	0.00	X	0.00062	25	7	0	18
22	0.00	X	0.00	X	0.00000	34	0	0	34
23	0.69	D	0.00	X	0.00076	31	15	1	15
24	0.00	X	0.00	X	0.00000	10	0	0	10
25	0.51	D	0.00	X	0.00056	39	16	2	21

Appendix D Morphology of dunes

Table D 1 The morphology data of cross sections of the studied dunes. $L_{Surface}$ refers to the length measured across the dune surface, L_{Bed} is the horizontal length on the bedrock platform providing dune wavelength in this study, and H is the highest point of the dune crest providing the dune height in this study.

Dune no (Month/ year)	$L_{Surface}$	L_{Bed}	H
11	0	0.00	0.00
(Sep 14)	0.5	0.48	0.15
	1	0.96	0.27
	1.5	1.44	0.41
	2	1.94	0.40
	2.5	2.44	0.42
	3	2.94	0.37
	3.5	3.41	0.20
	4	3.88	0.02
	4.5	4.38	0.00
12	0	0.00	0.00
(Sep 14)	0.5	0.48	0.15
	1	0.97	0.24
	1.5	1.46	0.33
	2	1.96	0.31
	2.5	2.46	0.27
	3	2.96	0.25
	3.5	3.45	0.15
	4	3.94	0.05
	4.5	4.44	0.00
15-1	0	0.00	0.00
(Mar 16)	0.5	0.50	0.05
	1	1.00	0.05
	1.5	1.42	0.33
	2	1.88	0.51
	2.5	2.38	0.52
	3	2.84	0.71
	3.5	3.33	0.83
	4	3.82	0.79
	4.5	4.32	0.73
	5	4.81	0.65
	5.5	5.26	0.43
	6	5.75	0.34
	6.5	6.24	0.23
	7	6.72	0.10
	7.5	7.22	0.09
	8	7.72	0.00

Dune no (Month/ year)	$L_{Surface}$	L_{Bed}	H
15-2	0	0.00	0.00
(Sep 14)	0.5	0.49	0.11
	1	0.96	0.26
	1.5	1.43	0.44
	2	1.92	0.56
	2.5	2.41	0.65
	3	2.91	0.69
	3.5	3.41	0.68
	4	3.90	0.64
	4.5	4.39	0.54
	5	4.86	0.37
	5.5	5.34	0.23
	6	5.81	0.05
	6.5	6.31	0.00
16-1	0	0.00	0.00
(Sep 14)	0.5	0.48	0.13
	1	0.97	0.23
	1.5	1.47	0.31
	2	1.95	0.42
	2.5	2.45	0.49
	3	2.95	0.50
	3.5	3.45	0.55
	4	3.94	0.61
	4.5	4.44	0.63
	5	4.94	0.54
	5.5	5.41	0.39
	6	5.89	0.26
	6.5	6.34	0.05
	7	6.84	0.00

Dune no (Month/ year)	$L_{Surface}$	L_{Bed}	H
16-2	0	0.00	0.00
(Mar 16)	0.5	0.50	0.06
	1	0.99	0.11
	1.5	1.43	0.18
	2	1.90	0.43
	2.5	2.40	0.59
	3	2.90	0.64
	3.5	3.40	0.65
	4	3.88	0.68
	4.5	4.38	0.57
	5	4.85	0.48
	5.5	5.34	0.33
	6	5.81	0.20
	6.5	6.31	0.03
	7	6.81	0.00
18-1	0	0.00	0.00
(Mar 16)	0.5	0.49	0.11
	1	0.95	0.29
	1.5	1.43	0.44
	2	1.89	0.63
	2.5	2.39	0.72
	3	2.87	0.84
	3.5	3.36	0.93
	4	3.86	0.89
	4.5	4.33	0.73
	5	4.81	0.58
	5.5	5.29	0.42
	6	5.75	0.23
	6.5	6.23	0.12
	7	6.73	0.12
	7.5	7.23	0.00

Dune no (Month/ year)	$L_{Surface}$	L_{Bed}	H
18-2	0	0.00	0.00
(Sep 14)	0.5	0.49	0.19
	1	0.96	0.27
	1.5	1.44	0.46
	2	1.93	0.59
	2.5	2.42	0.70
	3	2.92	0.76
	3.5	3.41	0.76
	4	3.91	0.67
	4.5	4.41	0.61
	5	4.90	0.57
	5.5	5.39	0.46
	6	5.88	0.38
	6.5	6.29	0.28
	7	6.79	0.14
	7.5	7.29	0.00
18-3	0	0.00	0.00
(Sep 14)	0.5	0.49	0.01
	1	0.98	0.08
	1.5	1.46	0.20
	2	1.93	0.34
	2.5	2.42	0.50
	3	2.90	0.60
	3.5	3.38	0.75
	4	3.87	0.89
	4.5	4.36	0.79
	5	4.85	0.70
	5.5	5.34	0.59
	6	5.84	0.50
	6.5	6.33	0.42
	7	6.82	0.32
	7.5	7.31	0.24
	8	7.80	0.14
	8.5	8.30	0.06
	9	8.80	0.00

Dune no (Month/ year)	$L_{Surface}$	L_{Bed}	H	Dune no (Month/ year)	$L_{Surface}$	L_{Bed}	H
19-1	0	0.00	0.00	20	0	0.00	0.00
(Sep 14)	0.5	0.50	0.06	(Mar 16)	0.5	0.50	0.36
	1	0.99	0.12		1	0.99	0.39
	1.5	1.48	0.22		1.5	1.49	0.47
	2	1.98	0.30		2	1.99	0.48
	2.5	2.45	0.46		2.5	2.47	0.43
	3	2.94	0.53		3	2.96	0.56
	3.5	3.44	0.53		3.5	3.45	0.69
	4	3.94	0.56		4	3.94	0.76
	4.5	4.44	0.59		4.5	4.43	0.85
	5	4.94	0.61		5	4.93	0.94
	5.5	5.44	0.60		5.5	5.43	0.95
	6	5.94	0.62		6	5.93	0.95
	6.5	6.44	0.60		6.5	6.42	0.95
	7	6.94	0.60		7	6.92	0.84
	7.5	7.44	0.56		7.5	7.41	0.81
	8	7.93	0.47		8	7.89	0.69
	8.5	8.42	0.38		8.5	8.38	0.57
	9	8.92	0.36		9	8.86	0.47
	9.5	9.42	0.29		9.5	9.35	0.31
	10	9.90	0.18		10	9.82	0.23
	10.5	10.37	0.00		10.5	10.32	0.06
19-2	0	0.00	0.00		11	10.82	0.00
(Mar 16)	0.5	0.50	0.15				
	1	0.98	0.21				
	1.5	1.45	0.33				
	2	1.94	0.51				
	2.5	2.44	0.57				
	3	2.94	0.58				
	3.5	3.44	0.60				
	4	3.94	0.58				
	4.5	4.44	0.59				
	5	4.94	0.62				
	5.5	5.44	0.69				
	6	5.93	0.66				
	6.5	6.43	0.62				
	7	6.92	0.61				
	7.5	7.40	0.52				
	8	7.88	0.36				
	8.5	8.35	0.21				
	9	8.85	0.06				
	9.5	9.35	0.00				
	10	9.85	0.00				

List of References

A.S.C.E. Task Force on Bed Forms in Alluvial Channels, 1966. Nomenclature for bed forms in alluvial channels. American Society of Civil Engineers, Proceedings, Journal of the Hydraulics Division, 92(no. HY3), pp.51–64.

Abbott, J.E. and Francis, J.R.D., 1977. Saltation and Suspension Trajectories of Solid Grains in a Water Stream. Philosophical Transactions of the Royal Society A: Mathematical, Physical and Engineering Sciences, 284(February), pp.225–254.

Allen, J.R.L., 1968. Current ripples: Their relation to patterns of water and sediment motion, Amsterdam: North Holland.

Allen, J.R.L., 1969. On the geometry of current ripples in relation to stability of fluid flow. Geografiska Annaler. Series A, Physical Geography, 51(1/2), pp.61–96.

Allen, J.R.L., 1970. Physical prosesses of sedimentation, London: Unwin University Books.

Allen, J.R.L., 1978. Computational models for dune time-lag: calculations using Stein's rule for dune height. Sedimentary Geology, 20, pp.165–216.

Allen, J.R.L., 1980. Sand waves: A model of origin and internal structure. Sedimentary Geology, 26(4), pp.281–328.

Allen, J.R.L., 1984. Sedimentary structures: their character and physical basis. Amsterdam: Elsevier Scientific Publishing Co.

Allen, J.R.L., 1987. Late flandrian shoreline oscillations in the Severn Estuary: the Rumney formation at its typesite (Cardiff Area), Philosophical Transactions of the Royal Society of London. Series B, Biological Sciences, 315(1171), pp. 157–184.

Allen, J.R.L., 1990. The Severn Estuary in southwest Britain: its retreat under marine transgression, and fine-sediment regime. Sedimentary Geology, 66(1-2), pp.13–28.

Allen, J.R.L., 1991. Fine sediment and its sources, Severn Estuary and inner Bristol Channel, southwest Britain. Sedimentary Geology, 75(1-2), pp.57–65.

Allen, J.R.L., 1993. Sedimentary structures: Sorby and the last decade. Journal of the Geological Society, 150(3), pp.417–425. Available at: http://jgs.lyellcollection.org/cgi/doi/10.1144/gsjgs.150.3.0417 [Accessed May 24, 2013].

Allen, J.R.L., 2004. Annual textural banding in Holocene estuarine silts, Severn Estuary Levels (SW Britain): patterns, cause and implications. The Holocene, 4, pp.536–552. Available at: http://centaur.reading.ac.uk/3180/.

Allen, J.R.L. and Duffy, M.J., 1998a. Medium-term sedimentation on high intertidal mudflats and salt marshes in the Severn Estuary, SW Britain: The role of wind and tide. Marine Geology, 150(1-4), pp.1–27. Available at: http://linkinghub.elsevier.com/retrieve/pii/S0025322798000516.

Allen, J.R.L. and Duffy, M.J., 1998b. Temporal and spatial depositional patterns in the Severn Estuary, southwestern Britain: Intertidal studies at spring-neap and seasonal scales, 1991-1993. Marine Geology, 146(1-4), pp.147–171.

Allen, J.R.L. Friend, P., Lloyd, A. and Wells, H., 1994. Morphodynamics of Intertidal Dunes: A Year-Long Study at Lifeboat Station Bank, Wells-Next-the-Sea, Eastern England. Philosophical Transactions of the Royal Society A: Mathematical, Physical and Engineering Sciences, 347(1682), pp.291–344.

Allen, J.R.L. and Fulford, M.G., 1990. Romano-British wetland reclamations at Longney, Gloucestershire, and the evidence for early settlement of the inner Severn Estuary. Antiquaries Journal, 70(2), pp.288–326.

Allen, J.R.L. and Fulford, M.G., 1996. Late Flandrian coastal change and tidal palaeochannel development at Hills Flats, Severn Estuary (SW Britain). Journal of the Geological Society, 153(1), pp.151–162. Available at: http://jgs.lyellcollection.org/cgi/doi/10.1144/gsjgs.153.1.0151 [Accessed May 24, 2013].

Allen, J.R.L. and Leeder, M.R., 1980. Criteria for the instability of upper-stage plane beds. Sedimentology, 27, pp.209–217.

Allen, J.R.L. and Rae, J.E., 1987. Late Flandrian Shoreline Oscillations in the Severn Estuary: A Geomorphological and Stratigraphical Reconnaissance. Philosophical Transactions of the Royal Society of London. Series B, Biological Sciences, 315(1171), pp. 185–230.

Allen, J.R.L. and Rae, J.E., 1988. Vertical salt-marsh accretion since the Roman period in the Severn Estuary, Southwest Britain. Marine Geology, 83, pp.225–235.

Andrews, E.D., 1983. Entrainment of gravel from naturally sorted riverbed material. Geological Society of America Bulletin, 94(10), pp.1225–1231.

Andrews, E.D., 1984. Bed-material entrainment and hydraulic geometry of gravel-bed rivers in Colorado. Geological Society of America Bulletin, 95(3), pp.371–378.

Andrews, E.D. and Smith, J.D., 1992. A theoretical model for calculating marginal bedload transport rates of gravel. Dynamics of gravel-bed rivers, pp.41–54.

Archer, A.W., 2013. World's highest tides: Hypertidal coastal systems in North America, South America and Europe. Sedimentary Geology, 284-285, pp.1–25. Available at: http://linkinghub.elsevier.com/retrieve/pii/S0037073812003326 [Accessed May 27, 2013].

Ashley, G.M., 1990. Classification of Large-Scale Subaqueous Bedforms: A New Look at an Old Problem-SEPM Bedforms and Bedding Structures., 60(1), pp.160–172.

Australia Maritime Safety Authority, A.G., 2015. Differential Global Positioning System. Available at: http://www.amsa.gov.au/navigation/services/dgps/ (Accessed: 29 April 2015).

Baas, J.H., 1994. A flume study on the development and equilibrium morphology of current ripples in very fine sand. Sedimentology, 41, pp.185–209.

Baas, J.H. and Best, J.L., 2002. Turbulence Modulation in Clay-Rich Sediment-Laden flows and some implications for sediment deposition. Journal of Sedimentary Research, 72(3), pp.336–340.

Bagnold, R.A., 1966. An approach to the sediment transport problem from general physics. U.S.Geological Survey Professional Paper, (422-I).

Baker, V.R., 1973. Paleohydrology of Catastrophic Pleistocene Flooding in Eastern Washington. Geological Society of America, Special Paper 144, p.79.

Baker, V.R., 1978. Large-scale erosional and depositional features of the Channeled Scabland. In V. R. Baker and D. Nummedal, eds. The Channeled Scabland. Washington, D.C.: National Aeronautics and Space Administration, pp. 81–115.

Barnard, P.L., Hanes, D.M. and Kvitek, R.G., 2006. Massive Bedforms and their Movement Mapped at the Mouth of San Francisco Bay using Multibeam Sonar. American Geophysical Union, Fall Meeting 2006. Available at: http://adsabs.harvard.edu/abs/2006AGUFMNS22A..01B.

Barrie, J.V., Conway, K.W., Picard, K. and Greene, H.G., 2009. Large-scale sedimentary bedforms and sediment dynamics on a glaciated tectonic continental shelf: Examples from the Pacific margin of Canada. Continental Shelf Research, 29(5–6), pp. 796–806. doi: 10.1016/j.csr.2008.12.007.

Bathurst, J.C., Graf, W.K. and Cao, H.H., 1987. Bed load discharge equations for steep mountain rivers. In R. D. Thorne, C.R., Bathurst, J.C., and Hey, ed. Sediment Transport in Gravel-bed Rivers. Chichester: John Wiley and Sons, pp. 453–477.

Bennett, S.J. and Bridge, J.S., 1995. The geometry and dynamics of low-relief bed forms in heterogeneous sediment in a laboratory channel, and their relationship to water flow and sediment transport. Journal of Sedimentary Research, A65, pp.29–39.

Bennett, S.J., Bridge, J.S. and Best, J.L., 1998. Fluid and sediment dynamics of upper stage plane beds. Journal of Geophysical Research: Oceans, 103(1), pp.1239–1274.

Berne, S. et al., 1993. Morphology, internal structure, and reverseal of asymmetryof large subtidal dunes in the entrance to Gironde Estuary (France). , 63(5), pp.780–793.

BERR, 2004. UK Atlas of Offshore Renewable Energy. Produced by ABPmer, the Met Office, Garrard Hassan and Proudman Oceanographic Laboratory. Available at: http://www.renewables-atlas.info/.

Best, J.L., 1992. On the entrainment of sediment and initiation of bed defects: insights from recent developments within turbulent boundary layer research. Sedimentology, 39, pp.797–811.

Best, J.L., 1993. On the interactions between turbulent flow structure, sediment transport and bedform development: some considerations from recent experimental research. In N. J. Clifford, J. R. French, and J. Hardisty, eds. Turbulence: Perspectives on flow and sediment transport. Chichester: Wiley, pp. 61–92.

Best, J.L., 1996. The fluid dynamics of small-scale alluvial bedforms. In P. A. Carling and M. R. Dawson, eds. Advances in Fluvial Dynamics and Stratigraphy. Chichester: Wiley, pp. 67–125.

Best, J.L. and Leeder, M.R., 1993. Drag reduction in turbulent muddy seawater flows and some sedimentary consequences. Sedimentology, 40, pp.1129–1137.

Beylich, A. a. and Laute, K., 2014. Combining impact sensor field and laboratory flume measurements with other techniques for studying fluvial bedload transport in steep mountain streams. Geomorphology, 218, pp.72–87. Available at: http://dx.doi.org/10.1016/j.geomorph.2013.09.004.

Blott, S.J. and Pye, K., 2001. GRADISTAT: a grain size distribution and statistics package for the analysis of unconsolidated sediments. Earth Surface Processes and Landforms, 26(11), pp. 1237–1248. doi: 10.1002/esp.261.

Boersma, J.R. and Terwindtt, J.H.J., 1981. Neap–spring tide sequences of intertidal shoal deposits in a mesotidal estuary. Sedimentology, 28(2), pp.151–170.

Bogen, J. and Moen, K., 2003. Bed load measurements with a new passive acoustic sensor. Proceedinngs of the workshop erosion and sediment transport measurement in rivers: Technological and Methodological Advances, (June 2002), pp.181–192. Oslo, Norway.

Bradley, R.W. and Venditti, J.G., 2016. Reevaluating dune scaling relations. Earth-Science Reviews. Elsevier B.V., 165, pp. 356–376. doi: 10.1016/j.earscirev.2016.11.004.

Breakspear, R., 2008. Hydrodynamics and sedimentary structures of antidunes in gravel and sand mixtures. University of Southampton.

Bridge, J.S., 1982. Bed shear stress over subaqueous dunes, and the transition to upper-stage plane beds. Reply: Sedimentology, 29, pp.744–747.

Bridge, J.S., 1985. Paleochannel patterns inferred from alluvial deposits: a critical evaluation. Journal of Sedimentary Petrology, 55(4), pp.0579–0589.

Bridge, J.S., 1993. The interaction between channel geometry, water flow, sediment transport and deposition in braided rivers. Geological Society, London, Special Publications, 75(1), pp.13–71.

Bridge, J.S., 2003. Rivers and floodplains : forms, processes, and sedimentary record, Oxford : Blackwell.

Bridge, J.S. and Best, J.L., 1988. Flow, sediment transport and bedform dynamics over the transition from dunes to upper-stage plane beds: implications for the formation of planar laminae. Sedimentology, 35(5), pp.753–763. Available at: http://doi.wiley.com/10.1111/j.1365-3091.1988.tb01249.x.

Bridge, J.S. and Best, J.L., 1997. Preservation of planar laminae due to migration of low-relief bed waves over aggrading upper-stage plane beds: comparison of experimental data with theory. Sedimentology, 44(2), pp.253–262. Available at: http://doi.wiley.com/10.1111/j.1365-3091.1997.tb01523.x.

Bucher, W.H., 1919. On ripples and related sedimentary surface forms and their palaeogeographic interpretation. American Journal of Science, 47, pp.241–269.

Buffington, J.M. and Montgomery, D.R., 1997. A systematic analysis of eight decades of incipient motion studies, with special reference to gravel-bedded rivers. Water Resources Research, 33(8), pp.1993–2029.

Butler, P.R., 1977. Movement of cobbles in a gravel-bed stream during a flood season. Bulletin of the Geological Society of America, 88(8), pp.1072–1074.

Cai, H., Savenije, H.H.G. and Toffolon, M., 2013. Linking the river to the estuary: influence of river discharge on tidal damping. Hydrology and Earth System Sciences, 10, pp. 9191–9238. doi: 10.5194/hess-18-287-2014.

Carling, P.A., 1983. Threshold of coarse sediment transport in broad and narrow natural streams. , 8, pp.1–18.

Carling, P.A., 1987. Bed stability in gravel streams, with reference to stream regulation and ecology. River channels: environment and process. Blackwell Scientific Publications, Oxford, UK, pp.321–347.

Carling, P.A., 1990. Particle over-passing on depth-limited gravel bars. Sedimentology, 37(2), pp.345–355.

Carling, P.A., 1996a. A preliminary palaeohydraulic model applied to late Quaternary gravel dunes: Altai Mountains, Siberia. In J. Branson, A. G. Brown, and K. J. Gregory, eds. Global Continental Changes: The Context of Palaeohydrology. pp. 165–179.

Carling, P.A., 1996b. Morphology, sedimentology and palaeohydraulic significance of large gravel dunes, Altai Mountains, Siberia. Sedimentology, 43(4), pp.647–664. Available at: http://doi.wiley.com/10.1111/j.1365-3091.1996.tb02184.x.

Carling, P.A., 1999. Subaqueous gravel dunes. Journal of Sedimentary Research, 69(3), pp.534–545.

Carling, P. A., 2013. Subaqueous “yardangs”: Analogs for aeolian yardang evolution. Journal of Geophysical Research: Earth Surface, 118(1), pp.276–287.

Carling, P.A. Chateau, C., Leckie, D., Langdon, C., Scaife, R.and Parsons, D., 2015. Sedimentology of a tidal point-bar within the fluvial–tidal transition: River Severn estuary, UK. In P. J. Ashworth, J. L. Best, and D. R. Parsons, eds. Fluvial-Tidal Sedimentology: Developments in Sedimentology 68. Elsevier, pp. 149–192. Available at: http://store.elsevier.com/Fluvial-Tidal-Sedimentology/isbn-9780444635297/.

Carling, P.A., Gölz, E., Orr, H. G. and Radecki-Pawlik, A., 2000. The morphodynamics of fluvial sand dunes in the River Rhine, near Mainz, Germany. I. Sedimentology and morphology. Sedimentology, 47(1), pp.227–252.

Carling, P.A. Radecki-Pawlik, A., Williams, J.J., Rumble, B., Meshkova, L., Bell, P.and Breakspear, R., 2006. The morphodynamics and internal structure of intertidal fine-gravel dunes: Hills Flats, Severn Estuary, UK. Sedimentary Geology, 183(3-4), pp.159–179. Available at: http://linkinghub.elsevier.com/retrieve/pii/S0037073805002551 [Accessed November 16, 2012].

Carling, P.A., Richardson, K. and Ikeda, H., 2005. A flume experiment on the development of subaqueous fine-gravel dunes from a lower-stage plane bed. Journal of Geophysical Research: Earth Surface, 110(4), pp. 1–15. doi: 10.1029/2004JF000205.

Carson, M.A., 1971. The mechanics of erosion, London: Pion.

Choi, K. and Jo, J., 2015. Morphodynamics and stratigraphic architecture of compound dunes on the open-coast macrotidal flat in the northern Gyeonggi Bay, west coast of Korea. Marine Geology, 366, pp.34–48. Available at: http://linkinghub.elsevier.com/retrieve/pii/ S0025322715001036.

Church, M. and Hassan, M. a., 1992. Size and distance of travel of unconstrained clasts on a streambed. Water Resources Research, 28(1), pp.299–303.

Clague, J.J. and Rampton, V.N., 1982. Neoglacial Lake Alsek. Canadian Journal of Earth Sciences, 19(1), pp.94–117. Available at: http://dx.doi.org/10.1139/e82-008.

Colebrook, C.F. and White, C.M., 1937. Experiments with Fluid Friction in Roughened Pipes. Proceedings of the Royal Society of London. Series A, Mathematical and Physical Sciences, 161(906 (Aug. 3, 1937)), pp. 367–381. doi: 10.1007/s11103-011-9767-z.Plastid.

Coleman, S.E. and Melville, B.W., 1996. Initiation of bed forms on a flat bed. Journal of Hydraulic Engineering,ASCE, 122, pp.301–10.

Collins, M., 1983. Supply, distribution, and transport of suspended sediment in a macrotidal environment: Bristol Channel, UK. Canadian Journal of Fisheries and Aquatic Sciences, 40(S1), pp.s44–s59.

Collins, M., 1987. Sediment transport in the Bristol Channel: a review. Proceedings of the Geologists' Association, 98(4), pp.367–383. Available at: http://eprints.soton.ac.uk/192537/.

Collins, N.R. and Williams, R., 1981. Zooplankton of the Bristol Channel and Severn Estuary. The distribution of four copepods in relation to salinity. Marine Biology, 64(3), pp.273–283.

Cooper, R.H., Peterson, A.W. and Blench, T., 1972. Critical Review of Sediment Transport Experiments. American Society of Civil Engineers, Proceedings, Journal of the Hydraulics Division, 98, pp.827–843.

Cornish, V., 1899. ON KUMATOLOGY . (The study of the waves and wave-structures of the atmosphere, hydrosphere, and lithosphere). The Geographic Journal, 13(6), pp.624–626.

Correggiari, A., Field, M.E. and Trincardi, F., 1996. Late Quaternary transgressive large dunes on the sediment-starved Adriatic shelf. , (117), pp.155–169.

Costello, W.R. and Southard, J.B., 1981. Flume experiments on lower - flow - regime bed forms in coarse sand. , 51(3), pp.849–864.

Crickmore, M.J., 1982. Data collection — tides, tidal currents and suspended sediment. In Institute of Civil Engineers (Eds.). The Severn Barrage. Thomas Telford, London, pp. 19–26.

Dalrymple, R.W., Knight, R.J. and Lambiase, J.J., 1978. Bedforms and their hydraulic stability relationships in a tidal environment, Bay of Fundy, Canada. Nature, 275(5676), pp.100–104.

Dalrymple, R.W. and Rhodes, R.W., 1995. Estuarine dunes and barforms. In G. M. Perillo, ed. Geomorphology and Sedimentology of Estuaries. Developments in Sedimentology. Amsterdam: Elsevier, pp. 359–422.

Dietrich, W.E. et al., 1989. Sediment supply and the development of the coarse surface layer in gravel-bedded rivers. Nature, 340(6230), pp.215–217.

Dinehart, R.L., 1989. Dune Migration in a Steep, Coarse-Bedded Stream. Water Resources Research, 25(5), pp.911–923.

Dinehart, R.L., 1992a. Evolution of coarse gravel bedforms: Field measurements at flood stage. Water Resources Research, 28(10), pp.2667–2689.

Dinehart, R.L., 1992b. Gravel-bed deposition and erosion by bedform migration observed ultrasonically during storm flow, North Fork Toutle River, Washington. Journal of Hydrology, 136(1-4), pp.51–71. Available at: http://linkinghub.elsevier.com/retrieve/pii/002216949290004F.

Draper, L., 1991. Wave climate atlas of the British Isles, Great Britain, Department of Energy.

Dyer, K.R., 1970a. Current velocity profiles in a tidal channel. Geophysical Journal International, 22(1970), pp.153–161. Available at: http://gji.oxfordjournals.org/content/22/2/153. short.

Dyer, K.R., 1970b. Grain size parameters for sandy-gravels. Journal of Sedimentary Research, 40(2), pp.616–620. Available at: http://jsedres.sepmonline.org/content/40/2/616. abstract.

Dyer, K.R., 1971. The distribution and movement of sediment in the Solent, southern England. Marine Geology, 11, pp.175–187.

Dyer, K.R., 1972. Bed shear stresses and the sedimentation of sandy gravels. Marine Geology, 13(2), pp.M31–M36.

Dyer, K.R., 1984. Sedimentation Processes in the Bristol Channel / Severn Estuary. Marine pollution bulletin, 15(2), pp.53–57.

Emmett, W.W., 2010. Observations of Bedload Behavior in Rivers and Their Implications for Indirect Methods of Bedload Measurement, US Geological Survey Scientific Investigations Report.

EO-MINERS, 2015. Earth Observation in the frame of EO-MINERS - Overview of remote sensing methods, sensors and applications. Available at: http://www.eo-miners.eu/earth_observation/eo_eof_msa_forthcoming_review.htm (Accessed: 8 May 2015).

Fahnestock, R.K. and Bradley, W.C., 1973. Knik and Matanuska rivers, Alaska: a contrast in braiding. In M. Morisawa, ed. Fluvial Geomorphology. Binghamton, New York: State University of New York Press, pp. 220–250.

Fahnestock, R.K., Bradley, W.C. and Leveen, L.S., 1969. Bed forms and flow phenomena during a Lake George breakout flood, Knik River, Alaska. In Geol. Soc. Am., Abstr. Prog. pp. 61–62.

Feng, Q., Sjögren, P., Stephansson, O. and Jing, L. (2001) 'Measuring fracture orientation at exposed rock faces by using a non-reflector total station', Engineering Geology, 59(1–2), pp. 133–146. doi: 10.1016/S0013-7952(00)00070-3.

Fenton, J.D. and Abbott, J.E., 1977. Initial Movement of Grains on a Stream Bed: The Effect of Relative Protrusion. Proceedings of the Royal Society of London A: Mathematical, Physical and Engineering Sciences, 352(1671), pp.523–537. Available at: http://rspa.royalsocietypublishing.org/content/352/1671/523.abstract.

Ferret, Y., Le Bot, S., Tessier, B., Garlan, T. and Lafite, R., 2010. Migration and internal architecture of marine dunes in the eastern English Channel over 14 and 56 year intervals: the influence of tides and decennial storms. Earth Surface Processes and Landforms, 35(12), pp.1480–1493. Available at: http://doi.wiley.com/10.1002/esp.2051 [Accessed April 17, 2015].

Flemming, B.W., 1978. Underwater sand dunes along the southeast African continental margin — Observations and implications. Marine Geology, 26(3-4), pp.177–198. Available at: http://www.sciencedirect.com/science/article/pii/0025322778900592 [Accessed March 17, 2015].

Flemming, B.W., 1988. Zur klassifikation subaquatischer, stro¨mungstransversaler Transportko¨rper. Bochumer Geologische und Geotechnische Arbeiten, 29, pp.44–47.

Flemming, B.W., 2000. The role of grain size, water depth and flow velocity as scaling factors controlling the size of subaqueous dunes. In T. Trentesaux, A., Garlan, ed. Workshop Marine Sandwave Dynamics Int Worksh Proc, 23–24 March 2000. University of Lille 1, France, pp. 55–60.

Fofonoff, N.P. and Millard, R.C., 1983. Algorithms for computation of fundamental properties of seawater. Symposium A Quarterly Journal In Modern Foreign Literatures, 44, p. 53. Available at: http://darchive.mblwhoilibrary.org:8080/handle/1912/2470.

Foley, M.G., 1977. Gravel-lens formation in antidune-regime flow: a quantitative hydrodynamic indicator', Journal of Sedimentary Petrology, 47(2), pp. 738–746.

Fraley, L., 2004. Methods of Measuring Fluvial Sediment, p. 47.

Francis, J.R.D., 1973. Experiments on the Motion of Solitary Grains Along the Bed of a Water-Stream. Proceedings of the Royal Society A: Mathematical, Physical and Engineering Sciences, 332(1591), pp.443–471.

Francken, F., Wartel, S., Parker, R. and Taverniers, E., 2004. Factors influencing subaqueous dunes in the Scheldt Estuary. Geo-Marine Letters, 24(1), pp.14–21. Available at: http://link.springer.com/10.1007/s00367-003-0154-x [Accessed May 24, 2013].

Fredsøe, J., 1975. The friction factor and height–length relationships in flow over a dune-covered bed,

Gabel, S.L., 1993. Geometry and kinematics of dunes during steady and unsteady flows in the Calamus River, Nebraska, USA. Sedimentology, 40(2), pp.237–269. Available at: http://doi.wiley.com/10.1111/j.1365-3091.1993.tb01763.x.

Galay, V.J., 1967. Observed forms of bed roughness in an unstable gravel river. In International Association for Hydraulic Research, 12th Congress. pp. 85–94.

Galay, V.J. and Neill, C.R., 1967. Nomenclature for bedforms in alluvial channels. American Society of Civil Engineers, Proceedings, Journal of the Hydraulics Division, 93(HY1), pp.130–133.

Gaudet, B.J.M., Roy, A.G., Best, J.L. and Jocelyn, M., 1994. Effect of Orientation and Size of Helley-Smith Sampler on Its Efficiency. Journal of Hydraulic Engineering, 120(6), pp. 758–766.

Germanoski, D., 1989. Linguoid gravel bars, parabolic actively migrating bedforms [unpublished Ph.D. thesis].

Germanoski, D., 1993. Braid bar development through dissection of stalled linguoid dunes in gravel-bed braided rivers (abstract). In Third International Geomorphology Conference, August 23–28, 1993. Hamilton, Ontario, Canada, Programme with Abstracts, p. 145.

Gilbert, G.K., 1914. The transport of debris by running water. U.S. Geological Survey Professional Paper 86, pp.1–263.

Gomez, B., Naff, R.L. and Hubbell, D.W., 1989. Temporal variations in bedload transport rates associated with the migration of bedforms. Earth Surface Processes and Landforms, 14(2), pp.135–156. Available at: http://doi.wiley.com/10.1002/esp.3290140205.

Gradowczyk, M.H., 1968. Wave propagation and boundary instability in erodible-bed channels. Journal of Fluid Mechanics, 33(01), p.93.

Griffiths, B.G.A., 1989. Form resistancein gravel channels with mobile beds. Journal of Hydraulic Engineering, 115(3), pp.340–355.

Gustavson, T.C., 1978. Bed forms and stratification types of modern gravel meander lobes, Nueces River, Texas. Sedimentation Engineering, 25, pp.401–426.

Gyr, A. and Schmid, A., 1989. The different ripple formation mechanism. journal of Hydraulic Research, 27, pp.61–74.

Hamilton, D., 1979. The high energy, sand and mud regime of the Severn Estuary, SW Britain. In Tidal Power and Estuary Management. Scientechnica Bristol, pp. 162–172.

Harbor, D.J., 1998. Dynamics of bedforms in the lower Mississippi River. Journal of Sedimentary Research, 68(5), pp.750–762.

Harms, J.C. and Fahnstock, R.K., 1965. Stratification, bedforms, and flow phenomena (with an example from the Rio Grande). In G. V. Middleton, ed. Primary Sedimentary Structures and Their Hydrodynamic Interpretation. Society of Economic Paleontologists and Mineralogists, Special Publication 12, pp. 84–115.

Harrison, A.S., 1950. Report on special investigation of bed sediment segregation in a degrading bed, University of California, Institute of Engineering Research.

Hashemi, M.R., Abedini, M. J., Neill, S. P. and Malekzadeh, P., 2008. Tidal and surge modelling using differential quadrature: A case study in the Bristol Channel. Coastal Engineering, 55(10), pp.811–819.

Hassan, M.A. and Church, M., 1992. The movement of individual grains on the streambed. Dynamics of gravel-bed rivers, pp.159–175.

Helley, E. J. and Smith, W., 1971. Development and calibration of a pressure-difference bedload sampler, Open-File Report. Available at: http://pubs.er.usgs.gov/publication/ofr73108.

Helly, J.R., 1969. Field Measurement of the Initiation of Large Bed Particle Motion in Blue Creek Near Klamath , California, Professional Paper. United States Geological Survey, 526G.

HjulstrÖm, F., 1935. Studies of morphological activity of rivers as illustrated by the River Fyris. Bulletin of the Geological Institute, University of Uppsala, 25, pp.221–527.

Hoekstra, P., Bell, P., Van Santen, P., Roode, N., Levoy, F. and Whitehouse, R., 2004. Bedform migration and bedload transport on an intertidal shoal. Continental Shelf Research, 24(11), pp.1249–1269.

Hubbell, D.W., Stevens, H.H., Skinner, J.V. and Beverage, J.P., 1987. Laboratory data on coarse-sediment transport for bedload-sampler calibrations. U.S.Geological Survey, Water-Supply Paperaper, (2299), p.iv, 31 p.

Hydraulics Research Station, 1979. Lower Severn Estuary — Wave Climate Study. Report EX 887. Hydraulics Research Station, Wallingford. 15 pp.

Hydraulics Research Station, 1980. Lower Severn Estuary — Wave Climate Study. Report EX 933. Hydraulics Research Station, Wallingford. 15 pp.

Hydraulics Research Station, 1981a. Lower Severn Estuary — Wave Climate Study. Report EX 944. Hydraulics Research Station, Wallingford. 20 pp.

Hydraulics Research Station, 1981b. The Severn Estuary: silt monitoring April 1980–March 1981, Report EX 995, Hydraulics Research Station: Wallingford.

Iacono, C. and Guillén, J., 2008. Environmental conditions for gravelly and pebbly dunes and sorted bedforms on a moderate-energy inner shelf (Marettimo Island, Italy, western Mediterranean). Continental Shelf Research, 28(2), pp.245–256. Available at: http://linkinghub.elsevier.com/retrieve/pii/S0278434307002579 [Accessed December 14, 2012].

IH, 1998. Hydrological Data United Kingdom, Oxon OX10 8BB: Institute of Hydrology, Wallingford.

Ikeda, H., 1982. An experimental study of the formation of openwork gravel layers under alluvial-flow conditions. Trans. Jap. Geomorphol. Union, 3, pp.57–65.

Ikeda, H., 1983. Experiments on bedload transport, bed forms, and sedimentary structures using fine gravel in the 4-meter-wide flume, University of Tsukuba, Japan, Environmental Research Centre, Paper 2. Available at: http://books.google.co.uk/books?id=TKJPAQAAIAAJ.

IMCORE project, no date. Severn Estuary and Climate Change. Available at: http://www.coastaladaptation.eu/index.php/en/9-experiences-3/severn-estuary/138-climate-change-and-coastal-management.

Inman, D.L., 1949. Sorting of Sediments in the Light of Fluid Mechanics. Journal of Sedimentary Petrology, 19(2), pp.51–70.

Iseya, F. and Ikeda, H., 1987a. Pulsation in bedload transport rates induced by a longitudinal sediment sorting: a flume study of sand and gravel mixtures. Geografiska Annaler, 69A, pp.15–27.

Iseya, F. and Ikeda, H., 1987b. Transport in Bedload Pulsations Rates Induced By a Sediment Sorting : Longitudinal a Flume Study Using Sand and. Geografiska Annaler. Series A, Physical Geography, 69(1), pp.15–27.

Jackson, R.G., 1975. Hierarchical attributes and a unifying model of bed forms composed of cohesionless material and produced by shearing flow. Geological Society of America, Bulletin, 86, pp.1523–1533.

Jackson, R.G., 1976. Sedimentological and fluid-dynamic implications of the turbulent bursting phenomenon in geophysical flows. Journal of Fluid Mechanics, 77, pp.531–560.

Joint, I.R., 1983. Development of an ecosystem model of a turbid estuary. Canadian Journal of Fisheries and Aquatic Sciences, 40(S1), pp.s341–s348.

Jordan, G.F., 1962. Large Submarine Sand Waves. Science, 136(3519), pp.839–848.

Karim, F., 1995. Bed configuration and hydraulic resistance in alluvial channel flows, Journal of Hydraulic Engineering, 121 (1)(5739), pp. 15–25.

Keim, R.F., Skaugset, A.E. and Bateman, D.S., 1999. Digital terrain modeling of small stream channels with a total-station theodolite. Advances in Water Resources, 23(1), pp. 41–48. doi: 10.1016/S0309-1708(99)00007-X.

Keller, E.A., 1970. Bed-load Movement Experiments: Dry Creek, California: NOTES. Journal of Sedimentary Research, 40(4), pp.1339–1344.

Kennedy, J.F., 1960. Stationary waves and antidunes in alluvial channels. California Institute of Technology.

Kennedy, J.F., 1963. The mechanics of dunes and antidunes in erodible-bed channels. Journal of Fluid Mechanics, 16(04), p.521.

Kirby, R., 1986, Suspended fine cohesive sediment in the Severn Estuary and inner Bristol Channel, UK. Report ETSU-STP-4042, Department of Energy, Energy Technology Support Unit, London.

Kirby, R. and Parker, W.R., 1982. A suspended sediment front in the Severn Estuary. , 295, pp.396–399. Available at: http://www.nature.com/nature/journal/v295/n5848/abs/295396a0.html#References.

Kirby, R. and Parker, W.R., 1983. Distribution and Behavior of Fine Sediment in the Severn Estuary and Inner Bristol Channel, U.K. Canadian Journal of Fisheries and Aquatic Sciences, 40(S1), pp.s83–s95. Available at: http://dx.doi.org/10.1139/f83-271.

Knaapen, M.A., van Bergen Henegouw, C.N. and Hu, Y.Y., 2005. Quantifying bedform migration using multi-beam sonar. Geo-Marine Letters, 25(5), pp. 306–314. doi: 10.1007/s00367-005-0005-z.

Knighton, D., 1998. Fluvial forms and processes: a new perspective, London: Hodder Education/Arnold.

Kohsiek, L.H.M. and Terwindt, J.H.., 1981. Characteristics of foreset and topset bedding in megaripples related to hydrodynamic conditions on an intertidal shoal. Holocene Marine Sedimentation in the North Sea Basin, Speci. Publis int Ass. Sediment., 5, pp.22–37.

Komar, P.D., 1996. Entrainment of sediments from deposits of mixed grain sizes and densities. In M. R. Carling, P.A., and Dawson, ed. Advances in Fluvial Dynamics and Stratigraphy. Chichester, U.K.: Wiley, pp. 127–181.

Kostaschuk, R. and Best, J., 2005. Response of sand dunes to variations in tidal flow: Fraser Estuary, Canada. Journal of Geophysical Research: Earth Surface, 110(4), pp.1–11.

Kuhnle, R.A., 1993. Fluvial transport of sand and gravel mixtures with bimodal size distributions. Sedimentary Geology, 85(1), pp.17–24.

Kuhnle, R.A. and Southard, J.B., 1990. Flume experiments on the transport of heavy minerals in gravel-bed streams. Journal of Sedimentary Petrology, 60, pp.687–696.

Lane, E.W. and Eden, E.W., 1940. Sand waves in the lower Mississippi River, Ko Hsueh.

Langhorne, D.N., Heathershaw, A.D. and Read, A.A., 1986. Gravel Bedforms in the West Solent , Southern England. , pp.225–230.

Lapointe, M., 1992. Burst-like sediment suspension events in a sand bed river. Earth Surface Processes and Landforms, 17(3), pp.253–270.

Larcombe, P. and Jago, C., 1996. The morphological dynamics of intertidal megaripples in the Mawddach Estuary, North Wales, and the implications for palaeoflow reconstructions. Sedimentology, 43(3), pp.541–559. Available at: http://doi.wiley.com/10.1046/j.1365-3091.1996.d01-16.x.

Le Bot, S. and Trentesaux, A., 2004. Types of internal structure and external morphology of submarine dunes under the influence of tide- and wind-driven processes (Dover Strait, northern France). Marine Geology, 211(1-2), pp.143–168.

Lee, H.J., J., H.R. and Yong, S.C., 2006. Dune Migration on Macrotidal Flats Under Symmetrical Tidal Flows: Garolim Bay, Korea. Journal of Sedimentary Research, 76(2), pp.284–291.

Lee, M.W.E., Bray, M.J., Workman, M., Collins, M.B. and Pope, D., 2000. Coastal shingle tracing: A case study using the (Electronic Tracer System) (ETS), in Foster, I. D. L. (ed.) Tracers in Geomorphology, pp. 413–435.

Leeder, M.R., 1983. On the interactions between turbulent flow, sediment transport and bedform mechanics in channelized flow. In J. D. Collinson and J. Lewin, eds. Modern and Ancient Fluvial Systems. International Association of Sedimentologists, Special Publication 6, pp. 5–18.

Leeder, M.R., 1982. Sedimentology: Process and Product, London: George Allen and Unwin.

Leica Geosystems AG, 2013. Specifications Leica TPS1200+ Series. Available at: http://www.leica-geosystems.co.uk/downloads123/zz/tps/tps1200/brochures/Leica_TPS1200+_brochure_en.pdf.

Leica Geosystems AG, 2011. Leica ScanStation C10 Datasheet. Available at: www.leica-geosystems.com/hds (Accessed: 5 May 2015).

Leica Geosystems AG, 2009. Leica GS09 GNSS Datasheet. Available at: http://www.arctron.de/uploads/media/Leica_GS09_GNSS_DS_en.pdf (Accessed: 5 May 2015).

Lennon, G.W., Gumbel, E.J., Barricelli, N.A. and Jenkinson, A.F., 1963. A frequency investigation of abnormally high tidal levels at certain west coast ports. In ICE Proceedings. Thomas Telford, pp. 451–484.

Leopold, L.B., Bagnold, R.A., Wolman, M.G. and Brush Jr., L.M., 1960. Flow resistance in sinuous or irregular channels. 111th edn, Professional Paper. 111th edn. Washington, D.C. Available at: http://pubs.er.usgs.gov/publication/pp282D.

Leopold, L.B. and Emmett, W.W., 1976. Bedload measurements, East Fork River, Wyoming. Proceedings of the National Academy of Sciences of the United States of America, 73(4), pp.1000–4.

Lisle, R.J., Brabham, P. and Barnes, J., 2011. Basic Geological mapping. 5th edn. Chichester: Wiley-Blackwell.

Mackie, A.S., James, J.W., Rees, E.I., Darbyshire, T., Philpott, S.L., Mortimer, K., Jenkins, G.O. and Morando, A., n.d. BIOMÔR 4: The Outer Bristol Channel Marine Habitat Study, Available at: http://www.marlin.ac.uk/obc/pdfs/report/chapter 2.pdf.

Maizels, J., 1989. Sedimentology and palaeohydrology of Holocene flood deposits in front of a jo¨kulhlaup glacier, south Iceland. In P. A. Beven, K.J., and Carling, ed. Floods: Hydrological, Sedimentological and Geomorphological Implications. Chichester, U.K.: Wiley, pp. 239–251.

Maizels, J., 1997. Jokulhlaup deposits in proglacial areas. Quaternary Science Reviews, 16(7), pp.793–819.

Manning, A.J., Langston, W.J. and Jonas, P.J.C., 2010. A review of sediment dynamics in the Severn Estuary: Influence of flocculation. Marine Pollution Bulletin, 61(1-3), pp.37–51. Available at: http://dx.doi.org/10.1016/j.marpolbul.2009.12.012.

Marion, A. and Fraccarollo, L., 1997. Experimental investigation of mobile armoring development. Water Resources Research, 33(6), p.1447.

Masselink, G. et al., 2009. Tide-driven dune migration and sediment transport on an intertidal shoal in a shallow estuary in Devon, UK. Marine Geology, 262(1-4), pp.82–95. Available at: http://dx.doi.org/10.1016/j.margeo.2009.03.009.

McCave, I.N., 1971. Sand waves in the North Sea off the coast of Holland. Marine Geology, 10(3), pp.199–225.

Menard, H.W., 1950. Sediment movement in relation to current velocity. Journal of Sedimentary Research, 20(3), pp.148–160. Available at: http://jsedres.sepmonline.org/content/20/3/148.abstract.

Meyer-Peter, E. and Müller, R., 1948. Formulas for Bed-Load Transport. Proceedings of the 2nd Meeting of the International Association of Hydraulic Research, pp.39–64.

Middleton, G. V, 1965. Antidune cross-bedding in a large flume. Journal of Sedimentary Research, 35(4), pp.922–927. Available at: http://jsedres.sepmonline.org/content/35/4/922.abstract.

Middleton, G. V, 1991. A short historical review of clastic tidal sedimentology.

Miller, M.C., McCave, I.N. and Komar, P.D., 1977.) Threshold of sediment motion under unidirectional currents, Sedimentology, 24(4), pp. 507–527. doi: 10.1111/j.1365-3091.1977.tb00136.x.

Mueller, E.R. and Pitlick, J., 2005. Morphologically based model of bed load transport capacity in a headwater stream. Journal of Geophysical Research, 110(F02016), pp.1–14.

Nainwal, H.C., Negi, B.D.S., Chaudhary, M., Sajwan, K.S. and Gaurav, A., 2008. Temporal changes in rate of recession: Evidences from Satopanth and Bhagirath Kharak glaciers, Uttarakhand, using Total Station Survey. Current Science, 94(5), pp. 653–660.

Nakayama, K., Ikeda, H., Yamamoto, K., Iijima, Kusaro, J. and Itakura, M., 1997. Preliminary report of flume experiments on movements and bedforms of pumice grains and volcanic

glass particles. Geological Reports of Shimane University, 16, pp.37–45 (in Japanese with English abstract).

Neuendorf, K.K.E., Mehl, Jr., J.P. and Jackson, J.J., 2005. Glossary of geology, Alexandria: American Geological Institute.

Neumeier, U., 1998. Tidal dunes and sand waves in deep outer-shelf environments, Bajocian, SE Jura, France. Journal of Sedimentary Research, 68(3), pp.507–514. Available at: http://jsedres.sepmonline.org/cgi/doi/10.2110/jsr.68.507.

Nichols, G., 2013. Sedimentology and Stratigraphy, Wiley. Available at: https://books.google.co.uk/books?id=Gcgp5oLFrZMC.

Nio, S.-D. and Yang, C.-S., 1991. Diagnostic attributes of clastic tidal deposits: a review.

Novak, I.D., 1973. Predicting coarse sediment transport: the Hjulstrom curve revisited. In M. Morisawa, ed. Fluvial geomorphology. Allen and Unwin: London, pp. 13–25.

Owens, J.S., 1908. Experiments on the transporting power of sea. , 31(4), pp.415–420.

Parker, G., Klingeman, P.C. and McLean, D.G., 1982. Bedload and size distribution in paved gravel-bed streams. Journal of the Hydraulics Division, 108(4), pp.544–571.

Pearce, M.A., Jones, R.R., Smith, S.F., McCaffrey, K.J.W. and Clegg, P., 2006. Numerical analysis of fold curvature using data acquired by high-precision GPS. Journal of Structural Geology, 28(9), pp. 1640–1646. doi: 10.1016/j.jsg.2006.05.010.

Phillips, M.R. and Crisp, S., 2010. Sea level trends and NAO influences: The Bristol Channel/Severn Estuary. Global and Planetary Change, 73(3-4), pp.211–218. Available at: http://linkinghub.elsevier.com/retrieve/pii/S0921818110001323 [Accessed May 24, 2013].

Pingree, R.D. and Griffiths, D.K., 1980. Currents driven by a steady uniform wind stress on the shelf seas around the British Isles. Oceanologica Acta, 3(2), pp.227–236.

Pitlick, J., 1988. Variability of bed load measurement. Water Resources Research, 24(1), pp. 173–177.

Pitlick, J., 1992. Flow resistance under conditions of intense gravel transport. Water Resources Research, 28(3), pp.891–903.

Potter, I.C., Bird, D.J., Claridge, P.N., Clarke, K. Robert, Hyndes, G. and Newton, L.C., 2001. Fish fauna of the Severn Estuary. Are there long-term changes in abundance and species composition and are the recruitment patterns of the main marine species correlated? Journal of Experimental Marine Biology and Ecology, 258(1), pp.15–37. Available at: http://www.ncbi.nlm.nih.gov/pubmed/11239623.

Radecki-Pawlik, A. Carling, P.A. and Breakspeare, R., 2006. Field investigations of sand-gravel bed forms within the Raba river, Poland. River Flow 2006 - Ferreira, Alves, Leal and Cardoso (eds) © 2006 Taylor and Francis Group, London., (1989), pp.979–984.

Raudkivi, A.J., 1963. Study of sediment ripple formation. Journal of Hydraulic Engineering,ASCE, 89, pp.15–36.

Raudkivi, A.J., 1966. Bed forms in alluvial channels. Fluid Mechanics, 26, pp.507–514.

Raudkivi, A.J., 1997. Ripples on stream bed. Journal of Hydraulic Engineering,ASCE, 116, pp.58–64.

Raven, E.K., Lane, S.N. and Ferguson, R., 2010. Using sediment impact sensors to improve the morphological sediment budget approach for estimating bedload transport rates. Geomorphology, 119(1-2), pp.125–134. Available at: http://dx.doi.org/10.1016/j.geomorph.2010.03.012.

Raven, E.K., Lane, S.N., Ferguson, R.I. and Bracken, L.J., 2009. The spatial and temporal patterns of aggradation in a temperate, upland, gravel-bed river. Earth Surface Processes and Landforms, 34, pp.1181–1197.

Reid, I., Frostick, L. and Layman, J.T., 1985. The incidence and nature of bedload transport during flood flows in coarse-grained alluvial channels. Earth Surface Processes and Landforms, 10, pp.33–44. Available at: http://doi.wiley.com/10.1002/esp.3290100107.

Reid, S.C., Lane, S.N., Berney, J.M. and Holden, J., 2007. The timing and magnitude of coarse sediment transport events within an upland, temperate gravel-bed river. Geomorphology, 83(1-2), pp.152–182.

Reynolds, O., 1883. An Experimental Investigation of the Circumstances Which Determine Whether the Motion of Water Shall Be Direct or Sinuous, and of the Law of Resistance in Parallel Channels. Proc. R. Soc. Lond. January.

Richards, K., 1982. Rivers: Form and Process in Alluvial Channels, Blackburn Press.

Richardson, K., Benson, I. and Carling, P. a., 2003. An instrument to record sediment movement in bedrock channels. , (June 2002), pp.228–236. Available at: http://eprints.soton.ac.uk/14845/.

Rickenmann, D. and Fritschi, B., 2010. Bedload transport measurements using piezoelectric impact sensors and geophones. In Proceedings of International Bedload-Surrogate Monitoring Workshop.

Rickenmann, D. and McArdell, B.W., 2007. Continuous measurement of sediment transport in the Erlenbach stream using piezoelectric bedload impact sensors. Earth Surface Processes and Landforms, 32(9), pp.1362–1378. Available at: http://dx.doi.org/10.1002/esp.1478.

Rickenmann, D., Turowski, J.M., Fritschi, B., Klaiber, A. and Ludwig, A., 2012. Bedload transport measurements at the Erlenbach stream with geophones and automated basket samplers. Earth Surface Processes and Landforms, 37(9), pp.1000–1011. Available at: http://dx.doi.org/10.1002/esp.3225.

Robert, A., 1990. Boundary roughness in coarse-grained channels. Progress in Physical Geography, 14, pp.42–70.

Robins, P.E., Skov, M.W., Lewis, M.J., Giménez, L., Davies, A.G., Malham, S.K., Neill, S.P., McDonald, J.E., Whitton, T.A., Jackson, S.E. and Jago, C.F., 2016. Impact of climate change on UK estuaries: A review of past trends and potential projections. Estuarine, Coastal and Shelf Science, 169, pp.119–135.

Rubey, W.W., 1938. The force required to move particles on a stream bed - ed., Available at: http://pubs.er.usgs.gov/publication/pp189E.

Rubin, D.M. and McCulloch, D.S., 1980. Single and superimposed bedforms: a synthesis of San Francisco Bay and flume observations. Sedimentary Geology, 26(1-3), pp.207–231. Available at: http://www.sciencedirect.com/science/article/pii/0037073880900123 [Accessed March 17, 2015].

Ryan, S.E. and Porth, L.S., 1999. A field comparison of three pressure-difference bedload samplers. Geomorphology, 30(4), pp. 307–322. doi: 10.1016/S0169-555X(99)00059-8.

Scott, K., 1982. Erosion and sedimentation in the Kenai River, Alaska. Available at: http://pubs.usgs.gov/pp/1235/report.pdf.

Sear, D.A., Lee, M.W.E., Oakey, R.J., Carling, P.A. and Collins, M.B., 2000. Coarse Sediment Tracing Technology in Littoral and Fluvial Environments: A Review, in Foster, I. D. L. (ed.) Tracers in geomorphology. Chichester: John Wiley and Sons, p. 560.

Seminara, G., Colombini, M. and Parker, G., 1996. Nearly pure sorting waves and the formation of bedload sheets. Journal of Fluid Mechanics, 312, pp.253–278.

Seminara, G. and Tubino, M., 1989. Alternate Bars and Meandering : Free, Forced and Mixed Interactions. In S. Ikeda and G. Parker, eds. River Meandering. American Geophysical Union, Water Research Monograph, pp. 267 – 320.

Shaw, J. and Gorrell, G., 1991. Subglacially formed dunes with bimodal and graded gravel GRAVEL DUNES 545 in the Trenton Drumlin Field, Ontario. Ge´ographie Physique et Quaternaire, 45, pp.21–34.

Shaw, J. and Kellerhals, R., 1977. Paleohydraulic interpretation of antidune bedforms with applications to antidunes in gravel. Journal of Sedimentary Petrology, 47(1), pp.257–266.

Shields. A., 1936. Anwendung der Aehnlichkeitsmechanik und der Turbulenzforschung auf die Geschiebebewegung. University Berlin.

Shuttler, R.M., 1982. The wave climate in the Severn estuary. Severn Barrage., Thomas Telford, London.

Simons, D.B. and Richardson, E.V., 1971. River Mechanics: Flow in alluvial sand channels, Privately Published, Fort Collins, Colorado, USA.

Simons, D.B., Richardson, E.V. and Nordin, C.F.J., 1965. Sedimentary structures generated by flow in alluvial channels. The Society of Economic Paleontologists and Mineralogists Spec Publ, 2, pp.34–52.

Smart, G.M. and Jaeggi, M.N.R., 1983. Sediment transport on steep slopes. Eidgeno¨ssische Technische Hochschule, Zurich, Versuchsanstalt fu¨r Wasserbau, Hydrologie und Glaziologie, Mitteilungen, 64, pp.89–191.

Smith, N.D., 1978. Some comments on terminology for bars in shallow rivers. In A. D. Miall, ed. Fluvial Sedimentology. CSPG Special Publications (Canadian Society of Petroleum Geologists, Memoir 5), pp. 85–88.

Snishchenko, B.F., Muhamedov, A.M. and Mazhidov, T.S., 1989. Bedload composition effect on dune shape parameters and on flow characteristics. In Proceedings of the International Association for Hydraulic Research, 23rd Congress. p. B–105 – B–112.

Somerville, C., 2005. Coast : a celebration of Britain's coastal heritage, London: BBC Books.

Soulsby, R., 1997. Dynamics of marine sands: a manual for practical applications, Wallingford UK: HR Wallingford.

Soulsby, R. L. and Dyer, K. R. (1981) 'The form of the near-bed velocity profile in a tidally accelerating flow', Journal of Geophysical Research, 86(C9), p. 8067. doi: 10.1029/JC086iC09p08067.

Southard, J.B., 1971. Representattions of bedforms in depth-velocity-size diagrams. Journal of Sedimentary Petrology, 41, pp.903–915.

Southard, J.B. and Boguchwal, L.A., 1990. Bed configuration in steady unidirectional water flows; Part 2, Synthesis of flume data. Journal of Sedimentary Petrology, 60, pp.658–679.

Southard, J.B. and Dingler, J.R., 1971. Flume study of ripple propogation behind mounds on flat sand beds. Sedimentology, 16, pp.251–263.

Sundborg, Å., 1956. The River Klaralven: A Study of Fluvial Processes. Geografiska Annaler. Wiley on behalf of Swedish Society for Anthropology and Geography, 38(3), pp. 238–316. doi: 10.2307/520285.

Sundborg, Å., 1967. Some Aspects on Fluvial Sediments and Fluvial Morphology I. General Views and Graphic Methods. Geografiska Annaler, Series A, 49(2/4), pp.333–343. Available at: http://links.jstor.org/sici?sici=0435-3676(1967)49:2/4<333:SAOFSA>2.0.CO;2-B.

Terwindt, J.H.J. and Brouwer, M.J.N., 1986. The behaviour of intertidal sandwaves during neap-spring tide cycles and the relevance for palaeoflow reconstructions. Sedimentology, 33(1), pp.1–31. Available at: http://doi.wiley.com/10.1111/j.1365-3091.1986.tb00742.x.

Tinytag, 2011. Tinytag Plus Shock (0 to 100g): Datasheet. Available at: https://www.micronmeters.com/descriptions/productspecs/gemini/plus/tgp-0610.pdf.

UNAVCO, 2016. Terrestrial Laser Scanning (TLS) Project Support. Available at: https://www.unavco.org/projects/project-support/tls-support/tls-support.html (Accessed: 12 April 2017).

Uncles, R.J., 1981. A note on tidal asymmetry in the Severn estuary. Estuarine, Coastal and Shelf Science, 13(4), pp.419–432.

Uncles, R.J., 1982. Computed and observed resid ual curren ts in the Bristol Channel. Oceanologica Acta, 5, pp.11–20.

Uncles, R.J., 1984. Hydrodynamics of the Bristol Channel. Marine Pollution Bulletin, 15(2), pp.47–53.

Uncles, R.J., 2010. Physical properties and processes in the Bristol Channel and Severn Estuary. Marine pollution bulletin, 61(1-3), pp.5–20. Available at: http://www.ncbi.nlm.nih.gov/pubmed/20106490 [Accessed May 24, 2013].

Uncles, R.J. and Jordan, M.B., 1980. A one-dimensional representation ofresidual currents in the Severn Estuary and associated observations. Estuarine and Coastal Marine Science, 10(1), pp.39–60.

United Kingdom Hydrographic Office, Bathymetric Survey - 2013-10-15 - Severn Estuary. Available at: http://data.gov.uk/dataset/bathymetric-survey-2013-10-15-severn-estuary.

Valeport Limited, 1998. Valeport Limited: Operating Manual Model 808 Electromagnetic Current Meter.

Valeport Limited, 2003. Valeport Limited: Operating Manual Model 730D Directional Wave and Tide Recorder.

Van den Berg, J.H., 1982. Migration of Large-Scale Bedforms and Preservation of Crossbedded Sets in Highly Accretional Parts of Tidal Channels in the Oosterschelde, SW Netherlands. Geologie en Mijnbouw, 61, pp.253–263.

Van den Berg, J.H., Boersma, J.R. and van Gelder, A., 2007. Diagnostic sedimentary structures of the fluvial-tidal transition zone - Evidence from deposits of the Rhine and Meuse. Geologie en Mijnbouw/Netherlands Journal of Geosciences, 86(3), pp.287–306.

van Lancker, V., Lanckneus, J., Hearn, S., Hoekstra, P., Levoy, F., Miles, J., Moerkerke, G., Monfort, O. and Whitehouse, R. (2004) 'Coastal and nearshore morphology, bedforms and sediment transport pathways at Teignmouth (UK)', Continental Shelf Research, 24(11), pp. 1171–1202. doi: 10.1016/j.csr.2004.03.003.

van Rijn, L.C., 1982, Prediction of bed forms, alluvial roughness and sediment transport: Delft Hydraulics Laboratory, Report S 487 III, Delft, The Netherlands.

van Rijn, L. C. (1986) Sediment transport measurements, manual, Delft Hydraul. Lab., Delft, The Netherlands. Available at: http://onlinelibrary.wiley.com/doi/10.1029/JC094iC10p14315/pdf.

van Rijn, L. C. (1984) 'Sediment Transport, Part III: Bed forms and Alluvial Roughness', Journal of Hydraulic Engineering, 110(12), pp. 1733–1754.

Vanoni, V.A., 1974. Factors Determining Bed Forms of Alluvial Streams. American Society of Civil Engineers, Proceedings, Journal of the Hydraulics Division, 100, pp.363–377.

Vanoni, V.A., 1977. Sedimentation Engineering: New York, American Society of Civil Engineers, 745 p.

Vanoni, V.A. and Nomicos, G.N., 1959. Resistance properties of sediment-laden streams. Journal of the Hydraulics Division, 85(HY5), pp.77–107.

Vatne, G. et al., 2008. Bed load transport in a steep snowmelt-dominated mountain stream as inferred from impact sensors. Norsk Geografisk Tidsskrift-Norwegian Journal of Geography, 62(2), pp.66–74. Available at: http://apps.isiknowledge.com/full_record.do?product=WOS&search_mode=GeneralSearch&qid=8&SID=4CK7MLGhc6GpjaA1JKL&page=1&doc=7.

Venditti, J.G., Church, M. and Bennett, S.J., 2005. On the transition between 2D and 3D dunes. Sedimentology, 52, pp.1343–1359.

Villard, P. V. and Church, M., 2005. Bar and dune development during a freshet: Fraser River Estuary, British Columbia, Canada. Sedimentology, 52(4), pp.737–756.

Wang, Z. and Larsen, P., 1994. Turbulent structure of water and clay suspensions with bed load. , 120(5), pp.577–600.

Wang, Z.B., Jeuken, C. and Vriend, H.J. De, 1999. Tidal asymmetry and residual sediment transport in estuaries: a literature study and application to the Western Scheldt.

Welch, F.B.A. and Trotter, F.M., 1961. Geology of the country around Monmouth and Chepstow. Memoirs of the Geological Survey of Great Britain,

Wentworth, C.K., 1922. A scale of grade and class terms for clastic sediments. The Journal of Geology, 30(5), pp.377–392.

White, C.M., 1940. The Equilibrium of Grains on the Bed of a Stream. Proceedings of the Royal Society of London. Series A, Mathematical and Physical Sciences, 174(958), pp.322–338.

Whiting, P.J., Dietrich, W.E., Leopold, L.B., Drake, T.G. and Shreve, R.L.., 1988. Bedload sheets in heterogeneous sediment. Geology, 16, pp.105–108.

Whitney, J.D., Ling, Q., Miller, W.M. and Wheaton, T. A., 2001. A DGPS yield monitoring system for Florida citrus. Applied Engineering in Agriculture, 17(2), pp. 115–119.

Whittaker, J.G. and Jaeggi, M.N.R., 1982. Origin of Step-Pool Systems in Mountain Streams. American Society of Civil Engineers, Proceedings, Journal of the Hydraulics Division, 108, pp.758–773.

Wilbers, A., 2004. The development and hydraulic roughness of subaqueous dunes: Volume 323 of Netherlands geographical studies, Royal Dutch Geographical Society, Utrecht University.

Wilcock, P.R., 1992. Experimental investigation of the effect of mixture properties on transport dynamics. In P. Billi et al., eds. Dynamics of gravel-bed rivers. pp. 109–131.

Williams, G.P., 1967. Flume experiments on the transport of a coarse sand, Professional Paper. Available at: http://pubs.er.usgs.gov/publication/pp562B.

Williams, G.P., 1983. Paleohydrological Methods and Some Examples from Swedish Fluvial Environments. I. Cobble and Boulder Deposits. Geografiska Annaler. Series A, Physical Geography, 65(3/4), pp.227–243. Available at: http://www.jstor.org/stable/520588\nhttp://www.jstor.org/stable/pdfplus/520588.pdf?acceptTC=true.

Williams, J.J., Carling, P.A. and Bell, P.S., 2006. Dynamics of intertidal gravel dunes. Journal of Geophysical Research: Oceans, 111(C6), p.C06035. Available at: http://www.agu.org/pubs/crossref/2006/2005JC003000.shtml [Accessed November 21, 2012].

Williams, P.B. and Kemp, P.H., 1971. Initiation of ripples on flat sediment beds. Journal of Hydraulic Engineering,ASCE, 98, pp.1057–1070.

Wolf, J., 1987. A 3-D Model of The Severn Estuary. In J. C. J. Nihoul and B. M. Jamart, eds. Three-Dimensional Models of Marine and Estuarine Dynamics. Elsevier, pp. 609–624 (Liege Colloquium, 1986).

Yalin, M.S., 1964. Geometrical properties of sand waves. Journal of the Hydraulics Division,ASCE, 90, pp.105–119.

Yalin, M.S., 1972. Mechanics of sediment transport, Oxford; New York: Pergamon Press.

Yalin, M.S., 1977. Mechanics of sediment transport 2nd ed., Oxford: Pergamon Press.

Yalin, M.S., 1992. River Mechanics, Oxford: Pergamon Press.